FZR - 319

April 2001

Report
July 1999 - December 2000

Institute of Nuclear and Hadron Physics

Editors:

F. Dönau, W. Enghardt, E. Grosse,
B. Kämpfer, M. Schlett, Ch. Schneidereit

Explanation of special symbols:

The letters given in brackets in the following text and used as appendix in the title of the scientific contributions do express our grateful acknowledgement to the funding, sponsoring or grants provided by several institutions.

Research projects were funded by the Federal Ministry of Education and Research BMBF (B), by the Saxon Ministry of Education and Arts SMWK (S), by the German Research Community DFG (D), by the German Academic Exchange Service DAAD (A), by the European Commission (E), by the GSI Darmstadt (G), by the KFA Jülich (K) and by the special program HSP III (H) or were sponsored within Scientific agreements with eastern European countries (W).

CONTENTS

Preface

The Forschungszentrum Rossendorf (FZR) at Dresden is a research centre devoted to investigations using radiation and radioactivity in bio-medical, environmental, material, safety and nuclear science; it belongs to the Wissenschaftsgemeinschaft G. W. Leibniz (WGL), one of the German national institutions responsible for extra-university research. Among the five institutes of the FZR the Institute of Nuclear and Hadron Physics (IKH) is special in the sense that it is equally engaged in fundamental research on subatomic systems as well as in the transfer of knowledge to other fields of science. It especially investigates and exploits the possibilities for introducing experimental and theoretical techniques from particle and nuclear physics to the life sciences.

The most remarkable example of such technology transfer is the strong involvement of the institute in the work on the Radiation Source ELBE at the FZR. This instrument is centered around a superconducting electron linac; thus nuclear physicists can well contribute with their experience gained at accelerators outside of Rossendorf. From the projected electron beam of 1 mA at up to 40 MeV intensive secondary radiation shall be produced: for the medium and far infrared (IR) the free electron laser (FEL) principle will be used, whereas keV-X-rays can be produced via electron channeling or Compton backscattering. Bremsstrahlung photons in the MeV range are a very interesting probe for investigations in nuclear spectroscopy and astrophysics; they also allow the generation of fast neutrons in short bunches, which are of special interest for cross section measurements using time-of-flight techniques.

The first chapter of this Report describes the progress made in the completion of ELBE. It contains contributions from various FZR-groups as well as the institute's work on components of ELBE, especially on the production stations for the different kinds of secondary radiation and on the experimental equipment to be installed for their use. The conceptual and theoretical design studies for the IR-FEL and the detailed work on the magnetic undulators constitute a very important contribution to the FEL aspect of ELBE, which very likely will be especially attractive to outside users. Similarly, the numerical simulations performed for the optimization of the X-ray and the MeV-photon production stations and the experimental areas indicate that in both fields ELBE is apt to allow experiments with reduced background conditions.

Hadron Physics at the IKH - as described in the second chapter - is deals with hadronic interactions as such and also within the hadronic medium formed in collisions between nuclei or in violent astrophysical events like supernovae. Experiments related to such questions were performed at the proton cooler synchrotron COSY at the Forschungszentrum Jülich and at the heavy-ion synchrotron SIS at GSI Darmstadt. Theoretical studies refer to these experiments and to data obtained at higher energy accelerators, where a phase transition to a quark gluon plasma has been predicted to occur.

The third chapter combines experimental and theoretical research in Nuclear Physics. Here the work mainly deals with electromagnetic processes in nuclei, with special emphasis on those triggered by impinging bremsstrahlung photons. Special attention is given to studies of collective excitations of nuclei as well as their interplay to single nucleon degrees of freedom. The secondary ELBE beams also may play an important

role in the simulation of processes occurring during the stellar synthesis of the elements and they are of interest as the source of exotic nuclei whose spectroscopic properties shall be studied; here photon or neutron induced fission will be applied. Neutrons in the MeV range can also be used for determining cross sections of importance for the selection of materials for fusion reactors as well as for new nuclear technologies like waste transmutation or accelerator driven fission and spallation.

Last but not least this Annual Report contains a chapter on Biomedical Research performed by using nuclear technology. In the past the main contribution of the institute to this field came from Positron Emission Tomography (PET) and the outstanding achievement here is the successful operation of a PET scanner simultaneously to the irradiation of tumors with heavy ion beams. A significant number of patients was treated at GSI in the last years and the reliability and reproducibility of such radiation therapy had been improved considerably by in-situ PET, as developed at the institute. In the upcoming years biomedical research will be performed increasingly with the beams coming from ELBE: The quasi-monochromatic X-rays of easily variable energy as produced in electron channeling will be used as a probe for the elementary processes responsible for radiation damage in tissue. For a corresponding experimental study a cell laboratory is installed at ELBE, which will also be used for investigating the interactions of cells with the tunable FEL-radiation in the infrared as available at ELBE as well. Interesting research in biophysics and biochemistry will become possible; here the rather low damage of IR combined with its potential sensitivity to selected bio-molecular bonds may play an increasing role.

The scientific activities of the institute have benefitted from generous support from various sources. First of all, we gratefully acknowledge the close and fruitful collaboration with the colleagues from the Technical University (TU) Dresden and many other scientific institutions in Germany and abroad; such contacts are of vital importance for our institute. Specific projects were subsidized by the Federal Ministry for Education and Research (BMBF), the Saxon State Ministry for Science and Art (SMWK), Forschungszentrum Jülich and GSI Darmstadt. We express our gratitude to all these as well as to the Deutsche Forschungsgemeinschaft (DFG) and to the European Union (EU) for agreeing to support several ELBE research projects initiated by the institute.

The Radiation Source ELBE

At the Forschungszentrum Rossendorf (FZR) a major new installation is approaching its completion - the "Strahlungsquelle ELBE". This radiation source will use the high brilliance electron beam from a linac with superconducting rf-cavities to produce various secondary beams for experiments in nuclear, solid-state, environmental and bio-medical physics as well as in various other fields. To present a comprehensive status report of this important and innovative project, the present Annual Report combines contributions made to it by several groups and departments of the FZR. The Departments "Experimental Facilities and Information Technology" and "New Accelerators" as well as the ELBE-beam-diagnostics-group have carried out numerous developments within the ELBE project; the most important are described mainly in the beginning of this Report. The subsequent contributions from groups of the IKH are more strongly focused on the production and future use of the different kinds of secondary radiation.

Physics with IR-FEL's and their radiation

The high brilliance electron beam produced by a super-conducting linac like ELBE allows the investigation of various processes which produce high quality electromagnetic radiation in various energy (i.e.) ranges. An especially illustrative and theoretically clear example for the generation of radiation is the Free-Electron-Laser (FEL). With the electron energy range available at ELBE coherent infrared radiation from 300 μm (corresponding to 1 THz) to 3 μm (equivalent to 0.4 eV) can be produced in short pulses of a few ps and with a large repetition rate finally allowing tens of watts average intensity. At the long wavelength side the limitation results mainly from the difficulties in handling the strong diffraction effects. Various theoretical and numerical studies have been performed on this problem and on the resulting IR-beam properties; laboratory experiments to test some of these calculations are presently being set up. For the short wavelengths the quality of the electron pulses and the undulator field is crucial. Our newly perfected pulsed-wire field scan allows to cross-check the detailed field maps obtained with Hall-probes and it will be used to document 'in situ' future variations in magnetic field strength. Research making use of IR- radiation in the 10 μm-range has been performed at existing FEL facilities and with Fourier- transform (FTIR)-spectroscopy methods. A FTIR-spectrometer operable in conjunction with a reflection-optic microscope is newly available at the institute to be used in conjunction with the IR-studies on biomedical probes to be performed at the FEL in the next years by scientists from the IKH.

X-rays, Bremsstrahlung Photons and Neutrons

Quasi-monochromatic X-rays can be generated from the fast electrons either by using the channeling process in single crystals (esp. diamond) or by Compton scattering of intense laser light from the electrons. For both processes a very high brilliance e-beam has to be realized which requires a beam transport system allowing for the reduction of unwanted emittance growth effects. At ELBE a decrease of the transverse emittance beyond present values is expected from improvements of the e-gun and finally the use of a photo cathode gun directly coupled to a superconducting cavity. Space charge effects can be minimized by enlarging the repetition rate from 13 up to 260 MHz - at constant average beam intensity. Studies will be performed to enhance the yield of channeling X-rays by resonant variation of the crystal parameters using a variable frequency ultra-sound field; additionally an improvement of the X-ray-to-bremsstrahlung-ratio will be strived for by inserting polycristalline carbon segments between radiator and probe. To promote the radiation damage studies planned by the IKH for the X-ray beam a cell-laboratory has

been set up in the ELBE building.

In the case of MeV-bremsstrahlung to be used for nuclear spectroscopy a reduction of the background seen by the high resolution Ge-detectors will be aimed for by installing: (a) a vacuum tube to transport the beam from the radiator to the nuclear target, (b) a graded collimator made from pure Al, a material with low neutron production yield, (c) an extended photon beam stop formed by a hydrocarbon surrounded by Pb, (d) anti-coincidence shields from BGO around the detectors and (e) a coincidence circuit suppressing radiation delayed with respect to the e-bunches. First experiments on this beam-line will study the dipolar response of Mo-nuclei to photons of 5 to 15 MeV in dependence of their neutron number. Even more neutron-rich isotopes in this mass range will be accessible for spectroscopy as products from photon-induced fission in the future; such studies also deliver information of importance for the detailed understanding of the stellar synthesis of the heavier chemical elements.

The fast neutrons produced from the ps-e-bunches available at ELBE can be tagged such that a rather good energy resolution is obtained already after a few meter of flight path. The research envisaged here includes the investigation of fast neutrons with matter, especially with material for or from fission or fusion reactors. Also novel studies in the field of nuclear spectroscopy or nuclear astrophysics may become possible.

Collaborations

Within the FZR a close collaboration was established with the two departments responsible for the installation and operation of ELBE (i.e. Experimental Facilities / Information Technology and New Accelerators / ELBE-beam-transport and -diagnostics). Intense contacts also exist with the other Rossendorf institutes planning to use ELBE:
1) The Institute of Ion Beam Physics & Materials Research and the IKH are jointly installing equipment in the optics laboratories including a fs-laser system which will be synchronized to the ELBE e-bunches thus allowing studies of the temporal e-bunch structure as well as investigations of ultra-fast processes involving IR-pulses from the FEL.
2) The Institute of Radiochemistry and the IKH are jointly working on improving the sensitivity of IR-spectroscopical methods by replacing conventional thermal sources by the intense FEL- radiation; first exploratory studies in this field have been started at the CLIO-FEL at Orsay.
3) The Institute of Safety Research has joined the DFG-project on the "Interaction of fast neutrons with matter, esp. with materials for and from fusion and fission reactors", which also includes groups from IKH as well as from Dresden University.
Various collaborative efforts have been or are being formed to make use of the various novel research possibilities offered by ELBE and its secondary beams. As a typical example the EU-project THz-Bridge is mentioned here; it brings together scientists from IKH, from Frankfurt and Stuttgart universities and from four other EU-countries in a study on the interaction of far-IR and THz radiation with living cells.

Optimization of Transverse Emittance of the Thermionic Injector at ELBE

P. Michel, A. Büchner, P. Evtushenko, K. Möller, C. Schneider, J. Teichert

The injector concept for ELBE

To meet the different electron beam requirements according to the concept of ELBE to produce a wide range of radiation (Infrared radiation from FEL's, MeV-bremsstrahlung, X-rays, neutrons) an injector with optimum parameters for all these applications and easily changeable operation modes is needed. For example: to drive the FEL an electron beam with fixed repetition rate (13 MHz) at maximum peak current is necessary whereas for producing X-rays as channeling radiation the transverse emittance should be as low as possible (< 2 mm mrad, rms). To make Time-of-Flight experiments with neutrons the pulse to pulse distance should be variable up to micro seconds. These demands are well accomplished by an electronically grid-pulsed thermionic gun [1], which can be operated with variable frequency and bunch charge. A macro pulser based on a circular magnetic bending system interrupts the beam with adjustable duty cycle and allows a very flexible time structure of the beam. The gun is operated at 250 kV. Bunch compression is done by two bunchers operating at 260 MHz and 1.3 GHz, respectively. At two locations in the injector beam line insertable apertures are installed with three different diameters to optimize beam size and transverse emittance. The described injector set up is shown in Fig. 1.

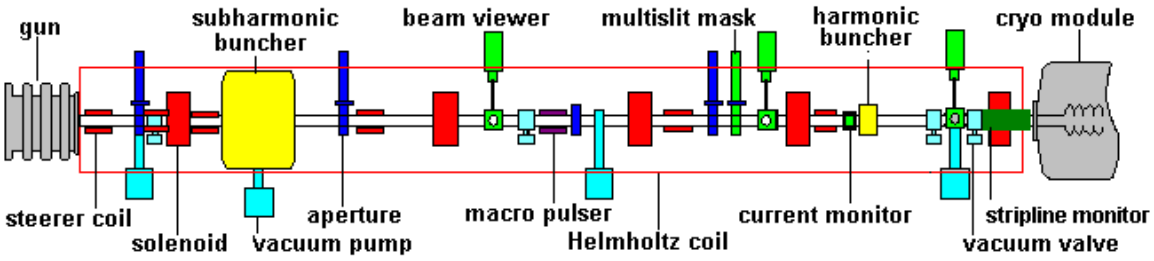

Fig. 1 *Set up of the thermionic ELBE injector*

Transverse emittance measurement

The electron beam from the gun and bunching stage (injector) was studied using a diagnostic module (Fig. 2). A multislit mask and a beam viewer allow to measure the transverse emittance in the range from 1 to 20 mm mrad with two different mask geometries. Fig. 3 shows the measured transverse geometric emittance of the ELBE injector at 13 MHz and 260 MHz pulse repetition rates. The 260 MHz regime allows operation at very low bunch charges which is important to achieve low emittance values. For comparison, Fig. 3 presents the results of a numerical simulation, too [2]. It can be seen that in the FEL mode the transverse emittance only slightly exceeds 13 mm mrad, which is sufficient to produce IR radiation down to a few microns. For Radiation Physics the emittance requirements can be

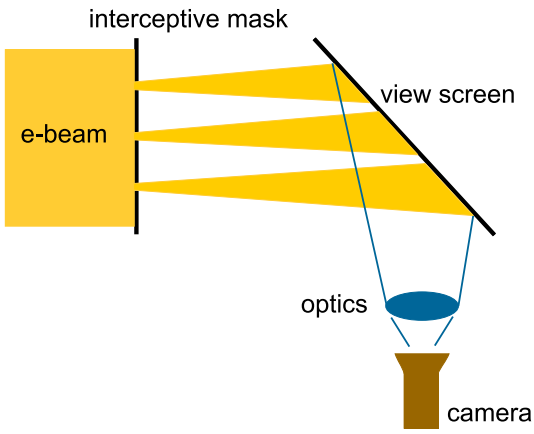

Fig. 2 *Multislit set up for transverse emittance measurement*

met by increasing the repetition rate up to 260 MHz and reducing the transverse phase space by two apertures.

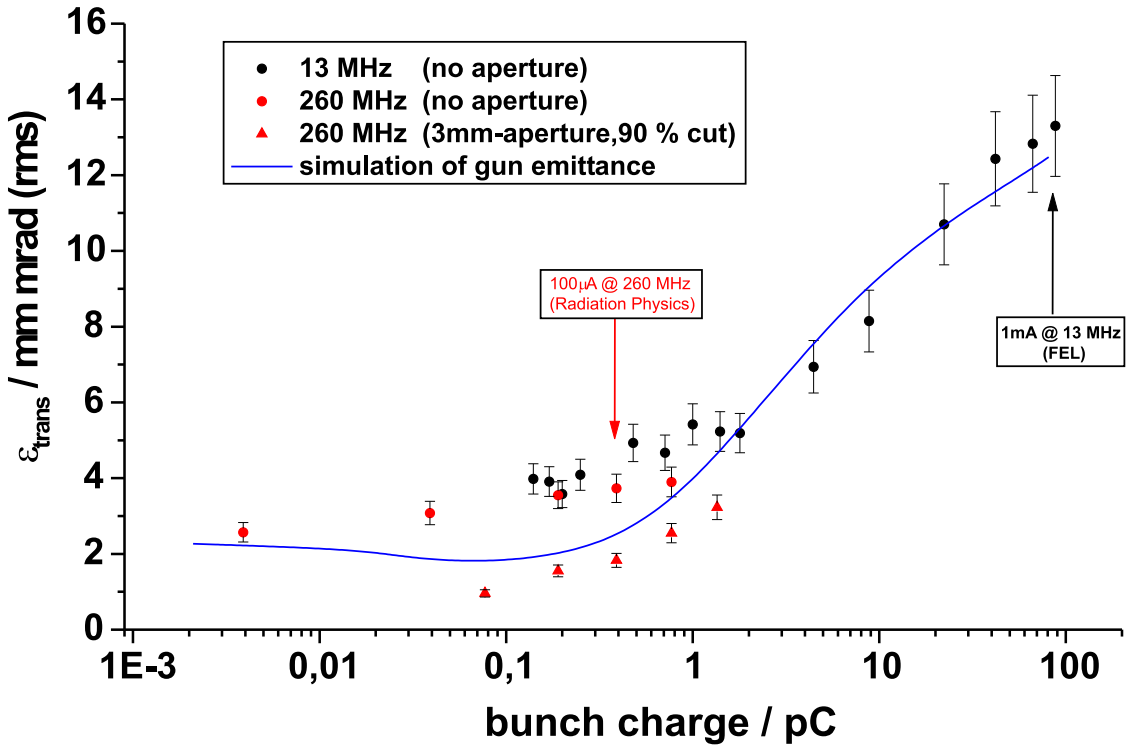

Fig. 3 *Transverse emittance of the thermionic ELBE injector*

References

[1] ELBE Design Report, FZR (1998)
[2] J. Teichert, this Report

Computation of the Transverse Emittance of a Thermionic Electron Gun Including Control Grid Effects

J. Teichert, P. Michel

Recently the injector beam parameters of the superconducting electron linear accelerator [1] were measured. For the transverse emittance an increase with bunch charge was found [2]. It grows from about 2 mm mrad for low bunch charges to nearly 14 mm mrad at a bunch charge of 85 pC. More detailed studies showed that this behaviour was rather independent of the injector operating parameters (bunching, pulse repetition rate) and that the emittance growth already takes place in the electron gun. The electron gun is a thermionic triode type with 250 kV cathode voltage and two-step acceleration. The gun has a cathode of 8 mm diameter and a 200 μm grid about 150 μm in front of it. By means of the grid, electron pulses are formed with either 13 or 260 MHz and a pulse length of about 600 ps. The maximum peak current is 140 mA which corresponds to a bunch charge of 77 pC and an averaged current of 1 mA at 13 MHz.

Numerical simulations were performed in order to understand the increase of the transverse emittance with bunch charge. Possible reasons which may cause the emittance growth and are considered within the simulations are: the thermal energy spread of the electrons, influence of the electrostatic accelerating field formed by the electrodes (geometrical aberrations), space charge effects, and the influence of the control mesh. For the calculations the program EGUN [2] was used.

As an example of the electrode geometry effect, Fig. 1 shows the influence of the Pierce electrode angle on the transverse emittance. It can be seen that the emittance decreases if the angle is increased. But this result is independent of the bunch charge and the emittance values are always much lower than the measured ones. The space charge effect is presented in Fig. 2 which shows the transverse emittance as function of the peak electron current. A significant effect on the transverse emittance is found for peak currents higher than about 1 A.

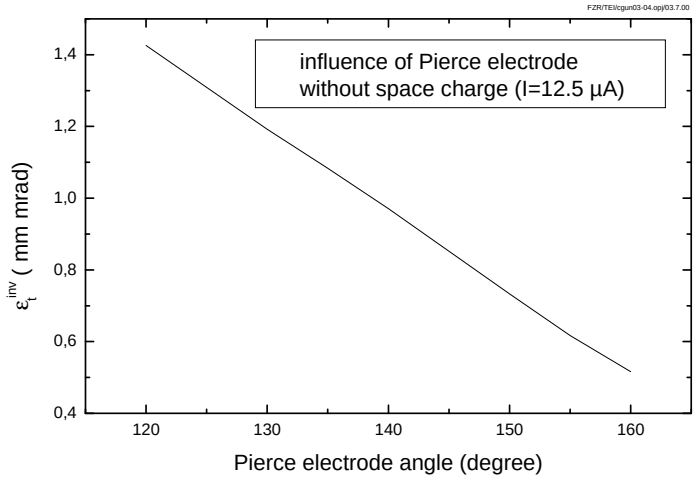

Fig. 1 *Transverse emittance (RMS) as a function of Pierce electrode angle.*

The control grid is a source of emittance growth because the strong acceleration field penetrates through the mesh holes, and for the electrons each hole acts as a lens. In order to estimate this effect a formula was derived by Reiser [4]. But this formula cannot be applied in the present

case where the mesh is always on negative potential. Therefore the grid effect was studied numerically by modifying the GUN code. For the electron transmission through the potential barrier of the mesh the free electron gas approximation with a local penetration probability , a Maxwell energy distribution, and Lambert's law were applied. Although the model is rather simple and stationary calculation with circular mesh holes are performed, the experimental results are well described by the calculation, as can be seen in Fig. 3. Thus, it can be assumed that the emittance growth is mainly caused by the grid. Furthermore the computer simulation predicts that smaller transverse emittance can be obtained at the ELBE injector by means of a smaller cathode diameter or/and a finer control mesh.

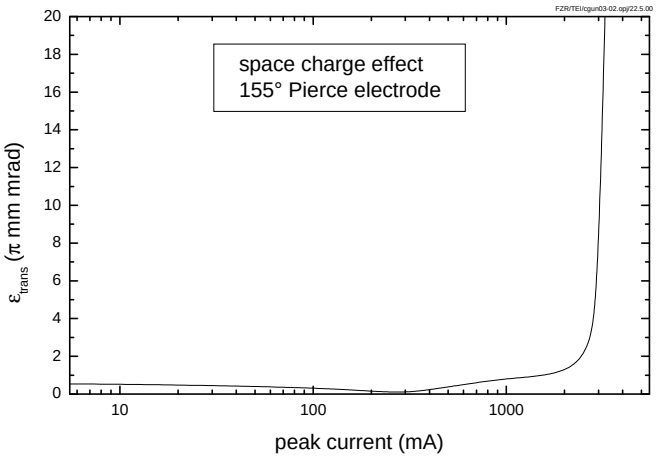

Fig. 2 *Transverse emittance (RMS) as a function of peak current (space charge effect).*

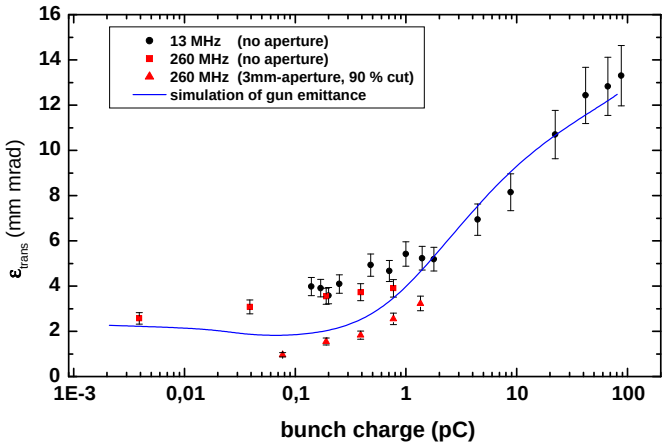

Fig. 3 *Transverse emittance (RMS) as a function of bunch charge measured at the ELBE injector for 13 and 260 MHz pulse repetition rate and with an additional aperture. The curve presents the calculation result of the grid effect.*

References

[1] F. Gabriel et al., Nucl. Instr. Meth. B 161-163 (2000) 1143
[2] P. Michel, this Report
[3] W.B. Hermannsfeldt, Report SLAC-331-UC-28, Stanford University, 1988
[4] M. Reiser, Theory and Design of Charged Particle Beams, Wiley, New York, 1994, p. 97

Status of the Superconducting RF Gun

D. Janssen

The development of a superconducting RF photocathode gun (SRF gun) is under way. SRF guns are the most advanced type of electron injectors, which combine high brightness and large bunch charges of normal conducting RF guns with the cw-mode and large average current of superconducting cavities. Numerical calculations of beam parameters for this gun show excellent results [1]. In the framework of the ELBE project we need this gun for the following reasons:
The minimal lenghts of the electron bunch, which can be obtained by this gun is smaller than 100 μm. This leads for an average electron current of 1 mA to a coherent undulator radiation in the order of 1 W with a wave lengths of 100 μm [2]. In this way for wavelengths $\lambda \geq 100\,\mu$m the SRF gun allows the generation of an intense, coherent infrared light without the optical resonator, used in the FEL.
In order to obtain intense and monochromatic radiation in the X-ray region with an electron beam energy equal or less than 40 MeV (which is the maximal energy of the accelerator), in the framework of the ELBE project different methods are planned and under discussion. In all of these methods (channeling radiation, transition radiation, parametric X-rays, Compton back scattering) the radiation output increases with decreasing of transversal emittance. Furthermore, the output of the Compton backscattering increases with increasing bunch charge. The SRF gun provides for a given bunch charge essential lower transversal emittances than the conventional injector, which is installed in the first phase of the ELBE project [1].
In the ELBE project time-of-flight measurements of fast neutrons for experiments in astrophysics, nuclear physics and for transmutation experiments are planned. For these measurements a point like neutron source with intense neutron pulses and variable time structure is necessary. These neutron pulses can be obtained by the interaction of an electron bunch with a target, where the electron bunch has the same properties as one expects for the neutron pulse. So for these experiments an electron beam with large bunch charge, small emittance and variable time structure is necessary. The possibility to create such an electron beam is one of the advantages of the SRF gun [1].
The design of the SRF gun is described in [3]. The status of its five parts is the following:

1. The main part is the cryostat with the gun cavity, the RF input coupler and the tuning mechanics for the cavity.
   The cryostat has been assembled and vacuum tested. The gun cavity has been prepared in the clean room of DESY. In a test cryostat excellent values for the maximal electric field and the Q-value were measured, see Fig. 1 and [3]. Also at DESY the cavity has been assembled together with the neighbouring beam tubes, with the coupler and with the cathode insertion device. All these parts are now installed in the cryostat at Rossendorf.

2. The photocathode preparation chamber together with the transfer tube for the photocathodes have been build and tested. In this chamber first $TeCs_2$ photolayers have been prepared. The mechanical transfer of the cathodes under vacuum from the chamber into the gun cavity inside the cryostat have also been checked.

3. The beam diagnostic module contains a viewscreen and a beamdump at the end, where beam of 2 kW can be absorbed. It has been assembled and vacuum tested. We are able to measure the beam profile and the current.

4. The fourth part is a mode locked UV laser together with a optical transfer line from the laser table to the photocathode inside the cavity. A first version of the laser has been developed at the Max Born Institute in Berlin.

5. The RF power supply together with the wave guide to the RF coupler and the control panel have been installed and tested.

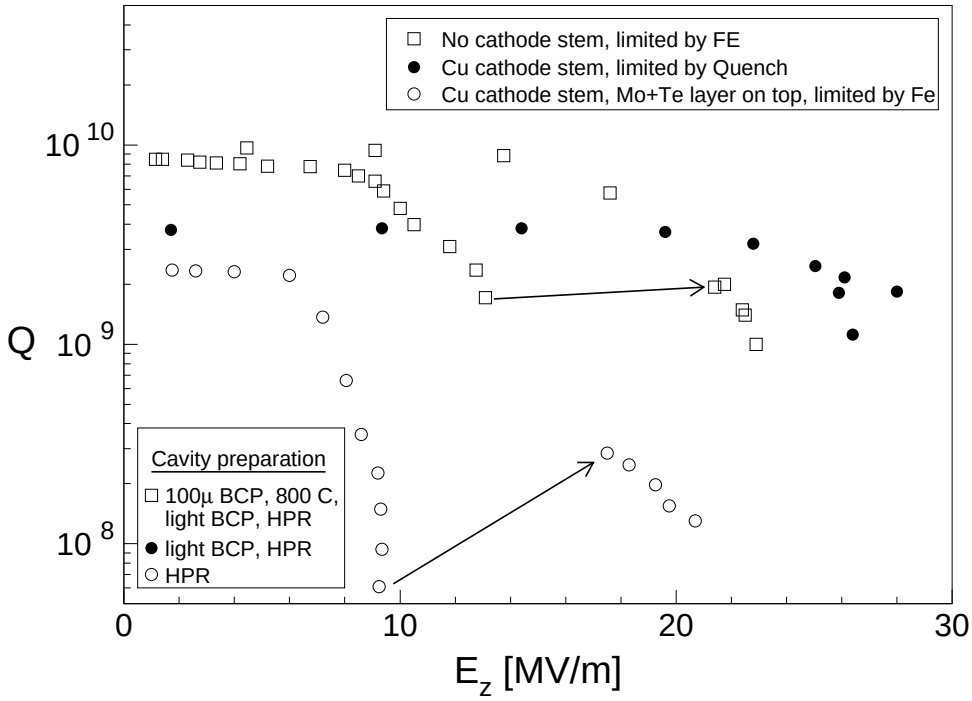

Fig. 1 *Results of the Vertical Cavity Tests obtained at a liquid Helium temperature of 2 K.*

References

[1] D. Janssen, V. Volkov
RF - focusing, an instrument for beam quality improvement in superconducting RF guns
Nucl. Instr. Meth. A 452 (2000) 34-43

[2] V. Volkov, D. Janssen, R. Wünsch
Generation of sub-picosecond electron bunches from superconducting 3+1/2 cell gun
Submitted to PAC 2001, Chicago

[3] E. Barthels et al.
On the way to a superconducting RF - gun, Nucl. Instrum. Meth. A 445 (2000) 408-412

Electron Beam Diagnostics at ELBE

A. Büchner, P. Evtushenko, U. Lehnert, P. Michel, K. Möller,
C. Schneider, J. Teichert

To optimize and control the electron beam at the ELBE facility a comprehensive system of diagnostics has to be provided similar to other facilities such as CEBAF, TTF, S-DALINAC or MAMI. In general there are two types of diagnostics. For destructive diagnostics a special diagnostics mode of beam operation was defined in order to limit the dissipated beam power. Nondestructive diagnostics can be used at all times to monitor the full-power operation of the beam. The system of diagnostics at ELBE will contain the following components:

Beam viewers

The beam viewers are operated in the diagnostics mode at an average beam current of about 1 μA and nominal bunch charge. The beam current is then controlled by the macro pulse parameters. The beam viewers are used to adjust the beam by optical inspection of the position and the size of the beam spot. Beam profiles can be determined using image analyzing software. In energy dispersive regions of the beamline viewers can be applied to measure the energy spread. In connection with multi slit masks or quadrupoles the transverse emittance of the beam can be measured. The described beam viewer concept was succesfully tested at the injector using the following equipment: screens – 500 μm Al_2O_3 ceramic (fluorescence) or 8 μm Al foil (OTR), cameras – Vidicon KH500 with Saticon tube XQ1300SF (radiation resistant), in some cases CCD cameras KAM02E, external target illumination, video multiplexing system (remote control) and a PCI-1407 frame grabber board which delivers at maximum 25 images/s synchronized to the macropulse.

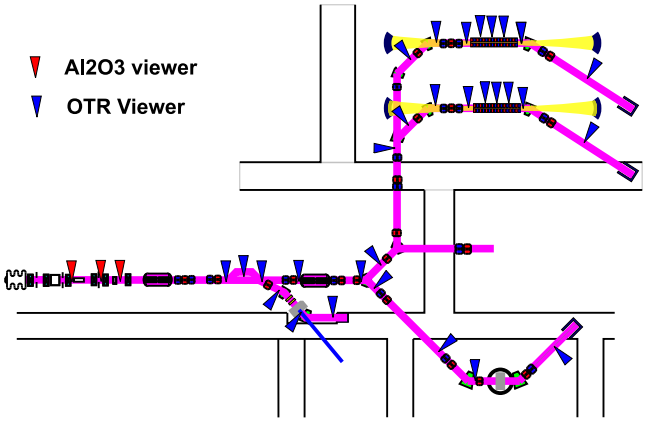

Fig. 1 *ELBE beam viewers*

Beam position and beam current monitors

These monitors are realized as strip line monitors with the following details: 35 mm diameter, signal filter 1.3 GHz with 60 MHz band width, signal conversion using an AD 8313 logarithmic rms-to-DC converter chip (0.1 - 2.5 GHz; 70 dB) into a 12(16) bit ADC. One prototype of the proposed strip line monitor was tested at the injector. A spatial resolution of < 30 μm was achieved in the current range of 10 - 1000 μA. The analysis of the strip line monitor signal with respect to its time behaviour allows the measurement of the bunch length with time resolution < 100 ps. Thereby the strip line monitors can be used for optimization of the bunch compression in the injector to deliver an optimized beam to the accelerator section. Additionally to the strip line monitors information on the beam current can

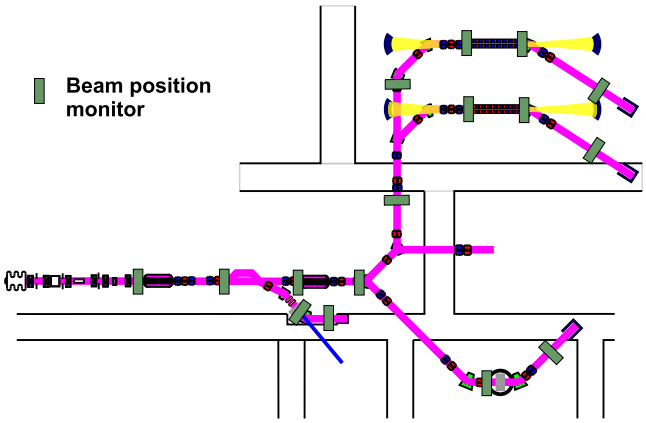

Fig. 2 *ELBE beam position monitors*

also be obtained at the various apertures and wall current monitors and at the beam dump.

Martin-Puplett Interferometer (DESY-design)

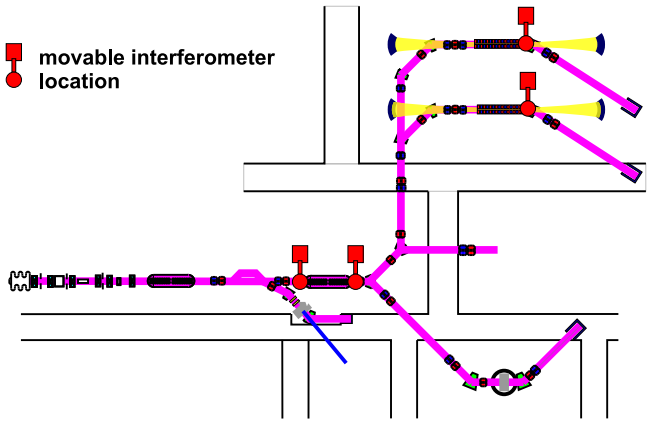

Fig. 3 *ELBE bunch length measurement*

The interferometer serves for measuring the bunch length in the submillimeter range by measuring the autocorrelation function of the coherent transition radiation. Golay cells are used to register IR radiation, the bunch length is calculated by the Kramers-Kronig method. The assembly of the interferometer is finished. At present the software for analysis is being developed.

Beam loss monitors

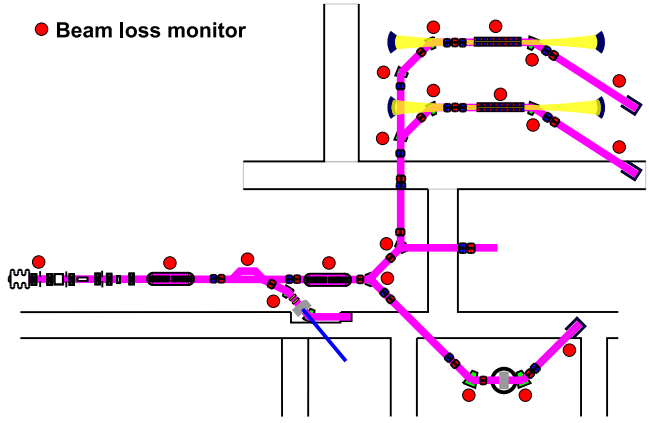

Fig. 4 *ELBE beam loss monitors*

The aim of these monitors is to measure the beam loss at a number of positions to ensure full beam transmission and to have some protection against thermal and radiation damages. They consist of „low cost“ photomultipliers (EMI9125) measuring bremsstrahlung radiation produced by electrons striking the beam tube and a count-rate integrator using VC 110 f/V-converter chips that deliver a radiation-dose signal into an ADC input. An optical test pulse will be used to ensure fail-safe operation. During tests at the injector this simple concept turned out to be fully efficient delivering signals proportional to the radiation dose.

Status of the Stripline Beam Position Monitors System at ELBE

P. Evtushenko, A. Büchner, K. Jordan[1], P. Michel

The ELBE accelerator needs a system to monitor the electron beam position in full power mode. The system will be used for optimization of the electron beam transport in the accelerator and for control of the electron beam position at the targets. The system must be nondestructive and should not affect the electron beam quality. Required resolution is about 100 μm for ± 5 mm from center. For this reason a system of stripline beam position monitors (BPM) is under design. The stripline BPM is a nondestructive device with negligible influence on the beam behavior. It is known that with stripline BPMs one can easily achieve a resolution considerably smaller than 100 μm.

To verify the basic principles of the stripline BPM and to get information about the BPMs signal behavior we did a set of measurements on the ELBE injector with a CEBAF FEL stripline BPM. We have to note that the CEBAF BPM was build for an accelerator with the fundamental frequency 1.5 GHz (as compared to 1.3 GHz at ELBE) and another beam pipe diameter. So this BPM has properties slightly different from BPM designed for ELBE. But nevertheless the general behavior of the BPM is the same and therefore the measurements were very useful for our understanding. The measurements were also necessary for the design of the BPM electronics. By means of a spectrum analyzer we measured the amplitude of the BPM signal at 1.5 GHz as a function of the beam current. The measurements gave the dynamic range of the signal which we have to take in to account in the electronic design. We also measured the amplitude of the signals from two opposite strips as a function of the beam position. The position of the beam was measured by a cromox viewscreen with a resolution much better than the BPM resolution. From this measurements we estimated the sensitivity and the achievable resolution of the BPMs.

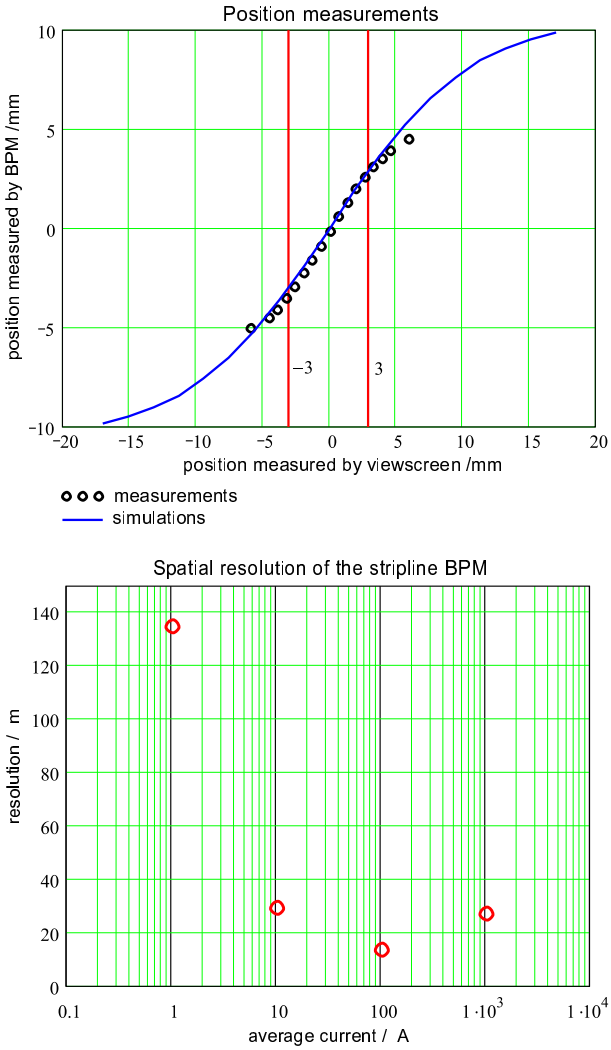

Fig. 1: *Calculated and measured response of the BPM (up), measured resolution (down).*

We also did simulations of the BPM signal behavior. The simulations were done by a simple Mathcad code. The code gives the capability to calculate the spectrum of the BPM signal as a function of bunch charge, bunch length and beam position. Here we present the results of the simulations together with results of the measurements as described above.
The measured sensitivity of the BPM is 243 mV/mm versus calculated 232 mV/mm such that there is a difference of 4.5 %. The deviation between measurements and simulation for the beam displacements of more than $3 \div 4$ mm is due to the fact that during the measurements the BPM

was installed downstream of the dipole with relatively small gap (the electron beam was cut by the vacuum chamber in the dipole).

One of the BPMs will be installed downstream of the first cryomodule. The BPM will serve for measurements of the electron beam position at the entrance of the cryomodule and for setting the correct phase and power of both bunchers of the injector. The electron bunch from the injector must enter into the module in the accelerating phase of the RF field and must have minimal length. Since the power spectrum of the beam depends on the bunch length measurements in the frequency domain can give information about the bunch length and one thus gains important information to set the bunchers. To check this possibility we did two sets of measurements. By means of a spectrum analyzer we measured the power of the 1.5 GHz peak in the BPM signal spectrum with different settings of the first subharmonic buncher.

The maximum of the signal corresponds to the minimum of the bunch length. Thus the optimum settings of the subharmonic buncher are turned out to be 500 W power and 5^o phase.

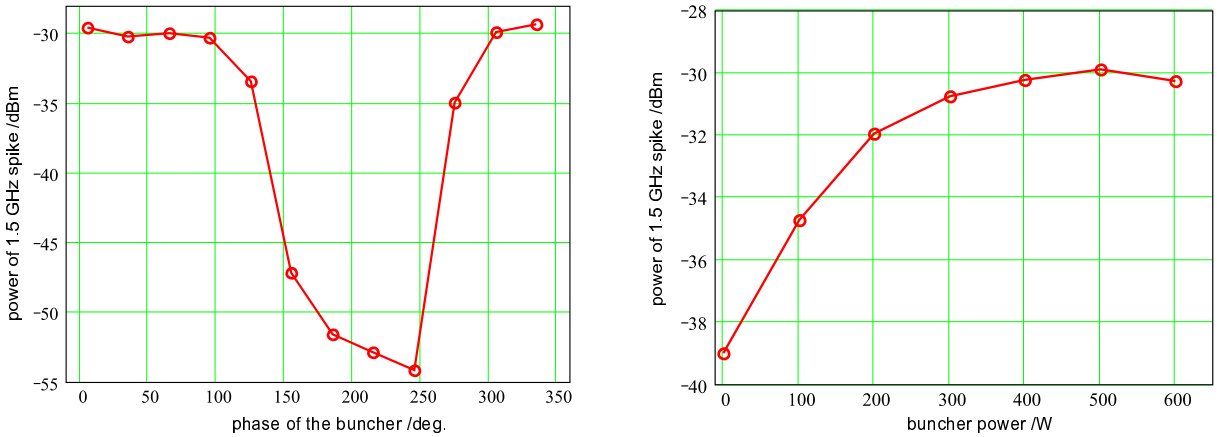

Fig. 2 *Measured power at 1.5 GHz with the following conditions: (left) dependence of the signal on the buncher phase with the power of the buncher set at 500 W; (right) dependence of the signal on the buncher power with the buncher phase constant at 5^o.*

[1] *Thomas Jefferson National Accelerator Facility, Newport News, Virginia 23606, USA*

Design of Electronics for the Stripline BPM

P. Evtushenko, A. Büttig, K. Jordan[1], P. Michel

The ELBE accelerator is operated with a time structure of the electron beam which is either cw or pulsed mode with a macropulse length down to 100 μs. Because of this time structure it is straightforward to use electronics operating in the frequency domain for the beam position monitors (BPM). The stripline BPM has a large bandwidth, at least 6 GHz, which we can see by means of a Network analyzer. The idea is to take a part of the BPM RF signal and to send it through electronics which will give a rms of the RF signal; in other words the electronics will convert the RF signal to DC with an amplitude proportional to the power of the RF signal. Microchips with 2.5 GHz bandwidth which can treat RF signals in this way are now available. There are two possible schemes of the BPM electronics under development. The first one is based on the logarithmic amplifier AD8313, the other one on the rms-responding true power detector AD8361. The features of the chips are shown in Fig.1.

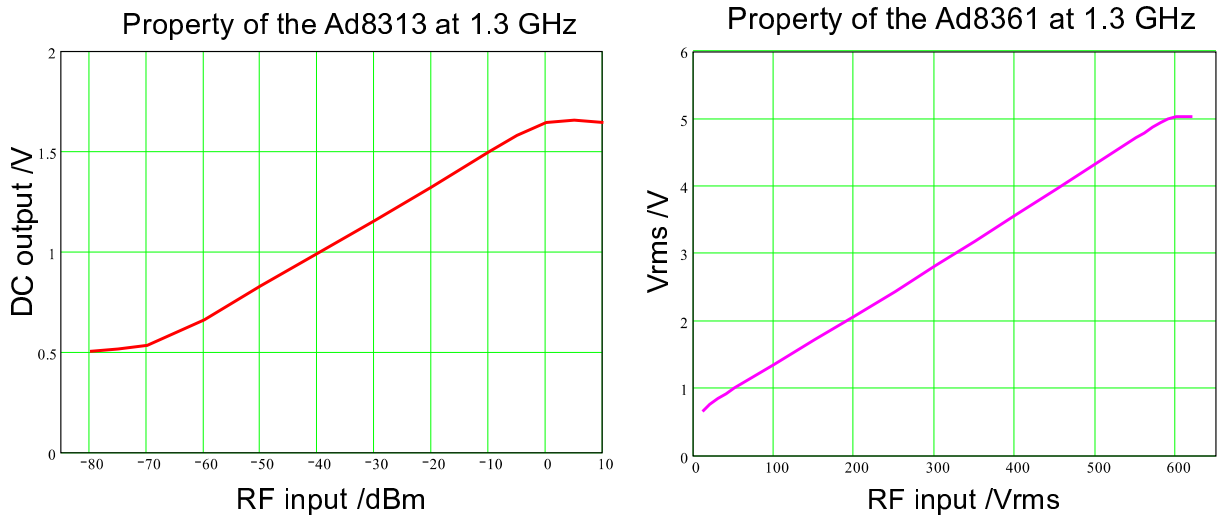

Fig. 1 *Characteristics of the chips which are used for the BPM electronics.*

The block-diagrams of the proposed electronics are given in Fig. 2.

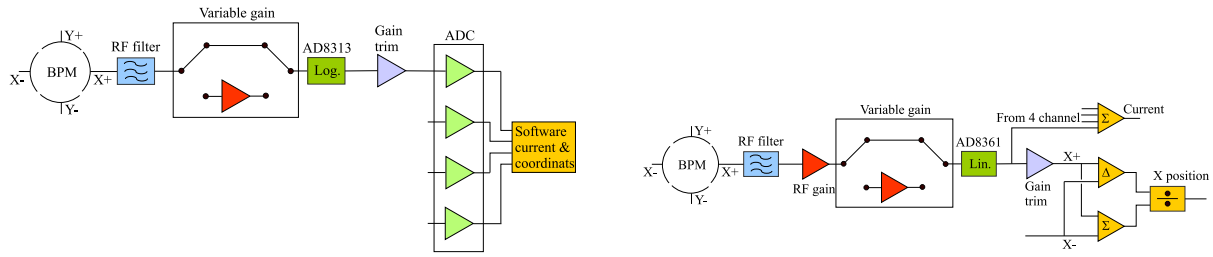

Fig. 2 *Proposed schemes of the BPM electronics, based on the logarithmic amplifier AD8313 (left) and on rms-responding true power detector AD8361(right).*

The electronics based on the AD8361 allows to calculate the electron beam position in an analog device and thus it can be more useful in time critical measurements. The scheme based on the logarithmic amplifier does not give such a possibility. In this case position and current will be calculated by software which results in a longer evaluation time. Such software for the BPM system was done in LabView.

[1] *Thomas Jefferson National Accelerator Facility, Newport News, Virginia 23606, USA*

Diagnostic Software at ELBE

Ch. Schneider

The control and data acquisition system of ELBE is a PC-based system using standard net technologies like e.g. OPC (Object Linking and Embeding (OLE) for Process Control) to interface the system components. The part of the system from which the diagnostics value are achieved is subdivided into two scopes of duties. The first is the section which acquires the raw data and processes the data (referred to as the DAQ/IMAQ). For this an example is: images from the beam distribution are grabbed from a VIDICON camera and vertical and horizontal profiles are extracted from the image data. The second is the section which processes the data in further steps to achieve more complex diagnostic variables and prepare indicators for the operator user interface (referred to as the diagnostic software). Whereas LabWindows is the development tool for the DAQ/IMAQ part for historical reasons, in general LabView will be used for the diagnostic software; it provides a well established link to LabWindows. The communication between these two system parts is realized through the DataSocket technology [1].

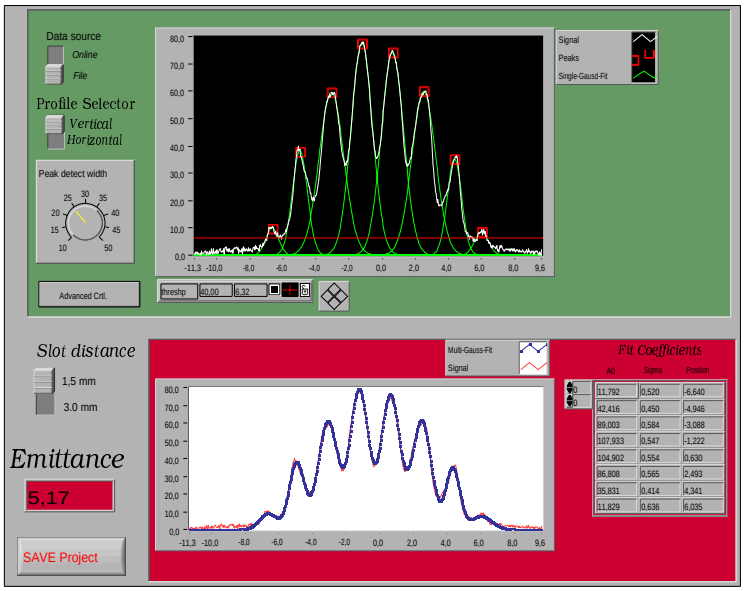

Fig. 1 *Tool to determine the emittance by the multi slit methode*

One of the important tasks in the diagnostic is the control of the beam emittance. This is done in the injector part of the accelerator with two methods. One is the multi slit method which demonstrates what kind of requirements the diagnostic software has to fulfil. In the multi slit method parts of the beam are cut out by a slit mask and are recorded from a detection screen with a camera. From the Image acquisition system IMAQ the profile data are sent to the diagnostic software. Here the image profile is fitted by a multi Gaussian function and the emittance is calculated from the fit parameters (see fig. 1).

Therefore the diagnostic software must provide complex signal analysing tools like the multi Gaussian fit and on the other hand support flexible operator controls and data indicators. In the tool displayed in fig. 1 it may be necessary to adapt the base line below the peaks or smooth the raw curve by an operator controlled width to find the correct number of peaks, which is a prerequisite for a successful multi Gaussian fit.

Unlike in other development tools a graphic programming language is used in LabView. The basic philosophy is to reflect the measurement hardware and signal acquisition in the software through the so-called (graphic) virtual instruments (VI). In that way it is consistent to reflect the diagnostic tasks like emittance, energy spread, beam profile, beam positions measurements and so on into single VIs. Since partly identical (e.g. read image profiles) subtasks have to be fulfilled much the same basic VI or subVI can be used in the program development. The data transfer between the VIs (like to the DAQ/IMAQ) is consequently realised with the DataSocket technology.

References

[1] http://www.ni.com/datasocket/wp1680.pdf

Beam Transport behind the LINAC 1

A. Büchner

The beam transport to the FELs has to perform a bunch compression and for that a chicane was planned between LINAC 1 and the „S“-arc. To design it the required transport matrix element R_{56} should be determined. This value depends on the longitudinal phase space after LINAC 1 and the desired longitudinal phase space in the FELs. Due to the complexity of the problem no exact values could be obtained from numerical simulations. As an estimate of the maximum required R_{56} a value of 450 mm was fixed. A variable chicane is planned which allows to vary R_{56} from 0 to this maximum. This gives an enormous flexibility in connection with LINAC 2, which for instance makes it possible to measure the longitudinal phase space.

To allow two-colour experiments at „ELBE“ with two FELs running synchronously in the future the beam transport has to be suitably designed. Even if these steps are not realized now the needed place for them has to be reserved. Because of tight space there is no other possibility than to combine the variable chicane with the beam separation for two-colour experiments and the beam transport to the nuclear physics experiments. A side effect of such a combination is the saving of extra dipoles for these tasks. As a consequence the size of the chicane is completely determined by the geometry resulting from the deflection angles of both energies at two-colour experiments. These angles were set to 30 and 45 degrees corresponding to a RF induced energy modulation of ± 5.23 MeV for a 30 MeV beam. This results in an even higher maximum R_{56} of the chicane of 633 mm with a maximum beam offset of 513 mm in its center. In Fig. 1 an overview of the chicane with the combined beam separation is given.

There exist five different beam paths in this design:

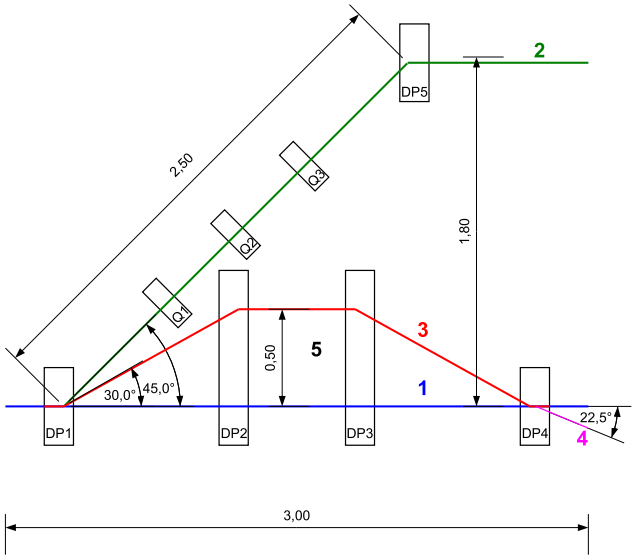

1 - Straight through to the radiation physics and neutron physics caves (all dipoles off).

2 - A separate path for the beams with sufficiently low energy.

3 - A path for the higher energy beam back to the continuation of line 1. For two-colour experiments this path and path 2 are used alternatively by subsequent pulses.

4 - A beam path to the nuclear physics cave (only dipole 4 switched on).

5 - A variable beam path for normal chicane operation.

Fig. 1: *Design of beam separation combined with variable chicane*

Beam transport calculations for all five beam paths were performed and it is possible to match the beam to the different requirements. The position of the viewscreens and beam adjustment rules are defined.

Design of the Electron-Beam Transport to the ELBE Experimental Caves

U. Lehnert

For the FEL beamlines an S-shaped design with achromatic bends was chosen which performs a compression of the electron bunch on its way to the FEL undulators. Both bends of the S use a dipole-quadrupole-dipole layout. Position and focusing power of the quadrupoles have to be adjusted to achieve zero position and momentum dispersion. For the first bend this leads to an asymmetric quadrupole position, given the asymmetric pole-face angles of the used dipole magnets. For each bend a beam matching is possible which results in equal beam radii at the entrance and exit of the bend. Given the positions of the dipole magnets the phase shift in longitudinal phase space is fixed to R_{56}=93 mm. A preparation of a certain longitudinal phase-space correlation which leads to an upright phase-space ellipse at the undulator is done with a variable-R_{56} chicane in between the two accelerator cryomodules.
The straight beamline section between the bends is mainly determined by mechanical limitations as the beam has to go through a 2.4 m thick concrete wall in front of which a beam shutter is placed. Considering this, the quadrupole-doublet magnetic lens has to be placed inside the concrete wall immediately behind the shutter in order to limit the beam magnification. Including two single quadrupoles at the ends of the straight section an imaging of the matched beams of the bends onto each other is possible.
The undulator of the mid-infrared FEL consists of two 1 m long segments. Their spacing varies from 245 to 345 mm determined by the resonance condition between the optical and the electron beam. Due to the field-free drift space beween the undulator segments an ideal matching which would yield a constant-radius envelope is impossible. Instead, a symmetric matching condition was choosen which has a beam waist between the undulator segments. The beam diameter at the waist is determined as to produce minimal betatron oscillations and thus a minimal average beam diameter over the undulator. The beamline to the undulator contains a quadrupole triplet, which does not allow an ideal matching, as there are only three degrees of freedom for four matching conditions. However, there exist decent matching compromises for all possible undulator settings, yielding a reasonably small beam diameter in comparison to the optical beam.

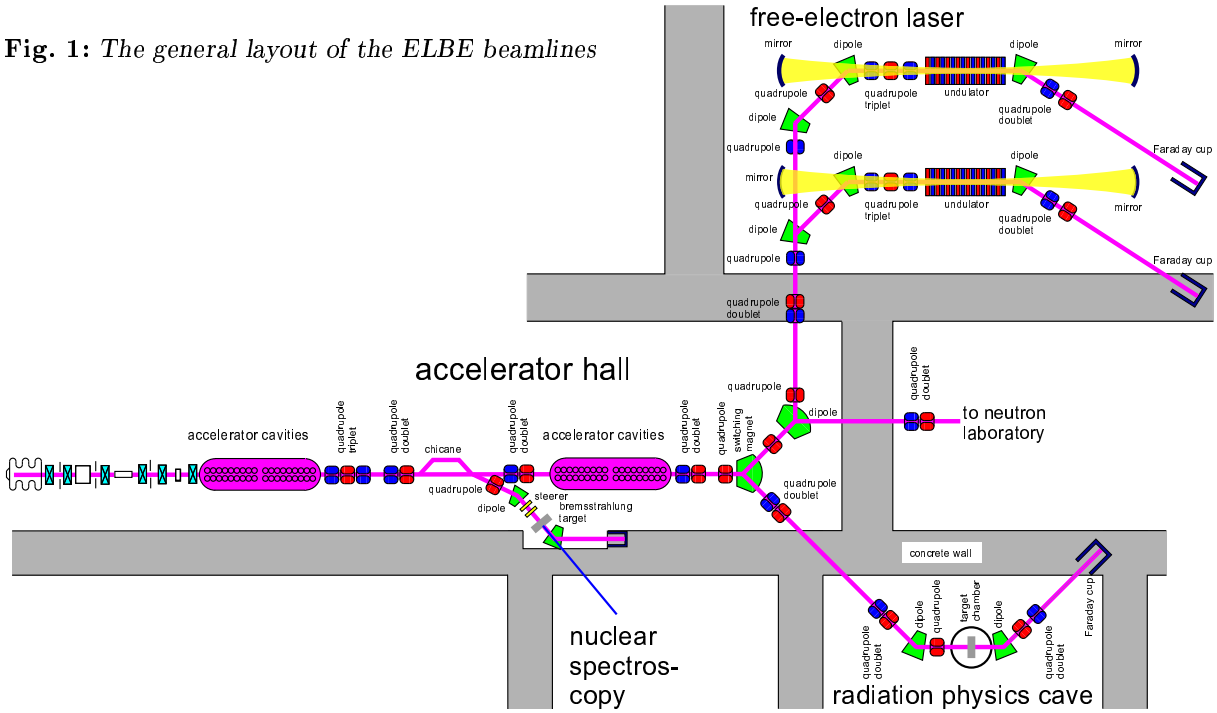

Fig. 1: *The general layout of the ELBE beamlines*

Space-charge effects on the electron beam transport were studied using the PARMELA [1] beam transport code. Electron beams which should allow an FEL operation can be supplied down to 10 MeV beam energy. The longitudinal phase shift R_{56} increases with decreasing energy from its design value R_{56}=93 mm at 20 MeV to R_{56}=160 mm at 10 MeV which has to be compensated for by tuning the chicane. At the same time, the longitudinal emittance and the energy spread of the beam are growing significantly. At 10 MeV the longitudinal emittance already triples but the beam quality still is just sufficient for the FEL operation.

The electron beam transport to the radiation physics cave has to be designed achromatic in order to conserve the low transverse emittance of the beam. This is achieved with a dispersion-crossover in the 45 deg section of the beamline. This crossover is placed asymmetrically in order to be situated outside the concrete wall and to be accessible for beam diagnostics. The necessary focussing is provided by quadrupole doublets before and after the wall that separates the accelerator hall from the radiation physics cave.
At the position of the channeling target a beam waist is created which diameter can be adapted to different experimental requirements. Either large focal spot sizes with very low beam divergence or rather narrow foci can be tuned using the two single quadrupoles situated before the switching magnet and after the first dipole in the radiation physics cave. The actual position of the focus is variable as well, thus allowing to use an alternative channeling target downstream the goniometer chamber, which design is optimized for the production of high-flux photon beams but lacks some of the flexibility of the goniometer.

For the nuclear physics beamline the last dipole magnet of the chicane is used in connection with one additional dipole and a quadrupole in between to achromatically deflect the electron beam by 45 degrees. A quadrupole doublet provides the necessary focusing onto the radiator target. A set of steerers is used to vary the angle of incidence of the electron beam with respect to the collimator axis, thus allowing experiments using partially polarized bremsstrahlung radiation emitted off the forward direction. The thickness of the radiator is limited by electron scattering and the according radiation background from electrons hitting the tubing. Therefore, special attention has to be paid to the design of the beam path from the radiator target to the beam dump, which has to be as short as possible and well shielded.

References

[1] L.M. Young, J.H. Billen, Los Alamos National Laboratory, LA-UR-96-1835

Measurements of the Electron Beam Profile and Position Inside Undulator by means of a Moveable YAG Screen

P. Evtushenko, P. Michel

Motivation

For operation of an FEL the overlap of the electron beam and the optical beam inside an undulator must be maximized. Both of them must be located in the magnetic axis of the undulator. To realize this one must be able to measure the electron beam position and profile inside the undulator with an accuracy of about 100 μm. These requirements are connected to the size of the electron beam and the optical mode in the undulator.

Scheme of the diagnostic system

The proposed diagnostics is shown on Fig 1. The system works in the following way: a moveable screen travels in the vacuum chamber which is located in the undulator. The travel length of the screen in the case of the undulator U27 is the length of the undulator (2×98 cm) plus a gap between the two parts of the undulator (~ 30 cm). In the case of undulator U50 the travel length is approximately the length of the undulator (~ 225 cm). That means the travel length of the screen is approximately the same for both undulators.

When the electron beam hits the YAG screen radiation with maximum intensity at 550 nm is produced. Downstream of the undulator there is a dipole magnet to bend the electron beam. The distance between the undulator and the dipole is approximately 140 cm. An insertable mirror is located behind the dipole. The mirror is used to deflect the YAG radiation from the vacuum chamber though a vacuum window. Near the vacuum window a lens is placed for imaging the screen to a CCD chip. Since the screen is moveable and we need to keep the optical path length between the screen and the lens constant we have to insert an element which has a variable optical path length. We can use a moveable roof mirror plus two mirrors 2 and 3, see Fig 1. The travel length of the roof mirror is half of the screen travel length. The mirror 4 and a very sensitive cooled CCD camera are located on the floor. The camera has to be shielded by a lead housing.

Choice of the screen material

As also hard X-rays will be produced, when the electron beam strikes the screen, the undulator magnets may loose magnetic strength in this high radiation environment; thus the screen should be as thin as possible. From this point of view an OTR screen would be preferable, since it is possible to make such screen from aluminium foil as thin as 10 μm. But in diagnostic mode with average current about 1 μA at an electron beam energy of 15 MeV $\div$ 40 MeV the radiation level in our collection solid angle is too small. Thus using an OTR is not sufficient for this diagnostic. The YAG crystal is a good alternative to the OTR screen in this case. Direct comparisons of the effective conversion efficiency, spatial resolution, and time response of the screens have been performed [1,2]. The light intensity of the YAG crystal is about 1000 times larger than with the OTR screen. A beam size growth has been observed for the YAG data relative to the OTR data above average current 60 mA. The fluorescence time of a the crystal has been measured [2]. The light intensity decay time was measured to be about 80 ns. YAG crystals with thickness 0.1 mm are commercially available [3].

The cooled CCD ST-237 [4] was chosen for the diagnostic, since it is sensitive enough and still not too expensive.

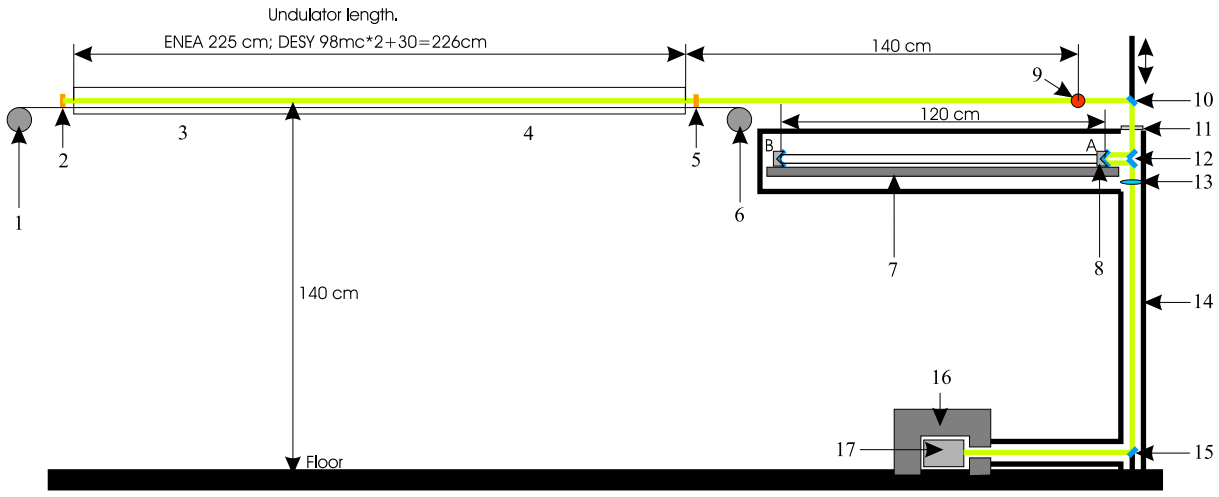

Fig. 1 *Scheme of the diagnostics. 1 - stepmotor 1, 2 - screen in position A, 3 - first part of the undulator U27, 4 - second moveable part of the undulator, 5 - screen in position B, 6 - stepmotor 2, 7 - linear motor stage with travel length 1.3 m, 8 - roof mirror on position A, 9 - position of the dipole, 10 - insertable mirror, 11 - window, 12 - mirrors, 13 - lens, 14 - light shielding, 15 - mirror, 16 - lead shielding, 17 - CCD camera.*

References

[1] A.H. Lumpkin, Nucl. Instr. and Meth. A 429 (1999) 336-340
[2] W.S. Graves, E.D. Johnson, A high resolution electron beam profile monitor, Proc. of Particle Accelerator Conf. 1997, Vancouver, Canada, Vol. 2, p. 1993
[3] http://www.crytur.cz/
[4] http://www.sbig.com/sbwhtmls/online.htm

Estimates of Absorbed Dose Rates around a Beam Dump at ELBE

B. Naumann[1]

Beam dumps will be used to aborb the electron beam energy of the radiation source ELBE. In the FEL cave it is planned to install the beam dump in front of a 3.6 m thick concrete wall and to shield it by iron and heavy concrete. The planned thickness of the iron layer in beam direction is about 30 cm resp. three tenth-value layer thicknesses of iron. For an axial symmetrically geometry (Fig. 1) the absorbed dose has been calculated using the particle transport code FLUKA [1]. The dose distribution in the described area for an electron beam with an energy of 50 MeV is shown in Fig. 2.

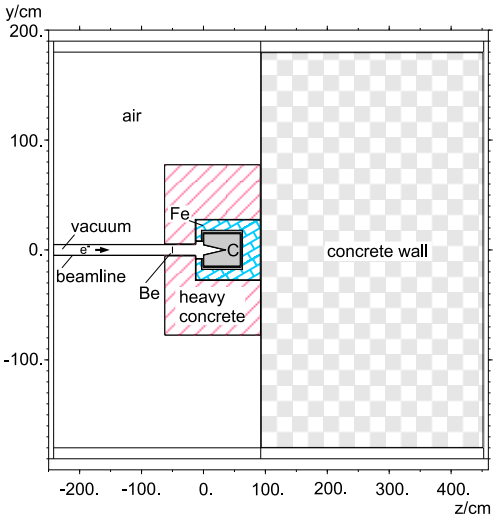

Fig.1 : *The placement of a graphite beam dump surrounded by iron and concrete shielding in front of a 3.6 m thick concrete wall.*

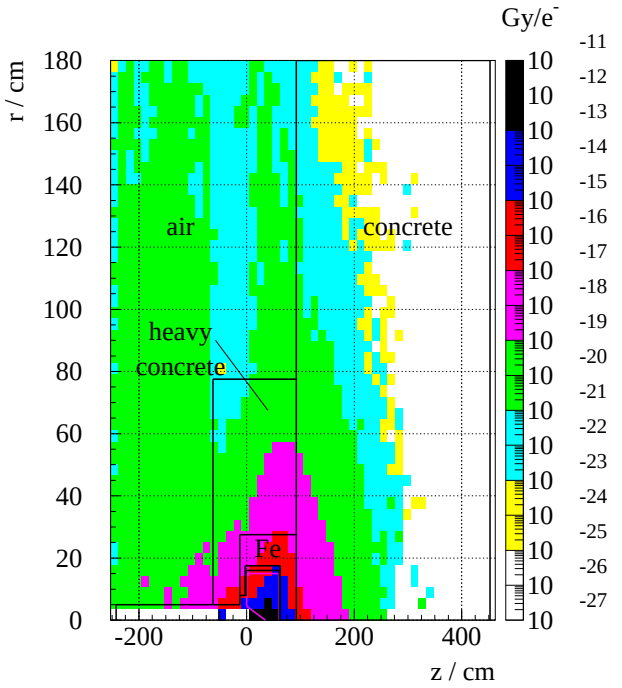

Fig.2 : *The dose distribution for a cylindrical geometry at an electron beam with 50 MeV energy.*

Assuming that the maximum dose is obtained along the beamline, the dose distribution into the inner radial section has been extracted from the dose distribution of Fig. 2. The dose distribution along the beamline inside the concrete wall (Fig. 3) has been calculated up to a depth of about 1 m with good statistics and the tenth-value layer thickness of the concrete has been obtained to 34.9 cm. This value is in a good agreement with data given in [2]. After passing the concrete wall the absorbed dose has been estimated approximately to $1.6 \cdot 10^{-27}$ Gy/e$^-$ and the dose rate to 0.04 μGy/h, which is two orders of magnitude lesser than the maximum value of dose rate for controlled areas $\dot{D}_{max} = 5\,\mu$Gy/h.

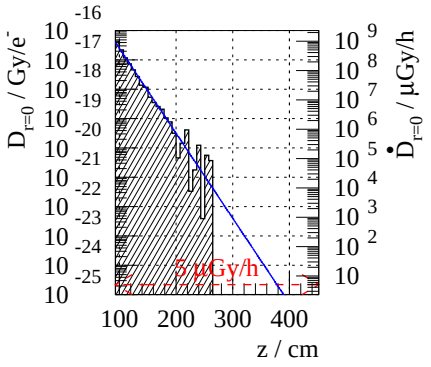

Fig.3 : *Dose and dose rate distributions along the beamline axis z inside the concrete wall.*

[1] *Institut für Kern- und Teilchenphysik, TU Dresden*

References

[1] A. Fasso et al., Proc. of the III Spec. Meeting on Shielding Aspects, Sendai (1997)61-74.
[2] Report NCRP-51, Radiation protection design guidelines, Washington (1977).

Calculations of the Power Dissipation and the Temperature Distribution in Beam Dumps at ELBE

B. Naumann[1], M. Werner[2]

The beam dumps for ELBE must be capable of absorbing an average beam power of 50 kW at an electron beam energy of 50 MeV. After passing a 500 μm thick beryllium foil the incident electron beam enters a purified graphite absorber ($\varrho = 1.7\,\mathrm{g/cm^3}$). The power dissipation for a first design of the beam dump was calculated using the particle transport code GEANT [1,2]. Further calculations have been performed with the transport code FLUKA [3], which makes possible to consider nuclear reactions like the (γ,n) process. Two geometrical shapes of the graphite core (V1, V2) have been compared with respect to the power dissipation and the temperature distribution. Version V1 corresponds to the first layout [1] with a radius of 15 cm and a cone-shaped hole of 35 cm depth. The power dissipation for V1 is shown in Fig. 1. After reducing of the radius to 10 cm, the implementation of a second cone-shaped hole at the entrance (10 cm deep) and the elongation of the first cone-shaped hole up to 45 cm, the power dissipation in this version V2 is more homogeneously distributed as shown in Fig. 2.

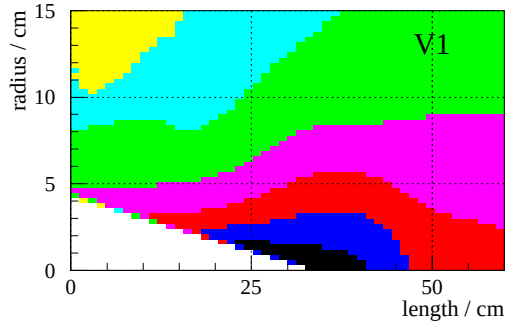

Fig. 1: *Power released in graphite core V1.*

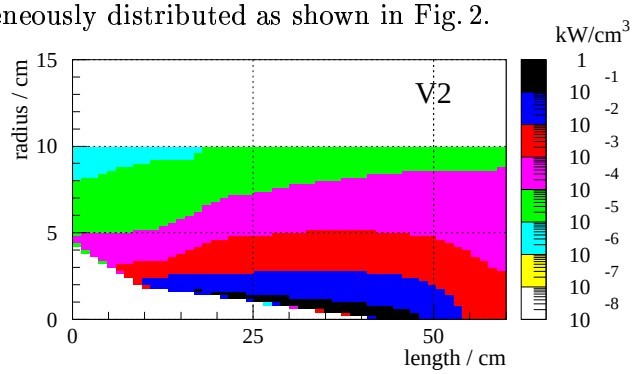

Fig. 2: *Power released in graphite core V2.*

On the base of the power dissipations the thermal loads were calculated for the two graphite cores using the Finite-Element-Code ANSYS [4]. The model comprises the heat transfer in the graphite and the radiation effect according to the Stefan Boltzman equation between the surface and the water cooling which surrounds the graphite core. The resulting temperature curves along the outer lines of the halfmodel for the two graphite cores are shown in Fig. 3. The maximum surface temperature at the centerline in V1 amounts to 2834 K and is near to the graphite sublimation temperature of 3300 K at a pressure of 5 mbar [1]. The improved geometry in V2 results in a smaller maximum surface temperature of 2256 K.

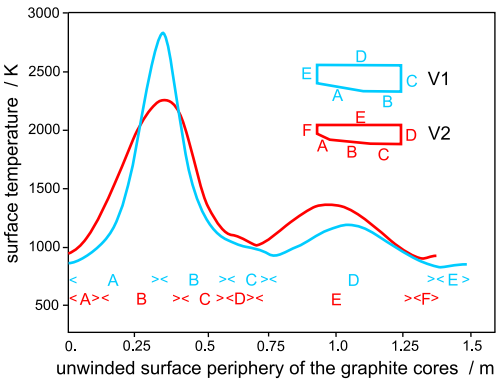

Fig. 3: *Profiles of the surface temperatures for two graphite core versions at an electron beam energy of 50 MeV.*

[1] *Institut für Kern- und Teilchenphysik, TU Dresden*
[2] *Institut für Sicherheitsforschung, FZ Rossendorf*

References

[1] B. Naumann et al., Strahlfänger für maximale Energien an ELBE, FZR Report FZR-267 (1999); Annual Report 1998/1999, FZR-271 (1999) 36.
[2] GEANT-Detector Description and Simulation Tool, CERN Program Library W5013 (1994).
[3] A. Fasso et al., Proc. of the III Spec. Meeting on Shielding Aspects, Sendai (1997) 61-74.
[4] ANSYS User's Manual for Rev. 5.6., Swansons Analysis Systems, Inc. (1999).

Field Measurements on the ELBE Undulator U27

P.Gippner, E. Grosse, W. Seidel, J. Pflüger[1], A. Schamlott, U. Wolf

In order to produce at ELBE an intense FEL radiation in the infrared region we shall install the undulator U27 which consists of two sections with a length of $0.98\,m$ each and a short region in between with three adjustable magnetic dipoles. Each section consists of $N_u = 34$ magnetic periods with a length of $\lambda_u = 27.3\,\mathrm{mm}$. The magnetic structures for both units were test modules for the TTF-Facility at DESY, Hamburg [1,2] and the carriages have been constructed and delivered by DANFYSIK. The fig. 1 shows the carriages before the magnets have been mounted. For optimization of the phase-matching of the two sections the distance between them is adjustable over a wide range by using a stepping motor.
The carriages are designed such that the gap of both sections can be varied independently. For special applications they can also be tapered individually, what should result in an increase of the extraction efficiency [3,4]. The undulator field was measured and tuned at HASYLAB (DESY) by means of the Hall probe shown in fig. 2.

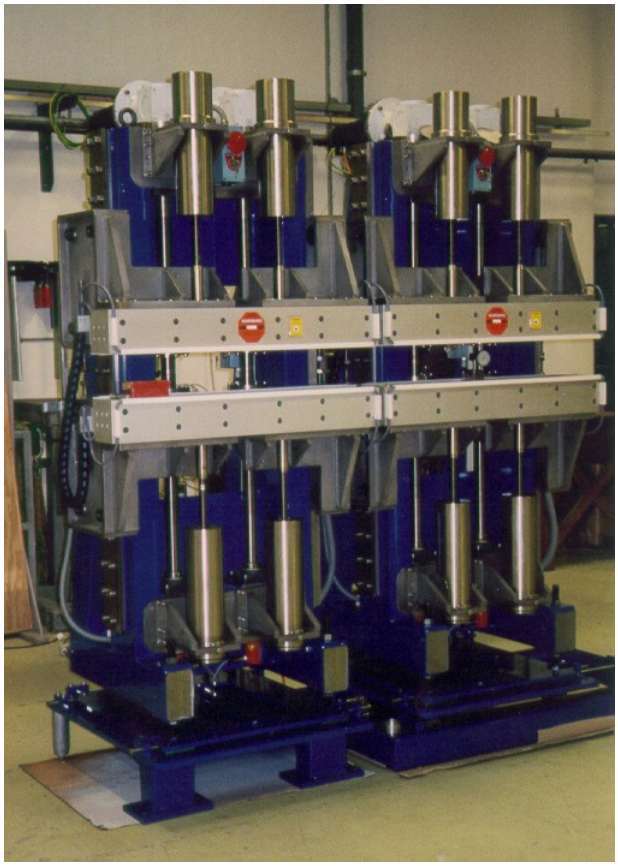

Fig. 1 *The undulator carriages with girders before mounting the magnetic structures.*

The probe is mounted on a goniometer with six degrees of freedom for right adjustment within the magnetic structures. The poles were tuned with the aim to get a minimum electron displacement at the exit sides of the modules as well as a peak field roughness lower than 0.4 %. As a result of the measurements the fig. 3 shows the field component $B_y(0,0,z)$ in the middle plane of both undulator units for a gap of $g = 12\,\mathrm{mm}$ and a distance $d = 250\,\mathrm{mm}$ between the sections (a) and the first integral over the measured field (b). The trajectory of a reference electron with an energy of $E = 20\,\mathrm{MeV}$ in the wiggle plane is shown in part (c). Fig. 4 shows the magnetic field distribution $B_y(x,0,z_5)$ perpendicular to the electron beam at different gaps , where z_5 is the center of the 5th pole.
In order to make the gap variation more convenient we tried to design a "passive" undulator. Thereby the elongation of the electrons for a given energy should be nearly independent of the gap width, whereas the displacement Δ and the slope of the trajectory at the exit should be as small as possible. Corresponding calculations have been done with the code RADIA [5] and have already been reported [6]. However the fringe field turns out to be not absolutely passive against gap widening but causes a weak dependence of Δ on the gap. This can be corrected by coils mounted at the entrance sides of both sections and allowing to inject the electrons under a small angle relatively to the z-axis. Only weak magnetic fields of about $2\,\mathrm{mT}$ are necessary to keep the electrons within the optical mode.
Presently the influence of shimming on the fringe field is under investigation.

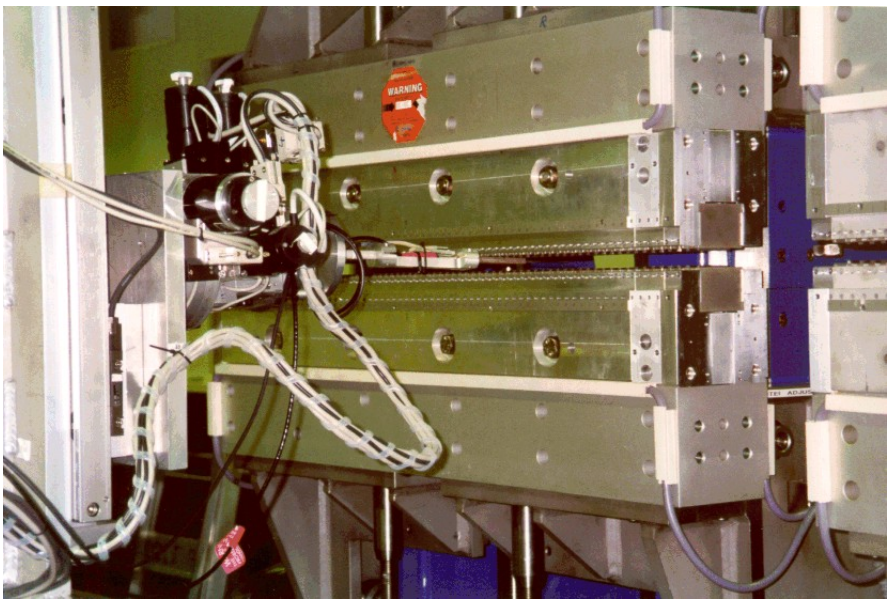

Fig. 2 *The Hall probe mounted on a goniometer for field measurements on the axis of one of the undulator sections.*

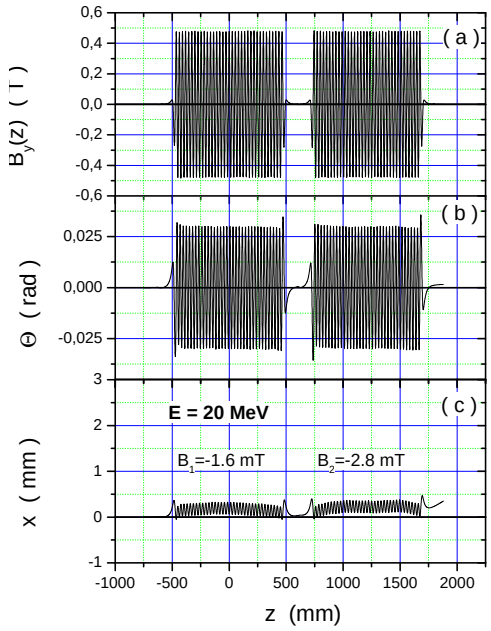

Fig. 3 *The field distribution $B_y(z)$ in the middle plane of the two undulator systems along the axis z for a gap width of $g = 12$ mm (see text).*

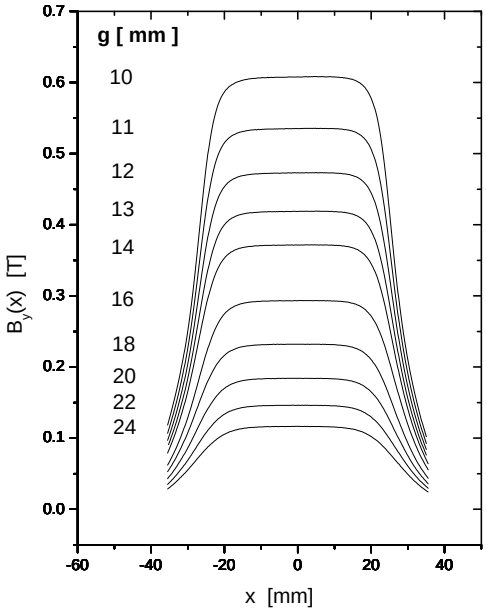

Fig. 4 *Magnetic field $B_y(x, 0, z_5)$ perpendicular to the electron beam at different gaps, where z_5 is the position of the 5th pole.*

[1] *HASYLAB at Deutsches Elektronen Synchrotron DESY, Hamburg*

References

[1] B. Faatz, J. Pflüger and Y.M. Nikitina, Nucl. Instr. Meth. A 375 (1996) 618
[2] Y.M. Nikitina and J. Pflüger, DESY Report TESLA-FEL 96-03
[3] E.L. Saldin, E.A. Schneidmiller and M.V. Yurkov, Phys. Lett. A 185 (1994) 469
[4] D. Jaroszynski et al., Phys. Rev. Lett. 72, 2387 (1994)
[5] P. Elleaume, O. Chubar and J. Chavanne, J. Synchr. Rad. 5 (1998) 481
[6] P. Gippner, W. Seidel and A. Schamlott, Annual Report 1998, FZR-271, p.16

Phase Matching of the Two Sections of the U27 Undulator

P. Gippner, J. Pflüger[1]

The U27 undulator consists of two 0.98 m long separate sub-systems which have individual mechanical drives for gap adjustment. Thus for variable gaps the radiation wavelength is changed and consequently the phasing between the two undulator systems has to be changed as well. This has to be done by properly choosing the electron flight path d between the two sections.
The optical phase in an undulator has been analyzed in detail by Walker[1]. It can be expressed by

$$\Psi(z) = \frac{2\pi}{\lambda_R}\left[\frac{z}{2\gamma^2} + \frac{\int^z dz'\Theta(z')^2}{2}\right]. \qquad (1)$$

Here z is the coordinate along the beam axis, λ_R is the radiation wavelength, γ is the electron kinetic energy in units of its rest mass and Θ is the electrons deflection angle. The terms in the bracket have the following descriptive meaning: the first gives the contribution to the phase, if the electron travels just a distance z in free space, the second term represents the additional contribution due to the magnetic field. The function $\Theta(z)$ can be derived from $B_y(z)$ by

$$\Theta(z) = \frac{e}{\beta\gamma m_0 c}\int^z dz' B_y(z'). \qquad (2)$$

Using the eqs. (1) and (2) the phasing of the two undulator sub-systems can be determined experimentally by measuring $B_y(z)$ along the axis of the entire undulator.
The phase on the poles in the second section varies with the distance d, which depends on the K-value and has to be chosen appropriately. Moreover, phase matching is obtained periodically after an increase of d by $\Delta d = \lambda_u(1 + \frac{1}{2}K^2)$. The deviation of the optical phase angle from its nominal value obtained for a perfect undulator is denoted by $\Delta\Psi(z)$. For a gap $g = 17\,mm$ measurements for $\Delta\Psi(z)$ are shown in fig. 1. The K-value for this case was 0.6688. The nominal phase deviation on the poles is nearly zero, only at the end poles before and after the interspace the phases deviate from zero. The proper choice of the distances d as functions of the K-value as determined experimentally is shown in fig. 2. Six different curves have been measured. They are shifted horizontally by $\Delta d = \lambda_u(1 + \frac{1}{2}K^2(g))$. These curves have to be used to choose phasing distances d_{ph} in dependence on the gap g.

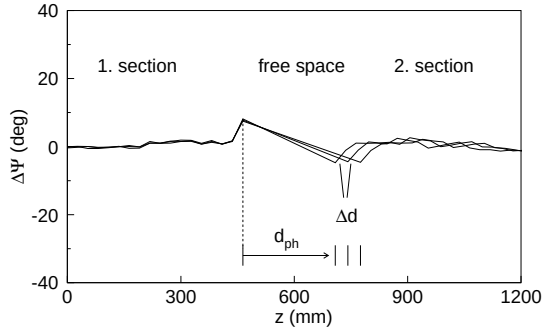

Fig. 1 *Phase differences $\Delta\Psi(z)$ for a gap g = 17 mm. The K-value is 0.6688. Three phasing distances d_{ph} are shown.*

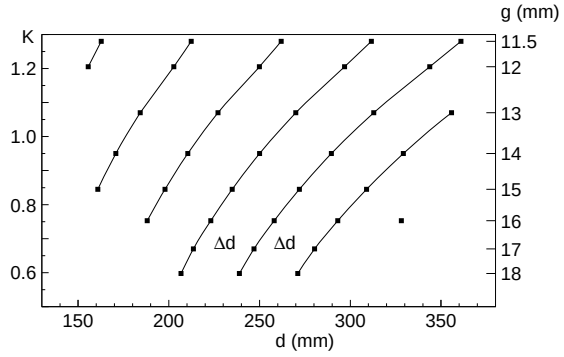

Fig. 2 *Phasing distances d_{ph} (points) between the two sections of U27. The right axis shows the gap widths g, for which the values d_{ph} have been found, the left axis shows the corresponding K-values in a linear scale.*

[1] *HASYLAB at Deutsches Elektronen Synchrotron DESY, Hamburg*

References

[1] R. P. Walker, Nucl. Instr. Meth. A 335 (1993) 328
[2] B. Faatz, J. Pflüger, P. Pierini, Nucl. Instr. Meth. A 375 (1996) 441-444

Tapering of the ELBE-Undulator U27

P.Gippner, E. Grosse, A. Schamlott, U. Wolf

If the FEL works with maximum power the energy factor γ of the electrons decreases by $\Delta\gamma = \gamma/2N_u$ (for the first harmonic) along the electron path due to the interaction of the electron beam with the electromagnetic field, where $N_u = 68$ is the total number of magnetic periods in the two undulator units [1]. The electron energy changes continuously from the undulator entrance to the exit leading to a resonance wavelength $\lambda(z)$ which depends on the coordinate z along the undulator

$$\lambda(z) = \frac{\lambda_u}{2\gamma^2(z)}(1 + \frac{1}{2}K^2). \tag{1}$$

Within a certain interval of λ this effect can be compensated by differentially increasing the gap, and hence decreasing the magnetic field along the undulator. To compensate the energy loss dγ by a reduction dB of the magnetic field one has to ensure

$$d\lambda = \frac{\partial\lambda}{\partial\gamma}d\gamma + \frac{\partial\lambda}{\partial K}dK = 0 \tag{2}$$

from which follows

$$\frac{dB}{B} = \frac{2 + K^2}{K^2}\frac{d\gamma}{\gamma}. \tag{3}$$

For hybrid undulators, the Halbach equation allows one to estimate the widening of the gap g needed for the variation dB of the field corresponding to equation (3). Figure 1 shows the effect of field tapering in both sections of the undulator U27, which would be used in a situation typical for high intensity lasing.

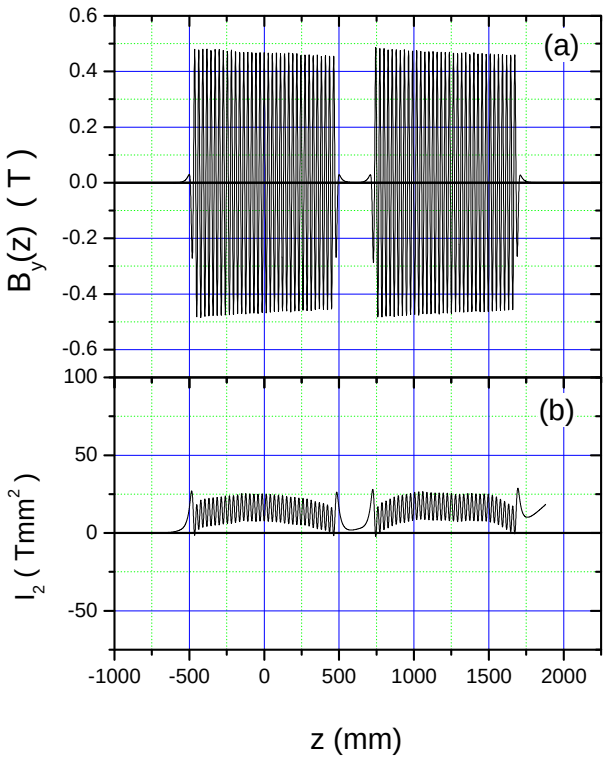

Fig. 1
(a) Measured field distribution $B_y(z)$ in the middle plane for a gap width $g = 12\,mm$ and a tapering of $0.3\,mm$ on the exits of both undulator sections.
(b) Second field integral I_2 of the undulator U27 as a function of the coordinate z. Within the scale used an influence of the tapering on the form of $I_2(z)$ is not noticeable. For conversion of I_2 in μm the formula $x[\mu m] = 300 \cdot I_2[T\,mm^2]/E[MeV]$ must be applied.

References

[1] P. Gippner, E. Grosse, W. Seidel, J. Pflüger, this Report

Application of the Pulsed Wire Technique to the Undulator U50

P. Gippner, U. Wolf, A. Schamlott, B. Rimarzig

In 2000 the ENEA undulator U50 was moved from Frascati to Dresden, but up to now we had no the possibility to control the magnetic structure of this equipment for damages originating by shocks during the transport. Corresponding measurements are normally made point by point using a Hall probe. Thereby great care must be taken for a precise mechanics and for the minimization of nonlinearities and calibration errors of the probe. Such measuring technique is not available at our institute. To find new irregularities of the magnetic field $B_y(z)$ arising from the transport we used the pulsed wire method [1, 2], which seems to be a much simpler technique than the Hall probe is. Parts of the equipment for this method and the software for data acquisition were delivered by ACCEL[1].

The pulsed wire method enables an in situ measurement of the first and second field integrals $I_1(z)$ and $I_2(z)$ of the magnetic structure depending on the current pulse form [1,2]. To measure these functions we used a CuBe wire with a diameter of $d = 50\,\mu$m and length of $L = 7500$ mm. The tension was produced by a mass of $m = 85$ g, resulting in a tensile force of $P = 0.83$ N and a tension of $T = 4.24 \cdot 10^4$ N/cm^2. In a first attempt an additional calibration magnet outside the undulator was not applied. The table 1 contains the electric parameters of the measurements.

Table 1

	I_1	I_2
current pulse length	12 μs	20 ms
current pulse high	900 V	40 V
frequency	0.5 Hz	0.1 Hz

The measured integrals $I_1(z)$ and $I_2(z)$ in arbitrary units for a gap width of $g = 25$ mm are shown in fig. 1. The field component $B_y(z)$ is the derivative of $I_1(z)$ and was calculated by the data acquisition program.

The fig. 2 allows a comparison with the results obtained at ENEA with the Hall probe technique before the transport to the FZR was carried out. In general one can conclude that no additional field errors arised.

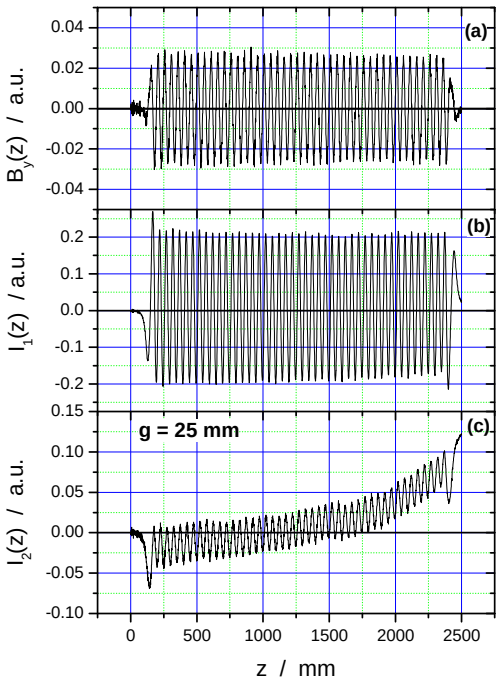

Fig. 1 *First field integral $I_1(z)$ (part b) and second field integral $I_2(z)$ (part c) measured with the pulsed wire method. The derivative $B_y(z)$ was not measured.*

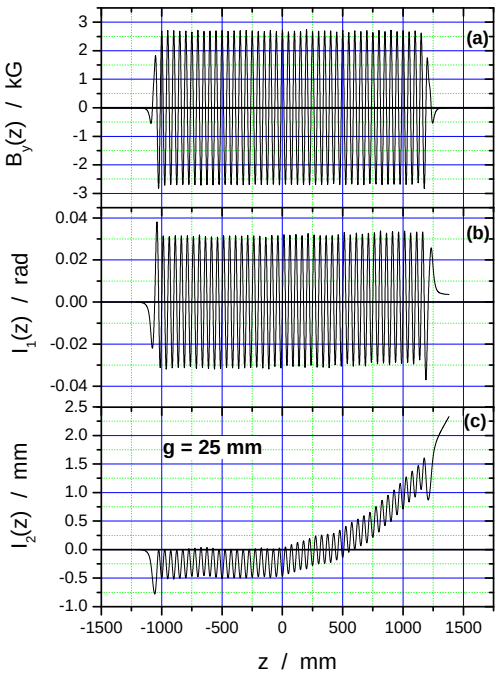

Fig. 2 *The field component $B_y(z)$ in the middle plane (a) measured with the Hall probe technique. The functions $I_1(z)$ and $I_2(z)$ are obtained by integration of $B_y(z)$.*

Finally, fig. 3 shows the second field integrals without and with an application of a homogeneous external field of $B = 3.3\,\mathrm{G}$ to correct the behaviour of this function. A bending effect can clearly be seen, which will help to guide the electron trajectories through the waist within the optical resonator. More quantitative investigations will be done in near future.

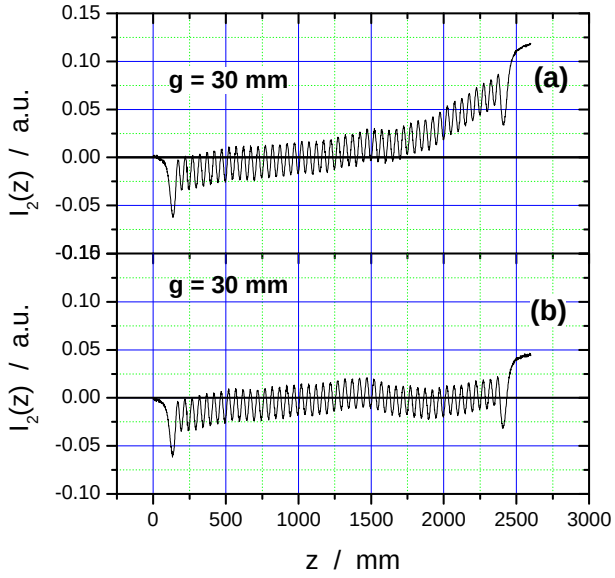

Fig. 3 *The integral $I_2(z)$ obtained by the pulsed wire method at a gap of $g = 30\,mm$ without (a) and with an additional homogeneous field (b) of $B = 3.3\,G$ in the exit part of the undulator.*

[1)] *ACCEL Instruments GmbH, Bergisch-Gladbach*

References

[1] R.W. Warren, Nucl. Instr. Meth. A 272 (1988) 257

[2] A. Geisler, M. Ridder and Th. Schmidt, Delta-Rep. 94-8,
University of Dortmund, Dept. of Accelerator Physics, unpublished

Magnet Field Errors of the ELBE Undulators and their Effect on the Laser Gain

P. Gippner, R. Wünsch

Two undulators (U27 and U50) are intended to be installed at the beam of ELBE to produce intense coherent radiation in the mid and far infrared range. To estimate the quality of the undulator we have measured the field strength B along the undulator axis z. In particular we consider the standard deviations σ_B and σ_Ψ of the magnetic field amplitude B and of the optical phase Ψ from their values in case of an ideal magnet. In an undulator with period length λ_U and rms parameter $K_{\rm rms}$, the optical phase is given by [1]

$$\Psi(t) \equiv k\,[ct - z(t)] = k\left[\frac{z}{2\gamma^2} + \frac{\int^z x'^2\,dz'}{2}\right] \qquad \left(k = \frac{2\pi}{\lambda}\right), \tag{4}$$

where $z(t)$ is the electron coordinate along the undulator axis and $x' \equiv dx/dz = e/(\gamma mc)\int^z dz'\,B_y(z')$ is the angle the electron makes with the z-axis in the transverse magnetic field B_y (m, $-e$ and γ denote mass, charge and energy of the electron; λ is the resonance wavelength $\lambda = (1 + K_{\rm rms}^2)\,\lambda_U/2\gamma^2$). In an ideal planar undulator, the phase (1) oscillates uniformly with half the undulator period around a constant value if the resonance condition is fulfilled. For a realistic undulator, strength and period of the field scatter around the values in case of ideal field.

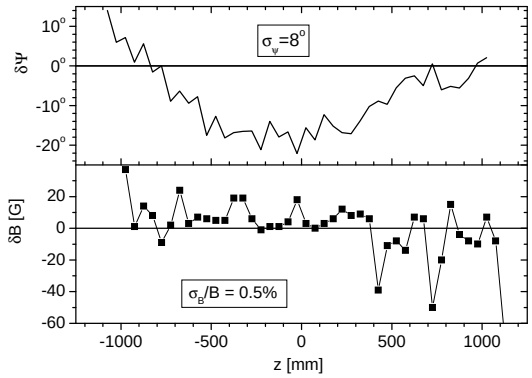

Fig. 1 *Deviations $\delta\Psi, \delta B$ of phase (1) and field amplitudes from their values in case of perfectly sinusoidal magnetic field as measured for the U50 undulator at the gap g=20 mm. $\sigma_{\Psi,B}$ denotes the variance of the corresponding quantity.*

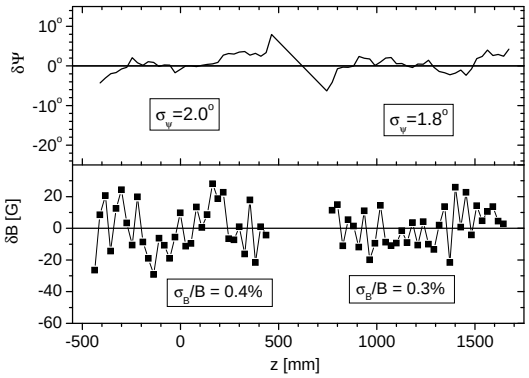

Fig. 2 *The same as in Fig. 1 for the two units of the U27 undulator at the gap g=14 mm. Similar results have been obtained for other gaps.*

Apart from the drift length between the two undulator units, where the electron does not interact with the field, the phase deviation for U27 (Fig. 2) is significantly smaller than for U50 (Fig. 1). That is the result of the meticulous tuning procedure applied to the U27 undulator.

The effect of the field errors on the lasing process has to be related to the electron energy spread σ_E. Both the deviations from their average values cause a line broadening σ_λ in the spontaneous emission spectrum which is also relevant for the degradation of the laser gain

$$\frac{\sigma_\lambda}{\lambda} = 2\frac{\sigma_E}{E} + \frac{2K_{\rm rms}^2}{1+K_{\rm rms}^2}\frac{\sigma_B}{B}. \tag{5}$$

For the ELBE beam ($\sigma_E \approx 90\,$keV) the first term in eq. (2) amounts to roughly 0.5% at E=40 MeV so that $\sigma_B/B \approx 0.5\%$ is only just small enough not further to reduce the laser gain considerably. On the other hand, the investigations of Bobbs et al. [2] have shown that a phase deviation smaller than 10^o does not significantly affect the laser gain.

References

[1] B. Faatz, J. Pflüger and P. Pierini, Nucl. Instr. Meth. A 375 (1996) 441-444

[2] B. L. Bobbs et al., Nucl. Instr. Meth. A 296 (1990) 574-578

The Magnetic Field Profile in the Wiggle Plane of the ELBE Undulators

C. A. J. van der Geer[1], P. Gippner, R. Wünsch

In an ideal undulator the magnetic field is assumed to be independent of the position in the wiggle plane (x-coordinate). In a real undulator consisting of finite magnets the field strength has a plateau in the center of the magnets ($x = 0$) and diminishes when moving toward their ends. The drop in the field strength defocuses the electron beam, i. e. electrons moving off the undulator axis and/or with a finite angle to it are deflected such that the beam size increases.

To study this effect we have measured and calculated the field profile in the wiggle plane of our undulators. We noticed a significant difference between the hybrid configuration (U27) and the Halbach construction (U50) even though their magnet blocks have the same width ($w = 50\,\mathrm{mm}$). Fig. 1 shows the measured field profiles for either configuration for a variety of undulator gaps. Generally, the hybrid magnetic configuration has a much more pronounced plateau than the Halbach construction has. At gaps below 10 mm, the first even has a small dip at $x = 0$, which is too small ($< 1\%$) to be visible on the scale of fig. 1

To investigate the effect on the electron beam we have calculated the average beam radius σ_x for either field configuration at the undulator exit for different gaps when starting with the same parallel beam of radius (0.4 mm) at the entrance. Fig. 2 clearly illustrates the pronounced defocusing effect in the Halbach undulator around a gap of 10 mm, in particular at lower energies. We also see the slight focusing action of the hybrid-type undulator at very small gaps. Note however that for a realistic simulation the beam divergence and the space charge have to be taken into account.

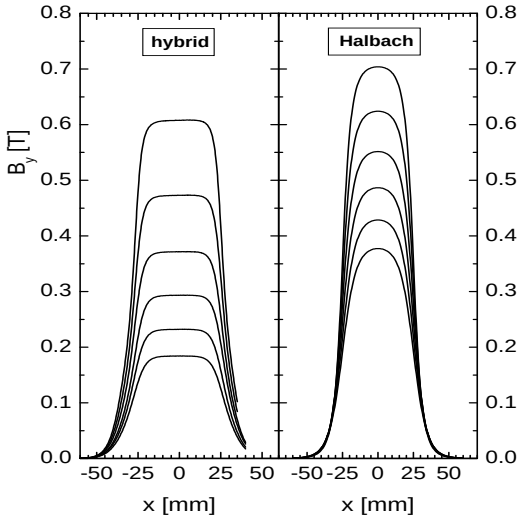

Fig. 1 *Measured transverse magnetic field profile of a hybrid undulator (left panel) in comparison to a Halbach construction (right panel) for the gaps g = 10, 12, 14, 16, 18 and 20 mm (from top to bottom). For the Halbach construction, only g = 16 and 20 mm have been measured. The other profiles have been calculated using the code RADIA [1] with parameters fitted to the measured profiles.*

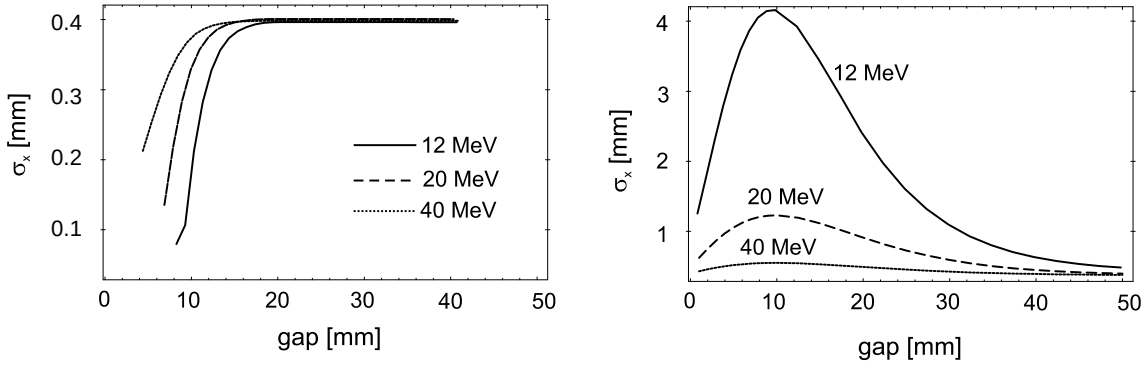

Fig. 2 *Beam radius (rms) σ_x in the wiggle plane after passing the undulator in either configuration as a function of the undulator gap for three different beam energies (indicated). Left panel: hybrid undulator (U27); right panel: Halbach construction (U50). $\sigma_x = 0.4\,\mathrm{mm}$ at the entrance. Code GPT [2].*

[1] *FOM Institute for Plasma Physics Rijnhuizen, The Netherlands*

References

[1] P. Elleaume, O. Chubar and J. Chavanne, J. Syn. Rad. 5 (1998) 481-484

[2] Pulsar Physics, General Particle Tracer, http://www/pulsar.nl

Considerations on Cavity Loss Measurements for a Partial Waveguide Resonator FEL

M. Tecimer[1], E. Grosse, W. Seidel

A symmetric waveguide resonator configuration incorporating toroidal mirrors and a waveguide structure extending along the undulator section has been proposed for the 30 μm-150 μm far infrared FEL [1].

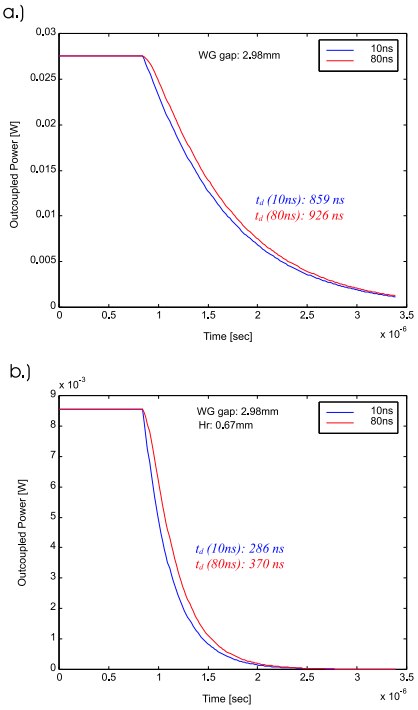

Fig. 1 *Simulated dependence of the outcoupled-power decay time on the pump-laser switching-off duration. In Fig.1b, additional losses due to a 1.35 mm diameter outcoupling hole has been taken into account leading to a shorter decay time.*

The use of toroidal resonator mirrors with optimized radius of curvatures helps to reduce cavity losses arising from the transition of the free space propagating mode into a wave guided one. The experimental study of the loss mechanism will be accomplished by means of a test resonator that is scaled down to the dimensions of an optical bench, according to the wavelength (10.6 μm) of the employed cw CO_2 seed-Laser. Measurements of the cavity ring down (CRD) time will determine the Q-Factor of the cavity and the associated resonator losses.

To be able to apply the CRD method, it is important to have the switching-off time of the pump laser being considerably shorter than the intracavity power decaying due to the loss mechanism (Fig. 1). In the planned experiments, after reaching steady-state, the power in the optical cavity will be switched-off within 80 ns using a acusto-optical modulator (AOM). The time dependence of the light intensity inside the cavity is then monitored by detection of the outcoupled light through the resonator mirror (Fig. 2) using a liquid-nitrogen cooled HgCdTe detector (MCT). A lens configuration located in front of the coupling mirror provides the necessary matching of the injected laser-mode profile into the lowest order hybrid mode excited in a parallel-plate waveguide.

In order to obtain an estimate for the losses and the associated cavity power decay time, a code has been developed based on the scalar diffraction theory [2]. It models the loss mechanism accounting for effects such as field outcoupling through the hole, mode conversion due to the hole and waveguide aperture, clipping-off the optical field at waveguide ends, transverse mode-matching of the injected laser-mode into hybrid modes, cross-coupling among the excited modes as well as temporal profile of the pump-laser decaying .

[1] *Tel Aviv University, Physical Electronics*

References

[1] M. Tecimer and R. Wünsch, this Report

[2] A. E. Siegman, Lasers, University Science Books, Sausalita CA, 1986

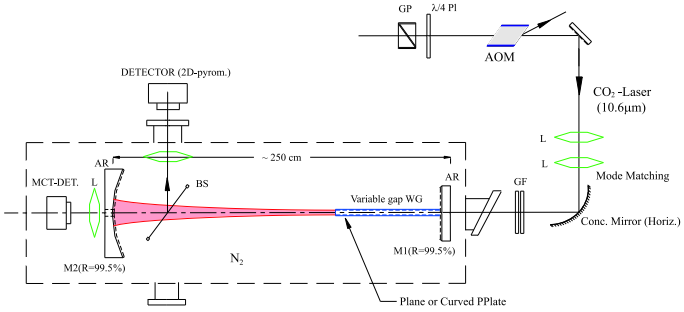

Fig. 2 *Schematic of the cavity ring down measurement setup.*

Losses in a Partial Waveguide Resonator of a FEL

M. Tecimer[1], R. Wünsch

The undulator U50 [1], which is a long-term loan from the ENEA Institute in Frascati, should at ELBE provide far infrared radiation up to roughly 150 μm. Already at 30 μm the transverse extension of the Gaussian mode in an open resonator is larger than allowed by the vacuum chamber located inside the undulator, leading to significant losses of optical power. To minimize these losses we propose a partially waveguided resonator 10 mm high that is guiding the wave along the undulator (240 cm) in the vertical dimension while the chamber is wide enough (40 mm) to allow the propagation of a Gaussian beam in horizontal direction. The currents induced by such a hybrid mode in the waveguide walls are small and the resulting ohmic losses are negligible [2]. Outside the undulator the vacuum chamber is large enough to ensure free propagation in either direction.

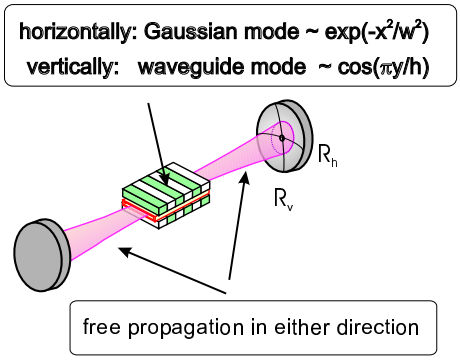

Fig. 1 *Optical beam in a resonator FEL with a waveguide mode inside the undulator and a Gaussian mode outside of it. The resonator mirrors have different radii of curvature R_h and R_v in the horizontal and vertical plane, respectively.*

Since the horizontal propagation of the optical beam is not affected by the waveguide, the horizontal radius of curvature R_h of the resonator mirrors is determined by the the gaussian optics. We choose a radius corresponding to a Rayleigh range z_R=1 m with a waist located at the center of the undulator.

The radius R_v in vertical direction determines the coupling of the waveguide mode inside the undulator with a free space mode outside of it. A detailed numerical analysis of mode coupling losses has been carried out using the code GLAD [3] and applying the diffraction theory based on the Huygens-Fresnel principle [4]. The results of computation (Fig. 2) show that at wavelengths larger than 30 μm the losses can be minimized by a mirror with a fixed radius of curvature R_v which corresponds to the distance D between mirror and waveguide exit. Below 30 μm the Fresnel number becomes so large that the appropriate radius of curvature depends strongly on the wavelength.

The simulated resonator characteristics will be investigated experimentally on a scaled down test resonator structure, excited by the radiation of a CO_2 laser at 10.6 μm. The Q-Factor of the cavity and the associated resonator losses will be then defined by means of a cavity ring down experiment.

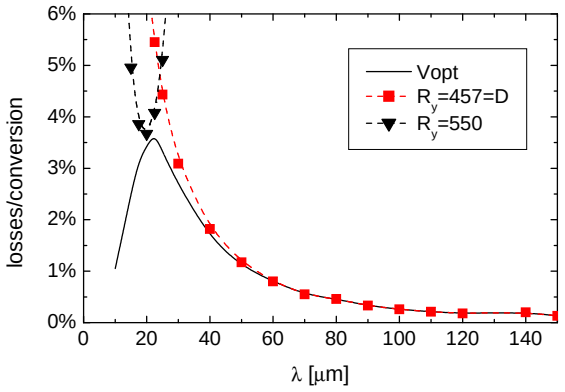

Fig. 2 *Losses of a single mode conversion in dependence on the wavelength λ of the radiation for two different radii of curvature R_v of the mirror. The full line shows the minimum losses which can be obtained with any mirror of constant curvature.*

[1] *Tel Aviv University, Physical Electronics*

References

[1] F. Ciocci et al., Nucl. Instr. Meth. A 250 (1986) 134-137
[2] L. Elias and J. Gallardo, Appl. Phys. B 31 (1983)
[3] G. Lawrence, GLAD, Applied Optics Research, Austin TX, USA
[4] A. E. Siegman, Lasers, University Science Books, Sausalito CA, 1986

Design of the Optical Cavity for a Far Infrared FEL with the ENEA Undulator for a Wavelength of 30 - 150 μm

B. Wustmann, A. Wolf

Design and construction of the optical Cavity of a far infrared FEL for the handling of long wavelengths is a great challenge. Tab. 1 shows the optical cavity and mirror parameters derived from the numerical simulations performed in [1] and [2] for the propagation of the optical mode in the 11,5 m long optical cavity using a partial waveguide within the undulator. These parameters were determined by the following boundary conditions:

Table 1

Resonator length	11530.5 mm
Position shift of a mirror	2 mm
Stability of the mirror distance	1 μm
Distance resolution	< 0.5 μm
Increment	< 0.5 μm
Direction change hysteresis	< 0.5 μm
Angle error of the cavity mirror	< 5 μrad
Error of the mirror surface	2 μm
Horizontal mirror diameter	145 mm
Vertical mirror diameter	270 mm
Mirror thickness	25 mm
Horizontal radius of curvature	5995 mm $\pm$ 0.25%
Vertical radius of curvature	4585 mm $\pm$ 0.25%
Diameter of the outcoupling hole	6 mm
Waveguide heigth	10 mm $\pm$ 0.1 mm
Waveguide width	40 mm
Waveguide length	2360 mm
Waveguide surface roughness	1...2 μm

The partial waveguide within the undulator guides the optical mode in the vertical direction through the narrow 20 mm magnetic gap in form of a fundamental waveguide mode with cosine distribution. The optical mode in horizontal direction has a Gauss-shaped freely spreading mode form both within and outside of the waveguide.
Due to this hybrid structure and the different divergence of the optical mode in horizontal and vertical direction outside the waveguides so-called bifocal concave toric mirrors with an elliptical cross section have to be used.
As the outlet of the optical gap in the waveguide amounts to 10 mm, the strong beam divergence in vertical direction results in a necessary mirror diameter of 270 mm for a wavelength $\lambda = 150\mu$m.
The mirror chambers have a diameter of about 300 mm. In fig. 1 and 2 they are shown with the necessary assembly nipples for the diagnostic and servo units.
The outcoupling of the laser radiation is made by means of a centric 6mm hole in one of the cavity mirrors. Additionally a horizontal insertable scraper mirror [3] should be able to outcouple a variable part of the laser.
For the alignment of the magnetic axis of the undulator, the electron beam axis and the axis of the optical cavity three insertable Berillium viewscreens with a centric hole of 1 mm are used within the waveguide (fig. 3).
The production technology for the waveguide is being verified by practical attempts. The detail construction of the mirror chambers has started and the draft design and version comparison of the optical cavity have been finished.
The dimensions of the scraper mirror and its vibration-free mounting are open problems.

References

[1] R. Wünsch, FZR-276 (1999)
[2] M. Tecimer and R. Wünsch, Losses in a Partial Waveguide Resonator of a FEL, this Report
[3] R. Nagai et al., An Optical Resonator with Insertable Scraper Output Coupler for the JAERI Far Infrared Free Electron Laser, 22th Free Electron Laser Conference, Durham, North Carolina, August 13-18, 2000

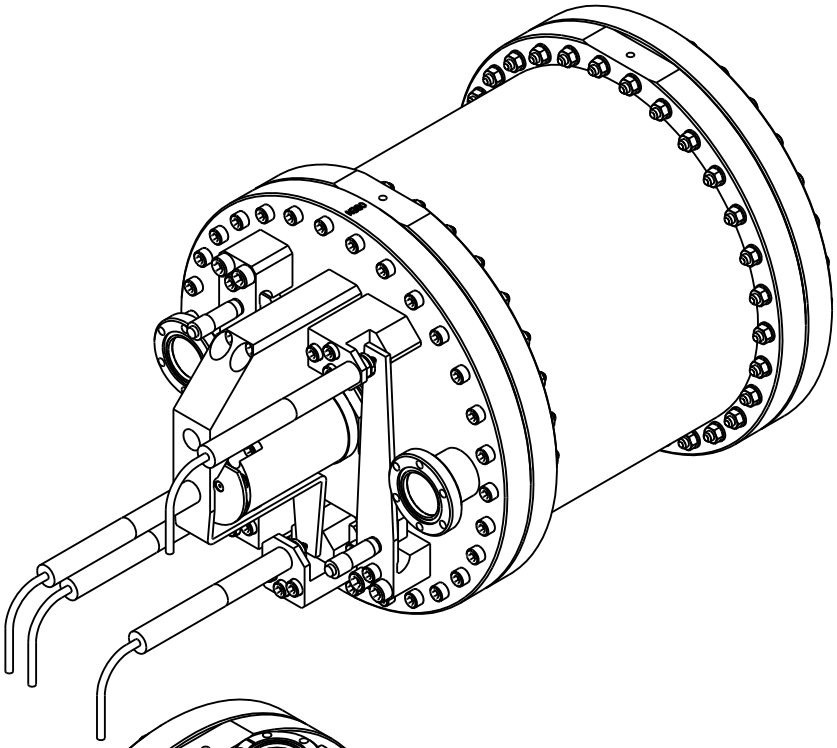

Fig. 1 *Mirror Chamber 1*

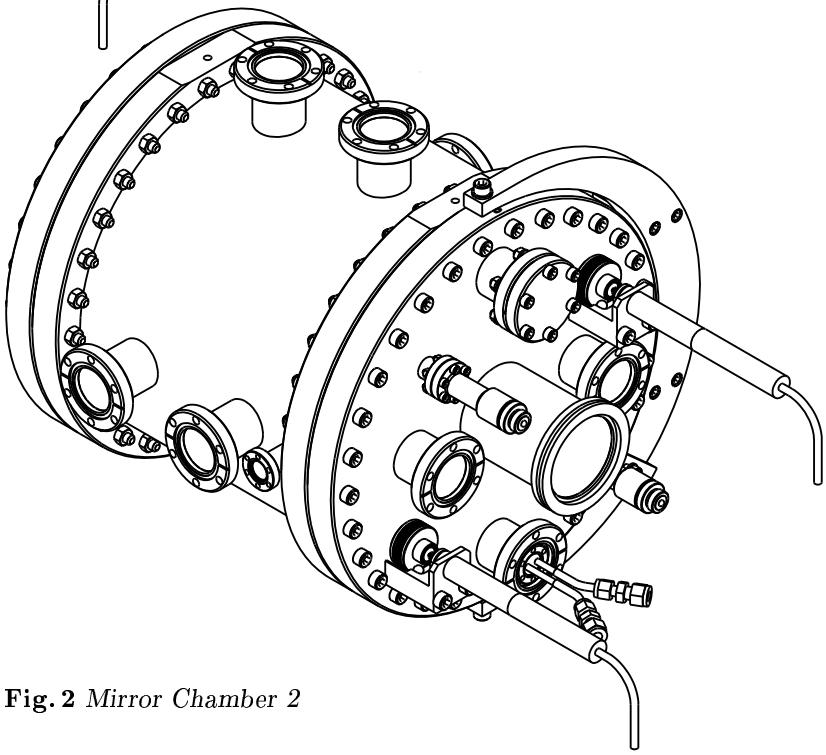

Fig. 2 *Mirror Chamber 2*

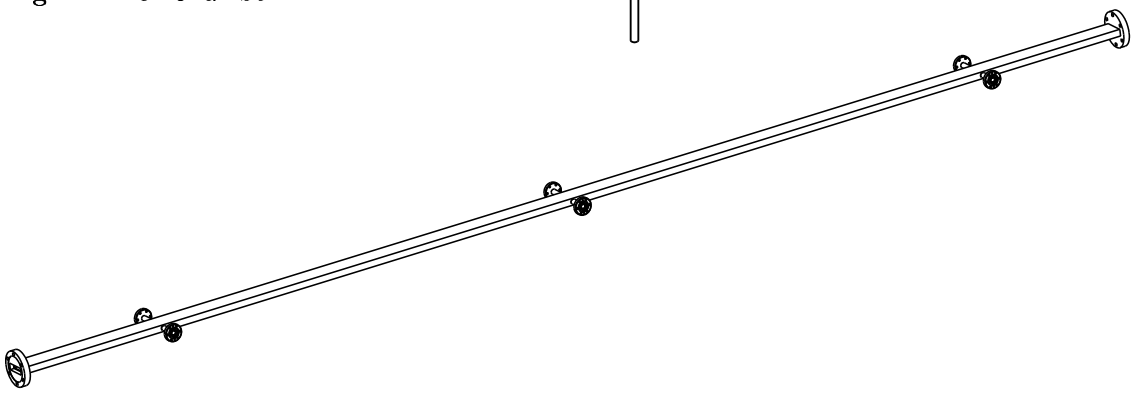

Fig. 3 *Wave Guide*

Infrared-Microspectroscopy of Environmental Samples

W. Seidel, A. Schamlott, D. Kalionska, K.H. Heise[1], R. Nicolai[1], J.-M. Ortega[2], F. Glotin[2], R. Prazeres[2]

The goal of this application of infrared radiation is the microspectroscopy of organic components and their heavy metal complexes in solid or liquid environmental samples.
The absorption bands due to the vibrational transitions are in the wavelength region of $\lambda = 2 - 200\,\mu$m ($5000 - 50\,cm^{-1}$). The absolute amounts of the components are very small. The concentration of solved organic components in environmental water samples is usually lower than 10^{-6} Mol/l. The conventional infrared spectrometry requires a particular sample preparation. Different measuring techniques are known, but the sensitivity and the position resolution are not satisfactory.
In order to improve the sensitivity of infrared measurements we are developing a thermo optical detection method based on the mirage effect [1]. A solid sample is periodically irradiated by a beam of monochromatic light produced by the free-electron laser (FEL) CLIO at Lure/Orsay in France. An absorption induces a temperature gradient which leads to an increase of the refractive index gradient. This deflects a probe beam (i. e. He-Ne laser) propagating along the surface of the sample (mirage effect). The periodic deflection of the probe beam is monitored by the use of a high resolution position detector placed at a suitable distance away from the illuminated sample. The magnitude of this periodic deflection can then be related to the absorption coefficient of the material under investigation. This results in an extremely high sensitivity (absorbances as low as 10^{-6} to 10^{-8} have been measured in the visible light by this method). We have carried out absorption measurements in the wavelength range from 9 μm up to 40 μm with different samples. In these measurements we could reproduce some features of the absorption of the samples, corresponding to the FTIR spectra. With the incident energy being modulated, the heat generation will show a corresponding time dependence. A temperature profile then develops in the sample via heat diffusion. For a heat source with a modulation frequency f the heat diffusion can be described by the thermal diffusion length

$$D = \sqrt{\frac{\kappa}{\pi \varrho C f}}$$

κ denotes the thermal conductivity, ϱ the material density and C the specific heat of the sample. Only heat generated within one thermal diffusion length will be able to reach the surface with an appreciable magnitude. For SiO_2 one finds D $\sim 1.5\,\mu$m for f = 1 MHz. This result means that if the signal is measured about 1 μs after the beginning of the laser pulse, the heat had time to diffuse only over a length shorter than 2 μm. Therefore, one can hope for a spatial resolution much smaller than the FEL wavelength, thus allowing eventually microspectrometry. In that case the He-Ne laser would have to be focused on a sufficiently small spot, which has not yet been done in the present, preliminary, experiments.
We started first resolution test experiments with synthetic samples in May and October 2000. For this runs we prepared samples with the IR absorption in a controlled manner. The pellets are made from KBr as matrix with homogeneous inclusions of interested materials (humic acid). Furthermore, we measured one natural sample of calcite containing humic acid inclusions.

We have carried out absorption measurements in the wavelength range from 9 μm up to 15 μm ($1100 - 670$ cm^{-1}). The average IR-power of CLIO was in the order of 1 W over the wavelength range. The laser time structure contains 10 μs trains (consist of short micropulses, which have a duration of < 10 ps and are separated by intervals of 16 ns) with 25 Hz repetition rate. For the measurement of the absorbance we have averaged the maximum deflection of the He-Ne laser beam over 20 macropulses at each wavelength. In different measurements we could reproduce the structure of the absorption spectra of the samples, corresponding to the FTIR spectra.

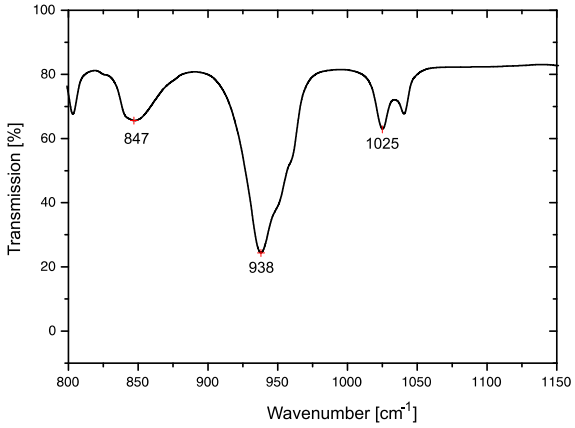

Fig. 1 *FTIR spectrum of the test sample (the substructure in the peak at 938 cm^{-1} is smeared out due to the reduced resolution of this measurement).*

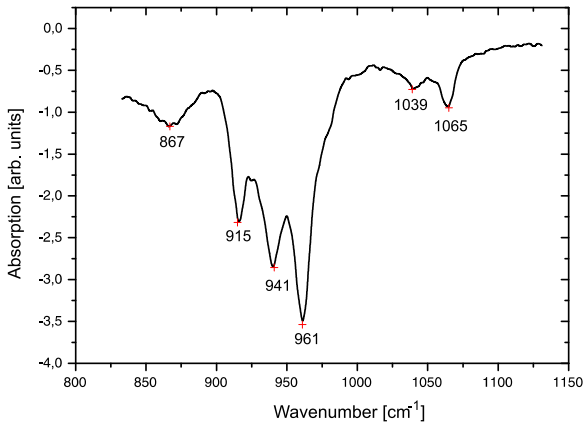

Fig. 2 *Spectrum obtained by the mirage effect at the CLIO FEL.*

Fig. 1 shows the FTIR-spectrum of a test sample (0.74 mg $UO_2(NO_3)_2 \times 6\ H_2O$ in 300 mg KBr-pellet) measured with a Perkin-Elmer Mod 2000 spectrometer, the spectrum measured at the CLIO FEL is shown in fig. 2. The splitting of the wide absorption peak around 941 cm^{-1} into tree peaks was not observed in the samples with lower concentrations of nitrate and will be investigated more detailed in near future. In a next series of FEL experiments we would like to test this method at longer wavelength in order to show that it will be a good possibility for spectroscopic investigation with spatial resolution. Preliminary results have already been obtained on Teflon between 25 μm and 40 μm showing the applicability of the method at long wavelengths.

[1] *Institute of Radiochemistry*
[2] *LURE, Orsay, France*

References

[1] A.C. Boccara, D. Fournier, and J. Bodez, Appl. Phys. Lett. 36, 130 (1980)

Calculating the Spectral Distribution of Bremsstrahlung

A. Wagner, S. Fan, H. W. Barz, E. Grosse, R. Schwengner

One area of research of the new ELBE facility at the FZR will be devoted to nuclear spectroscopy studies by means of nuclear resonance fluorescence experiments using polarized photons and by means of photon-induced fission producing radioactive nuclei of interest. For these experiments detailed knowledge about the spectral distribution of photons from Bremsstrahlung production is mandatory. Therefore, three different approaches to determine the spectral distribution of photons emerging from a thin foil irradiated with electrons have been taken. Two calculations are based on Monte-Carlo simulations with commonly available software packages, GEANT [1] and EGS4 [2], and the third one is based on an analytical treatment in a quantum electrodynamics (QED) approach as described by Itzykson and Zuber [3]. Only the QED approach gives a result for the polarization of photons. All calculations have been done for 20 MeV and 30 MeV incident electron energy using a radiator thickness of 20 μm in the Monte-Carlo calculations. The QED spectrum has been scaled arbitrarily to match at 50% of the maximum photon energy. In order to limit the time needed for the simulations the low energy cutoff for the propagation of particles and photons in GEANT is set to 100 keV whereas it is set to 1.5 MeV for electrons and 100 keV for positrons and photons in the EGS4 calculations. Generally, the agreement between the different calculations is quite good and deviations mainly show up in the high-energy part of the spectra. Nevertheless, as shown in Fig. 2, EGS4 gives a better agreement to the QED calculations for photon energies close to the end-point as compared to GEANT. The GEANT calculation overestimates the spectra by at least 10% for the upper 10% of the spectra. The slight relative enhancement of both Monte-Carlo spectra for the low-energy part as shown in Fig. 2 indicates the influence of absorption inside the radiator which are neglected by the analytical treatment.

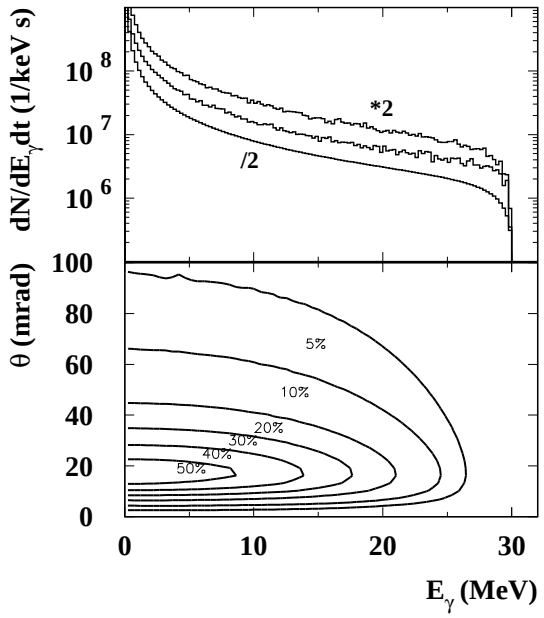

Fig. 1 *Upper part: Bremsstrahlung photon spectrum for a 20μm Aluminum radiator and incident electron energy of 30 MeV calculated by GEANT (middle), EGS4 (upper, multiplied by factor of 2), and QED (lower, divided by factor of 2). Lower part: Degree of polarization of Bremsstrahlung photons as function of photon energy and polar angle of observation for incident electrons of 30 MeV (QED).*

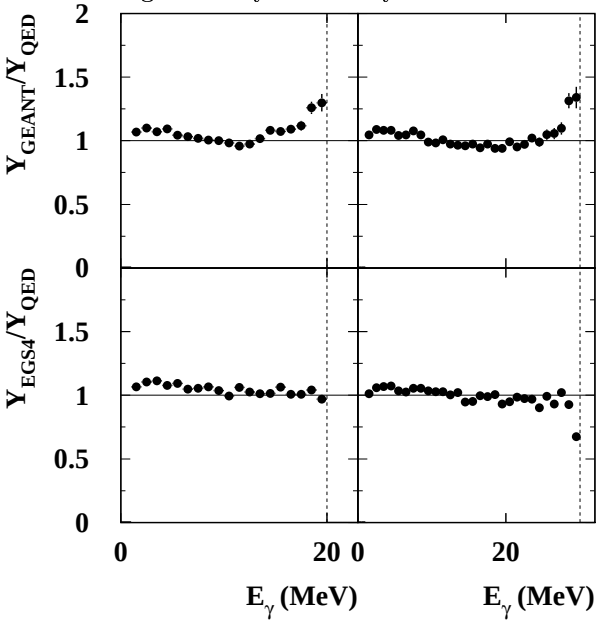

Fig. 2 *Energy dependence of the ratio of bremsstrahlung-spectra from GEANT (upper row) to the QED calculation and EGS4 (lower row) to the QED calculation for incident electron energies of 20 MeV (left column) and 30 MeV (right column).*

References

[1] CERN Program Library Long Writeup Q121, CERN, Geneva (CH), 1994
[2] The EGS4 code system, SLAC-R-265, UC-32, Stanford University
[3] C. Itzykson, J.-B. Zuber: Quantum Field Theory, McGraw-Hill, 1988

Postneutron Yield of Bremsstrahlung-Induced Fission of ^{238}U with an Endpoint Energy of 12 MeV

S. Fan, A. Wagner, E. Grosse

In order to examine the feasibility of studying neutron rich nuclei close to the astrophysical r-process path at ELBE we investigated the production cross sections of fission fragments from photo-induced fission. The isotopic fragment distribution from bremsstrahlung-induced fission of ^{238}U using bremsstrahlung from incident electron energies E_e can be written as

$$Y(Z/A) = \frac{N_i \int_0^{E_e} F_p(E) exp - \frac{(Z - Z_p(E(E_e)))^2}{2\sigma_Z^2} N(E(E_e))\sigma_F(E)dE}{\sqrt{2\pi}\sigma_Z \int_0^{E_e} N(E(E_e))\sigma_F(E)dE}$$

where the bremsstrahlung spectrum $N(E(E_e))$ was calculated using EGS4 [1], the photofission cross section σ_F was taken from Ref. [2]. Z_p denotes the most probable charge in a Gaussian distribution and was calculated using the Z_p model [3]. The width parameter σ_Z of the charge distribution from photofission of ^{238}U was found to be 0.34 [4], and N_i denotes the normalization parameter. The correction factor $F_p(E(E_e))$ for the proton odd-even effect is defined [4] as

$$F_p(E) = \frac{1+\delta_p}{1-\delta_p} \text{ for even Z, } F_p(E) = \frac{1-\delta_p}{1+\delta_p} \text{ for odd Z with}$$

$$\delta_p = \frac{\int_0^{E_e} \delta_p^{mono}(E) N(E(E_e))\sigma_F(E)dE}{\int_0^{E_e} N(E(E_e))\sigma_F(E)dE}$$

where $\delta_p^{mono}(E)$ was deduced from experimental data[4].
Fig. 1 shows the postneutron mass distribution for the ^{238}U(γ, f) reaction with bremsstrahlung from 12 MeV electrons [5]. Fig.2 depicts the elemental mass distribution and Fig.3 shows the isotopic distribution of postneutron fission fragments (colored), nuclei with known half-lifes are shown as open boxes, stable nuclei are shown as filled boxes. Also drawn is the limit of nuclei with mean lifetimes against β-decay of more than 43 ms from theoretical predictions by Moeller [6].

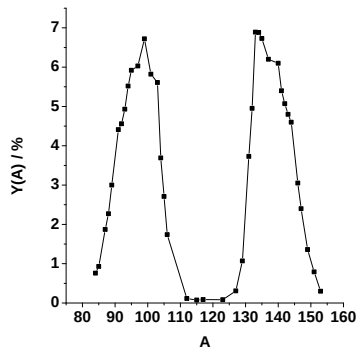

Fig. 1 *Postneutron mass distribution for ^{238}U(γ, f) reactions with bremsstrahlung from 12 MeV electrons [5].*

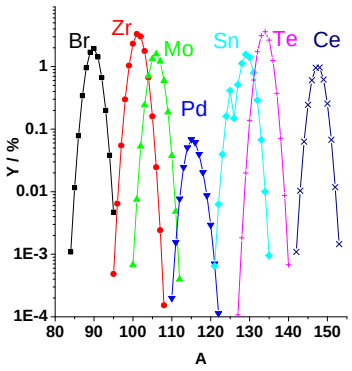

Fig. 2 *Elemental mass distribution (conditions as for Fig. 1).*

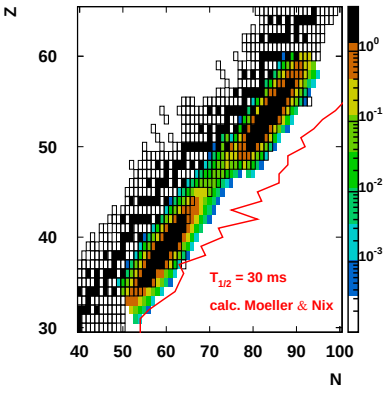

Fig. 3 *Isotopic distribution of fission fragments (colored). The contour line for expected half-lifes of 30 ms from theoretical calculations [6] is shown in red.*

References

[1] W.R. Nelson et al., SLAC-Report-265 (1985).
[2] B.L. Berman et al., Phys. Rev. C 21 (1980) 1215.
[3] R.K. Gupta et al., Phys. Rev. C 30 (1984) 395.
[4] K. Persyn et al., Nucl. Phys. A 620 (1997) 171.
[5] E. Jacobs et al., Phys. Rev. C 21 (1980) 237.
[6] P. Moeller et al., Atomic Data Nucl. Data Tables 66 (1997) 131-343.

A Beam Dump for Energetic Photons

A. Wagner, F. Dönau, E. Grosse, L. Käubler, K.-D. Schilling, R. Schwengner, W. Schulze

Nuclear spectroscopy studies at the new ELBE facility will make use of energetic photons from Bremsstrahlung production. In order to minimize the background from scattered photons the secondary photon beam has to be removed after passing through the experiment's target. Several different solutions have been studied by thorough Monte-Carlo simulations using the GEANT [1] program package. As a result, the configuration shown in Fig. 1 gives the minimal backscattering of photons towards the target area. It consists of a cylindrical inner absorber made from Polyethylene (PE) with a diameter of 80 cm and a length of 70 cm. This inner absorber is surrounded by a lead shielding with a thickness of 20 cm in axial and 10 cm in radial direction.

The selection of a low-density material like PE appears disadvantageous since it results in a large setup. Nevertheless, the high neutron production threshold and low (γ, n) cross section of 18.7 MeV for Carbon (for the most abundant isotope C-12) clearly favours PE as compared to lead. Moreover, Compton backscattering of photons for PE is reduced as compared to water by the lower mean atomic number density in PE. This lower atomic number of PE additionally lowers pair production and subsequently positron annihilation photons.

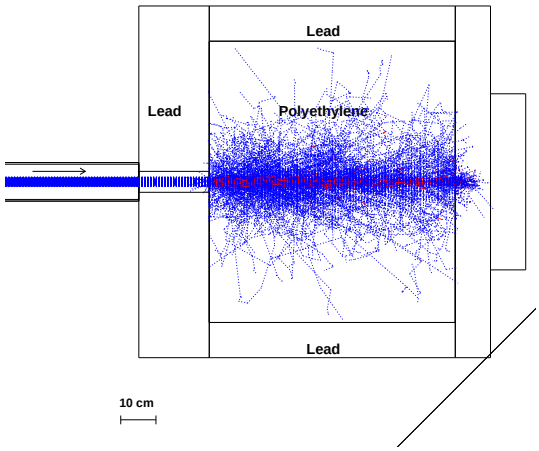

Fig. 1 *Simulated photon propagation of 20 MeV photons inside the photon beam dump. The photon beam is impinging from the left. Blue lines indicate photons, red lines indicate electrons.*

isotope	abundance	S_n(MeV)
H-2	0.02 %	2.22
C-12	98.9 %	18.7
C-13	1.1 %	4.95
O-16	99.8 %	15.7
O-17	0.04 %	4.14
O-18	0.2 %	8.04
Pb-204	1.4 %	8.39
Pb-206	24.1 %	8.09
Pb-207	22.1 %	6.74
Pb-208	52.4 %	7.37

Table 1 *Natural abundances and one-neutron separation energies for different isotopes used in the calculations.*

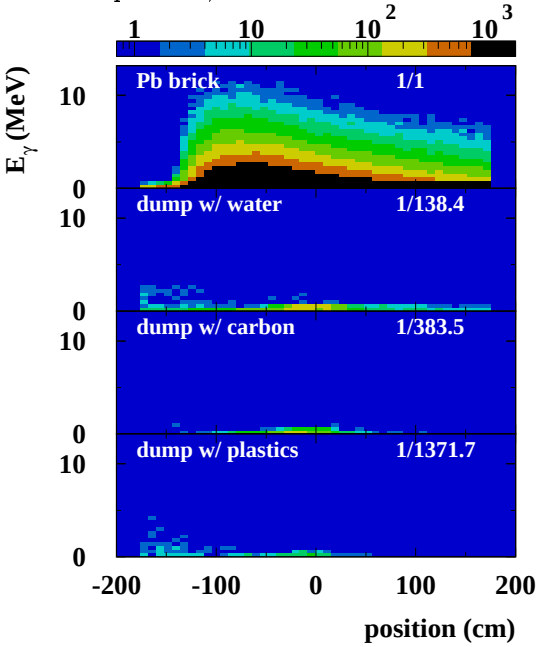

Fig. 2 *Spectral (ordinate) and position distribution (abscissa) of photons emerging from the photon beam dump and crossing a plane tilted by an angle of $\pi/4$ with respect to the photon beam. Different setups for the internal absorber of the beam dump are indicated with the integrated yield normalized to the first alternative featuring simply a lead brick at the end of the beam pipe. Different intensities follow a logarithmically scaled geographical colour map as shown on top.*

References

[1] CERN Program Library Long Writeup Q121, CERN, Geneva (CH), 1994

Optimization of a Quasi-Monochromatic X-ray Source for Cell Irradiations [B]

W. Neubert, W. Enghardt, U. Lehnert, B. Naumann, A. Panteleeva, J. Pawelke

Among the various secondary radiation sources proposed for the superconducting electron linear accelerator ELBE we consider the realization of an X-ray source for radiobiological investigations. For measuring relative biological effectivenesses of photons ($E_x \simeq 10 \div 100$ keV) by cell survival studies a channeling X-ray source is being developed. However, the quasi-monochromatic channeling radiation (CR) is contaminated by bremsstrahlung, which results both from the crystal and from the interaction of scattered electrons with the beam tube. Furthermore, neutrons are produced since the photon energy exceeds the threshold for photo-neutron reactions.
The beam line from the accelerator hall to the radiation physics cave was designed for a dispersion-free beam transport with minimal loss using the PARMELA code [1]. The system delivers an electron beam with $3\,\pi$ mm mrad normalized transverse emittance to the target crystal at focal spot diameters ranging from 4 mm to less than 1 mm. These parameters of the incident beam are chosen to meet the channeling condition. The channeling radiation yield was analytically calculated using the dipole approximation [2] for 20 MeV electron channeling along the (110) plane of a 100 μm thick diamond crystal. The maximum energies of channeling radiation emitted in forward direction are 17.1 keV (2→1 transition) and 29.9 keV (1→0 transition). But the interaction of the electron beam with the target strongly increases the beam divergence leading to collisions of electrons with beam line elements (Fig. 1). This causes a considerable bremsstrahlung background that may influence the radiobiological measurements, while the background contribution originating from the beam delivery to the target is negligible. Therefore, the complete setup downstream of the target crystal has been taken into account in GEANT [3] simulations as displayed in Fig. 1. For background calculations the electron beam was started at 1 cm in front of the carbon target that simulates the diamond crystal. The input (electron momentum distribution) was taken from the beam transport calculations. Multiple scattering in the target was found to be the dominating process which determines the beam divergence. Initially, the background calculations assumed a configuration with a distance of 123 cm between the crystal and the center of the dipole magnet which separates the electron beam from the photons. The full beam transport without consideration of electron scattering favours this solution but the electron tracking by GEANT shows too much bremsstrahlung production at the entrance of the dipole magnet. A significant reduction of the bremsstrahlung background in the GEANT simulations was achieved by increasing the beam tube diameters from 40 to 63 mm and the gap of the magnet from 60 to 90 mm. This way, the bremsstrahlung could be reduced to the level of the unavoidable contribution from the target. Secondary neutron production from these components has been treated by multiplying the bremsstrahlung photon

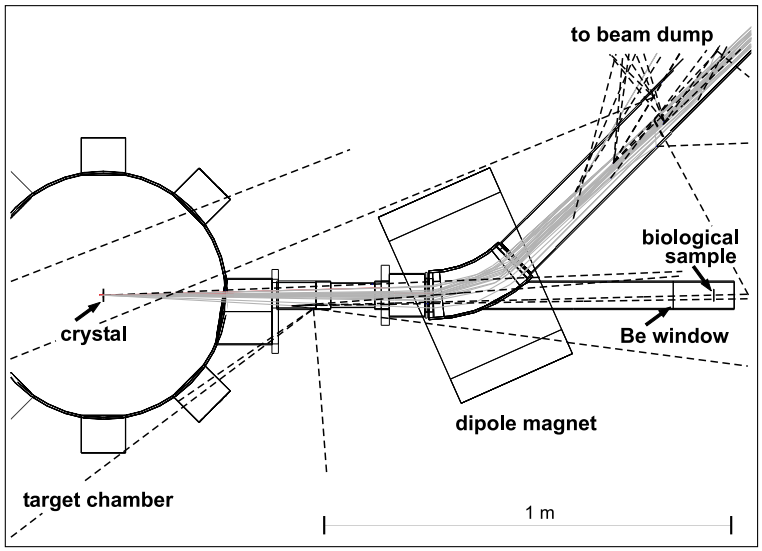

Fig. 1 *Top view of the channeling radiation source with tracks of electrons (grey) and photons (dashed).*

distribution with photo-neutron cross sections using the method described in [4]. In the optimized layout, the contamination of the X-ray dose delivered to the cell layer by neutrons is expected to be less than 1 %. The biological sample is assumed to consist of a monolayer of fibroblast cells (4 μm thick) placed on a 10 μm cellulose membrane and covered with a 8 mm thick medium layer. Fig. 2 shows the dose distribution in this sample produced by the photon beam after passing a 100 μm Be vacuum window calculated with the EGS 4 code [5]. We studied both tracking and energy deposition in such thin layers. A thickness greater than 1 μm was found to be necessary to perform dose calculations with EGS 4 in the photon energy range from 1.5 keV to 30 keV. The dose provided by the discrete channeling lines exceeds the bremsstrahlung background by at least one order of magnitude. But the integral dose of the bremsstrahlung is comparable to that of the channeling radiation. The introduction of an additional 70 μm Al absorber allows to reduce the low energy bremstrahlung contribution below 10 keV. It shows, however, that energy differential precision measurements of doses in biological samples require monochromatization of the photon beam, e.g. by reflection at a curved pyrolytic graphite crystal.

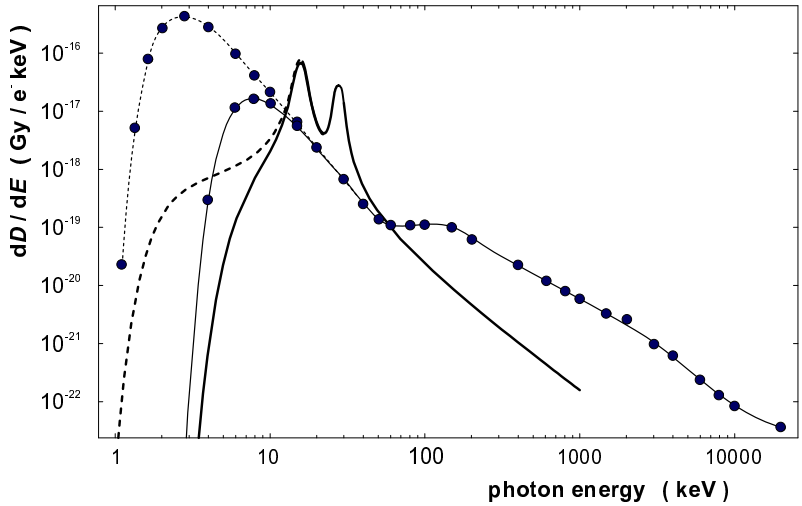

Fig. 2 *Dose distributions obtained by EGS 4 simulations for the described biological sample irradiated by bremsstrahlung (dots) and channeling radiation (thick line). The dotted and dashed lines are the corresponding calculations without the 70 μm Al absorber.*

Table 1 *Expected doses in the biological sample.*

Photon energy	Dose in 10^{-16} Gy / e$^-$	
	with 100 μm Be window	with additional 70 μm Al absorber
1...10 keV background	13.00	0.70
10...100 keV background	1.04	0.86
$\geq$ 100 keV background	0.29	0.29
17 keV CR line	3.23	2.82
29 keV CR line	1.53	1.49

References

[1] L.M. Young, Los Alamos National Laboratory LA-UR-96-1835 (1996)
[2] M. Kumakhov and R. Wedell, Radiation of Relativistic Light Particles during Interaction with Single Crystals (Akademie-Verlag, Berlin 1991)
[3] GEANT-Detector Description and Simulation Tool, CERN Program Library W5013
[4] B. Naumann et al., Report FZR-267, Dresden (1999)
[5] W.R. Nelson et al., The EGS 4 code system, SLAC-Report-265 (1985)

Channeling in an Ultrasonic Superlattice [W,S]

L. Sh. Grigoryan[1], W. Wagner

A quantum mechanical description of channeling under the influence of ultrasound (US) excited in a single crystal has been developed [1–2]. It was shown that a resonant interaction between a longitudinal standing ultrasonic wave and planar or axially channeled relativistic charged particles can take place if the frequency of US approaches some critical value. This value corresponds to the energy difference between two neighbouring states a and b of transverse motion. The quantum numbers N of these states obey the selection rules $\mid N_a - N_b \mid = 1, 2, 3...$ for axial and $\mid N_a - N_b \mid = 2, 4, 6...$ for planar channeling.
The frequency of US necessary for resonance reads

$$\nu_n^* = \frac{v_s}{c} \frac{\mid \varepsilon_a - \varepsilon_b \mid}{n\,h}$$

where ε denotes the corresponding energy level of the channeled particle and v_s the velocity of US inside the crystal. Since the effect resembles a parametric resonance, an integer $n = 1, 2...$ appears in the denominator of the formula. This is of great practical importance because it opens the possibility of resonant interaction even at frequencies ν_s lower than typically 10 GHz for $n = 1$. At the same amplitude of crystal potential modulation, higher values of n, of course, diminish the effect of US.
Probability distributions of a planar channeled electron are shown in Figs. 1 and 2 versus the dimensionless coordinates $X = \alpha x$ and $Z = k_s z$ where the spatial coordinate z is chosen along the channeling direction, x is the transversal one, α denotes a scaling parameter of the crystal potential and k_s is the wave number of US. The only difference between the two figures consists in the US-frequency. At resonance (Fig. 1) US strongly mixes the corresponding channeling states a and b. Even a slight deviation of ν_s from the resonant value ν_1^* (Fig. 2) results in an abrupt reduction of the influence of US on the state of the channeled particle.

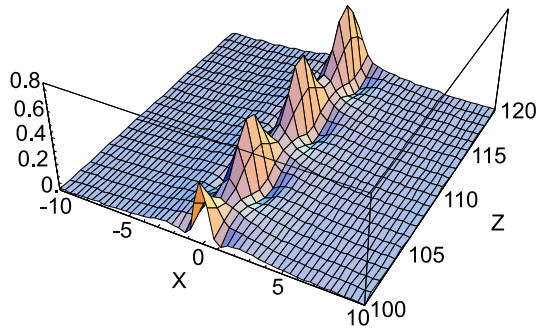

Fig. 1 *Probability distribution $P(X, Z)$ of a planar channeled electron at resonance ($\nu_s = \nu_1^*$).*

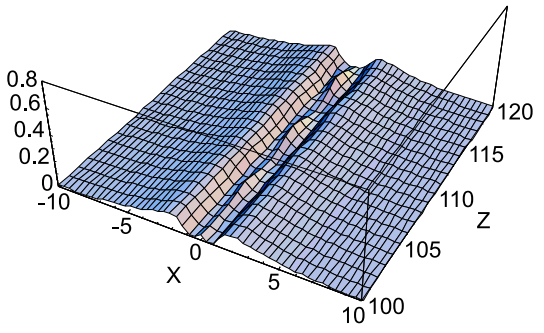

Fig. 2 *The same as in Fig. 1 but slightly out of resonance ($\nu_s = 0.95\,\nu_1^*$).*

[1] *Institute of Applied Problems in Physics, NAS Yerevan, Armenia*

References

[1] L.Sh. Grigoryan et al., Rad. Eff. & Def. in Sol. 152 (2000) 225; ibid. p. 269
[2] L.Sh. Grigoryan et al., Rad. Eff. & Def. in Sol. 153 (2000) 13

Mechanism of Channeling Radiation Stimulation by Ultrasound [W,S]

L. Sh. Grigoryan[1], W. Wagner

The interaction of a channeled relativistic charged particle with a standing ultrasonic wave excited in a single crystal leads to the splitting of the projection of its momentum in the channeling direction (z) : $p_z \Rightarrow (p_z - \hbar k_s\,,\, p_z\,,\, p_z + \hbar k_s)$. Here $\hbar k_s$ denotes the momentum associated with an acoustic phonon. The wave function of the channeled particle then represents a superposition of three plane waves with the phases $(p_z - \nu \hbar k_s)\, z/\hbar$, $\nu = 0, \pm 1$.

Theoretical considerations on the influence of ultrasound (US) on channeling [1] formally predict the occurrence of additional radiative transitions which may amplify the total intensity of channeling radiation (CR). The mechanism of this effect instantly becomes reasonable from the following graphical treatment of CR.

Fig. 1 schematically illustrates the dispersion relation [2] $E = c\sqrt{m^2c^2 + p_z^2} + \varepsilon_N$ of a channeled particle for three stationary states ($N = 1, 2, 3$) of transverse motion with the energy levels ε_N. Because of $E \gg \mid \varepsilon_N \mid$ the slope of these curves $\partial E/\partial p_z \approx v_z$ is determined by the particle velocity (v_z). By applying $\Delta E/\Delta p_z$ for the triangles CBD and CBA the known formula for the energy of CR emitted under an angle θ due to the transition AC :

$$\hbar\omega = \frac{\varepsilon_2 - \varepsilon_1}{1 - \beta\cos\theta}\ ,\ \beta = v_z/c$$

can directly be obtained from the ratio of these two expressions. In an analogous way, from the triangles GBA and GBF, one can for instance derive the adequate equation for an inverse transition AG accompanied with the emission of an acoustic phonon :

$$\hbar\omega = \frac{\varepsilon_2 - \varepsilon_3 - \nu\, c\hbar\, k_s}{1 - \beta\cos\theta}\ ,\ \nu = -1\ ,\ c\hbar k_s > \mid \varepsilon_2 - \varepsilon_3 \mid .$$

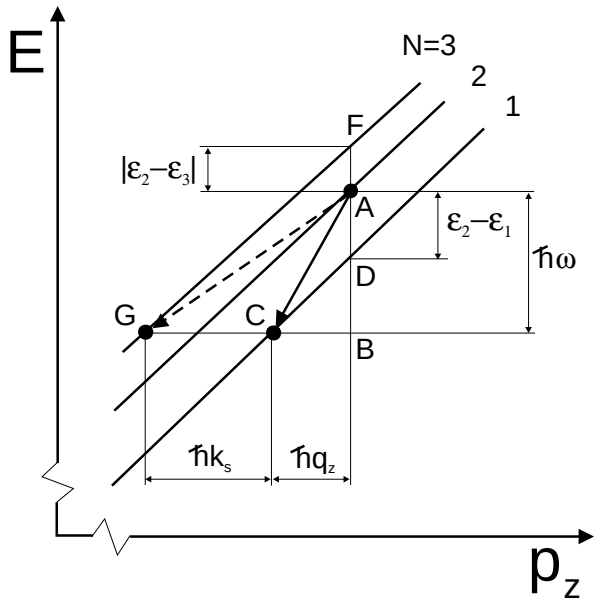

After such a *radiative* transition the channeled particle occupies a state with *larger* transverse energy; i.e. a CR-photon was emitted together with an acoustic phonon, and the quantum number N is increased.

Since in general $\nu = 0, \pm 1$ [1], the direct $(\varepsilon_i > \varepsilon_f)$ as well as inverse $(\varepsilon_i < \varepsilon_f)$ radiative transitions associated with the emission or absorption of an acoustic phonon are induced *additionally* to such with $\nu = 0$ which are not influenced by US. Consequently, US enables the channeled particle to emit multiple CR-photons during its traverse through the acoustically excited crystal that should result in an increase of the CR intensity.

Fig. 1 *Schematic dispersion curves with two transitions (arrows) of a channeled particle.* $\hbar q_z = \hbar q\cos\theta$ *denotes the projection of the photon momentum* $q = \omega/c$ *onto the channeling direction.*

[1] *Institute of Applied Problems in Physics, NAS Yerevan, Armenia*

References

[1] L.Sh. Grigoryan et al., Rad. Eff. & Def. in Sol. 152 (2000) 225; ibid. p. 269; vol. 153 (2000) p. 13

[2] J.O. Kephart, Stanford University, Ph.D. thesis (1987)

Hadron Physics

The production of strange hadrons and electromagnetic radiation from colliding hadron systems allows insights in the properties of dense nuclear matter as formed in violent cosmic processes like super-novae and as present in a certain phase of the big bang. In particular, the experimental research of the department focuses on in-medium modifications of hadrons, i. e. their behavior when embedded in strongly interacting matter. Various heavy-ion experiments in the 1 GeV range point to such changes in a medium. For instance, dedicated measurements by the KaoS and FOPI collaborations at the heavy-ion synchrotron SIS in Darmstadt can be interpreted by a slight mass enhancement of kaons and a significant mass reduction of anti-kaons. While these interesting findings can be attributed to an evidence for partial restoration of chiral symmetry in dense nuclear matter produced in the course of heavy-ion collisions, other interpretations are conceivable, too.

In this respect the measurements of kaon production in proton-nucleus collisions represent the missing link for systematically understanding strangeness production. During the last years the COSY-11 and TOF collaborations at the cooler synchrotron COSY in Jülich enlarged already the data basis for strangeness production in elementary hadron reactions. Now the final analysis of the experiments by the KaoS collaboration at SIS and the ANKE collaboration at COSY is eagerly waited for. Both experiments measure in complementary phase space regions kaons produced by a proton beam at various energies impinging on various target nuclei.

Hidden strangeness, e. g. in ϕ mesons, represents another facet of strangeness degrees of freedom. While ϕ production is presently a hot topic in hadron reactions with respect to the strangeness sea in nucleons and OZI rule violations, the ϕ multiplicity in heavy-ion collisions appears puzzling. The analysis of data taken previously with the FOPI detector points to a ϕ production probability being much larger than can be understood within the framework of transport models.

While selected hadron channels, in particular these with strangeness, are sensitive to in-medium effects, a direct measurement of spectral functions is desirable. This goal can be accomplished, e. g., via the dielectron decay channels. Indeed, the starting HADES project at SIS is aimed at studying the in-medium properties of ρ, ω and ϕ mesons in a nuclear environment. Since the fall of 2000, HADES is operating and begins with data taking while being completed. The first multi-wire chamber built in our detector workshop has proven to work successfully. The remaining 5 chambers from Rossendorf will be installed in the HADES detector system during 2001 thus enabling, together with the other chambers, the required high-precision resolution of charged particles tracks. HADES is expected to have a large scientific potential for various investigations with the pion, proton and heavy-ion beams delivered at the SIS.

The theory group in the hadron physics department is accompanying these experimental activities. Predictions and interpretations of selected topics in the realm of strange and rare electromagnetic probes are provided. Most of these calculations refer to the energy range covered by the experiments performed with FZR participation (see collaboration list below), others deal with various phenomenological aspects of deconfined matter, as a state with chiral symmetry restoration in the strongly interacting medium, produced in high-energy heavy-ion reactions. Whereas the investigations of dense and hot hadronic matter as produced in medium-energy collisions are of strong interest for the understanding of astronomical objects like supernovae and neutron stars, the quark-gluon phase transition studies are of relevance for more violent scenarios like the big bang.

Collaborations

ANKE: *Univ. Münster, FZ Jülich, Univ. Giessen, Univ. Bonn, Univ. Köln, Univ. Erlangen- Nürnberg, Fachhochschule München, FZ Rossendorf, JINR Dubna (Russia), Univ. Tblisi (Georgia), Petersburg Nuclear Physics Institute (Russia), ITEP Moscow (Russia), Russian Academy of Science Moscow (Russia), ECN-Nuclear Energy (Netherlands), Jagellonian Univ. Cracow (Poland), Moscow State University (Russia), Univ. College London (England), Soltan Institute for Nuclear Studies (Poland),*
spokesperson: K. Sistemich

FOPI: *Univ. Heidelberg, GSI Darmstadt, FZ Rossendorf, IPNE Bucharest (Romania), KFKI Budapest (Hungary), LPC and Univ. Blaise Pascal Clermont (France), ITEP Moscow (Russia), Kurchatov Institute Moscow (Russia), Korea Univ. Seoul (South Korea), IreS Strasbourg (France), Univ. Warsaw (Poland), RBI Zagreb (Croatia),*
spokesperson: N. Herrmann

HADES: *Univ. Frankfurt, TU München, Univ. Giessen, GSI Darmstadt, FZ Rossendorf, Institute of Physics Bratislava (Slovakia), LNS Catania (Italy), LPC and Univ. Blaise Pascal Clermont (France), Jagellonian Univ. Cracow (Poland), JINR Dubna (Russia), Univ. degli Studi di Milano (Italy), ITEP Moscow (Russia), INR Moscow (Russia), MEPhI Moscow (Russia), Univ. of Cyprus (Cyprus), Institute de Physique Nucleaire d'Orsay (France), Nuclear Physics Institute Rez (Tschechia), Univ. of Santiago de Compostela (Spain), Univ. of Valencia (Spain),*
spokesperson: J. Friese

KaoS: *TU Darmstadt, Univ. Frankfurt, Univ. Marburg, GSI Darmstadt, Jagellonian Univ. Cracow (Poland), FZ Rossendorf,*
spokesperson: P. Senger

TOF: *Univ. Bochum, FZ Jülich, Univ. Bonn, TU Dresden, Fachhochschule Jülich, Univ. Tübingen, Univ. Erlangen-Nürnberg, FZ Rossendorf, IUCF Bloomington (USA), INFN Torino (Italy), SINS Warsaw (Poland),*
local organizer: E. Roderburg

Kaon and Antikaon Production in Proton-Nucleus Collisions [G]

W. Scheinast[1] for the KaoS collaboration:
I. Böttcher[4], M. Dębowski[1], F. Dohrmann*, A. Förster[3], E. Grosse[7], B. Kamys[6], P. Koczoń[2], B. Kohlmeyer[4], F. Laue**, M. Menzel[4], L. Naumann[1], H. Oeschler[3], F. Pühlhofer[4], Ch. Schneider[1], E. Schwab[2], P. Senger[2], Y. Shin[5], H. Ströbele[5], Ch. Sturm[3], G. Surówka[6], F. Uhlig[3], A. Wagner[1], W. Waluś[6]

During the last year the analysis of the data on K^+ and K^- production in proton-nucleus collisions has continued and now first results can be presented. The experiment already described in the last annual report had taken place 1998 at SIS/GSI Darmstadt. In the kaon spectrometer a new 2nd level trigger enabled beam intensities above $10^9\,s^{-1}$ to be applied.

Fig. 1 shows double differential cross sections for $K^{\pm}$ production. The 3.5 GeV data exhibit structures which might be caused by a yet unknown problem with the trigger efficiency (the trigger was different for the 2.5 GeV data).

In the 2.5 GeV K^+ spectra the maximum of the differential cross section shifts to lower momenta with increasing mass number. Taking into account the observation angle of 40°, this is an evidence for the emission system being different in these targets. The K^+ are emitted more towards target rapidity in the p+Au system. Consequently they are either produced in secondary reactions or rescattered before leaving the nucleus.

Heavy ion data at comparable energies can well be described by Boltzmann distributions (e. g. in [1]). When trying this for the proton data, one has to know the kaon emission frame. Fig. 1 contains the fits of the 2.5 GeV spectra with a Boltzmann function in the proton-nucleus center-of-mass frame. An attempt to adjust this distribution in the nucleon-nucleon frame failed. This can be regarded as a hint for the K^+ being produced in multistep processes. The inverse slope parameters are $T = 123.5(9)$ MeV (Au) and $T = 115.5(8)$ MeV (C).

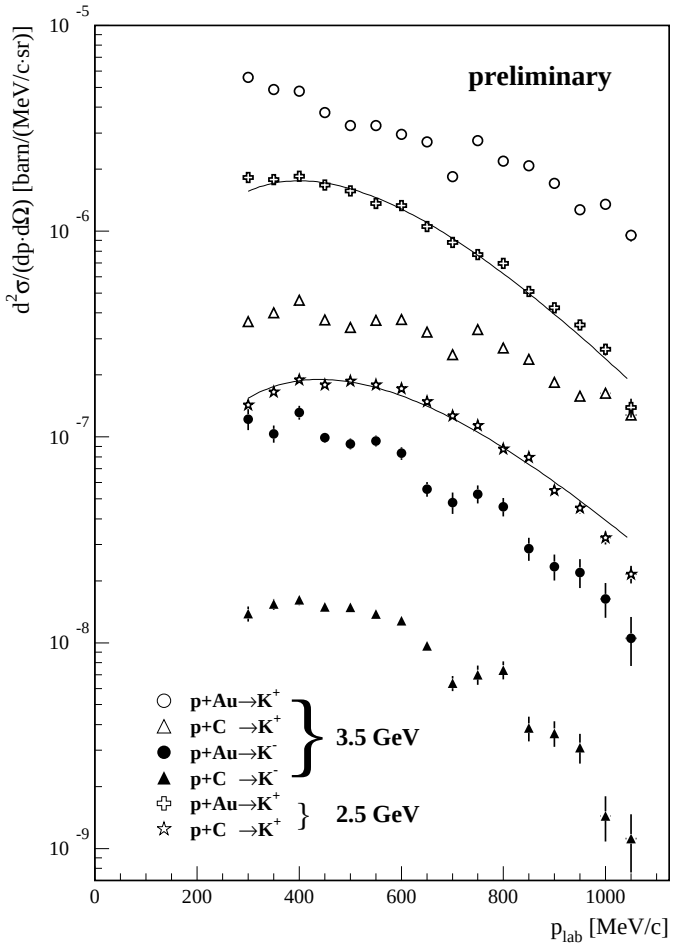

Fig. 1 *Inclusive double differential K-meson production cross sections versus momentum in the laboratory frame at a polar angle of 40°. Only statistical errors are plotted. Open symbols denote K^+, full symbols K^-.*

K^+ are scarcely absorbed in nuclear matter because strangeness exchange reactions are not possible. Antikaons do these reactions, e. g. $K^- + N \rightarrow \pi + \Lambda$, so they are strongly absorbed. In Fig. 2 two K^-/K^+ ratios at 3.5 GeV are plotted. The difference between carbon and gold target might be a hint for K^- absorption, but can also arise from a difference in the emission systems between K^+ and K^-.

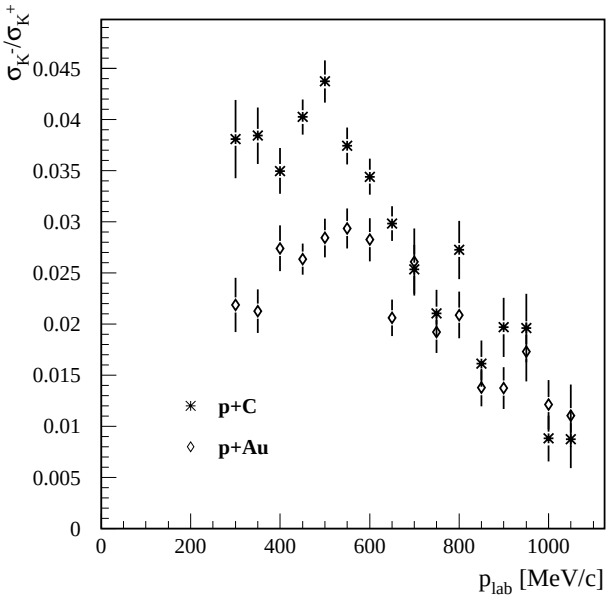

Fig. 2 *K^-/K^+ ratio at 3.5 GeV, from the spectra of Fig. 1.*

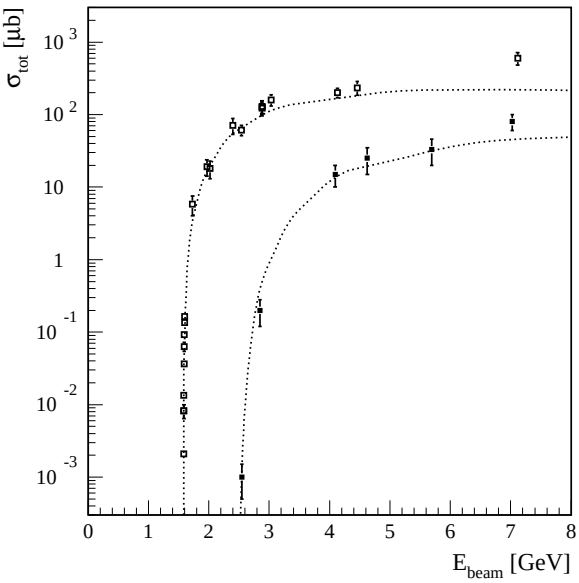

Fig. 3 *Compilation [2] of total cross sections on K^+ (left curve) and K^- (right curve) production in p+p collisions. The curves represent parametrizations [4].*

Over the shown momentum range this ratio is in the same order of magnitude as the ratio of total p+p cross sections, as can be seen in Fig. 3. So, the 3.5 GeV data seem not to exhibit obvious in-medium effects besides rescattering and absorption. If there are such effects, they must be visible more clearly in near-threshold data, i. e. 1.6 and 2.5 GeV. The future analysis will show this and will allow a comparison to complementary data from ITEP[3] and COSY/ANKE.

[1] *FZR*
[2] *GSI Darmstadt*
[3] *TU Darmstadt, Institut für Kernphysik*
[4] *Universität Marburg, Physikalisches Institut*
[5] *Universität Frankfurt, Institut für Kernphysik*
[6] *Jagiellonian University Cracow, Institute of Physics, Poland*
[7] *FZR and TU Dresden, Institut für Kern- und Teilchenphysik*
[*] *FZR, now at Argonne National Laboratory, Argonne IL, USA*
[**] *GSI, now at Ohio State University, Columbus OH, USA*

References

[1] C. Sturm et al., Phys. Rev. Lett. 86/1 (2001) 39
[2] P. Senger, H. Ströbele, J. Phys. G 25 (1999) R59
[3] Y. T. Kiselev et al., J. Phys. G 25 (1999) 381
[4] A. Sibirtsev, Phys. Lett. B 359 (1995) 29,
A. Sibirtsev et al., Z. Phys. A 358 (1997) 101

Centrality Dependence of Kaon and Antikaon Production in Ni+Ni Collisions at SIS Energies [B,G]

M. Menzel[4], I.M. Böttcher[4], M. Dębowski[5,6], F. Dohrmann[6], A. Förster[2], E. Grosse[6,7], P. Koczoń[1], B. Kohlmeyer[4], F. Laue[1,*], L. Naumann[6], H. Oeschler[2], F. Pühlhofer[4], W. Scheinast[6], E. Schwab[1], P. Senger[1], Y. Shin[3], H. Ströbele[3], C. Sturm[2], G. Surówka[5], F. Uhlig[2], A. Wagner[6], W. Waluś[5]

Kaons and antikaons are regarded as a promising probe to study hadron properties in dense nuclear matter. Recent experimental results obtained with the Kaon Spectrometer indicate modifications of the in-medium properties of K^+ and K^-. Remarkable results are that the K^-/K^+ ratio is enhanced compared to pp collisions [1,2,3], the spectral slope for the antikaons is steeper than for the kaons [2] and a preferential out-of-plane emission of K^+ is observed [4].

In order to study the kaon production as a function of the reaction centrality and the beam energy, we have measured K^+ and K^- mesons around midrapidity ($\theta_{lab} = 40° \pm 4°$) in Ni+Ni reactions at beam energies of 1.1 (K^+ only), 1.5 and 1.93 AGeV. The multiplicity of charged particles measured by a target hodoscope is used to determine the centrality. The data set is subdivided in five centrality bins MUL1 to MUL5 for each beam energy. From a measurement under minimum bias conditions the reaction cross section is determined. For all beam energies we find a reaction cross section of $\sigma_R = 2.9 \pm 0.3$ barn, which agrees with the geometric model. The relative reaction cross section for each centrality class $\sigma_{R,MUL}/\sigma_R$ is given in Table 1 for 1.5 and 1.93 AGeV. Errors of about 10 % have to be added to the ratio $\sigma_{R,MUL}/\sigma_R$.

Figure 1 shows the invariant cross sections of K^+ (full circles) and K^- (open circles) for central to peripheral collisions (see middle panel: MUL 5 to MUL 1) as a function of the center-of-mass kinetic energy at beam energies of 1.1, 1.5 and 1.93 AGeV. The K^- mesons are scaled by a factor of 20 (see lower panel) and the yields in the bins are scaled by factors of 10 (see upper panel). The error bars shown are due to statistics only and a systematic error of 10% has to be added, caused by beam normalization, acceptance determination and trigger efficiency. The lines represent

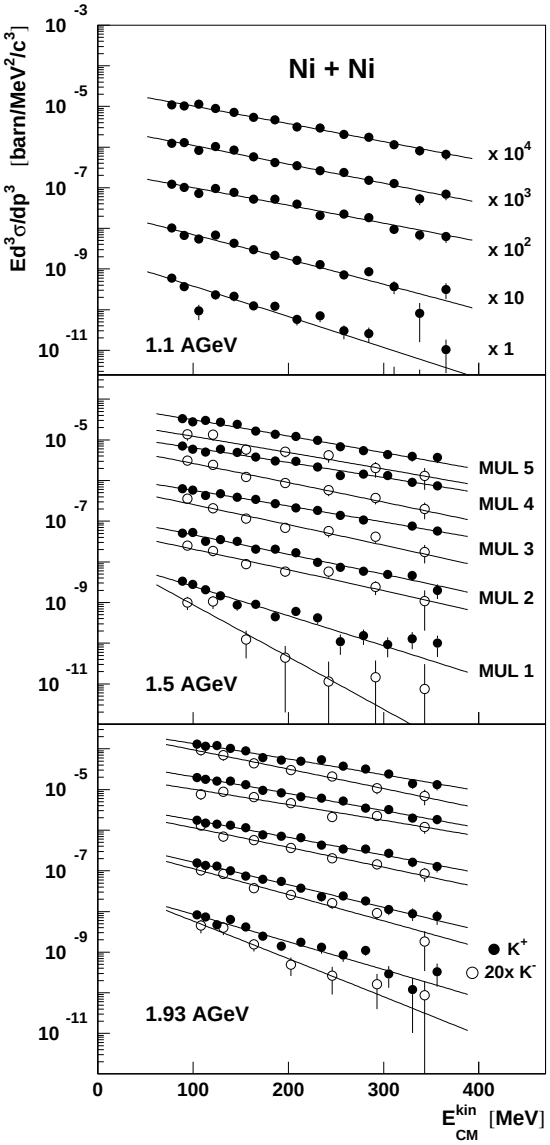

Fig. 1 *K^+ and K^- invariant cross sections as a function of the kinetic energy and the centrality of the reaction measured around midrapidity ($\theta_{lab} = 40° \pm 4°$) for Ni+Ni collisions at different beam energies (preliminary).*

Boltzmann distributions $d^3\sigma/dp^3 \propto exp(-E_{CM}/T)$ fitted to the spectra individually for each multiplicity bin. The integrated kaon cross sections $4\pi(d\sigma_K/d\Omega_{CM})$ and the inverse slope parameters T as a function of the centrality are given in Table 1 for 1.5 and 1.93 AGeV. The errors of both quantities include the systematic effects. For all beam energies the spectral slopes decrease (Figure 1) and the inverse slope parameters T increase (Table 1) with increasing centrality of the reaction for both, kaons and antikaons. We determined the average multiplicity per number of participating nucleons M_K/A_{part} as a function of the number of participating nucleons. M_K is calculated via $M_K = \sigma_K/\sigma_{R,MUL}$ with $\sigma_K = 4\pi(d\sigma_K/d\Omega_{CM})$ and with the reaction cross section for each multiplicity class $\sigma_{R,MUL}$. A_{part} is calculated from the number of nucleons in the overlap of the colliding nuclei. The impact parameter b is determined for the center of each multiplicity bin. The kaon and antikaon multiplicity per A_{part} (full circles: K^+, open: K^-) is shown in Figure 2 (different scaling factors) with a parameterization according

to $M_K \propto A_{part}^{\alpha}$ (lines). The multiplicities for MUL 1 are not shown because the errors in integrating the cross sections are larger compared to the other bins. Within the uncertainties of A_{part} we get a common $\alpha = 1.62 \pm 0.21$ for K^+ and K^- and for all beam energies. Values of α larger than unity indicate that the nucleons participate more than once in the kaon production.

Energy	MUL	$\frac{\sigma_{R,MUL}}{\sigma_R}$	$4\pi \frac{d\sigma_K}{d\Omega_{CM}}$ [mb]	T [MeV]
	1	0.41	2.2 ± 0.2	55 ± 4
1.5	2	0.23	4.5 ± 0.4	79 ± 6
AGeV	3	0.18	6.2 ± 0.5	96 ± 7
K^+	4	0.14	7.2 ± 0.5	101 ± 8
	5	0.05	3.3 ± 0.3	93 ± 7
	1	0.44	7.6 ± 0.7	58 ± 5
1.93	2	0.23	14.8 ± 1.2	70 ± 6
AGeV	3	0.16	18.1 ± 1.4	88 ± 7
K^+	4	0.11	21.4 ± 1.6	91 ± 7
	5	0.06	14.8 ± 1.2	97 ± 7
	1	0.41	0.06 ± 0.011	33 ± 3
1.5	2	0.23	0.10 ± 0.012	74 ± 6
AGeV	3	0.18	0.12 ± 0.013	78 ± 7
K^-	4	0.14	0.13 ± 0.014	80 ± 7
	5	0.05	0.07 ± 0.011	90 ± 10
	1	0.44	0.30 ± 0.06	43 ± 3
1.93	2	0.23	0.51 ± 0.07	63 ± 7
AGeV	3	0.16	0.56 ± 0.06	79 ± 10
K^-	4	0.11	0.57 ± 0.07	96 ± 8
	5	0.06	0.46 ± 0.05	81 ± 7

Table 1 *Relative reaction cross sections, K^+ and K^- production cross sections and inverse slope parameters as a function of the centrality for Ni+Ni collisions at beam energies of 1.5 and 1.93 AGeV (preliminary).*

In Figure 3 we present the K^-/K^+ ratio as a function of the impact parameter b for the beam energy 1.5 AGeV (full triangles) and 1.93 AGeV (full squares). Within the error bars the values are constant between 1.8 fm and 6 fm and the averaged ratios are 0.020 ± 0.004 for 1.5 AGeV and 0.031 ± 0.004 for 1.93 AGeV. The ratio for 1.93 AGeV agrees with the value of 0.031 ± 0.005 for non-central and near-central collisions in Ni+Ni measured for the full rapidity range ($\theta_{lab} = 28°$ to $64°$) at the same beam energy [3]. All measured K^-/K^+ ratios for Ni+Ni can be compared with the smaller system C+C [2] and the corresponding inclusive values of 0.025 ± 0.007 for the beam energy 1.8 AGeV and 0.038 ± 0.013 for 2.0 AGeV.

In conclusion, the K^-/K^+ ratio at a given bombarding energy is constant as a function of the centrality of the reaction and the size of the collision system. This observation is in agreement to the hypothesis, that the antikaon yiel d is coupled to the kaon yield via the strangeness exchange reaction $Y\pi \rightarrow K^-N$ (with $Y = \Lambda, \Sigma$).

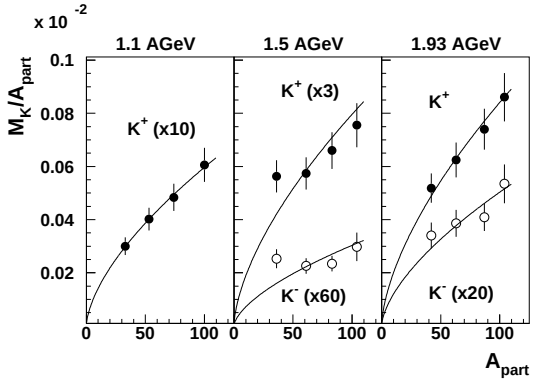

Fig. 2 *Kaon and antikaon multiplicity per A_{Part} as a function of A_{Part} for Ni+Ni collisions at beam energies of 1. 1, 1.5 and 1.93 AGeV (preliminary).*

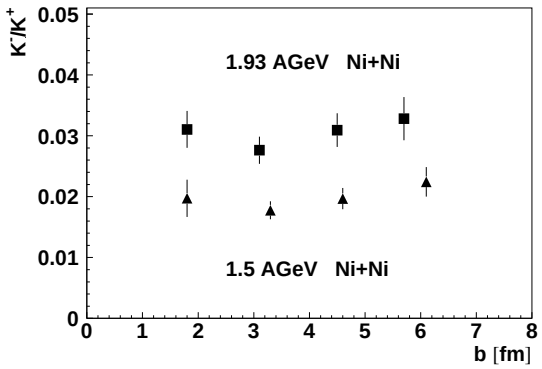

Fig. 3 *K^-/K^+ ratio as a function of the impact parameter b for Ni+Ni collisions at beam energies of 1.5 and 1.93 AGeV (preliminary).*

[1] *GSI Darmstadt* [2] *TU Darmstadt*
[3] *GSI Univ. Frankfurt* [4] *Univ. Marburg*
[5] *GSI Univ. Krakow* [6] *FZ Rossendorf*
[7] *TU Dresden* * *now at Ohio State Univ., Columbus, USA*

References

[1] R. Barth et al., Phys. Rev. Lett. 78 (1997) 4007
[2] F. Laue et al., Phys. Rev. Lett. 82 (1999) 1640
[3] M. Menzel et al., Phys. Lett. B 495 (2000) 26
[4] Y. Shin et al., Phys. Rev. Lett. 81 (1998) 1576

Comparison of First Results of K^+ Production at ANKE with Model Calculations [B]

Ch. Schneider, H. Müller and ANKE Collaboration

Kaon production in the reaction p+C→K^++X has been measured with the ANKE spectrometer [1] at beam energies of 2.3, 1.8, 1.5, 1.2 and 1.0 GeV. The calibration of the data is still in progress, nevertheless the detected and analysed Kaon rates can be compared with the ROC-model [2] calculations if the acceptance and efficiency of the detection process at ANKE is taken into account. Thus the ROC-model was used as a data generator for GEANT simulations of the ANKE side detector system.

In Fig. 1 the detection efficiencies for Kaons from such simulations are shown. They are plotted as a function of the telescope number, normalised to the total number of Kaons. Curve **b** shows the number of Kaons generated in the acceptance range of each considered telescope. The difference to the curve **a** represents the losses due to scattering and due to the gaps between the telescopes. Curve **c** takes into account the loss due to cuts on time of flight and energy loss in the scintillation counters. Curve **d** takes the lifetime of the Kaons on their way through the detector into acount. Curve **e** shows the finally counted particles in the veto counter with a decay time larger than 2.6 ns.

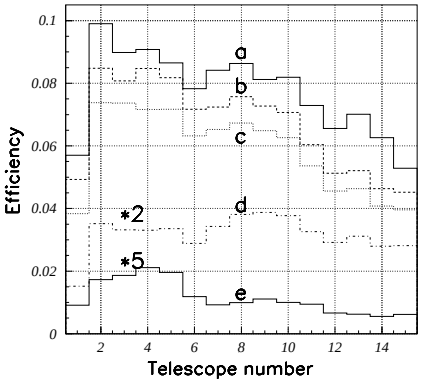

Fig. 1 *Simulation of K^+ verification with the ANKE side detector system as a function of telescope number. The curves are explained in the text.*

Very primilary results of the data analysis for beam energies of 1.0 GeV and 1.2 GeV are shown in Fig. 2. The raw numbers of extracted Kaons for the specified data collecting time are plotted as a function of the mean particle momentum measured in every telescope. A peliminiary normalisation to comparable experiment conditions results in a factor of ∼ 30 [3] between the cross sections at the two energies. The cross sections obtained from the ROC-Geant simulations are plotted in Fig. 3. They take into account all losses described in Fig. 1. The ratio of the measured production rate at 1.0 GeV and 1.2 GeV at the covered forward angle around 0° is comparable to the prediction of our simulation.

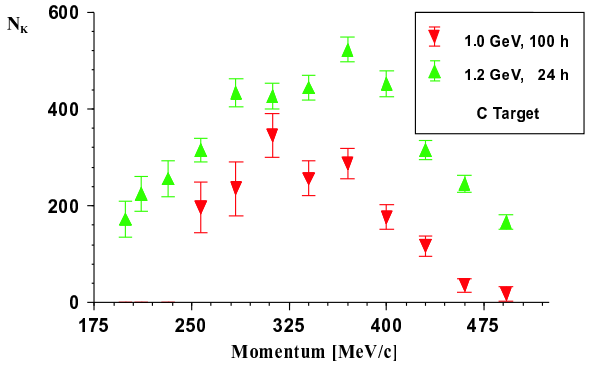

Fig. 2 *Number of indetified Kaons in each telescope from the experimental runs at 1.2 and 1.0 GeV [1]*

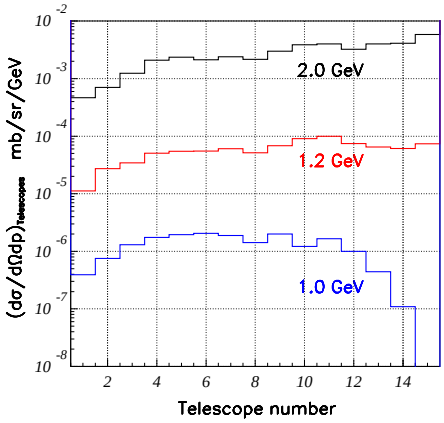

Fig. 3 *Simulated detection cross sections, when the ROC-model is used as a generator for GEANT simulation of the ANKE spectrometer*

References

[1] S. Barsov et al., Nucl. Phys. A 675, 230 (2000)
[2] H. Müller, Z. Phys. A 355, 223 (1996)
[3] M. Büscher et al., publication in preparation

Investigation of the Associated Strangeness Production in the Reaction $pp \to pK^+\Lambda$ [B,K]

K. Möller, S. Dshemuchadse

One of the main topics of the physics program of the COSY TOF collaboration is the investigation of the associated strangeness production in pp reactions at COSY energies up to 2.5 GeV. Quite a lot of data has been accumulated in recent beam times. So, there is an urgent need for analysing these data. To support and speed up the analysis a computer code was developed by the Rossendorf COSY TOF group for analysing the associated strangeness production of Λ hyperons. In this code a new concept was applied to search for primary and secondary tracks in the data.

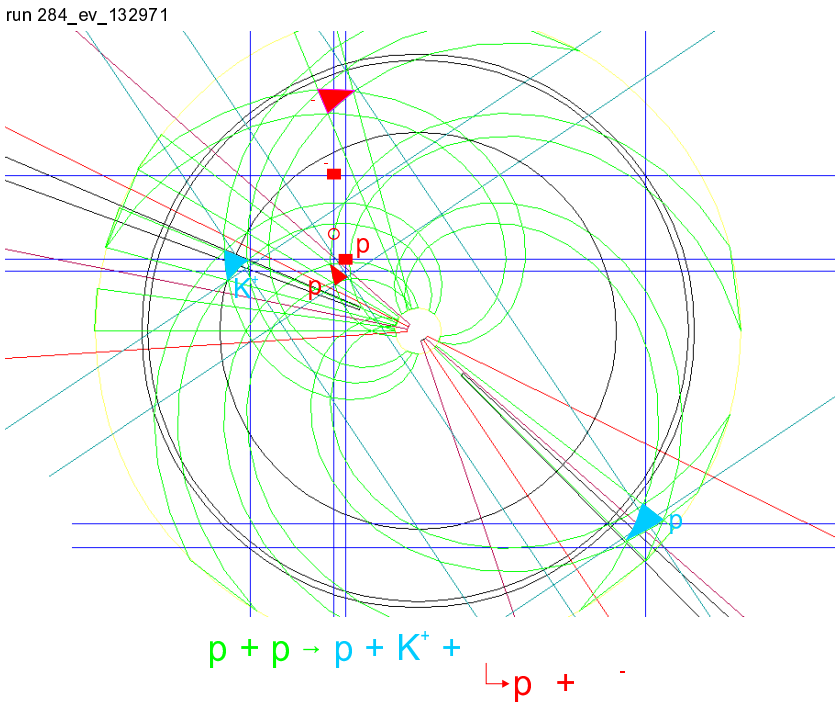

Fig. 1 *A $pK\Lambda$ event at proton momentum 2.85 GeV/c.*

One example is shown in Fig. 1 which demonstrates that the developed computer code is capable of detecting pKΛ events. In the figure a hit display is shown with the following colour assignments for the different position sensitive detector elements: start detector sectors (red), microstrip sector and ring elements (black), fiber hodoscope 1 (blue), fiber hodoscope 2 (blue-green) and the endcap (quirl) elements (green). In the first step of the pp-reaction shown in Fig. 1 a proton, a kaon and a lambda particle are generated with the latter one decaying into a proton and a pion in a secondary process. After the software development was finished in a first check a data tape was reanalysed which was analysed somewhat earlier by the Erlangen COSY TOF group. In most cases good agreement was found in the set of event numbers attributed to $pK\Lambda$ events. For events with event numbers which did not coincide the reason for the disagreement was analysed. This led to a further refinement of the computer codes. Thus by applying two different codes for data analysis the accuracy of the results obtained by the TOF collaboration can be significantly increased. After checking the reliability of the Rossendorf $pK\Lambda$ analysis concept the developed computer code is now ready to be applied to data not yet analyzed up to now. Due to the modular structure of the analysis program (written in C++) the code can easily be modified to analyse also channels other than the associated Λ production, e.g., the Σ production in the channels $pp \to pK^+\Sigma^0$ and $pp \to pK^0\Sigma^+$.

Strangeness in Quark Stars [B]

A. Peshier[1], B. Kämpfer, G. Soff[2]

There is the long standing conjecture that in the cores of neutron stars the matter resides in a deconfined state (cf. [1] and further references therein). Basing on the speculation of self-bound strange quark matter also pure strange quark stars have been predicted (cf. [2] for a reference list for this topic). The theoretical study of this subject was hampered up to now by the poorly known equation of state at large baryon density. However, recently a considerable progress has been made in calculating the equation of state at vanishing baryon density [3].

In [4] we have shown that the lattice QCD data can be described within a quasiparticle model. This model allows to map the lattice results to finite baryon density. Provided the quasiparticle nature does not change, the equation of state is accessible in such a way. Surprisingly, the numerically obtained results at vanishing temperature can be approximated by $p = \alpha e - 4\tilde{B}$, where p is the thermodynamical pressure, e the total energy density, $\alpha = 3.0 \cdots 4.5$ and $\tilde{B}^{1/4} = 200 \cdots 260$ MeV. The ranges of α and $\tilde{B}$ are a direct consequence of the yet existing uncertainty of the lattice QCD results.

Exploiting the given parameterization one can integrate the TOV equations to get the masses and radii of cold, pure quark stars in local β equilibrium, as displayed in Figs. 1 and 2. Due to the β equilibrium a large fraction of the quarks occurs as strange quarks.

Of course, the existence of pressure-free deconfined matter is questionable, therefore, one should study hybrid stars by *interpolating* from our high-density equation of state to nuclear matter densities, where the equation of state is fairly well known.

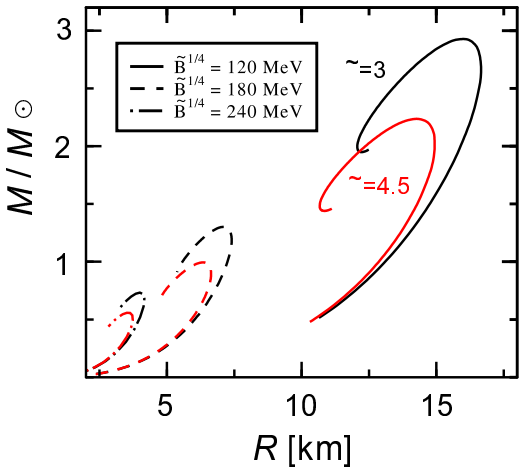

Fig. 1 *The dependence of the mass of pure quark stars with strangeness on the radius for several values of the parameters α and $\tilde{B}^{1/4}$.*

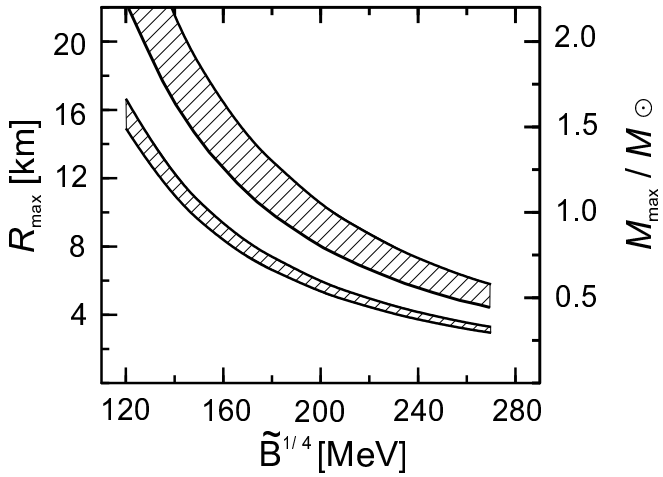

Fig. 2 *Maximum masses (upper hatched band, right scale) and corresponding radii (lower hatched band, left scale) of pure quark stars as a function of $\tilde{B}^{1/4}$. The upper (lower) limit of the bands is for $\alpha = 3$ (4.5).*

[1] *Dept. of Physics, Brookhaven Nat. Lab., Upton, NY 11973, USA*
[2] *Institut für Theoretische Physik, TU Dresden*

References

[1] B. Kämpfer, J. Phys. A 14 (1981) L471, Phys. Lett. B 158 (1984) 121
[2] K. Schertler, C. Greiner, J. Schaffner-Bielich, M.H. Thoma, Nucl. Phys. A 677 (2000) 463
[3] F. Karsch, E. Laermann, A. Peikert, Phys. Lett. B 478 (2000) 447
[4] A. Peshier, B. Kämpfer, G. Soff, Phys. Rev. C 61 (2000) 045203

Electroproduction of Kaons and Light Hypernuclei [B, W]

F. Dohrmann[1,2] for the Jefferson Laboratory Experiment E91-016 collaboration

Jefferson Laboratory experiment E91-016, "Electroproduction of Kaons and Light Hypernuclei" is a study of quasifree production of Kaons on targets of H, D, ^{3}He, ^{4}He, Carbon and Aluminum, at an incident electron energy of 3.245 GeV. For H and D targets, data were also obtained at E = 2.445 GeV. The scattered electron e' and emergent K^+ were detected in coincidence with the use of the HMS and SOS spectrometers, respectively, in Hall C of Jefferson Laboratory. Angular distributions for the (e,e'K^+)Y reactions were measured at forward angles with respect to the virtual photon for $Q^2 \simeq 0.35\,\mathrm{GeV}^2$. Particle identification utilizing time-of-flight detectors together with Aerogel Cerenkov detectors yields clean missing mass spectra [1], and allows subtraction of random backgrounds. The experiment was run in two time periods. The H and D targets were studied near the end of 1996 while the balance of the experiment, namely the $^{3,4}He$ targets were bombarded in the fall of 1999 when the FZR also collaborated on running the experiment. More than 1.4 TB of data were taken during that time.

The fundamental interaction being studied is N(e,e'K^+)Y where Y is either a Λ or Σ and N represents a nucleon. For the H target, the final state can only be a Λ or Σ, but for heavier targets, there is relative motion between the nucleons in the target that results in broadening of the peaks. For the D target, it is possible to separate the two peaks inasmuch as the Fermi broadening is not large compared to the mass difference [2]. For ^{3}He and ^{4}He, very preliminary missing mass spectra being shown in Fig 1, it will be more difficult to separate the yields for the various final states. Even in this early stage of analysis, it is quite clear that the width of the quasifree peak is greater in ^{4}He (more binding) than in ^{3}He.

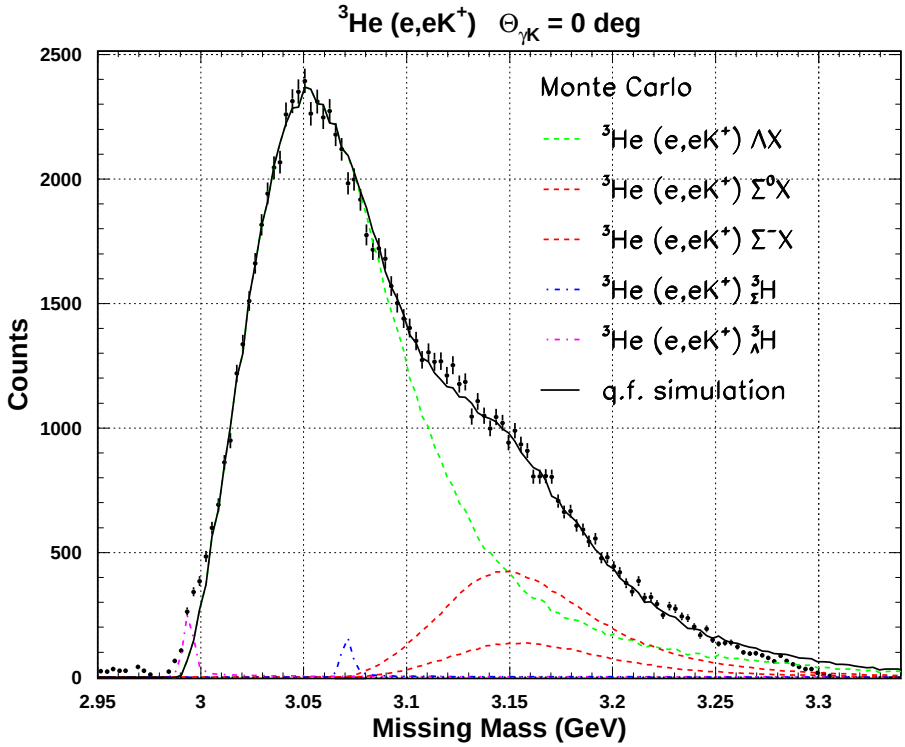

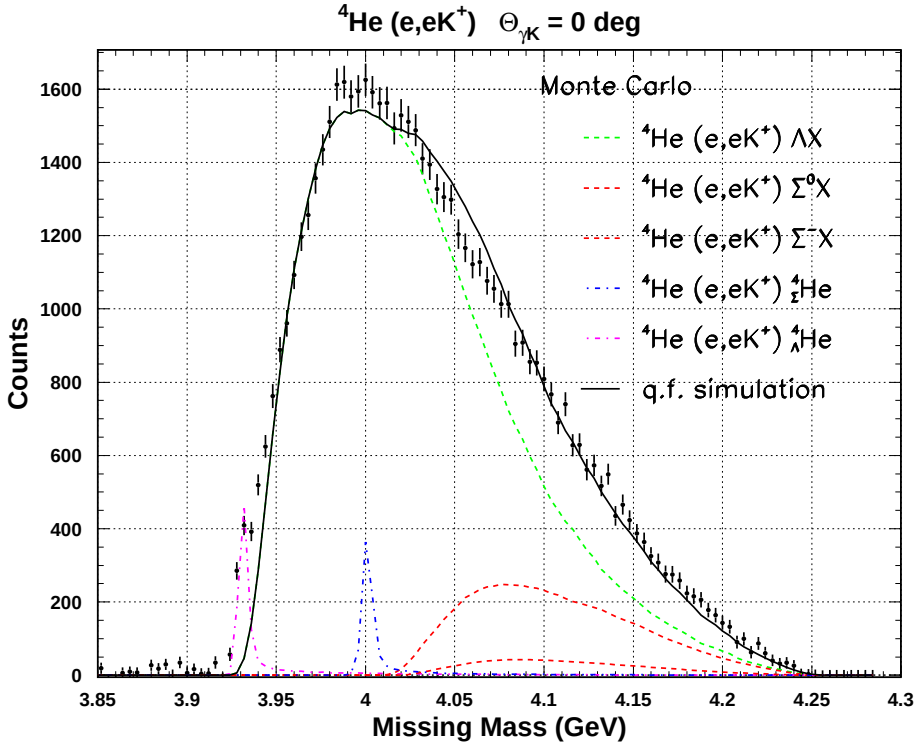

Fig. 1 *Preliminary missing mass spectra for* ^{3}He *and* ^{4}He$(e,e'K^+)$ *reactions for a relative angle of* 0 deg *in the lab between the virtual photon and the Kaon. The various Monte-Carlo simulations for the quasi-free contributions as well as their sum (solid line) are shown. They are preliminary and relatively crude. The location of "bound* Λ *and* Σ*" states is shown merely to suggest possible locations. It should be emphasized that much more analysis is required.*

For D, it is known that there is no bound Λ-nucleon state, but for both ^{3}He and ^{4}He targets we anticipate evidence for a bound hypernuclear states. Although the data shown in the figure are quite preliminary, it appears that bound Λ hypernuclear states are seen. The possibility of bound Σ hyper-nuclei also exists, but it is conjectural at this time. Construction of an optimal Monte-Carlo simulation will require considerably more effort before any conclusions can be drawn. The large number of final state configurations results in complications that must be analyzed prior to extracting final cross sections.

Together with Carbon and Aluminum the complete data set contains five different targets and provides a high-statistics study of the mass dependence of Kaon electroproduction on light nuclei.

[1] *FZR and Physics Division, Argonne National Laboratory, Argonne, Illinois 60439, USA*
[2] *presently Feodor Lynen Research Fellow at Argonne National Laboratory, Argonne, Illinois 60439, USA*

References

[1] ANL Annual Report # ANL99-12, Fig. III-6
[2] D. Abbott et al., Nucl. Phys. A 639 (1998) 205c

Production of ϕ Mesons in Near-Threshold πN and NN Reactions [B,W]

A.I. Titov[1], B. Kämpfer, B.L. Reznik[2]

In previous work [1] we have demonstrated that various observables in the reactions $NN \to \phi NN$ and $\pi N \to \phi N$ show some sensitivity to an admixture of hidden strangeness in the nucleon. It turns out, however, that, within the extended one-boson-exchange model, the effective coupling constants and cut-off parameters are poorly constrained. We have, therefore, continued our analysis to explore the ϕ production mechanism within a conventional one-boson-exchange model by including the recent results of the DISTO collaboration. Our calculated cross sections are displayed in Figs. 1 and 2 together with experimental data.

The data and other constraints of the model parameters are still insufficient to derive a unique set of parameters. Rather there is a wide range of the commonly used cut-off parameter $\Lambda_{\phi\rho\pi}$ entering the $\phi\rho\pi$ vertex. Some observables, such as the total cross section as a function of the excess energy and the angular distribution, are less sensitive to variations of $\Lambda_{\phi\rho\pi}$. Polarization observables and observables related to the subsequent decays $\phi \to e^+e^-$ and $\phi \to K^+K^-$ can serve as further constraints to the parameter space.

A detailed understanding of the ϕ production dynamics, in particular the cross sections at small excess energies, is a necessary prerequisite for a profound analysis of the kaon and dilepton channels in heavy-ion collisions.

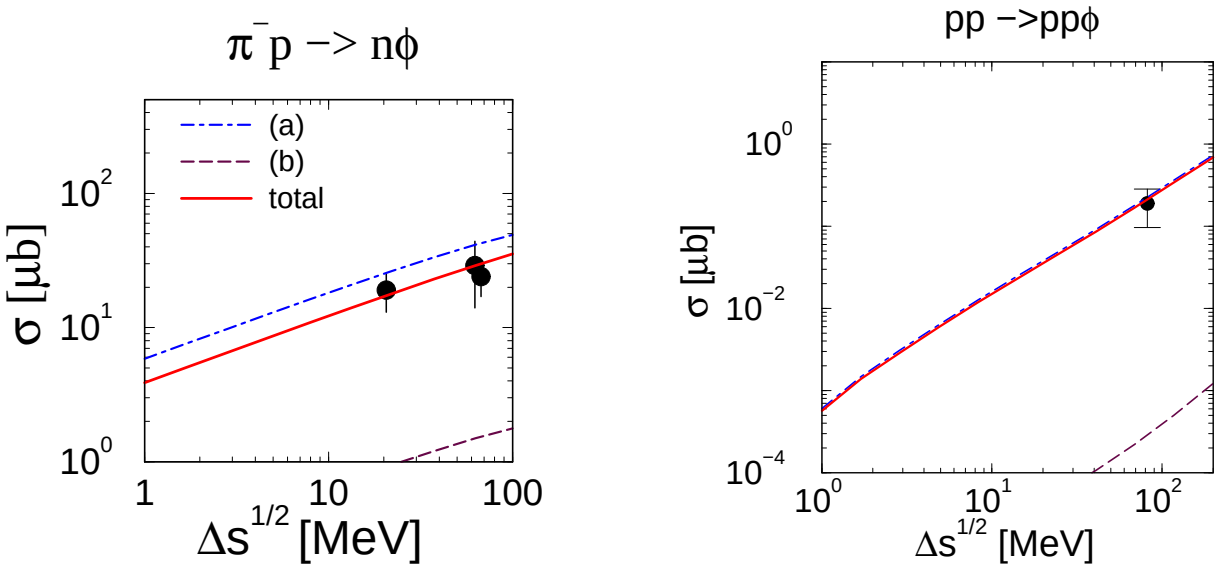

Fig. 1 *The calculated cross sections for the reactions $\pi^- p \to \phi n$ (left panel, data from [3]) and $pp \to \phi pp$ (right panel, data from [4]) as a function of the excess energy above the threshold. Dot-dashed curves: contribution from diagrams with a $\phi\rho\pi$ vertex, dashed curves: contributions from diagrams with direct ϕNN coupling, solid curves: resulting cross sections including interferences. Final state interaction has been included within the Jost function and phase-equivalent potential formalism. For further details see [2].*

[1] *Bogolyubov Laboratory of Theoretical Physics, JINR Dubna, Russia*
[2] *Far-Eastern State University, Vladivostok, Russia*

References

[1] A.I. Titov, B. Kämpfer, V.V. Shkyar, Phys. Rev. C 59 (1999) 999
[2] A.I. Titov, B. Kämpfer, B.L. Reznik, Eur. Phys. J. A 7 (2000) 543
[3] A. Baldini et al., Total cross sections of high energy particles, Springer-Verlag, Heidelberg, 1988
[4] F. Balestra et al. (DISTO Collaboration), Phys. Lett. B 468 (1999) 7

Sub-Threshold ϕ(1020) Meson Production in the Reactions Ni(1.93A·GeV)+Ni and Ru(1.69A·GeV)+Ru [B]

R. Kotte and the FOPI collaboration

First results on systematic investigations of sub-threshold ϕ meson production in heavy-ion reactions measured with the 4π detector system FOPI at GSI have been previously reported [1,2]. About $N_{ev} = 4.7 \cdot 10^6$ ($6.8 \cdot 10^6$) central events comprising about 9% (15%) of the total cross section have been analysed for the system Ni+Ni (Ru+Ru) at 1.93 (1.69) A·GeV. We select candidates of charged kaons measured with the subdetectors Helitron (Hel) and outer Plastic Wall (Pla) within the polar angle and velocity acceptance limits of $\Delta\theta_K$ ($15^o < \theta < 27^o$) and $\Delta\beta_K$ ($0.4 < \beta < 0.85$), respectively. These limits confine a phase space sector located near the region of highest intensity, i.e. at mid-rapidity ($\beta_{cm} \sim 0.7$) and at low transverse momentum [1]. The efficiency-corrected ϕ multiplicity is determined via $P_\phi(\Delta\theta_K, \Delta\beta_K) = \frac{N_\phi(\Delta\beta_K, \Delta\theta_K)}{N_{ev} \cdot \epsilon^2_{det,K}(\Delta\beta_K, \Delta\theta_K)}$ with $N_\phi(\Delta\beta_K, \Delta\theta_K)$ being the number of ϕ's reconstructed from their decay kaons and $\epsilon_{det,K}(\Delta\beta_K, \Delta\theta_K)$ representing the kaon detection efficiency (incorporating the matching efficiency of Hel tracks with Pla hits and the cut efficiency of kaon selection). The efficiency is taken from pseudo kaons, i.e. protons of similar angular and momentum range as kaons [1]. (This method does not work for the FOPI subdetectors CDC and Plastic Barrel, since the latter one alone does not allow for particle identification. There, all efficiencies are included in the ϕ acceptance factor which is determined with the GEANT package simulating the detector response [2]. Since the acceptance depends strongly on the ϕ phase space distribution which is generated as input, e.g. by using a thermal model with temperature T, any ϕ yield extrapolated to 4π would depend on these assumptions, i.e. it would be model dependent.) For the Ni+Ni (Ru+Ru) system, the deduced ϕ multiplicity per central event in the Hel/Pla acceptance given by $\Delta\beta_K$ and $\Delta\theta_K$ amounts to $P_\phi(\Delta\theta_K, \Delta\beta_K) \cdot 10^5 = 4.8 \pm 2.0$ (3.1 ± 1.2).

These numbers can be compared directly with the output of transport approaches when implementing the detector acceptance/geometry and the decay properties of both the ϕ mesons and the daughter kaons. Appropriate transport model calculations have been performed recently [3]. Extending the IQMD transport model to ϕ meson production a total of $3.5 \cdot 10^{-4}$ ($2.2 \cdot 10^{-4}$) ϕ mesons per central event has been calculated for the Ni+Ni (Ru+Ru) system. Filtering the decay kaons through the acceptance limits described by $\Delta\beta_K$ and $\Delta\theta_K$ and taking into account the branching ratio of the decay $\phi \rightarrow K^+K^-$ of 49.1% and the finite kaon lifetime ($c\tau = 3.71$ m) a ϕ yield of $1.8 \cdot 10^{-6}$ ($1.1 \cdot 10^{-6}$) is found for the Ni+Ni (Ru+Ru) system.

The ratio of the yields with/w.o. filtering gives a typical ϕ acceptance of 0.5%. Since the total ϕ rapidity and transverse momentum spectra of the transport approach can be well approximated by an isotropic thermal distribution with $T = 60 - 70$ MeV, quite similar acceptance factors (including the $\phi \rightarrow K^+K^-$ branching) are calculated also within our Monte-Carlo simulations when adopting this effective temperature [1].

For both considered systems, the ϕ yield predicted by the transport model is substantially smaller than the experimental values. Also, an earlier attempt to predict the ϕ production in the Ni+Ni reaction within the framework of another transport approach [4] delivered deviations of similar size though the involved elementary cross sections (esp. $pp \rightarrow pp\phi$) are quite different. The reason for this strong underestimation of ϕ meson production in both central heavy-ion reactions investigated at beam energies below the nucleon-nucleon threshold (2.54 A·GeV) is not yet understood. Therefore, further theoretical work is advisable [5].

References

[1] R. Kotte (FOPI collaboration), Proc. Int. Workshop XXVIII, Hirschegg, Austria, Jan. 2000, p. 112
[2] N. Herrmann (FOPI collaboration), Nucl. Phys. A 610 (1996) 49c
[3] C. Hartnack and J. Aichelin, private communication
[4] W.S. Chung, G.Q. Li, and C.M. Ko, Nucl. Phys. A 625 (1997) 347
[5] H.W. Barz, B. Kämpfer, G. Wolf, and M. Zétényi, this Report

The Role of Three-Body Collisions in ϕ Meson Production Processes Near Threshold [B]

H.W. Barz, B. Kämpfer

Currently there is much interest in subthreshold production of heavy mesons in relativistic nuclear collisions. It is expected that measurements will reveal the change of the properties of mesons in dense and hot nuclear matter. Recent measurements [1] of ϕ mesons in Ni+Ni and Ru+Ru collisions point to relatively large production cross-sections which could not be understood till now within the framework of transport models [2].

Therefore, we study whether three-body collisions could remarkably contribute to the production of ϕ mesons in heavy-ion collisions. Such processes have the advantage that three nucleons can share their energy. The cross section for the reaction N+2N $\rightarrow \phi$ + 3N is calculated using tree-level diagrams indicated in Fig. 1. If the momentum of an intermediate particle (ρ, π, B) in a diagram gets on shell its value becomes singular and the diagram describes two consecutive two-body processes. Such two-step processes are usually considered in the transport models. Therefore, we have defined the genuine tree-body process after separating the singular parts from the diagrams. The upper line in Fig. 2 shows the cross section for this genuine process. However, if absorption processes in the medium are included this cross section is strongly diminished and can even take a negative value. The two-step processes with intermediate π and ρ mesons give together a larger cross section than that calculated with the three-body diagrams, see Fig. 2.

We conclude that genuine three-body processes are not important in nuclear matter as most of the strength can be evaluated via consecutive two-body reactions. In the case considered here the two-step processes slightly overestimate the cross section. However, it is necessary that all intermediate particles which can reach the energy shell are treated properly within transport-model calculations as they essentially contribute to particle production.

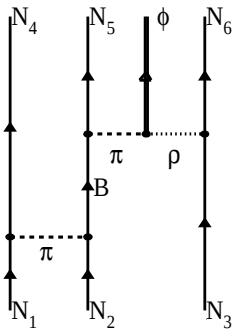

Fig. 1 *Topology of tree-level diagrams contributing to the three-body ϕ meson production. Further diagrams are used arising from time reordering and particle exchanges.*

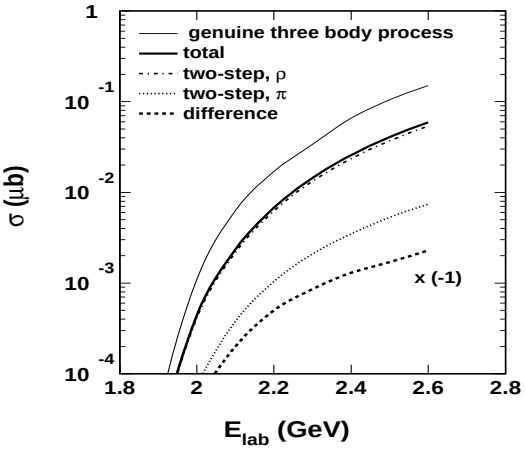

Fig. 2 *Cross section of ϕ meson production by a proton hitting a proton in a proton environment. The thin line gives the three-body cross section without intermediate rescattering whereas the other lines show the results with rescattering. For further details consult [3].*

References

[1] R. Kotte (FOPI collaboration), Proc. Int. Workshop XXVIII, Hirschegg, Austria, 2000, p. 112
[2] W.S. Chung, G.Q. Li and C.M. Ko, Nucl. Phys. A 625 (1997) 347
[3] H.W. Barz and B. Kämpfer, Nucl. Phys. A 683 (2001) 594

Cross Sections for ϕ Meson Production in ρ Meson–Baryon Collisions [B,A]

H.W. Barz, M. Zétényi[1]

Recently ϕ meson production was measured in subthreshold Ni+Ni and Ru+Ru collisions by the FOPI collaboration at the heavy-ion synchrotron at GSI Darmstadt [1]. The ϕ meson yield found in these experiments is considerably larger than the predictions of Boltzmann-Ühling-Uhlenbeck (BUU) calculations [2]. A possible explanation could be the existence of new ϕ production channels that have not been considered so far in BUU calculations. Therefore, we study the ϕ production cross sections in ρ-N and ρ-Δ collisions.

We calculate the isospin averaged cross sections in a one-boson exchange model. In this case a single pion exchange diagram contributes to both processes. The differential cross section can be written as

$$\frac{d\sigma}{d\Omega} = \frac{1}{64\pi^2 s}\frac{|\mathbf{p}_{out,CM}|}{|\mathbf{p}_{in,CM}|}|\mathcal{M}|^2. \tag{6}$$

The quantity $|\mathcal{M}|^2$ represents the squared matrix elements summed over the final and averaged over the initial spin and isospin states. These expressions read for the ρ-N channel

$$|\mathcal{M}|^2 = 32\left(\frac{A_{\rho N\to\phi N}}{p_\pi^2 - m_\pi^2}\right)^2 m_N^2\left(p_N\cdot p_{N'} - m_N^2\right)\left((p_\rho\cdot p_\phi)^2 - m_\rho^2 m_\phi^2\right) \tag{7}$$

and for the ρ-Δ channel

$$|\mathcal{M}|^2 = \frac{16}{9}\left(\frac{A_{\rho\Delta\to\phi N}}{p_\pi^2 - m_\pi^2}\right)^2 (p_\Delta\cdot p_N + m_\Delta m_N)\left((\frac{p_\Delta\cdot p_N}{m_\Delta})^2 - m_N^2\right)\left((p_\rho\cdot p_\phi)^2 - m_\rho^2 m_\phi^2\right). \tag{8}$$

Here, the incoming four-momenta are denoted by p_ρ, p_Δ and p'_N while the p_N and p_ϕ are the outgoing momenta. The factors A_i are given by $A_{\rho N\to\phi N} = (f_{\pi NN}f_{\pi\rho\phi}/m_\pi m_\phi)F_{\pi NN}(p_\pi^2)F_{\pi\rho\phi}(p_\pi^2)$ and $A_{\rho\Delta\to\phi N} = (f_{\pi N\Delta}f_{\pi\rho\phi}/m_\pi m_\phi)F_{\pi N\Delta}(p_\pi^2)F_{\pi\rho\phi}(p_\pi^2)$. Substituting the appropriate values for the coupling constants f_i and the cutoff parameters appearing in the form factors $F_i(p_\pi^2)$ and integrating Eq. (1) numerically over the angle we obtain the total cross sections. Their values are displayed in Fig. 1 as a function of the CM energy above threshold using the peak masses of the resonance states involved. For comparison we have included the cross section for the process $\pi + N \to N + \phi$ [2]. The obtained cross sections for ϕ meson production in ρ channels are much higher than that of the π-N channel, therefore the ρ-baryon channels can essentially contribute to ϕ production in heavy-ion collisions despite their relative small abundances.

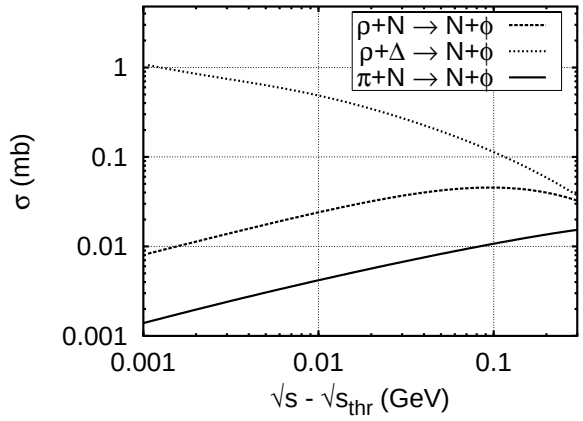

Fig. 1 *Total cross section of ϕ meson production in the reactions $\rho + N \to N + \phi$ and $\rho + \Delta \to N + \phi$. For comparison the cross section for the process $\pi + N \to N + \phi$ is also included. Note that the threshold for the $\rho+\Delta$ process lies in the incoming channel.*

[1] *KFKI Budapest, Research Institute for Particle and Nuclear Physics, H-1525 Budapest, POB 49, Hungary*

References

[1] R. Kotte (FOPI collaboration), Proc. Int. Workshop XXVIII, Hirschegg, Austria, 2000, p. 112
[2] W.S. Chung, G.Q. Li and C.M. Ko, Nucl. Phys. A 625 (1997) 347

Influence of ρ Meson Channels on ϕ Meson Production in Heavy-Ion Collisions [B,A]

H.W. Barz, B. Kämpfer, Gy. Wolf[1], M. Zétényi[1]

The study of meson production in heavy-ion collisions near threshold gives insight in the particle properties in dense matter. Furthermore information on the equation of state is provided as the particle production rates depend sensitively on the potentials the collision partners feel. Recently, the ϕ meson production was measured in reactions of Ni+Ni and Ru + Ru at energies of 1.93 and 1.69 A·GeV, respectively [1]. Extrapolations from the limited phase space available point to a larger cross section than standard Boltzmann-Ühling-Uhlenbeck (BUU) calculations [2]. These calculations usually do not consider the production of ϕ mesons by elementary collisions of ρ mesons and baryons. The cross sections of these reactions are larger than those of pions. To study the influence of these channels a version of the BUU code [3] was used which explicitly treated ρ mesons created in pion-pion collisions or in resonance decays. This version was applied to central collisions of Ru+Ru with an impact parameter smaller than 4.2 fm. We found that $2 \cdot 10^{-3}$ ϕ mesons are produced per event and roughly 2/3 of them stem from ρ-N and ρ-Δ collisions. In Fig. 1 we show the transverse mass spectrum at midrapidity from which an effective temperature of $T = 85$ MeV is deduced. Taking into account the detector acceptance of the FOPI apparatus [1] the expected ϕ meson distribution in the rapidity-transverse momentum plane is shown in Fig. 2, altogether there are $0.8 \cdot 10^{-5}$ particles per central event. This number is still by about a factor of four smaller than the experimental value of $(3.1 \pm 1.2) \cdot 10^{-5}$ [4].

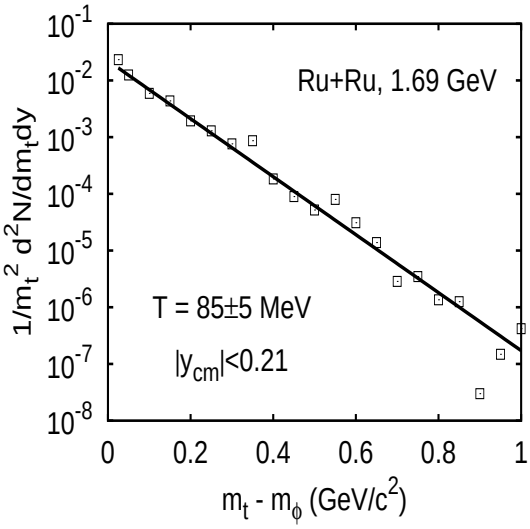

Fig. 1 *Calculated transverse mass spectrum (open squares) of ϕ mesons at midrapidity. The solid line shows the fit to the Boltzmann distribution $exp(-m_t/T)$.*

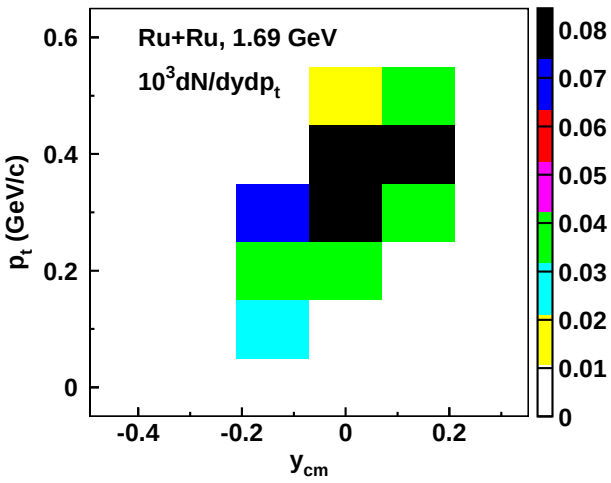

Fig. 2 *Calculated distribution of $dN/dydp_t$ of ϕ mesons per event in the rapidity - transverse momentum plane taking the FOPI detector acceptance into account.*

[1] *KFKI Research Institute for Particle and Nuclear Physics, H-1525 Budapest, POB 49, Hungary*

References

[1] R. Kotte (FOPI collaboration), Proc. Int. Workshop XXVIII, Hirschegg, Austria, Jan. 2000, p. 112
[2] W.S. Chung, G.Q. Li and C.M. Ko, Nucl. Phys. A 625 (1997) 347
[3] Gy. Wolf, W. Cassing, U. Mosel, Nucl. Phys. A 552 (1993) 549
[4] R. Kotte, this Report

Production of ω Mesons in pp Collisions at Q = 89 MeV

R. Dressler, I. Fröhlich[1], E. Grosse, W. Kühn[1], H.-W. Pfaff[1], J. Ritman[1]
for the DISTO collaboration

In the course of the experiments with the two-arm DISTO [1] spectrometer at the SATURNE accelerator in Saclay the exclusive production of ω mesons was measured at excess energies Q = 89, 207, and 320 MeV ($Q = \sqrt{s} - \sqrt{s_0}$). These beam energies are well suitable to close the considerable gap between the near-threshold data obtained in SPEC III experiments [2] at excess energies Q < 30 MeV and data at larger Q > 400 MeV (see e.g. [3]).
Data at the highest beam energy in DISTO experiments were analyzed and published so far [4-7]. The investigation of all data is still in progress. In this contribution first preliminary results on the analysis of the data at the lowest excitation energy for the ω meson are presented.
The exclusive reactions pp→ppη and pp→ppω were identified via the three pion decay (i.e. $\eta, \omega \to \pi^+\pi^-\pi^0$), where the braching ratios are taken from [8]. Only events with one negative and three positive charged particles were used in the data processing of η and ω mesons. A good separation was achieved for π^+ and p, also the π^- was clearly observed as shown in [4-6] using the light signal from the water filled Cerenkov detectors together with the particle momentum. Fig. 1 shows the $(M^{pp\pi^+}_{\rm inv})^2 - (M^{\pi^-}_{\rm miss})^2$ distribution, whereas the symbol $(M^{x}_{\rm inv/miss})$ denotes the invariant or the missing mass of the particle or particle combination x. In Monte Carlo simulations only the region above 0.4 $(\mathrm{GeV/c^2})^2$ was populated with η and ω mesons. Therefore, this behavior was used to suppress pure 4 body events (pp$\pi^+\pi^-$) in the data analysis, which are peaked at $(M^{pp\pi^+}_{\rm inv})^2 - (M^{\pi^-}_{\rm miss})^2 = 0\ (\mathrm{GeV/c^2})^2$.
To improve the resolution of the $(M^{pp\pi^+\pi^-}_{\rm miss})^2$ spectrum a kinematical refit assuming a missing π^0 meson was applied in a second fit procedure. The spectrum after this refit is shown in Fig. 2. The arrows depict the expected positions for the mesons taken from [8]. The main source of the remaining background is the non-resonant $\pi^+\pi^-\pi^0$ production. Unfortunately, the exact form of the background is unknown. Therefore, the spectrum was fit with Gauss peaks for the η and ω signals and the background was parametrized with a polynomial of third order and a wide Gaussian curve. In Fig. 2 are also depicted the fit result (full), the η and ω peak (dashed), and the background (dotted), respectively.

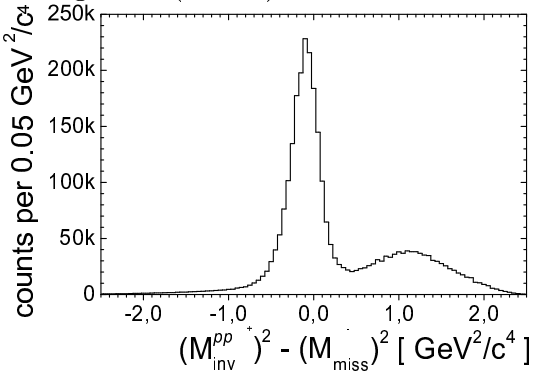

Fig. 1 *Distribution of* $(M^{pp\pi^+}_{\rm inv})^2 - (M^{\pi^-}_{\rm miss})^2$.

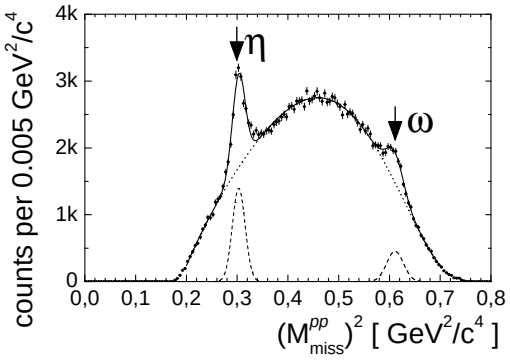

Fig. 2 $(M^{pp}_{\rm miss})^2$ *spectrum after kinematic refit.*

[1] *II. Physikalisches Institut, Justus-Liebig-Universität Gießen*

References

[1] F. Balestra et al., Nucl. Instr. Meth. A 426, 385 (1999)
[2] F. Hibou et al., Phys. Rev. Lett. 83, 492 (1999)
[3] R. Baldi et al., Phys. Lett. B 68 (1977) 381
[4] F. Balestra et al., Phys. Rev. Lett. 81, 4572 (1998)
[5] F. Balestra et al., Phys. Lett. B 468, 7 (1999)
[6] F. Balestra et al., Phys. Lett. B 491, 29-35 (2000)
[7] F. Balestra et al., Phys. Rev. C 63, 024004 (2001)
[8] D.E. Groom et al., Eur. Phys. J. C 15, 1 (2000)

Production of a_0^+ Mesons in the Reaction $pp \to da_0^+$ [B]

H. Müller

The structure of the lightest scalar mesons $a_0(980)$ and $f_0(980)$ is not well understood (see the "note on scalar mesons" of the particle data group [1]). In a recent paper [2] the necessity of new measurements of a_0 production and of a_0 branching ratios for clarifying the a_0 structure has been emphasized. Such an experiment is presently prepared at COSY [3].

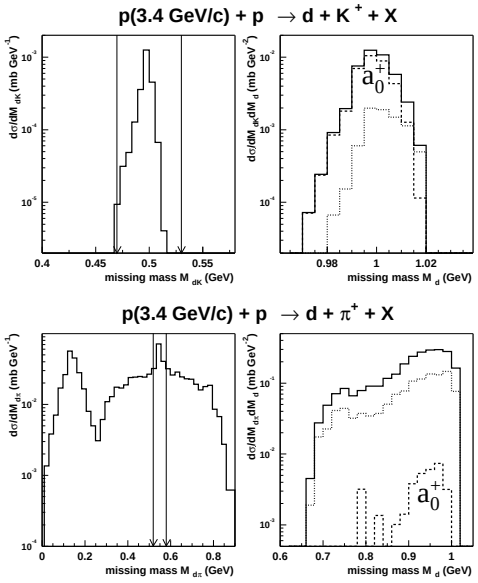

Fig. 1 *Missing mass distributions for the reactions $pp \to dK^+X$ (upper panels) and $pp \to d\pi^+X$ (lower panels) calculated at incidence momentum* 3.4 GeV/c *for polar angles $\Theta \leq 10°$ and 1.5% momentum resolution. The two arrows in the left hand panels indicate the windows in the M_{dK} and $M_{d\pi}$ distributions, which are used in the calculation of the M_d distribution shown in the right hand panels. The dashed histograms indicate the contributions from the reaction $pp \to da_0^+$, the dotted histograms those of the nonresonant channels $pp \to dK^+\bar{K}^0$ and $pp \to d\pi^+\eta$, respectively.*

Although in Ref. [2] predictions for the reaction $pp \to da_0^+$ at COSY energies have been given, no attempt has been made to compare the channels with a_0^+ production and subsequent decays, $pp \to da_0^+ \to dK^+\bar{K}^0$ and $pp \to da_0^+ \to d\pi^+\eta$, with the nonresonant channels $pp \to dK^+\bar{K}^0$ and $pp \to d\pi^+\eta$. For the measurement of a_0^+ production the latter channels might be rather disturbing if they are of high intensity. Another source of background are multipion channels, where two or three pions may have an invariant mass similar to the η mass. In Fig. 1 ROC model [4] predictions of the cross sections for a_0^+ production *together* with an estimate of the cross sections for the nonresonant and the multipion channels at the highest COSY energy are given. In these calculations the a_0^+ is considered as a usual quark model state with two decay channels $a_0^+ \to K^+\bar{K}^0$ and $a_0^+ \to \pi^+\eta$. The missing mass distributions of two particles are used to select the mass of the third particle defining thus the final channel. Then the signal from the a_0^+ is looked for in the missing mass distribution of the d. In case of strangeness production there are no background reactions, while channels with three or four pions may contribute to the η window in the $M_{d\pi}$ distribution. The difference between the full and the dotted histogram in the lower right panel of Fig. 1 is the contribution from these pion channels.

The main difficulty consists in differentiating between the channels via the a_0^+ meson and the channels with nonresonant production, especially in case of the channel $pp \to dK^+\bar{K}^0$, where the missing mass M_d varies only by about half the assumed width of the a_0^+ meson. The value of the calculated cross section for a_0^+ production is closely related to the assumption that the a_0^+ consists of light quarks. For the direct population of the channel $pp \to dK^+\bar{K}^0$ the creation of a $d\bar{d}$ and a $s\bar{s}$ pair is necessary. Strange quark production is suppressed and, therefore, the larger contribution to the final channel $dK^+\bar{K}^0$ comes from an intermediate a_0^+. In case of the decay channel, $a_0^+ \to \pi^+\eta$, the ROC model predicts higher cross sections for the nonresonant channel than for a_0^+ production. Therefore, the measurements should be carried out with high statistics.

References

[1] C. Caso et al., Eur. Phys. J. C 3 (1998) 1
[2] V. Y. Grishina et al., Eur. Phys. J. A 9 (2000) 2, 277, nucl-th/0007074
[3] V. Chernyshev et al., COSY Proposal #55: Study of a_0^+ mesons at ANKE (1997), cf. http://ikpd15.ikp.kfa-juelich.de:8085/doc/Anke.html
[4] H. Müller, Eur. Phys. J. C 18 (2001) 563, hep-ph/0011350

Tests of the First HADES Drift Chamber MDCIII [B,G,W]

R. Dressler, W. Enghardt, O. Fateev[1], E. Grosse, K. Heidel, J. Hutsch, R. Kotte, L. Naumann, M. Sobiella

The final design of the large trapezoidal low-mass drift chambers (MDCIII) of the HADES spectrometer tracking system has been performed at the detector laboratory of the FZ Rossendorf [1]. These drift chambers consist of 6 modules with an active area of 2.20 m^2 for each plane and a drift cell size of 8x12 mm^2. Each module has 6 drift cell layers, i.e. 6 anode and 7 cathode frames. The anode frames contain alternately signal wires (tungsten gold-coated, $\emptyset = 20$ μm) and field wires (aluminium, $\emptyset = 100$ μm) with a distance of 6 mm from each other. The wires in the anode frames have orientations of $-40°, +20°, -0°, +0°, -20°$ and $+40°$, respectively, whereas the wires in the cathode frames (aluminium, $\emptyset = 80$ μm) have always the same orientation $+90°$ and a distance of 3 mm. Over the last two years we have solved all physical and technical problems of the design and production of the MDCIII. A full size prototype was finished in February 2000, consisting of only one anode frame (orientation $+0°$) between two cathode frames and in addition the other 10 frames without wires. Thus, the total volume of this prototype (150 l) matches the volume of a final MDCIII sector. A mixture of helium and iso-butan (60% He, 40% i-C_4H_{10}) was used for test measurements, which should be applied in real experiments. A stable gas mixture can be guaranteed by a flow of 10 l/h because the leakage rates of both gas components differ slightly (0.15 l/h at a level of 0.5 l/h). The results of first measurements are depicted in the following figures. Fig. 1. shows the current versus the high voltage. It is obvious to see, that external light sources (e.g. fluorescent tubes) dramatically reduce the break-through voltage, due to the emission of photo electrons from the Al wires.

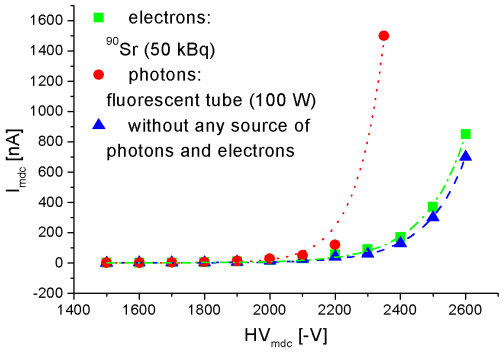

Fig. 1 *Current versus supplied high voltage for different working conditions.*

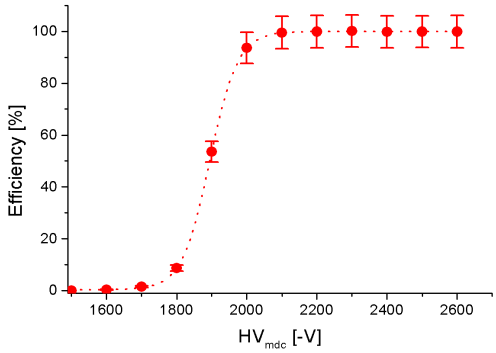

Fig. 2 *Counter efficiency versus supplied high voltage for the prototype.*

The counting characteristic of the prototype is depicted in Fig. 2. A ^{90}Sr source (50 kBq) was used to deliver electrons, which are additionally detected in a master scintillator telescope (20x20 mm^2), a 1 mm thick scintillator in front of the prototype and a 5 mm thick scintillator behind. The signal from the anodes was amplified by a factor of 50 with a fast current sensitive preamplifier [2] and further processed with NIM and CAMAC modules. Up to a high voltage of -2600 V the prototype works without break through. A large counting plateau of 500 V was found above -2100 V. Nearly hundred percent counter efficiency was reached for the individual drift layers and a value of 98% was determined for coincident signals in all six drift layers.

[1] *JINR, Dubna, Russia*

References

[1] http://www.fz-rossendorf.de/FWK/hp/hades.html
[2] K. Heidel et al., this Report

Status Report of the HADES Drift Chamber Read Out [B, G, W]

K. Heidel, R. Dressler, O. Fateev[1], R. Kotte, L. Naumann

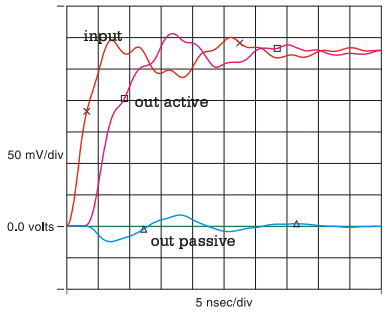

Fig. 1 *Crosstalk output active/passive (8%) for a 24 cm long PCB connector and a 27 cm long FPC cable.*

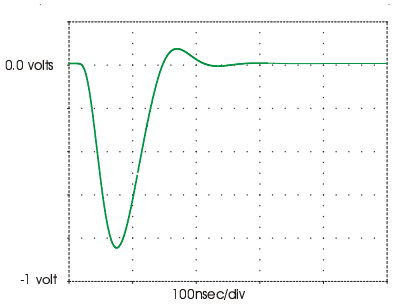

Fig. 2 *Simulated output signal for a 10 μA current signal and a detector capacity of 30 pF.*

The first module out of six multiwire drift chambers (MDC) designed for plane III of the HADES dielectron spectrometer [1] at GSI Darmstadt has been built and tested successfully [2]. The following report resumes the results of the electronics tests.

1. Simulation: In order to avoid secondary transmission line effects accurate pre-layout simulations, including crosstalk and reflection, have been performed for the printed circuit boards (PCB) developed to guide the signals from the MDC sense wires to the front-end electronics. The layout has been designed as a four-layer PCB with a thick dielectric between signal and ground layers and conductor widths of 0.1 mm to match the input impedance ($Z_0 = 115\ \Omega$) of the daughterboards (analog boards with ASD8 chips [3]). The simulation (cf. Fig. 1) yielded typical crosstalks of less than 8% for the common configuration of PCB and flex print cable (FPC [4]), where the latter one connects PCB and daughterboards. The capacity of MDC sense wire, PCB, and FPC, which is important for the input noise characteristics, was measured directly to be about 30 pF, depending on the wire length.

2. Pulse characteristics: A wire chamber acts as a current source with signals depending on the cell geometry, the gas filling and the electric field. A current-sensitive amplifier with a gain of $dV_{out}/dI_{in} = 100$ mV/μA has been developed [5] to match the small rise time of several ns (according to the collection time of electrons produced near to the sense wire) and the long fall time of about 50 - 100 ns (slow ion drift towards the cathode and field wires). Fig. 2 shows the result of the simulation for a 10 μA current signal. It is in agreement with the amplitude measured at the real amplifier output.

3. Concept of grounding: The front-end electronics consisting of daughterboards (incorporating the ASD8 chips with preamplifier, shaper, and discriminator; thus delivering logical time-above-threshold signals) and motherboards (carrying the TDC's to convert the information) is mounted at the edges of the detector frames. In order to obtain an optimum signal-to-noise ratio special attention has been payed to the grounding principle. The most effective grounding methods with respect to low noise level and small r.f. reception was figured out to be the following: 1) Using short flexible cables with high cross section, all PCB cards and also all analog and digital ground points of the daughterboards have been connected to a broad self-adhesive copper foil glued onto the frame below the motherboards. 2) A thick copper-track loop has been installed around the frame to conduct the reverse current (total 25 A!) back from the daughterboards and motherboards. With this arrangement an unrivaled low noise level of 20 mV (measured at the analog output of a daughterboard) without any disturbing r.f. crosstalk, e.g. arising from the 5 MHz quartz oscillator (clock) operating on the motherboard, has been attained.

[1] *JINR, Dubna, Russia*

References

[1] C. Müntz, for the HADES collaboration, Nucl. Phys. B 78 (1999) 139
[2] F. Dohrmann et al., this Report
[3] F.M. Newcomer et al., IEEE (1993) 630
[4] C. Müntz; http://www-hades.gsi.de/mdc/internal/techinfo/fpc/
[5] H. Langenhagen, FZ-Rossendorf, private information

First Beam Exposition of the HADES Drift Chamber MDCIII at SIS [B,G,W]

F. Dohrmann[1], R. Dressler, W. Enghardt, O. Fateev[2] E. Grosse, K. Heidel, K. Kanaki, R. Kotte, L. Naumann, M. Sobiella

The HADES spectrometer including all major detector units, read-out, data-acquisition and trigger electronics has been tested in the commissioning beam time in November 2000. It consists of ring imaging Cherenkov counters, multiwire drift chambers (MDC) of planes I to III, time of flight scintillation hodoscopes (TOF) and pre-shower modules [1]. The first large-area drift chamber MDCIII for the third tracking plane produced at FZ Rossendorf was installed in sector four of the HADES spectrometer (Fig. 1).
A 1.5 AGeV carbon beam with an intensity of $5x10^6$ per spill hits a carbon target. The spill length amounted to 5 seconds. Most of the reaction products crossing the spectrometer were protons and pions. The chamber volume of 150 l has been filled with a gas mixture of 40% iso-butane and 60% helium at a flow rate of 10 l/h. The leakage rate was 0.5 l/h

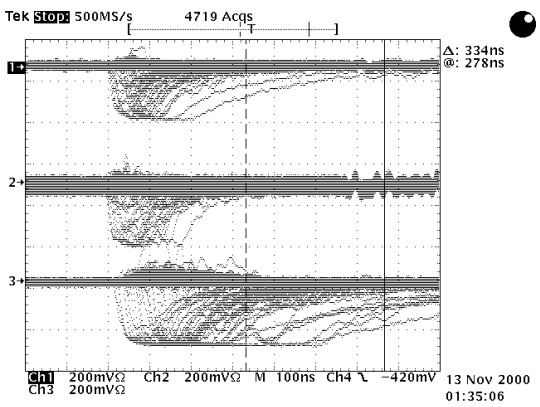

Fig. 2 *The analog signals monitored with a scope. The signals shown from top to bottom were measured on MDC planes I to III.*

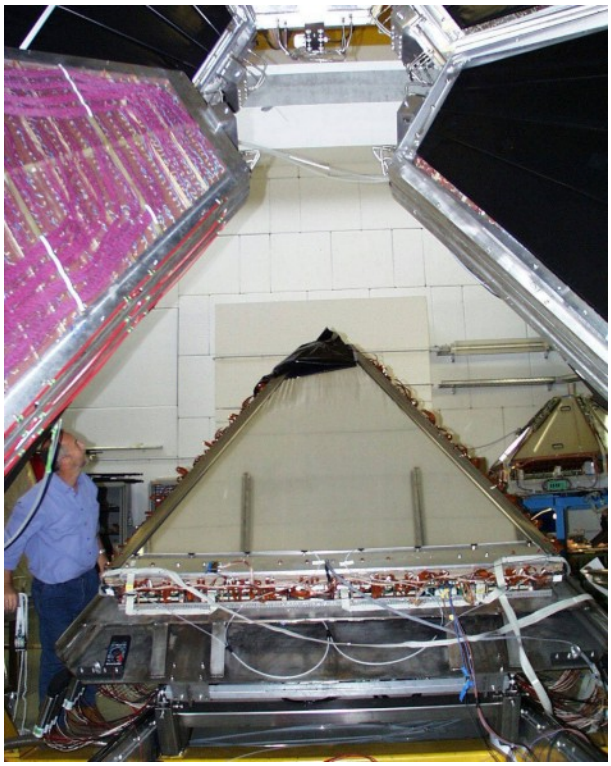

Fig. 1 *MDCIII mounted on the support frame of the HADES spectrometer. Under normal working condition the drift chambers are hidden inside the spectrometer core.*

The applied high voltage amounts to -2 kV for both the cathode and field wires. A selected anode wire is connected to an analog output to check the amplified signals as shown in Fig. 2. The shape of the signal shows a risetime of 30 ns up to the saturation level of the preamplifier.
The MDCIII is equipped with dedicated preamplifier/shaper/discriminator boards inserted into motherboards which itself contain the digitizers (TDC). These daughter- and motherboard components are mounted onto the detector frame under accurate consideration of the grounding [3].

The data acquisition was triggered by the TOF multiplicity $\geq$ 4. A typical TDC spectrum is shown in Fig. 3. The drift velocity was estimated to be 33 μm/ns based on a drift time distribution of 180 ns (FWHM) and the lateral half cell size of 6 mm. There is no visible effect of the strong magnetic field (0.2 T), created by superconducting solenoids in front of the MDCIII, onto the drift time spectrum.

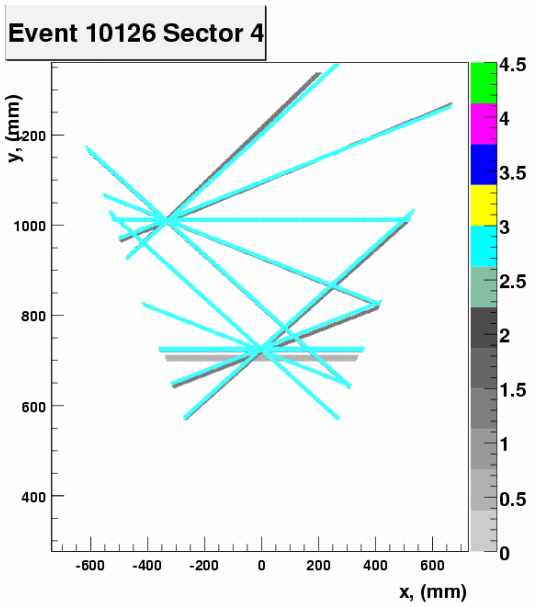

Fig. 4 *Two prongs of an event align between the target and the points of intersection in all three MDC's of sector four (bottom) of the HADES spectrometer. Each prong is characterised by the point of intersection of all fired signal wires in the two dimensional projection plane. The MDC plane numbers have been labeled by colors.*

[1] *ANL, Argonne, USA*
[2] *JINR, Dubna, Russia*

References

[1] http://www-hades.gsi.de
[2] H. Alvarez-Pol, privat information
[3] K. Heidel et al., this Report

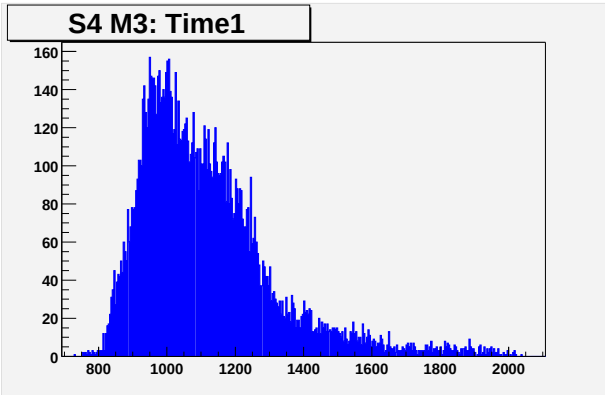

Fig. 3 *Drift time distribution of leading electrons in one anode layer of MDCIII (0.5 ns/channel). The time measurement started by a common signal, created by the TOF trigger, and stopped by an individual anode signal.*

A stereo optical positioning system [2] monitors with a resolution of 1 μm the three dimensional displacement between the MDC's before and behind the magnet. The mean observed displacement during all runs was less than 10 μm.
Fig. 4 shows as a highlight of the commissioning, a plot of the reconstruction of the linear flight paths of charged particles through three MDC planes without magnetic field. In each drift chamber the hit trajectory is defined by at least five anode layers giving a coincident signal. The hit positions have been defined by the dimensions of the drift cells only. The drift time information is not used for this plot.

Probing the Vector Meson Spectral Function by Multidifferential Cross Sections [B,W]

B. Kämpfer, O.P. Pavlenko[1], Gy. Wolf[2]

The starting experimental programme at the new detector facility HADES at SIS/GSI Darmstadt offers the access to dileptons in various reactions of heavy ions and hadrons (pions and protons) with various nuclear targets. One motivation of such experiments is the study of the in-medium change of the vector meson spectral functions. Within various models vastly different predictions are available ranging from a simple shift of the pole position of the spectral function to a strong broadening up to a fragmentation due to particle-hole excitations caused by the ambient matter.

While a moderate broadening of the most sensitive ρ meson spectral function leads probably to a disappearance of the ρ peak in the invariant mass spectrum $d\sigma/dM^2$, we have shown in [1] that, within a schematic blast wave model, measuring the double differential cross section $d\sigma/dM^2 dM_\perp^2$ in a sufficiently restricted interval of the transverse mass $M_\perp$ as function of the invariant mass M still allows to identify the ρ signal. As an example, in Fig. 1 the dilepton emission rate is displayed. Here, we assumed that the widths of the vector mesons are increased by a factor of 3 due to in-medium effects. Indeed, while in the invariant mass spectrum the ρ peak is not longer visible, selecting an narrow interval of values of $M_\perp$ the ρ is clearly seen.

This feature is persistent when integrating the rate over the space-time history of the radiating matter. Additional complications arise due to the suspected strong coupling of the widths and pole positions to the baryon density and temperature, which change in space and time.

Employing a transport calculation of BUU type we have checked that such background contributions as pn bremsstrahlung, η Dalitz and Δ Dalitz decays are sufficiently strongly suppressed when selecting the interval 850 MeV $< M_\perp <$ 950 MeV. The count rates for this range of $M_\perp$ are not too small to make such measurements feasible.

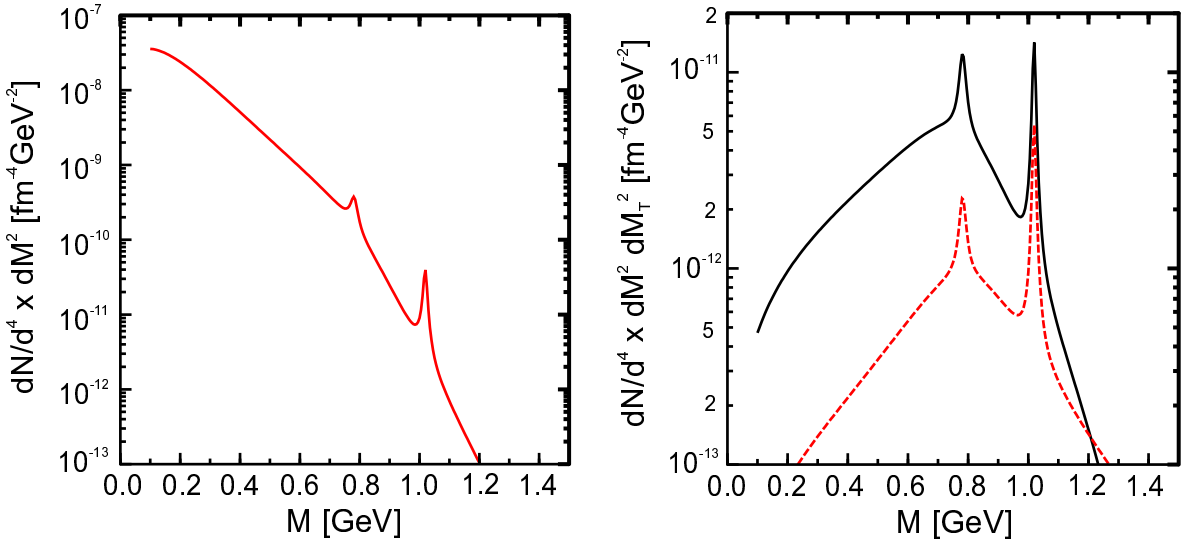

Fig. 1 *The dilepton emission rates $dN/(d^4x\,dM^2)$ (left panel) and $dN/(d^4x\,dM_\perp^2\,dM^2)$ (right panel, $M_\perp = 1.3$ GeV) for $T = 70$ MeV and radial expansion velocities of $v_r = 0.1$ (dashed curve) and 0.3 (solid curve).*

[1] *Institute of Theoretical Physics, Kiev, Ukraine*
[2] *KFKI Budapest, Hungary*

References

[1] B. Kämpfer, O.P. Pavlenko, Eur. Phys. J. A 10, 101 (2001)

Analysis of Dilepton Data from Heavy–Ion Experiments at CERN–SPS [B,W]

K. Gallmeister, B. Kämpfer, O.P. Pavlenko[1], C. Gale[2]

An excess of dileptons in lead–beam induced heavy–ion collisions has been reported (i) by the CERES collaboration in the low–mass region of dielectrons and (ii) by the NA50 collaboration in the intermediate–mass region of dimuons. This excess points to the existence of a system of thermalized matter emitting dileptons [1].

We achieve a good description of the mentioned data by a superposition of the thermal yield and either the hadronic cocktail in case of CERES data or both the contributions from correlated semileptonic decays of open charm mesons and the Drell–Yan process for NA50 data (see figs. 1 and 2 and [1] for details).

The thermal source is characterized by a mean temperature $\langle T \rangle = 170$ MeV. A similar value is found in an analysis of the dilepton data of the CERES, Helios/3 and NA38 collaborations with the sulfur beam [2]. In the dynamic scenario we find an initial temperature of the thermal system in the order of 200 MeV, i.e. a value larger than the expected deconfinement temperature.

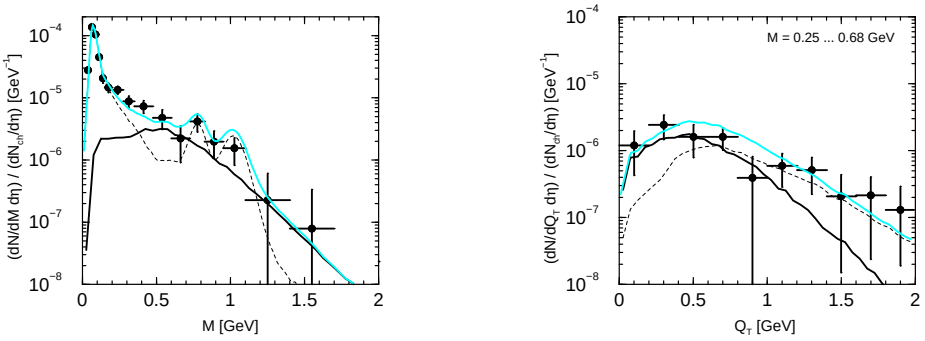

Fig. 1 *A comparison of our model with the CERES data. The dashed curves are the hadronic cocktail published by the CERES collaboration, the solid curves are the contributions from the thermal system. The sum is depicted by the gray curves. Left panel: the invariant mass spectrum, right panel: the transverse momentum spectrum for the invariant mass region* $M = 0.25 \ldots 0.68$ *GeV.*

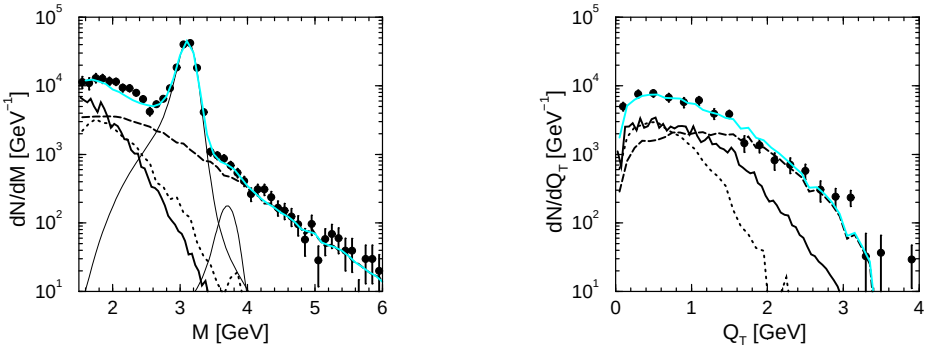

Fig. 2 *The data of the NA50 collaboration for the invariant mass spectrum (left) and the transverse momentum spectrum in the invariant mass region* $M = 1.5 \ldots 2.5$ *GeV (right). The dashed curves are the Drell–Yan contributions, the dotted curves show the contributions of open charm and the solid lines depict the yield of the thermal system. The sum is shown by the gray curves.*

[1] *Institute for Theoretical Physics, 252143 Kiev - 143, Ukraine*
[2] McGill University, Montreal, QC, H3A 2T8, Canada

References

[1] K. Gallmeister, B. Kämpfer, O.P. Pavlenko, Phys. Lett. B 473, 20 (2000)
[2] K. Gallmeister, B. Kämpfer, O.P. Pavlenko, C. Gale, Nucl. Phys. A 688, 933 (2001)

Analysis of the Direct Photon Data of the Experiment WA98 [B,W]

K. Gallmeister, B. Kämpfer, O.P. Pavlenko[1]

Recently the WA98 collaboration published data concerning the direct photon production in the reaction $Pb(158\ AGeV) + Pb$ [1]. Analog to our studies [2] of the dilepton spectra in similar reactions, we use a superposition of hard photon production processes and of the yields from thermalized matter in order to describe these data.

The contributions of the hard annihilation and Compton like diagrams within the framework of perturbative QCD are calculated using the event generator PYTHIA. The comparison of PYTHIA results and various direct photon data in proton induced collisions indicates that the shapes of the data are well described. Fig. 1 displays two examples of the comparison of our calculations and data.

The hard perturbative QCD contribution, calculated for pp collisions, is up–scaled such that the large–$p_\perp$ tail of the WA98 data is reproduced (cf. fig. 2). The thermal source is described by

$$\frac{dN}{d^3p/E} = N_{\rm eff}\,\frac{5\alpha\alpha_s T_{\rm eff}^2}{12\pi^2}\int_0^1 ds\ s^2 \int_{-1}^{+1} d\xi\ e^{-A}\log\left[1+\frac{2.912}{4\pi\alpha_s}A\right] \tag{9}$$

with $A = \frac{p_\perp \cosh y\,(1-sv_0\xi)}{T_{\rm eff}\sqrt{1-(sv_0)^2}}$, an effective temperature of $T_{\rm eff} = 170$ MeV and a space–time normalization factor $N_{\rm eff} = 3\times 10^4$ fm^4. These parameters are taken from our analysis [2] of dilepton data. Contrary to the SPS dilepton data, flow effects are visible in the photon $p_\perp$ spectra at values around 2 GeV. With a maximal radial expansion of $v_0 = 0.3c$ of the radiating fireball a good description of the data is achieved (see fig. 2).

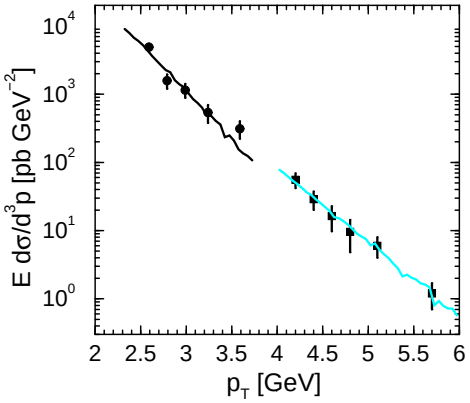

Fig. 1 *A comparison of calculations of the hard photon production in proton–proton collisions with data from E704 [3] at $\sqrt{s} = 19.4$ GeV (small $p_\perp$ values) and from UA6 [4] at $\sqrt{s} = 24.3$ GeV (large $p_\perp$ values). For more details cf. [5].*

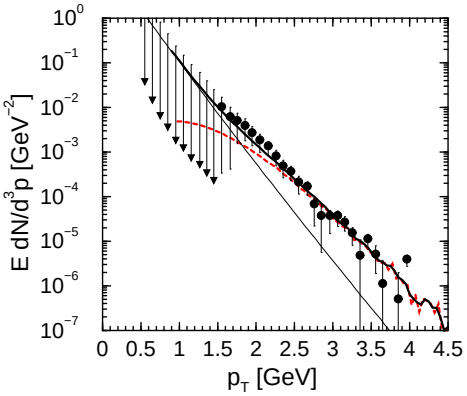

Fig. 2 *The data of the WA98 collaboration [1] compared with the hard direct photons (dashed curve) and the thermal contribution (thin curve). The sum of these contributions is depicted by the solid curve. A radial flow of $v_0 = 0.3c$ is assumed.*

[1] *Institute for Theoretical Physics, 252143 Kiev - 143, Ukraine*

References

[1] M. M. Aggarwal et al. (WA98), Phys. Rev. Lett 85 (2000) 3595
[2] K. Gallmeister, B. Kämpfer, O.P. Pavlenko, Phys. Lett. 473 (2000) 20
[3] D.L. Adams et al. (E704), Phys. Lett. B 345 (1995) 569
[4] G. Ballocchi et al. (UA6), Phys. Lett. B 317 (1993) 250
[5] K. Gallmeister, B. Kämpfer, O.P. Pavlenko, Phys. Rev. C 62 (2000) 057901

Solar Proton Burning Process Revisited [B,W]

L.P. Kaptari[1], B. Kämpfer, E. Grosse

Recently the solar proton burning process, $pp \to e^+\nu_e D$, has been revisited by various authors since the previous canonical value of the corresponding S_{pp} factor has been questioned. This stimulated us to calculate the relevant matrix elements within a fully covariant model of the deuteron D, based on the Bethe-Salpeter (BS) formalism. The relevant Feynman type diagrams are displayed in Fig. 1. Within our approach [1] a variety of quantities, including the total and differential cross sections, energy dependences, angular distributions etc. are accessible. Within the relativistic impulse approximation a covariant expression for the S_{pp} factor is obtained (see Fig. 2). Our result confirms the old canonical value of $S_{pp} \approx 4.00 \times 10^{-25}$ MeV b, which is in agreement with the energy balance of the sun and helioseismic data.

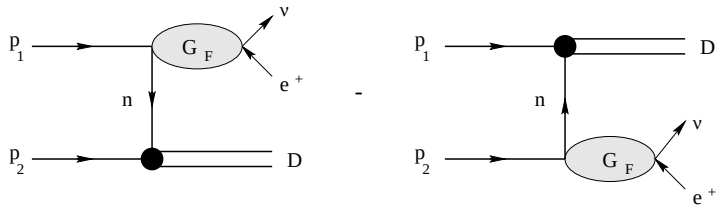

Fig. 1 *Feynman diagrams contributing to the processes* $pp \to e^+\nu D$.

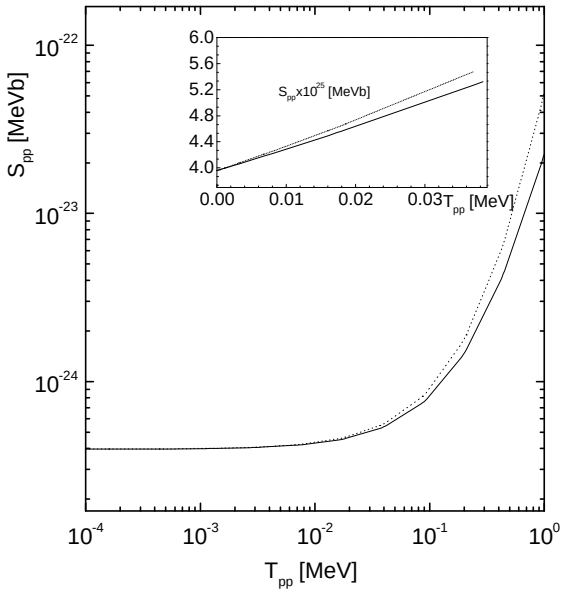

Fig. 2 *The* S_{pp} *factor for the reaction* $pp \to e^+\nu D$ *as a function of the relative kinetic energy of incident protons,* T_{pp}. *The solid line is the result of a calculation by using the full deuteron wave function, while the dotted line is the result of a computation with the deuteron wave function taken as constant (for details consult [1]). The inset shows* S_{pp} *vs.* T_{pp} *in linear scales.*

Encouraged by the applicability of our approach we have also studied the reaction $e^+D \to pp\bar{\nu}_e$ representing a cross channel of the solar burning process. In principle, such a reaction is feasible under laboratory conditions. For instance, at ELBE also a positron source is planned. However, the calculated cross section is exceedingly small. The competing electromagnetic deuteron disintegration reactions, $e^{\pm}D \to e^{\pm}pn$, have cross sections many orders of magnitude above the interesting weak disintegration process. Therefore, due to severe background problems, a dedicated experimental investigation of the astrophysically interesting weak deuteron disintegration seems to be far out of reach.

[1] *Bogolyubov Laboratory of Theoretical Physics, JINR Dubna, Russia*

References

[1] L. P. Kaptari, B. Kämpfer, E. Grosse, J. Phys. G 26 (2000) 1423

Nuclear Physics

The activities of the Nuclear Physics Department during the year 2000 concentrated on the following topics:

- *The design of the Bremsstrahlung facility at the ELBE accelerator with the aim to provide us an optimized source for intense polarized gamma radiation in an envisaged energy range up to 20 MeV was completed. Particular attention was paid to achieve a low background level of scattered photons and neutrons in the experimental cave. The electron beamline in the accelerator hall including the radiator target chamber and the electron beam dump as well as the aluminum collimator with an optional photon beam hardener is now under construction.*

- *In preparing future photon scattering studies at ELBE we performed an experiment at the Bremsstrahlung beam of the Dynamitron at Stuttgart in collaboration with the groups at the Universities of Stuttgart and Köln. In this experiment the semi-magic nucleus ^{87}Rb was investigated for the first time to find indications whether the N=50 neutron core excitations can contribute to the dipole states observed in photon scattering.*

- *The extensive data taken in an EUROBALL experiment of our group in Legnaro have been analysed and evaluated. Interesting new features concerning high spin structures of the N≈Z unstable nuclei produced by the ^{40}Ca+^{40}Ca reaction were found. For instance, rotational bands identified in ^{72}Br up to high spin values manifest a striking case of signature inversion. According to the applied Nilsson-Strutinsky model this observation provides evidence for a triaxial shape of this nucleus which continuously changes with spin. In the neighboring isotope ^{73}Br rotational structures were measured which persist to the extremely high spin value I=65/2ħ. The theoretical analysis has shown that one of those bands is observed up to its limiting spin where all particles of a given configuration have fully aligned their angular momenta along the nuclear symmetry axis. This is the first case of a so-called band termination in the mass region around A=80.*

- *In collaboration with the ISOL group at the GSI Darmstadt the nuclei ^{52}Fe and ^{93}Pd were studied. The detailed properties of these very neutron deficient nuclei are important for the understanding of the nucleosynthesis in rp-processes.*

- *Concerning the progress in nuclear structure theory further developments of the 3-dimensional cranking model were made to describe the chiral rotation which incorporates the highest degree of symmetry breaking occurring for the spin orientation. In fact, according to the latest experimental findings there exists an island of odd-odd isotones with N=75 around ^{134}Pr where this peculiar type of rotation shows up through the predicted signature of parallel sister bands.*

- *The integration method developed to calculate the RPA correlation energy was applied for realistic systems. These results demonstrate that quantal vibrations may considerably influence the rotational properties. Remarkably, these effects are sensitive against the specific features of the effective interaction.*

A special highlight in the year 2000 was the Workshop on Nuclear Spectroscopy and Nuclear Astrophysics held at the FZ Rossendorf from April 27 to April 29. The emphasis

of this international meeting was put on medium mass nuclei and its main goal was to discuss the new experimental possibilities for exploring nuclear structure at the limits of stability using the more intense radioactive beams being available soon. Another focus concerned the experimental nuclear physics program at the Bremsstrahlung facility of the ELBE accelerator.

The financial support from the Federal Ministry of Education and Research (BMBF) and the Saxon State Ministry for Science and Art (SMWK) enabled us to invite the international experts to our meeting.

Collaborations

We were benefiting from the successful and permanent cooperation with the spectroscopy groups from the German universities at Stuttgart, Köln, Göttingen and Darmstadt as well as with ISOL group of the GSI Darmstadt. We acknowledge also the fruitful cooperation with the Italian colleagues which were experimenting with us at the EUROBALL Legnaro, the colleagues from the Sofia University and University of Leuven. We are also grateful to the theoretical support from our colleagues at the University of Tennessee, and Notre Dame University, both in the US.

Chiral Symmetry in Nuclear Rotation

F. Dönau, Jing-ye Zhang[1], S. Frauendorf[2], V.I. Dimitrov[3]

Recently, in rotating nuclei a new type of symmetry breaking [1,2] was predicted which is called chiral symmetry breaking. This phenomenon appears in triaxially deformed nuclei if the direction of total angular momentum (a.m.) vector $\vec{J}$ is outside all the three principal planes spanned by the intrinsic axes of the nuclear density distribution. The different principal axes form under those conditions either a left-handed or a right-handed intrinsic system with respect to the space-fixed vector $\vec{J}$ which realizes two chiral symmetry types. In the ideal case two degenerate rotational bands appear corresponding to the chirally symmetric or antisymmetric intrinsic configuration with respect to the chiral operation $\chi = \mathcal{T}R_y(\pi)$ in which the rotation $R_y(\pi)$ about the space-fixed y-axis is combined with time reversal operation $\mathcal{T}$. Following the common phase conventions of [3] one gets straightforwardly for any tensor operators $Q_{\lambda\mu}$ the invariance property

$$\chi\, Q_{\lambda\mu}\, \chi^{-1} = Q_{\lambda\mu}. \tag{10}$$

The appropriate tool for describing these new features is the 3-dimensional Tilted Axis Cranking (TAC) model which enables us to calculate self-consistently the nuclear shape in conjunction with the off-plane orientation of the total spin which is crucial for obtaining chiral symmetry breaking. The 3d-TAC mean field Hamiltonian reads

$$\begin{aligned} h'_\omega(\beta,\gamma) \;=\; & h_o \;-\hbar\omega_\circ\beta\,(\,cos\gamma\,Q'_0 \;+\; sin\gamma\,(Q'_2+Q'_{-2})/\sqrt{2}\,) \\ & -\omega\,(sin\vartheta cos\varphi\,I_1 \;+\; sin\vartheta sin\varphi\,I_2 \;+\; cos\vartheta\,I_3\,) \end{aligned} \tag{11}$$

where ω is the rotational frequency, $Q'_{0,\pm2}$ and $I_{1,2,3}$ denote the body-fixed components of the intrinsic quadrupole operator and a.m.vector, respectively. The angles (ϑ,ϕ) define the selfconsistent a.m.direction i.e. a minimum in the corresponding potential energy surface. The chiral symmetry breaking appears for $0 < \vartheta,\phi < \pi/2$ which can only happen for a triaxial shape. In fig.1 such a situation is shown as calculated for the nucleus ^{134}Pr at the frequency $\hbar\omega = 0.35$ MeV.

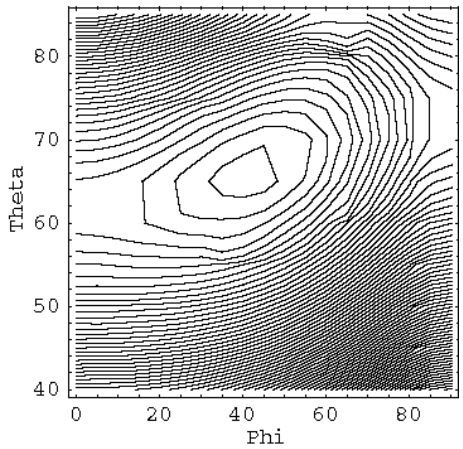

Fig. 1 *Potential energy surface $E(\vartheta,\phi)$ for ^{134}Pm which has a triaxial shape with $\gamma \approx 30^o$.*

In such a 3d-case the eigenfunctions $|\vartheta,\phi>$ of $h'_\omega(\beta,\gamma)$ become complex. The matrix elements of electromagnetic transitions can be calculated by projecting the wave function onto good chirality using the the relation

$$|\pm> = \frac{1}{\sqrt{2}}\,(1 \pm \chi)\,|\vartheta,\phi> \;. \tag{12}$$

The label $\pm$ distinguishes the different chiral branches of the rotational $\Delta I = 1$ bands. Evaluating the matrix elements of an electromagnetic operator $M(\lambda,\mu)$ by means of eq.(1) and for the

complex TAC eigenstates one derives

$$< \pm|M(\lambda,\mu)|\pm > = \Re e(< \vartheta,\phi|M(\lambda,\mu)|\vartheta,\phi >), \tag{13}$$

$$< \pm|M(\lambda,\mu)|\mp > = \Im m(< \vartheta,\phi|M(\lambda,\mu),|\vartheta,\phi >) \tag{14}$$

Hence, the transition amplitudes within a given chiral branch (+ or -) and in between different branches can be expressed by the real and imaginary part of the complex matrix element. One should mention, however, that these simple relations are valid only when neglecting the possible overlap between chirally reflected states, i.e. $< \vartheta,\phi|\vartheta,-\phi >= 0$.
Experimental band structures measured in the isotonic chain at N=75 are shown in fig. 2 which are suggested to be candidates for chiral doublets $|\pm >$. The lowest pair of positive parity bands in ^{134}Pr has been interpreted as a chiral doublet in [1,2]. New measurements at GAMMASPHERE extended the doublet seen for large frequency up to $\omega = 0.6\ MeV$ [4]. In order to exclude an accidental degeneracy the neighboring nuclei have been studied [5]. The systematic appearance of low-lying doublet bands of the same parity in the N=75 isotones with the disappearance of the energy difference in ^{134}Pr makes it likely that a small island of chiral rotation has been found which is surrounded by shores of soft chiral vibrations as is the case for other islands of broken symmetries, such as with quadrupole deformation, octupole deformation, and now rotational chirality. Clearly it would be interesting to study the neighboring isotone chains in order to map out the complete island.

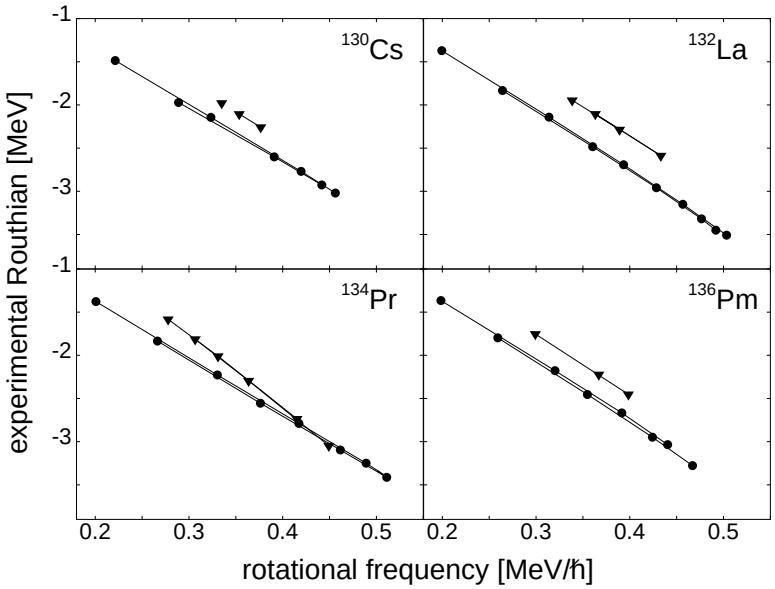

Fig. 2 *Experimental Routhians for the $\pi h_{11/2}\nu h_{11/2}$ main band (circles) and side bands (triangles) in the N=75 isotones studied. The Routhians are plotted up to a spin of I+11, where I is the bandhead spin. The distance between the two bands is the frequency of the chiral vibration. From [5].*

[1] *Department of Physics and Astronomy, University of Tennessee, TN 37996, USA*
[2] *on leave of absence at the Faculty of Physics, University of Notre Dame, IN 46556, USA*
[3] *Faculty of Physics, Sofia University, 1164 Sofia, Bulgaria*

References

[1] S. Frauendorf and J. Meng, Nucl. Phys. A 617, 131 (1997)
[2] V.I. Dimitrov, S. Frauendorf and F. Dönau, Phys. Rev. Lett. 84, 5732 (2000)
[3] A. Bohr and B.R. Mottelson, Nuclear Structure I, Benjamin, New York, 1969
[4] D. Fossan, private communication
[5] K. Starosta et al., Phys. Rev. Lett. 86, 971 (2001)

Chiral Symmetry and Particle Rotor Model

Jing-ye Zhang[1], P.B. Semmes[2], L.L. Riedinger[1], F. Dönau

The study of chiral bands in triaxially deformed nuclei [1] within the 3d-Tilted Axis cranking Model (TAC) has shown that the aplanar geometry of the angular momentum vector $< \vec{I} >$ exists only in a relatively short spin and frequency interval. This is because the energetical minimum stabilizing such an aplanar orientation is rather shallow and it can be easily driven towards a principal plane. Thus, for higher frequencies the favored a.m. direction returns to the normal (planar) tilt although the triaxial shape may still stay closely at maximal triaxiality $\gamma = 30^o$. Therefore, the question arises how sensitive is the aplanar spin orientation of the TAC model against the possible quantum interference (tunneling) in between the symmetry-related minima of the potential energy surface. This question goes beyond the TAC mean field model but can be investigated by symmetry restoration. A simple approach to it is the rotor plus particle model (RPM) in which a triaxial rotor core is coupled to two external high-j quasiparticles. The RPM is empirical with regard to the moments of inertia and the coupling to the deformed field which enter in terms of adjustable parameters. However, the above mentioned symmetry restoration of the RPM is by construction exactly carried out since the angular momentum is an exact quantum number of the model. In addition, the calculation of the important transition matrix elements is easily done and it automatically implies good a.m. states too.

Already Meng and Frauendorf [2] demonstrated in a schematic single j-shell RPM that the resulting bands have the chiral doublet pattern as predicted by the TAC model. Below we present the results from a similar calculation obtained with a more solid RPM description [3] in which both the pair and deformation field can be properly treated. This version allows one to study the energetical splitting of the chiral doublets and to calculate the inband and interband transition strength in a realistic manner. In this sense the RPM can be considered as a complementary approach to the TAC model. In Fig. 1 we show the lowest three bands calculated for the coupling of two quasiparticles ($\pi h_{11/2} \nu h_{11/2}$) to a rotor ($\gamma = 0$ and 30^o) for ^{134}Pr. Obviously, the chiral structures can not be formed with an axially deformed rotor in agreement with the prediction of TAC.

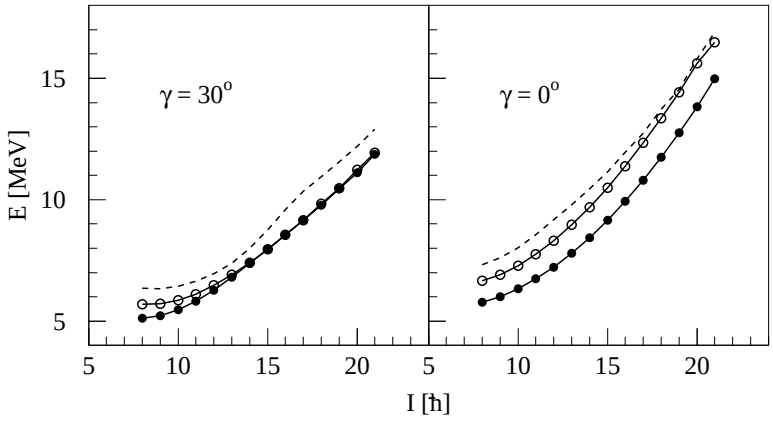

Fig. 1 *Calculated energy E vs. spin I for the three lowest bands of a rotor (left: γ=30^o, right: γ=0^o) plus two quasiparticle system. Only the triaxial rotor displays the chiral doublet structure.*

[1] *Department of Physics and Astronomy, University of Tennessee, TN 37996, USA*
[2] *Physics Department, Tennessee Technological University, Cookville, TN 38505, USA*

References

[1] V.I.Dimitrov, S. Frauendorf and F. Dönau, Phys. Rev. Lett. 84, 5732 (2000)
[2] S. Frauendorf and J. Meng, Nucl. Phys. A 617, 131 (1997)
[3] S. E. Larsson, G. A. Leander and I. Ragnarsson, Nucl Phys A 307 189 (1978)
I. Ragnarsson and P. B. Semmes, Hyperfine Interactions 43, 425 (1988)

A Hybrid Version of the Tilted Axis Cranking Model

V.I. Dimitrov[1], F. Dönau, S. Frauendorf[2]

The Tilted Axis Cranking (TAC) model [1] has turned out to be an appropriate theoretical tool for the description of the magnetic dipole bands. This model is a natural generalization of the cranking model for situations where the axis of rotation does not coincide with a principal axis of the density distribution of the rotating nucleus, and thus the signature is not a good quantum number. Since introduced, TAC has proven to be a reliable approximation for the energies and intraband transitions in both normally and weakly deformed nuclei. Hitherto the TAC calculations were based on the Nilsson Hamiltonian with the standard set of parameters [2]. This parameter set is known to have problems, for instance, in the $A = 130$ region where a better set has been suggested in [3]. On the other hand the Woods-Saxon potential with the universal parameter set [4] works very well around $A = 130$ and also in other mass regions. It is expected that this potential, which has a realistic radial profile instead of the artificial l^2- term of the Nilsson model, is more reliable when exploring mass regions where the Nilsson parameters have not been locally optimized. In addition, the l^2- dependence of the Nilsson potential is known to be problematic when the mean field is cranked at high angular velocity. In order to avoid the mentioned problems we developed an hybrid model which consists in adapting the Nilsson potential as close as possible to the Woods-Saxon one. Instead of the parameterizing the single particle levels of the spherical modified oscillator in the standard way by means of an ls- and an l^2-term, the hybrid model directly takes the energies of the spherical Woods-Saxon potential. The deformed part of the hybrid potential is an anisotropic harmonic oscillator. This compromise keeps the simplicity of the Nilsson potential, because coupling between the oscillator shell can be approximately taken into account by means of stretched coordinates [2], and it amounts to a minor modification of the existing TAC code. On the other hand, it has turned out to be quite a good approximation of the realistic flat bottom potential as long as the deformation is moderate. Another motivation for the hybrid potential is the considerably lower computation time (about a factor of 10) as compared with the full Woods-Saxon potential, which is important for the TAC calculations, which demand to achieve selfconsistency in two extra dimensions (the orientation angles).

Technically, the necessary replacements are rather simple, because the existing TAC code uses states of good l, j, m as a basis. The spherical Nilsson energies $e^{(nil)}_{N,l,j}$ are replaced by the spherical Woods - Saxon energies $e^{(ws)}_{N,l,j}$. It turns out to be unproblematic to associate the quantum numbers of the two different potentials. For a given combination l, j the third quantum number N is found by counting from the state with the lowest energy. The fact that the spherical Woods-Saxon code uses a harmonic oscillator basis permitted a check of the algorithm. The major component of the Woods-Saxon wavefunction agrees with the state found by our counting algorithm. In the high-lying part of the single-particle spectrum (three shells above the valence shell or higher) there are occasional ambiguities in assigning the states. Small errors of this kind are not expected to have any consequences at moderate or small deformation. These states do not couple strongly to the states near the Fermi surface.

[1] *Faculty of Physics, Sofia University, 1164 Sofia, Bulgaria*
[2] *on leave of absence at the Faculty of Physics, University of Notre Dame, IN 46556, USA*

References

[1] S. Frauendorf, Rev. Mod. Phys., in press
[2] S.G. Nilsson and I. Ragnarsson, Shapes and Shells in Nuclear Structure, Cambridge University Press, 1995
[3] Jing-ye Zhang, N. Xu, D. B. Fossan, Y. Liang, R. Ma, and E. S.Paul, Phys. Rev. C 39, 714 (1989) and Phys. Rev. C 42, 1394 (1990)
[4] S.Cwiok, J. Dudek, W. Nazarewicz, J. Skalski, and T. Werner, Comput. Phys.Commun. 46, 379 (1987)

Effects of Quadrupole RPA Correlations in Rotating Nuclei [B,W]

D. Almehed, F. Dönau, R.G. Nazmitdinov[1]

To study the influence of quadrupole shape vibrations on the rotation we have considered the following cranked Hamiltonian implying a residual isoscalar quadrupole-quadrupole interaction:

$$\hat{H}' = \hat{h}_0 - \hbar\omega_0\tilde{\kappa}\left[2\ell\cdot\mathbf{s} + \tilde{\mu}\left(\ell^2 - \left\langle\ell^2\right\rangle_N\right)\right] - \frac{\kappa}{2}\sum_m \hat{Q}_m\hat{Q}^*_m - \omega\hat{J}_z. \tag{15}$$

The first two terms denote the common spherical oscillator part and the spin-orbit potential which are chosen such that the mean field approximation of $\hat{H}'$ leads to the Nilsson Hamiltonian with the cranking term $-\omega\hat{J}_z$. In a first step of our calculations we determine the selfconsistent values of the deformation parameters ϵ, γ of the mean field potential as a function of the rotational frequency ω. In the second step the RPA treatment of the Hamiltonian $\hat{H}'$ is performed. Using the the spectral function integration method [1] the RPA correlation energy E'_{RPA} and their dependence on ω is obtained. This correlation energy contains the effects of the zero point quantum vibrations about the selfconsistent minimum of the potential energy surface. The total angular momentum J can be derived from the canonical relation $J(\omega) = -dE'/d\omega$ which is valid on mean field as well as on RPA level. There are two different options to construct the selfconsistent mean field solutions as the basis of the subsequent RPA calculation. The mean field approximation can be done straightforwardly with normal quadrupole operators $\hat{Q}_m$ [2]. Alternatively, when imposing additionally the constraint of volume conservation then the quadrupole operators have to be taken with doubly stretched coordinates [3]. In either way it is necessary to include the the $\Delta N = \pm 2$ mixing of oscillator shells caused by the quadrupole operators $\hat{Q}_m$. The different possibilities do only slightly change the results of the mean field calculation but produce rather different effects for the RPA.
As an example of a realistic calculation for the RPA correlations we choose ^{78}Sr. This nucleus has a rather stable prolate deformation and it is situated in a region with relatively low level density. Therefore, one can expect that the neglected pairing effects are of minor importance. The resulting total angular momentum J with and without RPA correlations is given in Fig. 1.

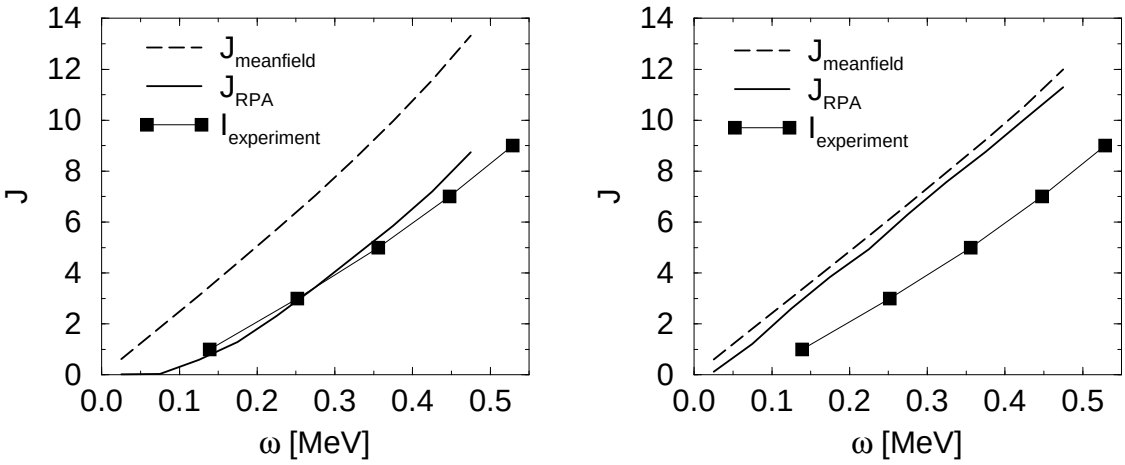

Fig. 1 *Angular momentum, in units of $\hbar$, of the ground state band in ^{78}Sr. Left panel: calculation with mean field approximation and RPA, respectively, with normal QQ force. Right panel: the same with doubly stretched QQ force. Experimental data are taken from [4].*

One notices that the mean field result for the angular momentum J is practically the same irrespectively whether the volume conservation is fulfilled or not. The moment of inertia is given by the ascent of the function $J(\omega)$. The resulting mean field value is much larger than the one seen in experiment. This is a well know result which is due to fact that ℓ^2 breaks the local

Galilean invariance. Concerning the quantum effects taken into account by the RPA there is a dramatic change when comparing the cases of normal and doubly stretched QQ-force. The RPA correlations obtained with the normal QQ-force reduce the moment of inertia by approximately 30 %. Applying the volume conservation together with doubly stretched quadrupole operators one has no reduction of the moment of inertia. There arises only a constant shift $\Delta J = \frac{1}{2}\hbar$ of the angular momentum related to its zero point motion. The better agreement of the RPA value with the experimental one, obtained for normal QQ-force is accidental.
The correlations are connected with the collective shape vibrations which is underlined by the fact that the size of these correlations is dependent on the curvature of the mean field potential.

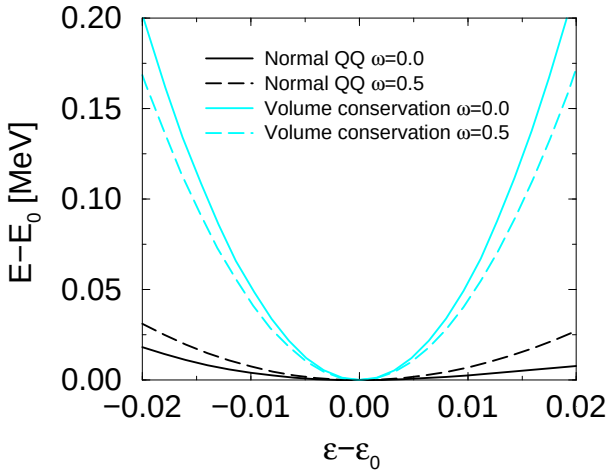

Fig. 2 *Potential energy as a function of deformation with the normal QQ-force (black lines) and with volume conservation (grey lines). The potential is plotted for the rotational frequencies* $\omega = 0$ *(solid lines) and* 0.5 *(dashed lines) MeV.*

In Fig.2 the potential energies $E(\epsilon) =< \hat{H}' >$ calculated for two frequency values ω in mean field approximation are shown as a function of the deformation parameter ϵ. The influence of the RPA correlation on the moment of inertia is determined by potential curvature with respect to ϵ and how the curvature is changing with the rotational frequency. One notices that the normal QQ-force leads to a much softer potential than the one with doubly stretched QQ-force. In addition, the stiffness of the potential increases with ω in the first case but decreases in the last case. To investigate these effects in more detail we have also considered a normal quadrupole interaction in which all $\Delta N = \pm 2$ matrix elements were neglected, i.e. the mixing between the oscillator mayor shells was omitted. In this approximation the RPA correlation effects of the normal QQ-force become similar to the one with volume conservation. This finding indicates the important role of the $\Delta N = \pm 2$ shell mixing which is known to be decisive for the formation of the Giant quadrupole resonances in nuclei. To get a more detailed understanding of the mechanism and the validity of different models in describing the effects of shape vibration in the ground state rotational band a more systematic investigation is necessary.

[1] *Joint Institute for Nuclear Research, 141980 Dubna, Russia*

References

[1] F. Dönau et al., Phys. Rev. Lett. 83, 280 (1999)
[2] D. Almehed et al., to be published in Physics of Atomic Nuclei
[3] S. Åberg, Phys. Lett. 157B, 9 (1985)
[4] D. Rudolph et al., Phys. Rev. C 56, 98 (1997)

The First Nuclear Resonance Fluorescence Experiment on ^{87}Rb [D,H]

L. Käubler, K.D. Schilling, R. Schwengner, D. Belic[1], P. v. Brentano[2], F. Dönau, C. Fransen[2], E. Grosse, U. Kneissl[1], C. Kohstall[1] A. Linnemann[2], P. Matschinsky[2], A. Nord[1], N. Pietralla[2], H.H. Pitz[1], M. Scheck[1], F. Stedile[1] and V. Werner[2]

As a result of nuclear resonance investigations of N=50 nuclei [1,2] the question arises to what extent neutron degrees of freedom play a role in the structure of low-spin states in such semi-magic nuclei. Moreover, nothing is known up to now about the response of the N=50 nucleus ^{87}Rb to real photons. The first (γ,γ') experiment on ^{87}Rb was performed with bremsstrahlung of an endpoint energy of 4.0 MeV delivered by the Dynamitron at Stuttgart. Gamma-rays scattered on a 2.507 g $^{87}Rb_2CO_3$ target (^{87}Rb enriched to 99.2 %) were measured with three HPGe detectors of 100 % relative efficiency. In Fig. 1 a portion of a γ-ray spectrum is shown.

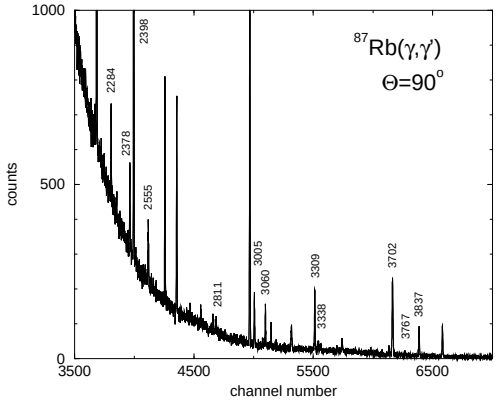

Fig. 1 *γ-ray spectrum of ^{87}Rb. Peaks denoted by their γ-ray energy belong to ^{87}Rb.*

The width Γ of 20 states could be measured for the first time. For ten levels for the first time γ-deexcitation was observed and for five for the first time γ-branchings. All observed states are dipole excitations, twelve of them M1 and six E1 excitations. For the 845 and 3837 keV transitions very large B(M1) and B(E1) values have been found, respectively. Shell model calculations [3] for ^{87}Rb have been performed. The shell model reproduces the right ordering of the experimentally observed magnetic dipole excitations and gives a fair reproduction of the excitation energies. There is a remarkable agreement of the measured B(M1) values with the calculated values (Fig. 2). The very strong 845 keV transition is the proton $p_{1/2}\rightarrow p_{3/2}$ spin-flip transition. Dominating proton $p_{3/2}$, $f_{5/2}$ and $p_{1/2}$ single particle character is found for the g.s., the 403 keV and 845 keV states, respectively. The other magnetic dipole excitations are dominated by three protons. Almost all negative parity states contain to some percent contributions of excitations of the N=50 neutron core. Even our large scale shell model calculations considering also the breakup of the N=50 core are not able to describe the electric dipole excitations.

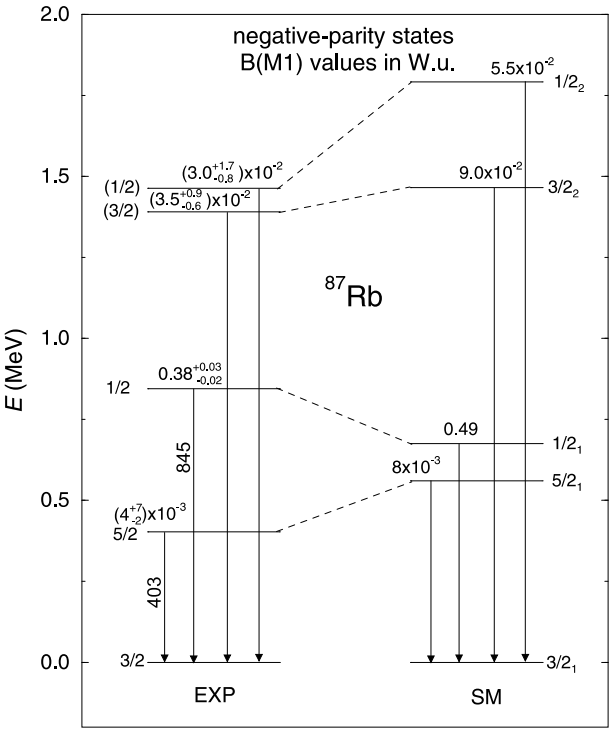

Fig. 2 *Experimental results for magnetic dipole excitations compared the results of large-scale shell model calculations.*

[1] *Institut für Strahlenphysik, Universität Stuttgart, 70569 Stuttgart*
[2] *Institut für Kernphysik, Universität zu Köln, 50937 Köln*

References

[1] J. Reif et al., Nucl. Phys. A 620 (1997) 1
[2] L. Käubler et al., Eur. Phys. J. A 7 (2000) 15
[3] E.A. Stefanova et al., Phys. Rev. C 62 (2000) 054314

A Scissors-Like State on Top of the Quadrupole Vibrational State in ^{88}Sr [D,H]

L. Käubler, H. Schnare, R. Schwengner, H. Prade, F. Dönau, E. Grosse, K.D. Schilling, A. Wagner
and the Köln[1] - Darmstadt[2] - Sofia[3] collaboration

A (γ,γ') experiment on ^{88}Sr was performed at the S-DALINAC accelerator of the TU Darmstadt with bremsstrahlung of 6.7 MeV endpoint energy using two EUROBALL CLUSTER detectors. In the search for the 1^- two-phonon state in the N=50 nucleus ^{88}Sr we found surprisingly $J^\pi = 1^+$ for the 4.742 MeV state [1] and a relatively large value of $B(M1)$=0.07 W.u. for the 4.742 MeV transition (Fig. 1) which is not reproduced by the quasiparticle-phonon model [2].

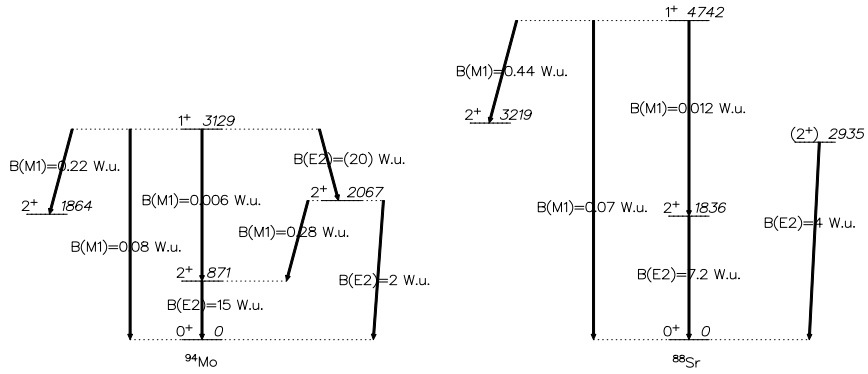

Fig. 1 *Comparison of ^{94}Mo and ^{88}Sr.*

In order to give an interpretation for the 1^+ state at 4.742 MeV, the picture of a new excitation mode called dynamic scissors mode is proposed: a superposition of the normal scissors mode (scissors-like isovector vibration of the deformed proton and neutron systems) with the dynamically deformed quadrupole vibrational state in a spherical nucleus. This idea is suported by the following two arguments: (i) For the first 2^+ state in ^{88}Sr a deformation of $\delta = 0.11$ is obtained for the maximum elongation. Based on empirical estimates (est) [3] the normal scissors mode in ^{88}Sr would occur for $\delta = 0.11$ at the centroid of energies of $E^{est}(1^+_{sc}) = 3.17$ MeV with a total strength of $B^{est}(M1; 1^+_{sc} \rightarrow 0^+_1) = 0.03$ W.u.. For the dynamic scissors mode state $E(1^+_{dsc})$ in ^{88}Sr one gets the estimate $E^{est}(1^+_{dsc}) = E^{exp}(2^+_1) + E^{est}(1^+_{sc}) = 5.01$ MeV. The estimates of 5.01 MeV and 0.03 W.u. are in fair agreement with the experimental results given above. (ii) There are many similarities of the deexcitation of the 4.742 MeV state in the spherical nucleus ^{88}Sr with that of the mixed symmetry scissors-like 1^+_{ms} state in the deformed N=52 nucleus ^{94}Mo [4], and also for the first three 2^+ states (Fig. 1). The 1^+ state in ^{94}Mo is considered to be the scissors mode in this nucleus having the structure $(2^+_1 \otimes 2^+_{ms})$, where 2^+_1 corresponds to the phonon of the isoscalar quadrupole vibration and 2^+_{ms} is the phonon of the isovector quadrupole vibration. For ^{88}Sr the energy sum of the 2^+ isoscalar quadrupole vibrational state (1.836 MeV) and the newly observed possible 2^+_{ms} isovector quadrupole vibrational state (2.935 MeV) results to 4.771 MeV in well accordance to 4.742 MeV for the 1^+ state. In summary, the 1^+ state at 4.742 MeV in the spherical $N = 50$ nucleus ^{88}Sr is a fingerprint for the existence of a scissors-like state. The picture of the dynamic scissors mode could be a schematic approach for this excitation giving a rough approximation to the real situation. The reality may be a complicated superposition of an isoscalar and isovector quadrupole vibration.

[1] *Institut für Kernphysik, Universität zu Köln, 50937 Köln*
[2] *Institut für Kernphysik, TU Darmstadt, D-64289 Darmstadt*
[3] *Institute of Nuclear Research and Nuclear Energy, Sofia, BG-1784 Sofia*

References

[1] L. Käubler et al., Eur. Phys. J. A 7 (2000) 15
[2] M. Grinberg and Ch. Stoyanov, Nucl. Phys. A 573 (1994) 231
[3] N. Pietralla et al., Phys. Rev. C 58 (1998) 184
[4] N. Pietralla et al., Phys. Rev. Lett. 83 (1999) 1303

Transition Strengths in Magnetic Dipole Bands in ^{82}Rb, ^{83}Rb and ^{84}Rb [A,E]

R. Schwengner, G. Rainovski[1], H. Schnare, A. Wagner, F. Dönau, M. Hausmann[2], O. Iordanov[2], A. Jungclaus[2], K.P. Lieb[2], D.R. Napoli[3], G. de Angelis[3], M. Axiotis[3], F. Brandolini[4], N. Marginean[3], C. Rossi Alvarez[4]

Searching for magnetic rotation in the mass region around $A = 80$ we studied the isotopes ^{82}Rb$_{45}$, ^{83}Rb$_{46}$ and ^{84}Rb$_{47}$. We found magnetic dipole ($M1$) sequences with varying properties in each nucleus. The $M1$ bands in the odd-odd nuclei ^{82}Rb and ^{84}Rb follow the regular rotational behaviour ($E \sim J(J+1)$, i.e. $J \sim \hbar\omega$) which can be seen in Fig. 1. $B(M1)/B(E2)$ ratios determined from branching ratios of transitions within the $M1$ bands reach values up to 25 $(\mu_N/eb)^2$ and decrease smoothly with increasing spin in a range of $13 \leq J \leq 16$. This behaviour is typical for magnetic rotation and caused by the gradual alignment of the spins of the involved proton and neutron orbitals (shears mechanism). The regular negative-parity $M1$ bands in ^{82}Rb and ^{84}Rb are well described within the tilted-axis cranking (TAC) model [1] on the basis of the lowest-lying four-quasiparticle (4-qp) configuration: $\pi(fp)\ \pi(g_{9/2}^2)\ \nu(g_{9/2})$ [2].

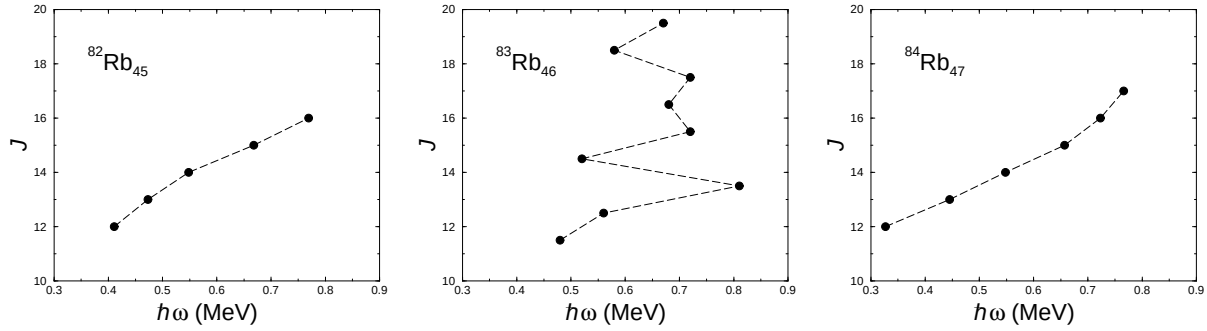

Fig. 1 *Spin as a function of rotational frequency in the $M1$ bands of ^{82}Rb (left panel), ^{83}Rb (middle panel) and ^{84}Rb (right panel). Lines are drawn to guide the eye.*

So far, the interpretation of the $M1$ bands was based on $B(M1)/B(E2)$ ratios deduced from γ-ray intensities. However, a detailed test of the predictions of the tilted-axis cranking model requires the knowledge of absolute $M1$ and $E2$ transition strengths. Therefore, we carried out a measurement of level lifetimes using the reaction ^{11}B + ^{76}Ge ($E = 45$ MeV) at the XTU tandem accelerator of the LNL Legnaro. Gamma rays were detected with the spectrometer GASP. A thick target was used to stop the recoil nuclei. Level lifetimes were deduced from a lineshape analysis applying the Doppler-shift-attenuation method.

Absolute experimental transition strengths within the $M1$ band of ^{84}Rb derived from the present lifetime measurement are compared with predictions of TAC calculations [2] in Fig. 2. The experimental $B(M1)$ values show a smooth decrease with increasing rotational frequency which may indicate the shears mechanism, but is not as pronounced as the calculated behaviour. The experimental $B(E2)$ values increase up to $\hbar\omega \approx 0.6$ MeV and decrease strongly towards higher frequency which may indicate a loss of collectivity due to a change of the structure. However, the calculated $B(E2)$ values stay almost constant over the considered frequency range.

In contrast to the odd-odd isotopes, the negative-parity $M1$ sequence in the odd-even nucleus ^{83}Rb is not regular, which can be seen in Fig. 1. Moreover, the $B(M1)/B(E2)$ ratios reveal a pronounced staggering that is not compatible with the shears mechanism [3] and cannot be described in the TAC model. Based on the present lifetime measurement we deduced absolute transition strengths within the negative-parity $M1$ sequence of ^{83}Rb which are shown in Fig. 3.

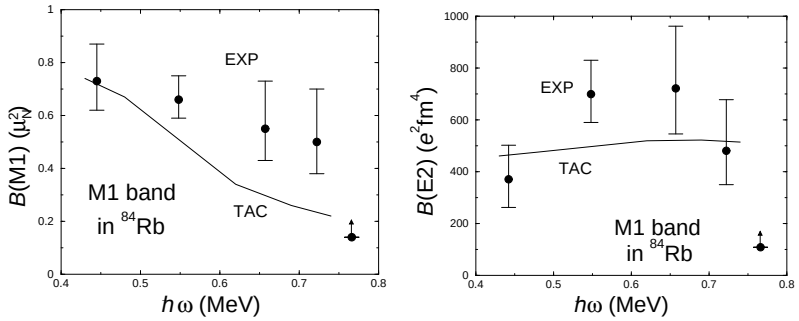

Fig. 2 *Experimental and calculated $B(M1)$ (left panel) and $B(E2)$ (right panel) transition strengths versus the rotational frequency in the $M1$ band of ^{84}Rb.*

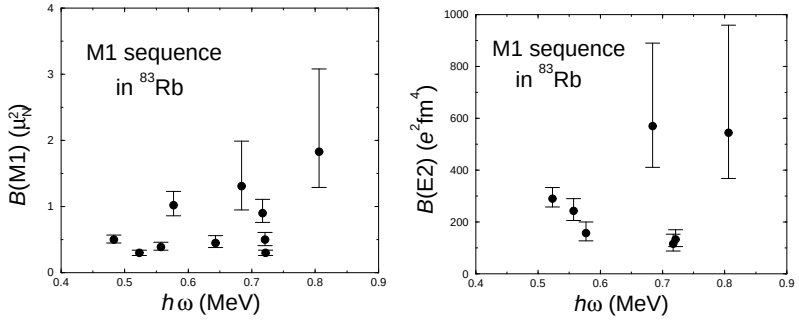

Fig. 3 *Experimental and calculated $B(M1)$ (left panel) and $B(E2)$ (right panel) transition strengths versus the rotational frequency in the negative-parity $M1$ sequence of ^{83}Rb.*

The experimental $B(M1)$ as well as the $B(E2)$ values show an irregular behaviour which is considered as the consequence of the even neutron number of this isotope in difference to the two odd-odd neighbours $^{82}Rb_{45}$ and $^{84}Rb_{47}$. In ^{83}Rb, the breakup of a neutron pair is necessary to generate excitations that include unpaired nucleons of both kinds. A possible configuration of negative parity is the 3-qp configuration $\pi(g_{9/2})\ \nu(g_{9/2})\ \nu(fp)$. This configuration has one $g_{9/2}$ particle less than the 4-qp configuration assumed for the odd-odd isotopes and, therefore, less possibilities to generate high spins. This and the specific neutron orbitals obviously lead to a spin coupling which cannot realize the shears mechanism. A further possible configuration similar to the one in the odd-odd isotopes is the 4-qp configuration $\pi(fp)\ \pi(g_{9/2}^2)\ \nu(g_{9/2}^2)$ which may occur at higher energy.

The different behaviour of the isotopes with odd numbers of $N = 45, 47$ on the one hand and an even number of $N = 46$ on the other hand demonstrates the delicate balance between irregular and coherent collective motion in this mass region.

[1] *FZR and Faculty of Physics, University of Sofia, 1164 Sofia, Bulgaria*
[2] *II. Physikalisches Institut, Universität Göttingen, 37073 Göttingen*
[3] *INFN, Laboratori Nazionali di Legnaro, 35020 Legnaro, Italy*
[4] *INFN and Dipartimento di Fisica dell'Universita di Padova, 35131 Padova, Italy*

References

[1] S. Frauendorf, Nucl. Phys. A 557, 259c (1993)
[2] H. Schnare et al., Phys. Rev. Lett. 82, 4408 (1999)
[3] R. Schwengner et al., J. of Res. of NIST 105, 133 (2000)

Shape Coexistence at High Spin in the N = Z + 2 Nucleus ^{70}Se [A,B,E]

G. Rainovski[1], H. Schnare, R. Schwengner, C. Plettner, L. Käubler, F. Dönau, I. Ragnarsson[2], J. Eberth[3], T. Steinhardt[3], O. Thelen[3], M. Hausmann[4], A. Jungclaus[4], K.P. Lieb[4], A. Müller[4], G. de Angelis[4], A. Gadea[5], D.R. Napoli[5], A. Algora[5], D. Jenkins[6], R. Wadsworth[6], A. Wilson[6], W. Andrejtscheff[7], V.I. Dimitrov[1],

The structure of nuclei in the vicinity of $N = Z$ in the mass region $A \approx 70 - 80$ reveals a rich variety of structural phenomena and provides a good test for nuclear models. The competition between proton and neutron shell gaps occurring at large oblate and prolate deformations near the nucleon numbers 36 and 38 results in a coexistence of different nuclear shapes [1]. The purpose of the present study is to extend the knowledge about the structure of nuclei close to $N = Z$ in the mass region $A \approx 70 - 80$. In particular, the information about high-spin states in such nuclei is scarce, since they can be produced in heavy-ion fusion reactions with small cross sections only. With the advent of large highly-efficient spectrometers as EUROBALL there are new prospects for the study of nuclei close to $N = Z$ which are populated in weak reaction channels.

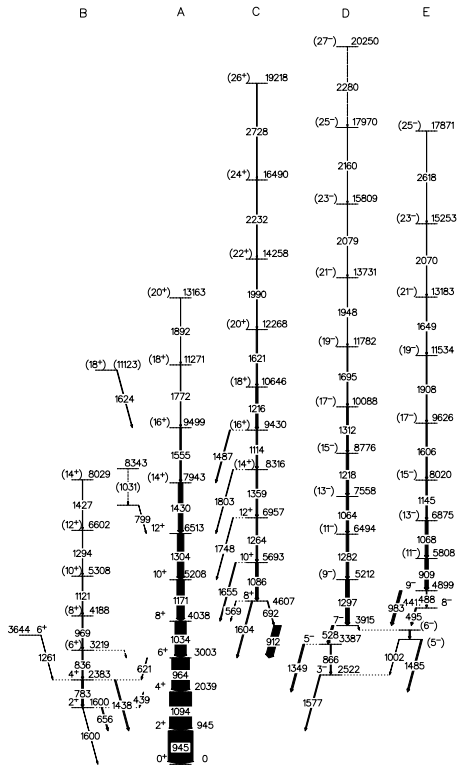

Fig. 1 *Level scheme of ^{70}Se deduced from the present experiment.*

Excited states in ^{70}Se were populated via the $2\alpha 2p$ exit channel of the reaction ^{40}Ca + ^{40}Ca at a beam energy of 185 MeV. The ^{40}Ca beam was provided by the XTU tandem accelerator at the Laboratori Nazionali di Legnaro. Gamma rays were measured with the EUROBALL III array consisting of 15 Cluster and 26 Clover detectors. Charged particles were detected with the silicon ball ISIS consisting of 40 $\Delta E - E$ telescopes. In the forward hemisphere, 50 neutron detector units filled with liquid scintillator BC501A were mounted.

The level scheme of ^{70}Se based on the present work is presented in Fig. 1. Excited states known from previous studies [2] were confirmed in our experiment. The positive-parity bands labelled A and C in Fig. 1 were considerably extended and a new positive-parity band (labelled B) was observed. Two new negative-parity bands (labelled D and E) were established on top of the irregular low-spin sequences.

The bands C, D and E are interpreted in terms of the configuration-dependent cranked Nilsson-Strutinsky model [3]. The potential energy surfaces show different minima that develop from configurations with the same numbers of nucleons lifted from the fp shell to the $g_{9/2}$ orbital. The newly observed negative-parity bands are thought to belong to such different minima. Thus, they represent a coexistence of different nuclear shapes at high spin.

[1] *FZR and Faculty of Physics, University of Sofia, 1164 Sofia, Bulgaria*
[2] *Department of Mathematical Physics, Lund Institute of Technology, 22100 Lund, Sweden*
[3] *Institut für Kernphysik, Universität zu Köln, 50937 Köln, Germany*
[4] *II. Physikalisches Institut, Universität Göttingen, 37073 Göttingen, Germany*
[5] *INFN, Laboratori Nazionali di Legnaro, 35020 Legnaro, Italy*
[6] *University of York, Physical Department, Heslington, Y015DD York, United Kingdom*
[7] *FZR and Institute for Nuclear Research and Nuclear Energy, BAS, 1784 Sofia, Bulgaria*

References

[1] W. Nazarewicz et. al, Nucl. Phys. A 435, 397 (1985)
[2] T. Mylaeus et. al, J. Phys. G 15, L135 (1989)
[3] A.V. Afanasjev et. al, Phys. Rep. 322, 1 (1999)

Signature Inversion Caused by Triaxiality in the ^{72}Br Nucleus [B,E]

C. Plettner[1], I. Ragnarsson[2], H. Schnare, R. Schwengner, L. Käubler, F. Dönau, A. Algora[3], G. de Angelis[3], A. Gadea[3], D.R. Napoli[3], J. Eberth[4], T. Steinhardt[4], O. Thelen[4], M. Hausmann[5], A. Müller[5], A. Jungclaus[5], K.P. Lieb[5], D.G. Jenkins[6], R. Wadsworth[6], A.N. Wilson[6]

Rotational structures in nuclei can be characterized by the signature quantum number α which defines the admissible spin sequence for a band through the relation $I = \alpha + 2n$ $(n = 0, 1, \ldots)$. This is a consequence of the well-known $D2$-symmetry of deformed intrinsic shapes reflected by the appearance of two signature partner bands with $\alpha = 0$ or 1 in even-mass nuclei. By investigating the relative position of the signature partners, important information about the structural changes ocurring in the nucleus with the increasing spin can be gained.

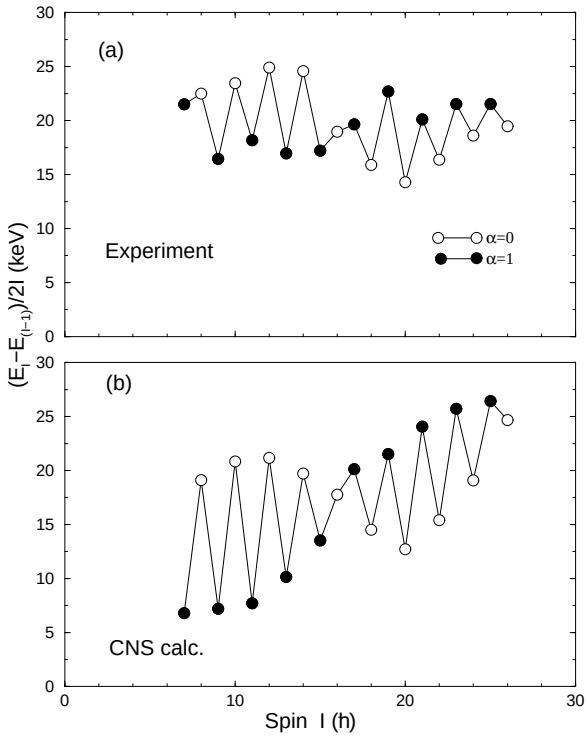

Fig. 1 *Energy difference between the states with spin I and spin (I - 1), divided by 2I, for the observed (upper panel) and calculated (lower panel) negative-parity bands in* ^{72}*Br.*

A peculiar feature of the negative-parity bands in ^{72}Br is the signature splitting that can be seen in the upper panel of Fig. 1. The $\alpha = 1$ branch is favoured up to $I \approx 16$ where a crossing of the branches takes place such that the $\alpha = 0$ branch is favoured at higher spins. This signature inversion in the negative-parity bands is unique in the chain of the odd-odd Br isotopes. In contrast, the ^{74,76,78}Br nuclei display signature inversions in the positive-parity bands at lower spin values of 9,10,11, respectively.

To understand the microscopic origin of the signature inversion in the negative-parity bands of ^{72}Br we performed calculations using the configuration-dependent cranked Nilsson-Strutinsky (CNS) [1] approach. A fully consistent calculation was performed, where the equilibrium deformation in the potential energy surface was searched for at each spin value separately. A comparison of the calculated signature splitting with the experimental one is presented in Fig. 1. This comparison shows that the main features, especially the energetic order of the signature partners and the spin, where the crossing takes place, are correctly reproduced. However, it should be mentioned that the signature inversion can not be reproduced in calculations with a fixed γ deformation [2]. The equilibrium deformation at low spin corresponds to negative γ deformation and gradually changes with increasing spin to positive values at the highest observed spins. This shows that the signature inversion is a consequence of changing triaxial deformation.

[1] FZR and Horia Hulubei NIPNE, Bucharest, P.O. Box MG-6, Romania
[2] Department of Mathematical Physics, Lund Institute of Technology, P.O. Box 118, 22100 Lund, Sweden
[3] INFN, Laboratori Nazionali di Legnaro, 35020 Legnaro, Italy
[4] Institut für Kernphysik, Universität zu Köln, 50937 Köln
[5] II. Physikalisches Institut, Universität Göttingen, 37073 Göttingen
[6] University of York, Physics Department, Heslington, York Y01 5DD

References

[1] I. Ragnarsson et al., Phys. Rev. Lett. 74, 3935 (1995)
[2] C. Plettner et al., Phys. Rev. Lett. 85, 2454 (2000)

Band Termination in the ^{73}Br Nucleus [B,E]

C. Plettner[1], H. Schnare, R. Schwengner, L. Käubler, F. Dönau, I. Ragnarsson[2], A.V. Afanasjev[3,4], A. Algora[5], G. de Angelis[5], A. Gadea[5], D.R. Napoli[5], J. Eberth[6], T. Steinhardt[6], O. Thelen[6], M. Hausmann[7], A. Müller[7], A. Jungclaus[7], K.P. Lieb[7], D.G. Jenkins[8], R. Wadsworth[8], A.N. Wilson[8]

The structure of the ^{73}Br isotope was investigated by using the EUROBALL spectrometer and the level scheme was published in [1].

To interpret the data, the configuration-dependent Cranked Nilsson-Strutinsky (CNS) approach was applied [2]. The calculations minimize the total energy of a specific configuration for a given spin with respect to the deformation parameters $(\varepsilon_2, \varepsilon_4, \gamma)$. The configurations are specified with respect to a $^{56}_{28}$Ni$_{28}$ core as having 7 active protons and 10 active neutrons. They are labelled by the shorthand notation $[p_1 p_2, n_1 n_2]$, where $p_1(n_1)$ stands for the number of protons (neutrons) in the $(p_{3/2}, f_{5/2})$ orbitals and $p_2(n_2)$ stands for the number of protons (neutrons) in $g_{9/2}$ orbitals. In addition, the sign of the signature of the last occupied orbital is given as a subscript, if the number of occupied orbitals in the specific group is odd. The calculated energies of the energetically lowest configurations are compared with experimental energies in Fig. 1, where a rigid rotor reference was subtracted. Based on this comparison the configurations [43$_+$,64] and [5$_+$2,64] were assigned to bands A and C, respectively. Band B is observed up to I = (63/2). The calculations suggest that the [5$_-$2,64] configuration can be assigned to this band at low and medium spin. It is the signature partner of the [5$_+$2,64] configuration assigned to band C. The [5$_-$2,64] configuration is crossed at spin 57/2 by the [43$_+$,7$_+$3$_+$] configuration. The predicted crossing is indeed observed in band B at spin (55/2$^-$). The latter configuration can be related to band B above the band crossing. In the calculations, the [43$_+$,7$_+$3$_+$] configuration (empty triangles in Fig. 1) undergoes a shape change from a collective shape (triaxiality parameter $\gamma \approx +30°$) to a non-collective oblate shape ($\gamma = +60°$) between spins 55/2 and 63/2. This means that collective rotation is no longer possible and the corresponding band terminates at spin 63/2. Since this is the highest spin observed for band B, we conclude that we observed band B up to its termination.

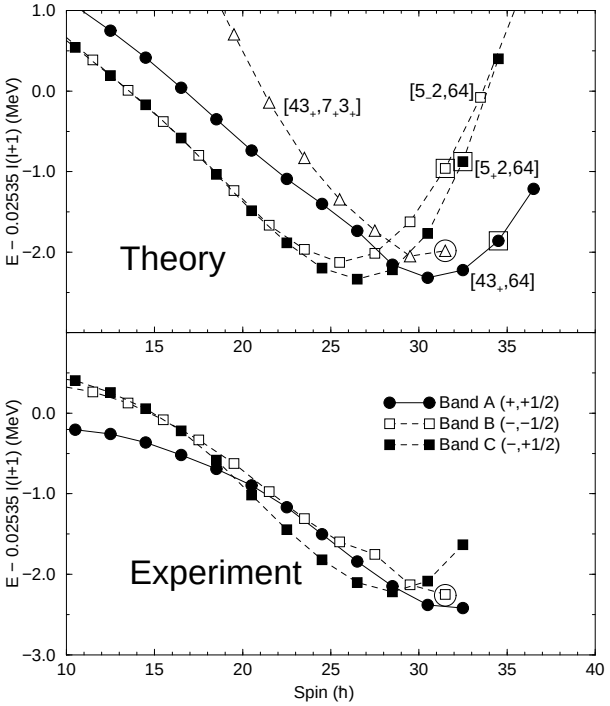

Fig. 1 *Comparison of experimental with calculated energies with respect to a rigid rotor reference.*

[1] *FZR and Horia Hulubei NIPNE, Bucharest, P.O. Box MG-6, Romania* [2] *Department of Mathematical Physics, Lund Institute of Technology, P.O. Box 118, 22100 Lund, Sweden* [3] *Physik-Department der Technischen Universität München, 85747 Garching* [4] *Laboratory of Radiation Physics, Institute of Solid State Physics, University of Latvia, LV 2169 Salaspils, Latvia* [5] *INFN, Laboratori Nazionali di Legnaro, 35020 Legnaro, Italy* [6] *Institut für Kernphysik, Universität zu Köln, 50937 Köln* [7] *II. Physikalisches Institut, Universität Göttingen, 37073 Göttingen* [8] *University of York, Physics Department, Heslington, York Y01 5DD, United Kingdom*

References

[1] C. Plettner et al., Phys. Rev. C 62, 014313 (2000)

[2] I. Ragnarsson et al., Phys. Rev. Lett. 74, 3935 (1995)

Influence of Neutron-Core Excitations on High-Spin States in ^{88}Sr [S]

E.A. Stefanova[1], R. Schwengner, J. Reif, H. Schnare, F. Dönau, M. Wilhelm[2], A. Fitzler[2], S. Kasemann[2], P. von Brentano[2], and W. Andrejtscheff[1]

High-spin states of the $N = 50$ nucleus ^{88}Sr were studied via the reaction ^{80}Se(^{11}B,$p2n$) at a beam energy of 45 MeV with the six-detector array OSIRIS CUBE at the University of Cologne. The level scheme of ^{88}Sr deduced from this experiment is shown in Fig. 1. On the basis of the analysis of directional correlations of coincident γ rays emitted from oriented states (DCO), spin assignments for all observed states were made. Mean lifetimes of three levels were determined using the Doppler-shift-attenuation method. They correspond to strong $M1$ transitions with $B(M1)$ values of about 0.3 to 1.4 W.u. Shell-model calculations in the model space $(0f_{5/2}, 1p_{3/2}, 1p_{1/2}, 0g_{9/2})$ for the protons and $(1p_{1/2}, 0g_{9/2}, 1d_{5/2})$ for the neutrons were performed. Experimental and calculated level energies of states in ^{88}Sr are compared in Fig. 2. Neutron-core excitations are predicted for the lowest 6^+ and 7^+ states in agreement with results of previous (d,p) experiments (e.g. [1]). Proton configurations of seniority $v = 4$ are predicted for the positive-parity states with $J^\pi = 8^+$, 10^+, 11^+ and 12^+. The calculations describe experimental high-spin level sequences with $J^\pi > 7^-$ and $J^\pi \geq 12^+$ linked by strong M1 transitions as $v = 4$ and 6 multiplets, respectively, which include proton excitations coupled to neutron-core excitations. A detailed description of this work is given in Ref. [2].

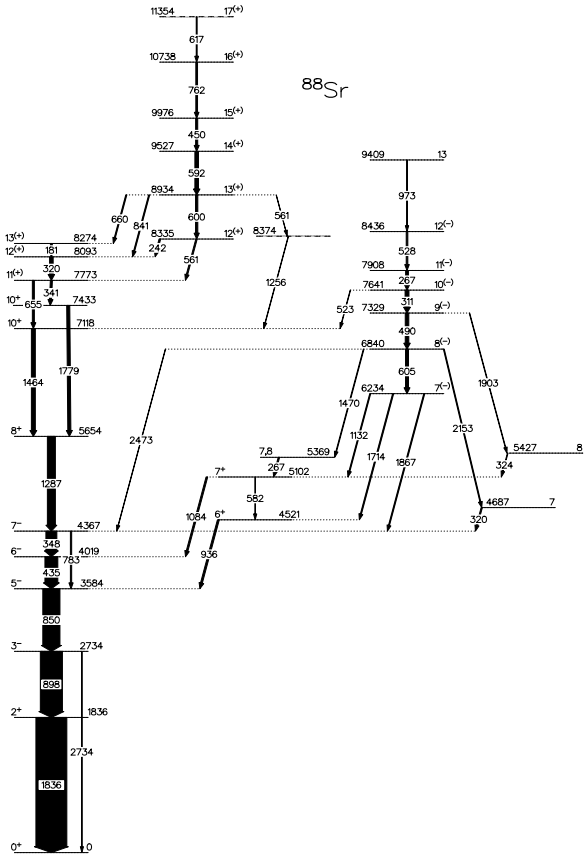

Fig. 1 *Level scheme of ^{88}Sr deduced from the present experiment.*

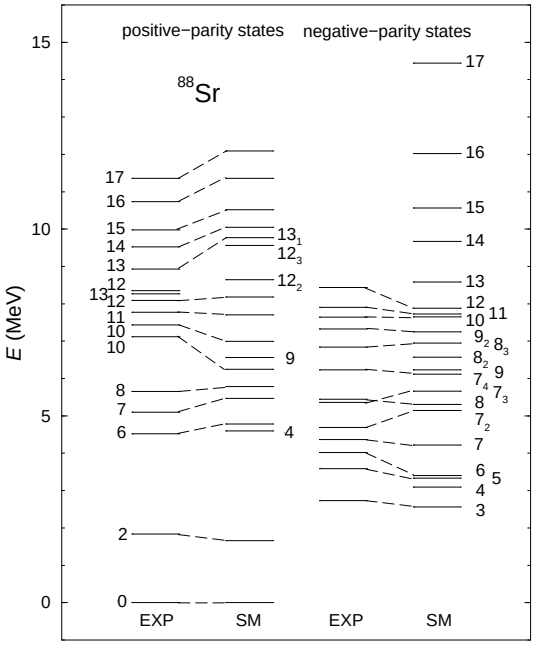

Fig. 2 *Comparison of experimental with calculated level energies in ^{88}Sr.*

[1] *FZR and Institute for Nuclear Research and Nuclear Energy, BAS, 1784 Sofia, Bulgaria*
[2] *Institut für Kernphysik, Universität zu Köln, 50937 Köln, Germany*

References

[1] P.C. Li et al., Nucl. Phys. A 462 (1987) 26
[2] E.A. Stefanova et al., Phys. Rev. C 62 (2000) 054314

Gamma and Beta Decay of the 12^+ Yrast Trap in ^{52}Fe [E,G]

A. Gadea,[1,2] S.M. Lenzi[3], D.R. Napoli[1], C.A. Ur[4], G. Martínez-Pinedo[5], M. Górska[6], M. Axiotis[1], G. de Angelis[1], F. Brandolini[3], D. Cano-Ott[2], E. Farnea[2], E. Nácher[2,6], B. Rubio[2], J. L. Tain[2], R. Borcea[6], J. Döring[6], H. Grawe[6], Z. Janas[6,7], R. Kirchner[6], M. La Commara[6], C. Mazzocchi[6,8], E. Roeckl[6], K. Schmidt[6], C. Fahlander[9], M. Hellström[9], L. Batist[10], A. Plochocki[7], J. Żylicz[7], C. Plettner, R. Schwengner

The spectroscopy of $1f_{7/2}$-shell nuclei provides a good test for shell-model calculations and the associated effective interactions. Recent advances in experimental techniques [1,2] have enabled detailed in-beam studies of high-spin states in many of the $N \approx Z$ nuclei in the $1f_{7/2}$ shell, and a similarly impressive progress has been made in large-scale shell-model (LSSM) calculations [3,4]. The high-spin spectrum of ^{52}Fe ($N = Z = 26$) represents a particular experimental challenge due to the presence of a 12^+ isomer which acts as a "trap" for the de–exciting γ–ray flux. In a recent work [5] performed with the γ–ray detector array GASP, the level scheme of ^{52}Fe has been extended up to the 10^+ state lying above the yrast 12^+ isomer. In the present report, preliminary results on the γ and β decays of the 12^+ state are presented. The experiment was performed at the GSI on-line mass separator, where a 2.5 mg/cm^2 thick ^{nat}Si target was bombarded by a 209 MeV ^{36}Ar beam. The mass 52 secondary beam was implanted in a tape which moved away every 80 s. The implantation position was viewed by a plastic scintillator with a β-detection efficiency of 85%, two composite germanium detectors of the Cluster and Clover type, and a 60% single germanium crystal. The absolute efficiency of the germanium detectors was 3.9% for a γ-ray energy of 1332 keV, which improves the detection sensitivity limit by a factor of 100 compared to that achieved in the previous study [6].

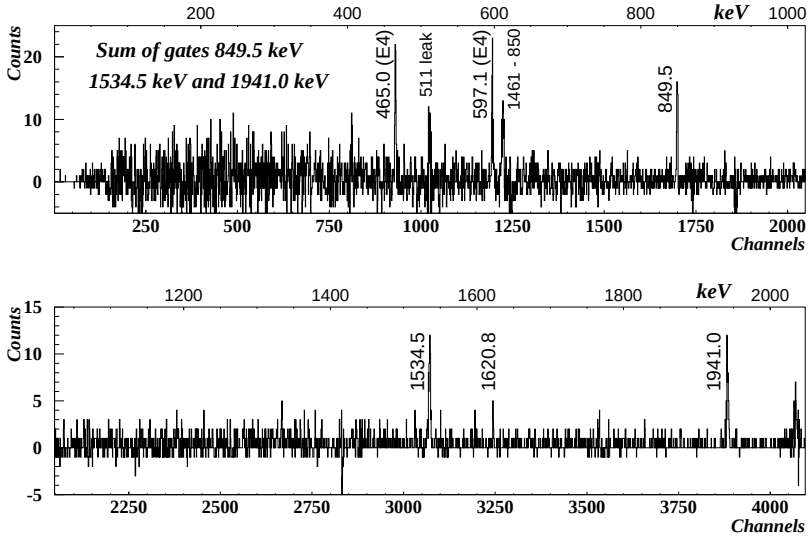

Fig. 1 *Spectrum gated on the main transitions in ^{52}Fe and in anti-coincidence with the β-counter.*

Events with β-γ-γ and γ-γ coincidences were recorded and afterwards sorted into 3D-cubes and 2D-matrices. The analysis of the γ-γ coincidences, including the "add-back" of the composite detectors and a veto condition derived from the β counter (see Fig. 1), allowed us for the first time to observe the γ de-excitation of the 12^+ isomer to the two 8^+ states via E4 transitions of 597.1 and 465.0 keV, thus giving the excitation energy of the isomer as 6957.5(4) keV (see Fig. 2). This value is significantly more accurate than the previous result deduced from β decay measurements [6] and yields better agreement with the LSSM predictions [5]. The intensities per total isomer decay have been estimated to be $1.3(4) \times 10^{-4}$ for the 597.1 keV $12^+ \rightarrow 8_1^+$ and

$0.9(3) \times 10^{-4}$ for the 465.0 keV $12^+ \rightarrow 8_2^+$ transition. We have also observed the second 11^+ state of ^{52}Mn populated in ^{52}Fe 12^+ β-decay (see Fig. 2) with an apparent feeding of 0.5%, which is in good agreement with the theoretical value of 0.3% predicted by the LSSM calculation.

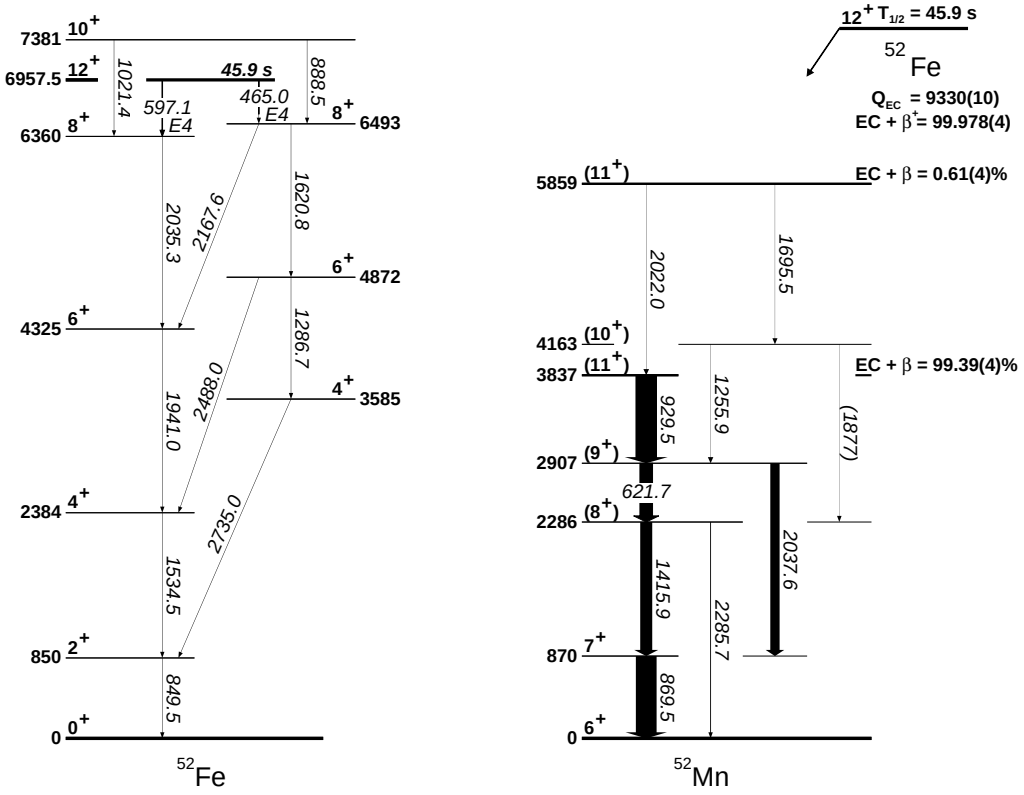

Fig. 2 *γ-decay (left) and β-decay (right) level schemes.*

[1] *LNL-INFN, Legnaro, Italy*
[2] *IFIC, Valencia, Spain*
[3] *Dipartimento di Fisica and INFN, Padova, Italy*
[4] *H. Hulubei NIPNE, Bucharest, Romania*
[5] *University of Aarhus, Denmark*
[6] *GSI, Darmstadt, Germany*
[7] *University of Warsaw, Poland*
[8] *Universitá degli Studi di Milano, Italy*
[9] *Lund University, Sweden*
[10] *PNPI, Gachina, Russia*

References

[1] S. M. Lenzi et al., Z. Phys. A 354, 117 (1996)
[2] S. M. Lenzi et al., Phys. Rev. C 56, 1313 (1997)
[3] E. Caurier et al., Phys. Rev. Lett. 75, 2466 (1995)
[4] G. Martínez-Pinedo et al., Phys. Rev. C 54, R2150 (1996)
[5] C.A. Ur et al., Phys. Rev. C 58, 3163 (1998)
[6] D.F. Geesaman et al., Phys. Rev. C 19, 1938 (1979)

Decay Properties of ^{93}Pd [A,G]

K. Schmidt[1,5], C. Mazzocchi[1,2], R. Borcea[1], J. Döring[1], S. Galanopoulos[3], M. Gośka[1], H. Grawe[1], S. Harissopulos[3], M. Hellström[4], Z. Janas[1], R. Kirchner[1], G. Kriembardis[3], M. La Commara[1], A. Ostrowski[5], G. Rainovski, E. Roeckl[1]

Neutron-deficient isotopes in the vicinity of the $N = Z$ line have attracted considerable experimental and theoretical attention over the last years. Among the key points of interest are investigations in the framework of the astrophysical rp-process [1] and studies of the residual proton-neutron interaction [2]. Reaction network calculations of the rp-process [3] identified, along with other isotopes such as ^{92}Pd and ^{96,97}Cd, the very proton-rich nucleus ^{93}Pd ($Z = 46, N = 47$) as a probable waiting point in the reaction path in X-ray burst scenarios. Calculations of this kind require, amongst other nuclear properties, β-decay half-lives as input parameters.

The nucleus ^{93}Pd was produced in the fusion-evaporation reaction ^{58}Ni(^{40}Ca,αn)^{93}Pd at a beam energy of 188 MeV. The reaction products were collected and ionised in a FEBIAD-E ion source. The mass-separated $A = 93$ beam collected from the GSI Online Mass Separator was implanted in a thin carbon foil in front of a $\Delta E - E$ silicon telescope which served as a detector for β-delayed protons. Figure 1 shows the energy spectrum containing 205 events, obtained within a measuring time of 14.3 hours. For part of the time, the beam was flipped between the collection position on the carbon foil and a beam dump, thus allowing for the recording of time-differential data. A comparison of the number of β-delayed protons registered during beam-on and beam-off periods yielded a half-life of $T_{1/2} = 0.7^{+0.2}_{-0.1}$ s.

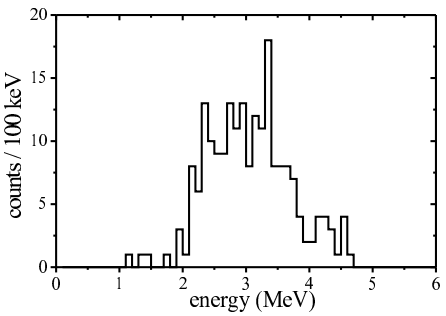

Fig. 1 *Energy spectrum of β-delayed protons recorded at mass $A = 93$.*

In addition to the measurement of β-delayed protons, β-delayed γ-rays were investigated by using an array of 13 germanium detectors and a plastic scintillator, mounted at a separate beamline. Gamma transitions of 239.7 keV, 381.7 keV, 621.7 keV, and 864.1 keV were identified in measurements of mass-separated $A = 93$ sources and preliminarily assigned to the decay of ^{93}Pd. The time characteristics of these γ-lines yield a half-life of $T_{1/2} = (1.0 \pm 0.3)$ s in good agreement with the value deduced from the proton data. Shell model calculations in the mass range $A = 86 - 100$ [4] predict a ground-state spin of either $7/2^+$ or $9/2^+$ for the isotope ^{93}Pd, while a low-lying $1/2^-$ isomer can not be excluded. The calculated disintegration mode of the ground-state is an allowed Gamow-Teller β-decay with a half-life of $T_{1/2} = 1.4$ s. Due to the good agreement with the calculations, we attribute the observed activity of β-delayed protons and γ-rays to the ground-state decay of ^{93}Pd. ^{93}Ag, on the other hand, is predicted [4,5] to be unbound with respect to direct proton emission from its ground state. The search for direct protons at mass $A = 93$ was unsuccessful.

[1] *GSI, D-64291 Darmstadt, Germany*
[2] *Universita degli Studi di Milano, I-20133 Milano, Italy*
[3] *N.C.S.R. Democritos, GR-15310 Aghia Paraskevi, Greece*
[4] *Lund University, P.O. Box 118, S-22100 Lund, Sweden*
[5] *University of Edinburgh, Edinburgh EH9 3JZ, United Kingdom*

References

[1] R.K. Wallace and S.E. Woosley, Astrophys. J. Suppl. 45, 389 (1981)
[2] A.L. Goodman, Phys. Rev. C 60, 014311 (1999)
[3] H. Schatz et al., Physics Reports 294, 167 (1998)
[4] H. Herndl and B.A. Brown, Nucl. Phys. A 627, 35 (1997)
[5] P. Möller et al., At. Data and Nucl. Data Tables 59, 185 (1995)

Static Quadrupole Moment of Five-Quasiparticle $K = \frac{35}{2}$ Isomer in ^{179}W Studied with the LEMS Method [B]

D. L. Balabanski[1,2] K. Vyvey[1], G. Neyens[1], N. Coulier[1], R. Coussement[1], G. Georgiev[1], A. Lèpine-Szily[1,3], S. Ternier[1], S. Teughels[1], M. Mineva[4], P. M. Walker[5], P. Blaha[6], D. Almehed, S. Frauendorf[7]

This study addresses the following question: is there a difference between the deformation of the nuclei in their ground states and in their high-seniority multi-quasiparticle excitations often observed as isomeric states. The importance of this question is related to the question of the quenching of the pairing correlations in atomic nuclei. The nuclear deformations are present as a parameter in many calculations, which requires that they should be determined experimentally. Prior to this experiment [1], only the quadrupole moments of the high-K isomers in ^{182}Os ($K^\pi = 25^+$), ^{178}Hf ($K^\pi = 16^+$) and ^{177}Lu ($K^\pi = \frac{23}{2}^-$) were known. For the latter two isomers the deformation which was deduced is similar to the ground-state deformation. In the case of ^{182}Os there is a considerable difference between the ground state and isomeric quadrupole moment.

The spectroscopic quadrupole moment of the high-spin, high-K five-quasiparticle isomer ($K^\pi = \frac{35}{2}^-, T_{1/2} = 750(80)$ ns, $E_i = 3349$ keV) in ^{179}W has been determined using the Level Mixing Spectroscopy (LEMS) method [1]. A value $Q_s = 4.00(^{+0.83}_{-1.06})eb$ was derived, which corresponds to an intrinsic quadrupole moment $Q_0 = 4.73(^{+0.98}_{-1.25})eb$ and to a quadrupole deformation $\beta_2 = 0.185(^{+0.038}_{-0.049})$. These values differ significantly from the deduced ground-state quadrupole moments and are in disagreement with the current theoretical predictions in this mass region.

Hartree-Fock-Bogolyubov calculations within the framework of the Tilted Axis Cranking (TAC) theory [2] permit us to take into account possible mixing between bands with different K values. Such effects were found to be small. TAC yields a value for the quadrupole moment of this isomer $Q_s = 6.223$ eb if pairing is treated with the particle number projection technique [3] and $Q_s = 6.343$ eb without it (the neutron pairing is zero in this case). These values of the quadrupole moment correspond to an axially symmetric nucleus with deformations $\epsilon_2 = 0.228$ and $\epsilon_4 = 0.038$, which coincide practically with the calculated ground-state deformations for ^{179}W: $\epsilon_2 = 0.226$ and $\epsilon_4 = 0.039$ but contradict with the measured quadrupole moment for the isomer.

In conclusion, we have measured the quadrupole moment of the $K = \frac{35}{2}$, $E_i = 3349$ keV isomer in ^{179}W. The deduced deformation of this state is smaller, compared to the systematic trend of the ground-state deformations of the nuclei in the region, and smaller than the theoretically predicted values. Further improvement of the experimental accuracy is probably needed. At the same time the exploration of other theoretical aspects is necessary, since it seems impossible to explain these differences within the well established schemes to calculate nuclear deformations in this mass region.

[1] *University of Leuven, IKS, Celestijnenlaan 200 D, Leuven, Belgium*
[2] *Faculty of Physics, St. Kliment Ohridski University of Sofia, BG-1164 Sofia, Bulgaria*
[3] *IFU, Sao Paulo, CP 20156, Sao Paulo, Brazil*
[4] *Department of Physics, Lund University, S-221 00 Lund, Sweden*
[5] *Department of Physics, University of Surrey, Guilford GU2 7XH, UK*
[6] *Institut für Physikalische und Theoretische Chemie, Technical University Vienna, A-1060 Vienna, Austria*
[7] *on leave of absence at the Department of Physics, University of Notre Dame, IN 46556, USA*

References

[1] D.L. Balabanski et al., Phys. Rev. Lett. 86, 604 (2001)
[2] S. Frauendorf, Nucl. Phys. A 557, 259c (1993)
[3] D. Almehed et al., Phys. Rev. C 63, 044311 (2001)

Biomedical Research

The activities of the institute in the field of biomedicine have been devoted to two topics: The continuous operation of positron emission tomography (PET) for quality assurance of heavy ion therapy and the improvement of this method, and as a further application of nuclear physics based technology to a biomedical issue, the preparation of an experimental facility at ELBE for cell radiobiology with quasi-monochromatic X-rays.

During the time period reported here (July 1999 – Dec. 2000) 46 Patients suffering from head and neck tumours received carbon ion therapy at the experimental therapy facility at GSI Darmstadt. All these irradiations have been monitored by means of the Rossendorf in-beam PET scanner BASTEI. It could be confirmed that the modifications of the treatment planning data base, which were initiated by PET observations of carbon ion range deviations especially in highly inhomogeneous target volumes, considerably improved the precision and the reliability of the treatments. This allowed the carbon ion therapy to be extended to more delicate situations. An evaluation of the 45 patients with skull base tumours irradiated with carbon beams between December 1997 and September 1999 was published earlier this year (J. Debus et al., Strahlenther. Onkol. 176 (2000) 211). After a mean follow-up of 9 months it revealed that the irradiations were well tolerated by all patients. Partial tumour remission was seen in 7 patients, one-year local control was 94 %, one patient deceased. No severe unexpected toxicity and no local recurrence within the treated volume were observed. The clinical effectiveness and the technical feasibility of the experimental therapy facility could be demonstrated. To evaluate the clinical relevance, larger patient numbers are necessary and, therefore, the treatments will be continued during three time slots of about 4 weeks a year. Continuing this project a new heavy ion accelerator exclusively for clinical use is planned to be constructed in Heidelberg. The facility will be capable of producing therapeutic beams ranging from protons to oxygen ions, it will be equipped with rotating beam deliveries (gantries) that will be combined with in-beam PET for therapy monitoring. These results and future plans determine the current work on the PET project:

- *To increase the flexibility in treatment planning the GSI therapy facility will be equipped with a chair in 2001 for treating patients in a sitting position. This required to built up a completely new PET gantry which allows the detector heads to be rotated around the beam axis.*

- *It is desirable to quantify deviations between the planned and the applied dose distributions on the basis of PET data. Such deviations are caused by slight mispositioning or by changes of the patient's physical condition during the treatment of more than 3 weeks duration. To prepare for this, improved attenuation and scatter correction methods of the measured data as well as refined models (positron range, photon scattering) for predicting the β^+-activity from the treatment planning have been introduced.*

- *Combining an in-beam PET scanner with an ion beam gantry for multi-field irradiations, as it is planned for the Heidelberg clinical facility, requires new technical solutions, namely new scanner configurations. To predict their imaging properties a versatile PET simulation and reconstruction tool has been developed. Gantry-based multi-field therapeutic irradiations may result in PET scans of rather low counting*

statistics and, thus, an optimization of the signal-to-noise ratio is required. For this we studied the possibility of using the new scintillator material Lutetiumorthosilicate (LSO), which is superior to the currently used Bismutgermanate (BGO) with respect to light output and fluorescence time. We analyzed the influence of the time microstructure of the synchrotron beam to the random coincidence rate registered by the positron camera as the basis for improving the signal-to-noise ratio of the PET images by an effective random coincidence rejection.

- *The investigation of an extension of our PET technique to proton therapy monitoring has been initiated.*

In preparation of radiobiological investigations with quasi-monochromatic X-rays produced by electron channeling in diamond at ELBE the following activities have to be reported:

- *The radiation physics beam line, where the radiobiological experiments will be performed, has been designed with special attention to an electron beam of low divergence for a high channeling radiation yield. On that basis the majority of the beam line components have been purchased.*

- *By means of Monte Carlo simulations the different radiation components (channeling X-rays, bremsstrahlung, neutrons) contributing to the dose in the cells have been quantified. The beam line configuration has been optimized to reduce the bremsstrahlung and the neutron background. A dedicated channeling radiation production target is under construction. Nevertheless, for energy dependent cell survival studies a further reduction of the bremsstrahlung background is necessary. This will be performed by means of filters of highly oriented pyrolytic graphite.*

- *The equipment for X-ray dosimetry has been purchased and set into operation. Due to the high attenuation of the rather soft X-rays a reliable dosimetry within the cell monolayers requires special care. As a possible solution the application of thermally stimulated exoelectron emission dosimetry has been studied.*

- *The experimental techniques for cell survival studies have been trained and successfully applied to the measurements of the relative biological effectiveness of 25 kV X-rays.*

- *The cell laboratory attached to ELBE has been designed, construction has been started and the main technical equipment (class 2 safety cabinet, incubator, autoclave, centrifuge and microscope) has been purchased.*

Collaborations

Heavy Ion Tumour Therapy
- GSI Darmstadt
- Radiologische Klinik of the Universität Heidelberg
- Deutsches Krebsforschungszentrum Heidelberg
- Institute for Bioanorganic and Radiopharmaceutical Chemistry (FZ Rossendorf)

Cell Radiobiology at ELBE
- Klinik für Strahlentherapie und Radioonkologie of the TU Dresden
- Institut für Strahlenschutzphysik of the TU Dresden
- Institut für Zoologie of the TU Dresden
- Institute for Bioanorganic and Radiopharmaceutical Chemistry (FZ Rossendorf)

The Redesign of the Positron Camera BASTEI for In-Beam PET Monitoring of Patients Treated with Carbon Ions in a Sitting Position [B,E,G]

W. Enghardt, F. Pönisch, M. Sobiella, P. Crespo[1], D. Schardt[1]

The heavy ion therapy facility at GSI is only capable of delivering a fixed horizontal beam, where the patients have been treated in supine position up to now. This reduces the flexibility in treatment planning for the most frequently treated skull base tumours [1] as a recent analysis of the treatment geometry of such tumours revealed: The heavy ion beam portals giving an optimum dose conformation to the target are found to have an inclination of about 10 to 45 deg with respect to the frontal plane of the patient in supine treatment position [2]. A maximum flexibility for choosing the beam portals as it is usual at medical electron linear accelerators for photon and electron therapy would be achieved with a rotating beam delivery (gantry) [3]. Since such a solution is not feasible at the GSI experimental heavy ion therapy unit, a chair for irradiating patients in a sitting position will be mounted at the therapy site in 2001.

The original design of the positron camera BASTEI [4] was based on the assumption that patients are exclusively irradiated in supine position and thus the detector heads were mounted below and above the table. Evidently they would interfere with a sitting patient. In this case the detector heads have to be rotated into a horizontal or oblique position. Since the positron camera cannot be moved from its park position being 110 cm upbeam to the treatment site before immobilizing the patient, and considering the size of the beam delivery (see Fig. 1), the gap between the heads has to be increased from 83.2 to 115 cm before rotating. After this the camera can be moved downbeam to the patient position and the heads are radially removed to their standard imaging distance of 83.2 cm. To meet these requirements the PET gantry had to be completely rebuilt (Fig. 1).

The gantry reconstruction has been coordinated by Dr.-Ing. Haderthauer, nukmed konstruktion, Tülau-Fahrenhorst, mechanical engineering was carried out by Bernd Flach, Maschinenbau & Kunststoffverarbeitung, Schönheide under the technical leadership of K. Spitzner, and the control system based on the SPS process control units of SIEMENS including the position readout via network by the PET workstation has been developed by Automatisierungstechnik Egbert Neuschulz GmbH, Salzwedel. The reliability of the new gantry was demonstrated during the therapy of Nov./Dec. 2000, when 535 PET scans have been performed.

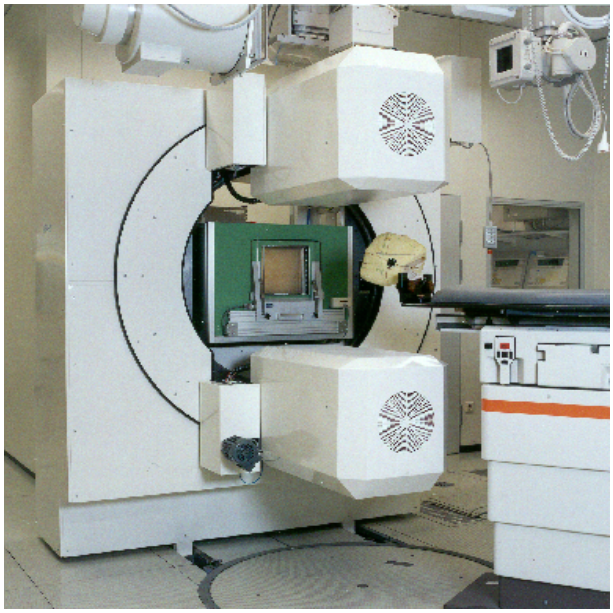

Fig. 1 *The new PET gantry in treatment position. (Photo: A. Zschau, GSI Darmstadt)*

[1] *Gesellschaft für Schwerionenforschung Darmstadt*

References

[1] J. Debus et al., Strahlenther. Onkol. 176 (2000) 211
[2] O. Jäkel, J. Debus, Phys. Med. Biol. 45 (2000) 1229
[3] K.D. Gross, M. Pavlovic (eds.), Proposal for a dedicated ion beam facility for cancer therapy, GSI Darmstadt, 1998
[4] W. Enghardt et al., Strahlenther. Onkol. 175/II (1999) 33

A Realistic Description of Positron Ranges Based on GEANT Simulations [G]

F. Pönisch, B. Naumann[1], W. Enghardt

The monitoring of dose localization at carbon ion tumour therapy at GSI Darmstadt by means of BASTEI [1] requires the comparison between the measurement and a model calculation of the positron activity distributions [2]. For this a realistic description of the positron range distribution in tissue is required. For that purpose a new model is developed and an improved numerical implementation to the code is used.

Up to now the probability distribution of the positron emitter range is supposed to be a bilinear exponential function [3] with three parameters depending on the maximum positron energy. These parameters have been estimated for β^+-endpoint energies up to 3.5 MeV, which is sufficient for PET applications to nuclear medicine. However, in the nuclear fragmentation reactions between the therapeutic carbon ion beam and the atomic nuclei of the tissue β^+-emitters of much higher endpoint energy (up to 16.7 MeV) are produced for which the parametrization of [3] is not proved. Therefore, the positron range distributions have been calculated by means of GEANT [4] simulations for all positron emitting isotopes that may be produced by the fragmentation of ^{12}C ions in tissue. The geometry used in the GEANT calculations consists of an isotropic point-like source in the centre of a water cube being sufficiently large for stopping all the positrons. The initial positron energy values were deduced from the β^+-energy spectra. In Fig. 1 the projection of the 3D spatial distribution on an arbitrary oriented axis (denoted with x) obtained by GEANT is compared with those of Hasch [2] and Derenzo [3]. A much more realistic description of the positron transport in the calculation of the β^+-activity distribution is expected if the 3D positron range distribution (Fig. 2) is applied. Now the distribution function method is used for sampling the range values. A cumulated distribution function (cdf) is constructed from the positron range distribution, which was derived from the GEANT results. The inverse function of cdf is stored in a lookup-table. This database is used for the sampling of the random quantity positron range by means of chosing equally distributed random numbers within the interval [0,1].

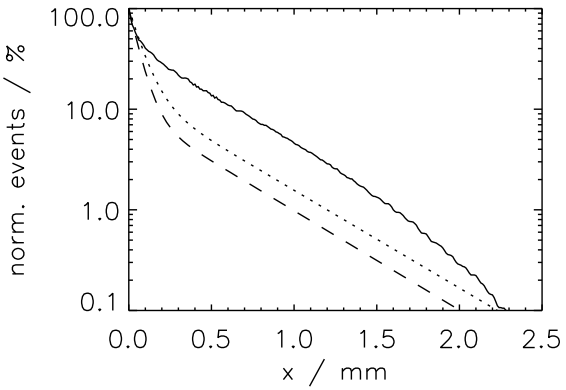

Fig. 1 *Projected point spread function by Derenzo (dashed), Hasch (dotted) and GEANT (solid) for ^{11}C.*

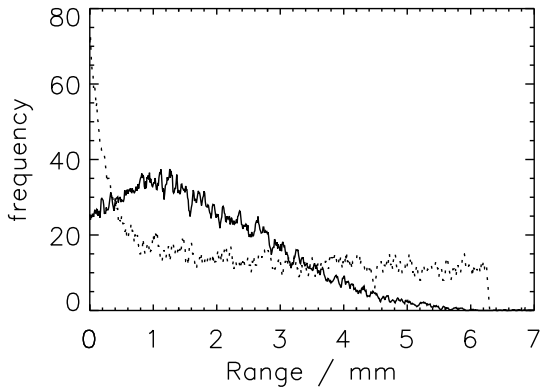

Fig. 2 *Positron range distribution of random quantities implemented by Hasch (dotted) and by GEANT (solid) for ^{15}O.*

[1] *TU Dresden, Institut für Kern- und Teilchenphysik*

References

[1] W. Enghardt et al., Annual Report 1999, FZR-271 (1999) 89
[2] B. G. Hasch et al., Annual Report 1996, FZR-179 (1997) 87
[3] S. E. Derenzo, IEEE Trans. on Nucl. Science, Vol. 33, No.1 (1986) 565
[4] GEANT-Detector Description and Simulation Tool, CERN Prog. Lib. W 5013 (1994)

An X-ray CT Based Attenuation Correction Method for PET [G]

F. Pönisch, W. Enghardt, K. Lauckner[1]

As reported [1] a maximum likelihood algorithm was adapted for the reconstruction of images from data taken by the limited angle double head camera BASTEI at the heavy ion therapy facility of GSI Darmstadt. The necessary attenuation correction algorithm differs from the one which is used in nuclear medicine. The information on tissue composition and densities within the camera field of view (FOV) are derived from X-ray computed tomograms (CT) which are taken for each patient for treatment planning. Additionally, a CT of the head rest is used. These two CT are automatically merged by means of our MERGECT IDL-code. The correct positioning of these CT with respect to the positron camera is derived from stereotactic coordinates used during the diagnostic CT scan and the tumour irradiation with simultaneous PET measurement. The created data set contains all information on the spatial distribution of matter within the positron camera FOV and is the basis for the calculation of attenuation correction factors. The Fig. 1 shows that there is a significant influence of absorption by the head rest on the detector response. The dashed lines denote the acceptance cone of the tomograph. By means of the HU-density calibration curve (Fig. 2) for a given Hounsfield unit (HU) the corresponding density is obtained. Due to the dependence of the mass attenuation coefficients on the tissue composition a segmentation of the HU range into air, soft tissue and bone is applied. The attenuation factors along each coincidence channel (4 millions) are calculated by a forward projection. From Fig. 3 the improvement is evident; whereas without attenuation correction spurious activity is observed inside the nasal cavity it is nearly completely removed after introducing the attenuation correction.

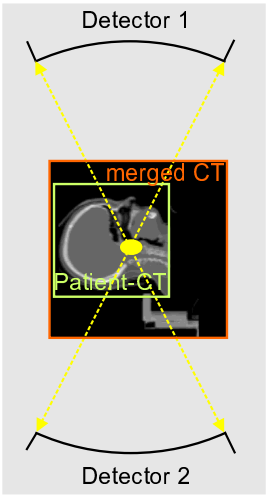

Fig. 1 *PET detector with a sagittal slice of a patient and head rest extended CT.*

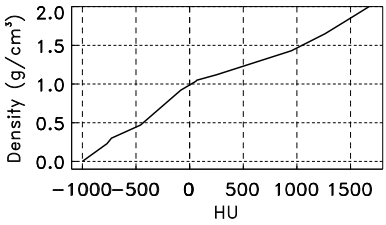

Fig. 2 *Density-Hounsfield unit calibration curve from Zaers [2].*

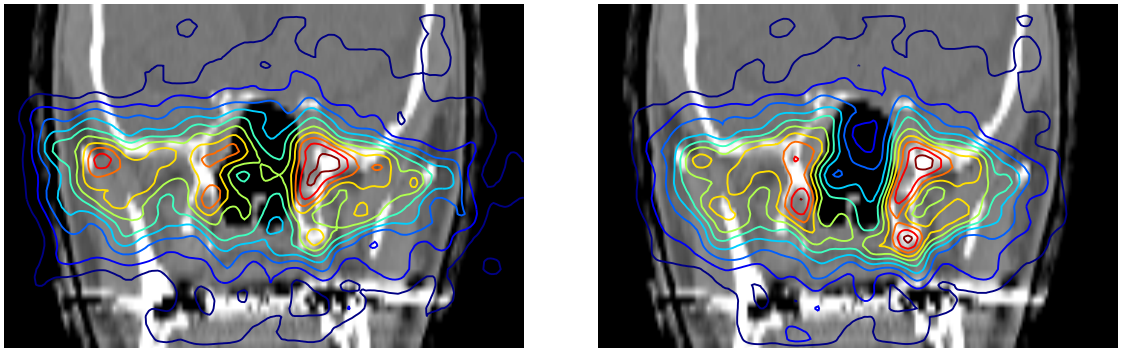

Fig. 3 *Comparison of β^+-activity distributions obtained without (left) and with (right) attenuation correction for a beam portal that is typical for treating skull base tumours. The beam enters the patient from the right side (left on the figure). The β^+-activity isolines are superimposed onto X-ray CT.*

[1] *Gesellschaft für Schwerionenforschung Darmstadt*

References

[1] K. Lauckner et al., Annual Report 1997, FZR-215 (1998) 70
[2] J. Zaers, DKFZ Heidelberg, priv. communication

The Description of Photon Scattering on the Basis of X-ray CT data [G]

F. Pönisch, W. Enghardt, J. Henniger[1]

The process of photon scattering considerably influences the image quality in positron emission tomography (PET): for head and neck imaging only about 20 % of the annihilation photons escape the patient without any interaction with the tissue. About 25 % of the registered true coincidences are influenced by Compton or Rayleigh scattering, which may destroy the correspondence between the source and the reconstructed radioactivity distribution, especially in highly inhomogeneous regions of the human body. In the PET application for quality assurance of carbon ion therapy [1] the scatter problem has to be considered not only with respect to the reconstruction of the source distributions from the measured data but, furthermore, to the prediction of the β^+-activity distribution from the treatment plan and the time course of the irradiation [2]. Since the decision on the correctness of an irradiation is based on the comparison of this prediction with the β^+-activity distribution reconstructed from the data acquired during the patient treatment, both data sets have to be processed the same way. Therefore, the first step of the prediction is a Monte Carlo calculation [2] that describes the stopping of the therapeutic ion beam in tissue, the decay of the β^+-emitters, the propagation of positrons and the annihilation photons and finally the γ-ray detection. This code produces a list mode data set like a measurement and thus it can be reconstructed in the same way as measured data. However, in the original Monte Carlo code photon scattering was processed in a simplified way by assuming a homogeneous scatter volume ($400 \times 200 \times 200\,\mathrm{mm}^3$, $\rho = 1.18\,\mathrm{g/cm}^3$) centered in the field of view (FOV) of the positron camera. Thus, the simulated data had to be reconstructed without attenuation correction. Obviously this approach is quantitatively incorrect and neglects the large tissue inhomogeneities of the head and neck region, as the typical target for carbon ion therapy at GSI. Therefore, a more comprehensive scatter description has been developed. It requires an attenuation map obtained from the X-ray computed tomograms (CT) of the patient and of the equipment for patient positioning within and nearby the camera FOV [3]. The positron and annihilation photon propagation is modelled by means of a Monte Carlo code that takes also into account multiple scattering. To reduce computing time the following approaches that do not influence the accuracy have been introduced: 1) Positron annihilation in air is neglected. 2) The points of interaction are determined by means of the Delta Scattering Photon Transport algorithm of ref. [4], leading to a run time being independent on the voxel size of the CT. 3) The processing of annihilation photons is stopped either after hitting a detector, after escaping the CT image stack or after reducing the photon energy below 250 keV (the lower energy threshold of the positron camera). 4) Due to the coincidence condition it is not necessary to follow the second photon of the annihilation pair if the first photon is not detected. The computing time is reduced by a factor of 4 in comparison with the original method. This CT based photon scatter estimation allows the reconstruction algorithm to be applied to the measured and simulated PET data sets in a similar way. This is, furthermore, the condition for including a scatter correction algorithm in the reconstruction in order to evaluate both simulated and measured data quantitatively.

[1] *TU Dresden, Institut für Strahlenschutzphysik*

References

[1] W. Enghardt et al., Annual Report 1999, FZR-271 (1999) 89
[2] B.G. Hasch et al., Annual Report 1996, FZR-179 (1997) 87
[3] F. Pönisch et al., „An X-ray CT based attenuation correction ...“, this Annual Report
[4] C.H. Holdsworth et. al, IEEE NSS Conference Record 1999, M10-66

Possible Effect of the Carbon Ion Beam Microstructure on In-Beam PET Measurements at GSI Darmstadt [B]

K. Parodi, W. Enghardt, H. Eickhoff[1], T. Haberer[1], P. Moritz[1], P. Forck[1], A. Peters[1]

The data acquired by the positron camera during the beam spills delivered by the heavy ion synchrotron SIS at GSI Darmstadt are affected by high noise level and are useless for the image reconstruction. A reason could be a wrong correction of random coincidences. The standard method of random correction, identifying random coincidences with delayed ones (delay time of 128 ns and coincidence window 12 ns wide), properly works in nuclear medicine, where the random background seen by the scanner is rather constant in time. In the therapy case, a background correlated in time with the beam microstructure on a time scale comparable to the delay time could lead to an underestimation of random coincidences and hence to the observed increase of noise. In Fig. 1 we sketch the background model used in our simulation approach for reproducing the experimental random (i.e. not related to β^+-activity) prompt and delayed coincidence rates acquired by the camera in spill. The periodical repetition of the bunch Gaussian shape represents the background radiation directly following the beam appearance, whereas the bias c introduces a delayed γ-ray component, due to isomeric de-excitations or radioisotope decay with half-lives longer than several ns.

Our model with FWHM and period values given by in-ring measurements of the beam microstructure at flat top voltage $U_{ft} = 2\,\mathrm{kV}$ (which is applied for a more homogeneous beam structure in time) could not explain all the experimental PET data. Therefore, the microstructure was measured after the extraction in the beam line of the medical cave. At $U_{ft} = 2\,\mathrm{kV}$ the time occurrence of the ions in one RF period (Fig. 2) revealed bunches of lower FWHM than in the accelerator ring. With the new measured T and w values, all the experimental prompt and delayed coincidence rates could be reproduced by simulation, provided that a bias c of some percent with respect to the Gaussian modulation was added. However, at $U_{ft} = 0\,\mathrm{kV}$ the microstructure vanished (Fig. 2), while the in spill PET data could be explained by a loss but not a completely suppression of time correlation at $U_{ft} = 0\,\mathrm{kV}$. Nevertheless, the disagreement could come from slight self-bunching effects, due to the higher beam intensity ($I \simeq 10^7 - 10^8$ ions/s) in the PET acquisitions than in the microstructure investigation ($I \simeq 10^5 - 10^6$ ions/s). On the basis of all these considerations, we want to measure the background radiation seen by the positron camera. If the experiment will confirm our model and hence prove the beam microstructure influence on the in spill PET acquisitions, the last step will be to destroy the microstructure or to find a new method of random correction, overcoming the limitations given by frozen software and hardware features of the scanner installed at GSI.

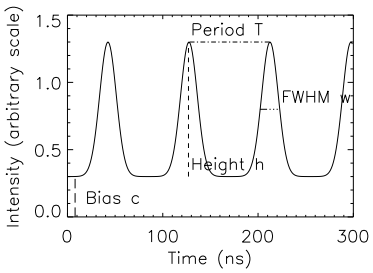

Fig. 1. *Model of the background radiation reaching the scanner during the beam spill.*

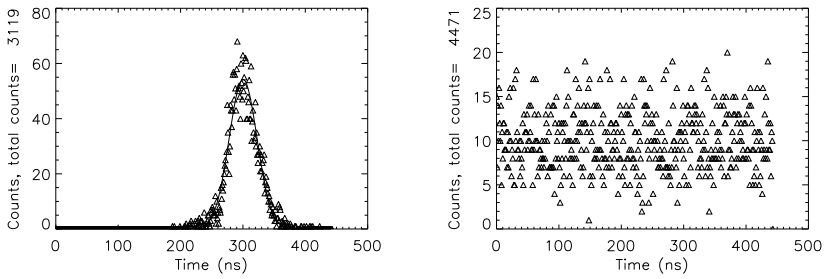

Fig. 2. *Left: example of beam microstructure at $U_{ft} = 2\,kV$. A Gaussian fit is superimposed onto the data. Right: example of not correlated time distribution measured at $U_{ft} = 0\,kV$.*

[1] *Gesellschaft für Schwerionenforschung Darmstadt*

Potential Extension of PET Technique to Proton Therapy Monitoring [B]

K. Parodi, W. Enghardt

In perspective of the proposed proton and heavy ion (up to oxygen nuclei) therapy facility at Heidelberg [1] and on the basis of the positive impact of positron emission tomography to quality assurance of carbon ion therapy at GSI Darmstadt [2], we investigated the potential of PET for proton therapy monitoring [3]. We simulated by means of the FLUKA Monte Carlo code the β^+-activation of a $9 \times 9 \times 30\,\mathrm{cm}^3$ PMMA target ($C_5H_8O_2$, $\rho = 1.19\,\mathrm{g/cm}^3$) irradiated by monoenergetic pencil-like proton beams (FWHM = 10 mm) in the energy range of interest for therapy ($70 - 200\,\mathrm{MeV}$). The selected target contains the most abundant elements of the human body and is very suitable for experimental investigations. The simulated yield of β^+-emitters of main relevance for the PET monitoring, namely ^{11}C, ^{15}O and ^{10}C, and the outcoming activity in 5 minutes (as a typical irradiation time) were found one order of magnitude lower than those induced by carbon ion irradiation at the same range and number of projectiles. But keeping into account the $\simeq 20$ times higher fluence of protons required in order to deliver the same physical dose and, furthermore, the lower relative biological effectiveness of protons in comparison to carbon ions, the activation induced by protons is expected to be at least twice as intense than for carbon ions. However, the spatial correlation between the positron emitter distribution and dose is poorer for protons, since they cannot experience the projectile fragmentation reaction leading to the sharp activity peak close to the dose maximum in the carbon ion case (Fig. 1, right). Nevertheless, the range and Bragg peak position of protons are still correlated to the distal edge of the β^+-emitter depth distribution (Fig. 1, left), depending on the energy threshold of the fragmentation reactions and on the O/C ratio of the irradiated target. Therefore, an important check of particle range and dose localisation seems to be possible for proton irradiation, too.
In practical clinical cases a strategy could be to compare the measured activity with a simulated pattern based on the treatment plan, as already done in the carbon therapy case [2]. Moreover, an in-beam PET scanner is required in order to exploit the quantitative gain in the activity signal, dominated by the contribution of ^{15}O ($T_{1/2} = 121.8\,\mathrm{s}$) according to our estimations in typical mean irradiation times. On the basis of these simulated results and of their agreement with a previous set of off-line PET measurements [4], sensitive only to the activity contribution coming from ^{11}C, a new experiment has been performed with the FZR in-beam PET scanner at GSI Darmstadt in December 2000. The data analysis is currently in progress.

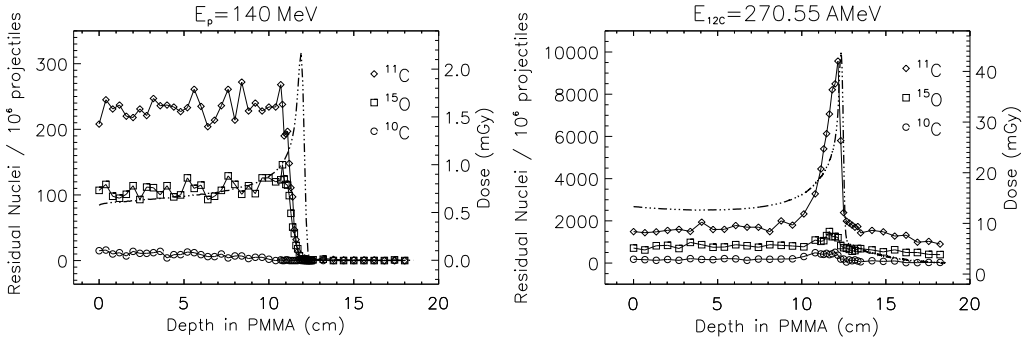

Fig. 1 *Simulated spatial depth distribution of β^+-emitters produced by 10^6 proton and carbon ion projectiles. The dashed-dotted line displays the dose profile. The factor of about 20 between the amount of dose delivered by the same number of primary particles can be seen.*

References

[1] K. D. Gross and M. Pavlovic (eds), Proposal for a dedicated ion beam facility for cancer therapy (GSI Darmstadt, 1998) pp 43-6
[2] W. Enghardt et al., Strahlenther. Onkol. 175 (1999) 33
[3] K. Parodi and W. Enghardt, Phys. Med. Biol. 45 (2000) N151
[4] U. Oelfke et al., Phys. Med. Biol. 41 (1996) 177

Feasibility Study for an LSO-Based In-Beam PET Scanner [B,E]

K. Lauckner[1], P. Crespo[1], W. Enghardt, J. Pawelke

Over the last 3 years in-beam PET has proven its capability of quality assurance in carbon ion tumour therapy at the pilot project of cancer therapy at the Gesellschaft für Schwerionenforschung (GSI) in Darmstadt, Germany [1]. It is planned to integrate a new positron camera into the proposed dedicated hospital-based facility for ion beam therapy in Heidelberg, Germany [2]. We have investigated the possibility of using LSO as the scintillation material for the next generation of in-beam PET cameras.

We address the issue of background coincidences arising from the natural radioactivity of LSO. Natural lutetium contains the radioactive isotope ^{176}Lu with an abundance of 2.59 %, causing a background activity of 280 Bq per cm^3 of LSO. ^{176}Lu undergoes β^--decay feeding excited levels of ^{176}Hf at 597 keV and 998 keV with probabilities of 99.66 % and 0.34 %, respectively. These levels are de-excited via a prompt γ-ray cascade of 307, 202 and 88 keV, which is topped by a 401 keV transition in the case of the 998 keV level. This results in undesired true coincidences when the electron and low-energy γ-rays deposit enough energy in the crystal, where the β^--decay takes place, and the γ-rays of higher energy escape and deposit their energy in an opposite crystal. Because the true count rate measured with the BGO-based dual-head positron camera BASTEI during the cancer treatment averages at only 100 coincidences/s we studied the influence of the LSO background on realistic in-beam PET images.

Therefore, we have estimated the background coincidences expected for the detector geometry of BASTEI assuming LSO as detector material. The estimation takes into account the energy distribution of the electron resulting from the β^--decay, together with all γ-ray combinations that lead to a background coincidence. This has been done for energy windows of 250 - 850 keV, 350 - 650 keV and 400 - 600 keV, two γ-ray combinations that are possible within the energy windows and an energy resolution of 15 % FWHM. Furthermore, the attenuation of the escaping 307 or 401 keV γ-rays due to the presence of the patient has been taken into account.

The analysis [3] shows that the major component of the background of true coincidences caused by ^{176}Lu originates from the escape of the 307 keV γ-ray and subsequent detection by another detector of the positron camera. If, however, an energy window between 350 - 650 keV or narrower is applied these background coincidences are effectively rejected and an influence on the reconstructed β^+-activity distribution can be avoided (Fig. 1).

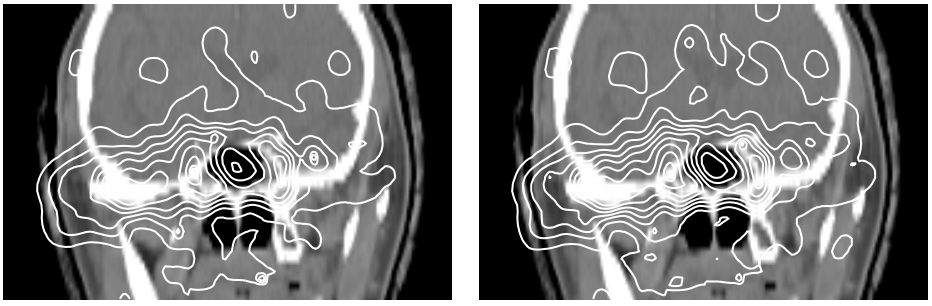

Fig. 1 *The left Figure shows a typical β^+-activity distribution as it was measured by the BGO-based positron camera BASTEI. The image on the right shows the same measured β^+-activity distribution but with background coincidences added to the original PET scan as they would be expected for an LSO-based BASTEI assuming an energy window of 350 - 650 keV.*

[1] *Gesellschaft für Schwerionenforschung Darmstadt*

References

[1] W. Enghardt et al, Nucl. Physics A 654 (1999) 1047c
[2] K.D. Gross, M. Pavlovic (eds.), Proposal for a dedicated ion beam facility for cancer therapy, 1998
[3] K. Lauckner et al, An LSO-based scanner for in-beam PET:
A feasibility study, IEEE NSS/MIC Conf. Rec., 2000

The Combination of an In-Beam PET Scanner with a Rotating Beam Delivery for Ion Tumour Therapy [B,E]

P. Crespo[1], K. Lauckner[1], W. Enghardt

Over the past three years the PET camera installed at the tumour therapy facility in GSI has proven its capability of contributing to the quality assurance of ^{12}C radiotherapy [1]. In this report, we present the first studies concerning the PET camera design and implementation onto a dedicated hospital-based ion beam facility for cancer therapy, proposed to be built in Heidelberg [2] due to the promising results achieved with the GSI pilot project [3]. In the proposed facility, due to the presence of a rotating gantry which will deliver the heavy ion beam - thus satisfying an important medical need [4], the flexibility of the PET camera must be enhanced so that it does not collide with the patient or the couch nor with the beam gantry, as well as it allows a fast access of the physicians to the patient.

Figures 1 and 2 depict possible PET scanner implementations. In Fig. 1, the scanner moves along the patient couch and, thus, can be positioned around the region being irradiated. An aperture on the tomograph ring allows the beam to pass through without touching the γ-ray detectors. This configuration can provide a full coverage of the volume under observation if the scanner rotates 180° around its axial direction (Z_{PET}) during the beam extraction cycle (spill off, $\sim$2 s). This detail, besides being relevant for the image quality, is also important for a quantitative analysis of the measured β^+-activity. If typical dimensions of a PET scanner are applied, an aperture of 30 cm for the beam is considered (param. 7) and the distance between the scanner and its support ring is 40 cm (param. 10), the map plotted in Fig. 3 is obtained. The black and dark grey areas correspond to beam gantry and patient couch angle combinations not suitable for therapy because the beam penetrates the patient through the trunk of the body (caudo-cranial direction). The angle combinations mapped in light grey are free for irradiation only if the beam leaving the target volume does not activate substantially the scanner support structure. In this configuration the scanner never approaches the patient.

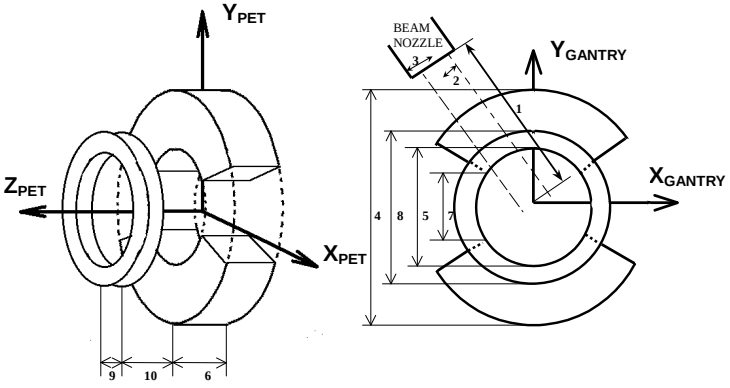

Fig. 1 *PET scanner connected with the patient couch. The couch lies along Z_{PET} and the camera rotates, before the beginning of the treatment, facing the beam with its aperture (not shown).* ***Legend:*** *1) Nozzle distance to isocenter, 2) Beam radius, 3) Nozzle radius, 4) Scanner outer radius, 5) Scanner inner radius, 6) Scanner width, 7) Scanner aperture for beam, 8) Support ring outer radius, 9) Support ring width and 10) Distance between scanner and its support ring.*

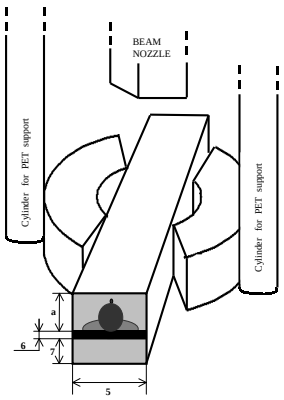

Fig. 2 *PET scanner connected with the gantry, placed perpendicular to the beam nozzle. The central parallelepiped represents the volume reserved for patient and couch.* ***Legend:*** *1) through 4) as in Fig. 1. 5) Couch width. 6) Couch thickness. 7) Vertical range. a) $\frac{couch\ width}{2}$*

In Fig. 2 the PET scanner is depicted, which is assumed to be connected to the gantry and to be placed parallel to the beam nozzle (the beam does not collide with the scanner or its support structure in any situation). A collision study yields a minimal scanner aperture of 75 cm in

order for no physical collisions to occur between scanner and patient/couch. If the scanner is placed parallel to the beam nozzle the minimum aperture needed decreases to 65 cm (the present dual-head PET scanner at the GSI therapy facility has 63 cm aperture). These collision studies did not take into account the movement of the scanner into the measurement position.

In addition to the collision studies summarized, we have developed the tools to quantify the spatial resolution degradation as one moves from a closed ring to an open ring PET camera configuration: (i) a simulation capable of treating several camera geometries and (ii) a flexible image reconstruction routine being capable of reading the output from the simulations. The reconstruction uses an iterative procedure based on the maximum likelihood estimation maximization algorithm. Due to the enormous amount of crystal combination possibilities (over 150 million), dynamic memory allocation is used in conjunction with a developed factorization scheme, which obliged the routine to differ substantially from the one presently used at the GSI therapy unit [5].

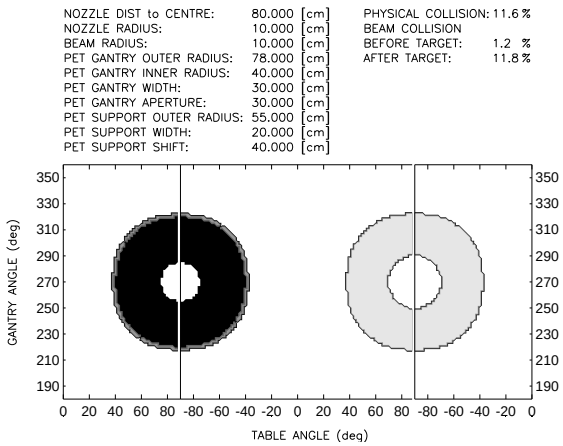

Fig. 3 *Collision study for the case PET connected with the patient couch. Black area: physical collision between beam gantry and scanner. Dark grey area: beam collides with scanner support ring* ***before*** *the target volume. Light grey area: as dark grey but* ***after*** *irradiating the target volume.*

In Fig. 4 we depict the first results on the spatial resolution degradation if one moves from a closed ring to an open ring detector assembly. No Compton scattering effects on the detector were simulated yet, the attenuation of the γ-rays in the crystals and thus the depth-of-interaction influence on the spatial resolution was taken into account. The degradation in spatial information experimentally observed for detector crystals coupled to photomultipliers according to the modified ANGER principle was also not included.

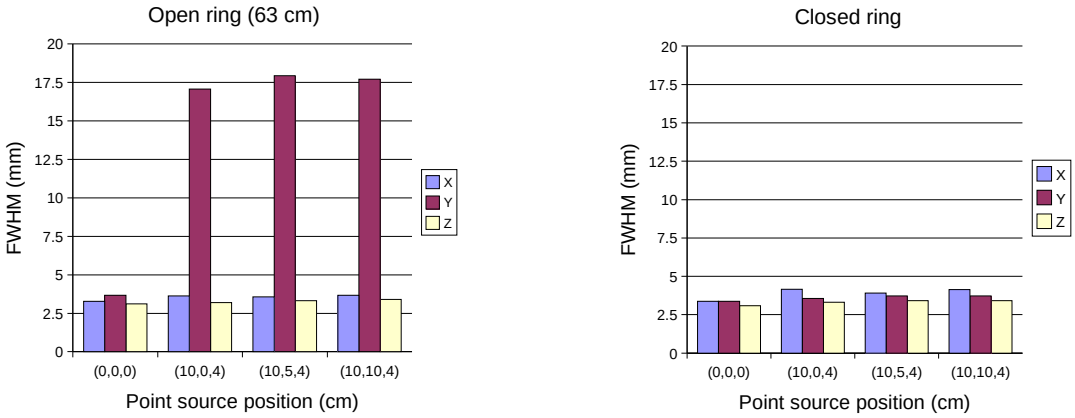

Fig. 4 *Comparison between the spatial resolution achieved with a closed ring versus an open ring positron camera (diameter: 82.3 cm, aperture: 63 cm, Fig. 1), built up of crystals of* $5.0 \times 4.5\,mm^2$ *frontal surface and 30 mm depth.*

[1] *Gesellschaft für Schwerionenforschung Darmstadt*

References

[1] W. Enghardt et al., GSI Scientific Report (1999) 164-5

[2] K.D. Gross, M. Pavlovic (eds.), Proposal for a dedicated ion beam facility for cancer therapy, GSI Darmstadt, 1998

[3] J. Debus et al., Strahlenther. Onkol., 176 Nr 5, (2000) 211-6

[4] O. Jäkel and J. Debus, Phys. Med. Biol. 45 (2000) 1229-41

[5] K. Lauckner, Ph.D. Thesis, Dresden University of Technology, 1999

TSEE Dosimetry of Soft X-rays

J. Pawelke, A. Panteleeva

The measurement of RBE by cell irradiation requires precise determination of dose, delivered to the cell target. Absolute dose measurements are usually done by an air-filled ionisation chamber. However, in the case of low energy X-rays (below 10 keV) it does not sample the cell target because of the high attenuation. Detection based on thermally stimulated exoelectron emission (TSEE) allows to sample the depth dose distribution in a cell monolayer ($\approx 5\,\mu$m thick), because the thickness of the sensitive detector layer is of the order of ~ 10 nm [1]. A TSEE prototype system (Dr. Holzapfel Messgerätelabor, Teltow) consisting of 3 types of thin-film BeO (100 nm) detectors and a counter based on a spherical anode Geiger-Müller methane gas-flow counter was tested. The irradiation was performed with a high-activity beta-source (^{90}Sr), a calibrated gamma-source (^{137}Cs) and a soft X-ray source (^{55}Fe). Highest response as well as stability were shown by detector type I (fig. 1, table 1, same results were obtained with ^{55}Fe source), which proves that the 200 nm Au layer contributes for better mechanical attachment of the BeO layer as well as for electrical stability. The saturation in the dose response (fig. 2) due to the limited pulse resolution of the gas-flow counter results in an upper detection limit of about 0.1 Gy and is far from the requirements of the cell survival studies (≤ 10 Gy). Therefore it cannot be used as online monitoring system. In order to determine the dose delivered to cells, measurements must be done in the presence of cell culture medium. Irradiations were made after wetting the surface and showed no change in the detector response due to any tribo-effect [2]. As expected detector response after irradiation of detectors covered with about 0.5 mm propanol with low energy X-rays from ^{55}Fe source and high energy photons from ^{22}Na source was reduced only due to attenuation in the liquid layer. However, the dependence of the detector response on photon energy and dose rate must still be studied.

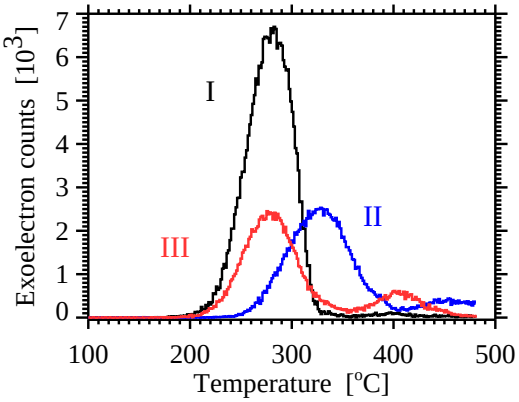

Fig. 1 *Typical glow curves of thin-film BeO detectors.*

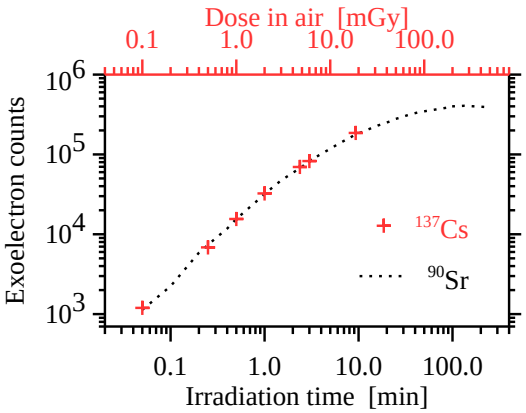

Fig. 2 *TSEE response of detector type I to electron (^{90}Sr) and photon (^{137}Cs) irradiation.*

Table 1 *Main detector properties.*

Detector type	Layer structure	Sensitive area [mm^2]	Peak range [^{o}C]	Reproducibility[a] [%]	Sensitivity[b] [counts/mGy]
I	BeO-Au-C	43.0	180...360	1.8	15538
II	BeO-C-Al	146.4	200...410	2.6	7603
III	BeO-C	146.4	180...360	9.6	6137

[a]) average error of the mean for a series of 8 measurements with ^{90}Sr [b]) ^{137}Cs, dose in air

References

[1] J.S. Durham et. al., Radiation Protection Dosimetry, Vol. 39(1991), No 1/3, pp. 67-70

[2] H. Eichenüller, Radiation Protection Dosimetry, Vol. 4(1983), No 3/4, pp. 281-285

The Determination of RBE of Soft X-rays

A. Panteleeva, K. Brankovic[1], W. Dörr[1], W. Enghardt, J. Pawelke, D. Slonina[2]

The superconducting electron linear accelerator ELBE, at present under construction at Forschungszentrum Rossendorf, is going to be used to produce various types of secondary radiation, among which are X-rays in the energy range 100 eV - 100 keV. At the first stage, monochromatic X-rays in the energy range 10 keV - 50 keV will be obtained by means of planar channeling of high-energy electrons in a diamond crystal. Such an unconventional X-ray source is rather compact, tuneable and allows the possibility of delivering a beam in picosecond pulses [1]. The relative biological effectiveness (RBE) of the X-rays in this energy range will be determined by studies of cell survival and cytogenetic damage. Precise RBE values are required for risk assessment in diagnostic radiology, such as mammography, and radiotherapy with soft X-rays (brachytherapy). It has been previously shown that soft X-rays are more effective in cell killing [2] and chromosome abberations induction [3]. In preparation of radiobiological studies at ELBE, experiments were performed with a 25 kV soft X-ray tube and a 200 kV reference X-ray tube at TU Dresden. The cell line NIH/3T3 mouse fibroblasts was chosen because it is widely used, easy to handle, and contact-inhibited. The cells were cultured in DMEM supplemented with 10 % bovine serum, 10 mM HEPES buffer, 1 mM Sodium Pyruvate, 1 % non-essential aminoacids, 100 U/ml penicillin and 100 μg/ml streptomycin (all from Biochrom Seromed) at 37^{o}C in air containing 5 % CO_2. Exponentially growing cells were irradiated in 25 cm^2 polystyrene flasks at dose rates 1.22 Gy/min (200 kV, 20 mA, 0.3 mm Al filter) and 1.67 Gy/min (25 kV, 20 mA, 0.5 mm Cu filter). After irradiation the cells were harvested, counted and seeded at appropriate densities (6-8 replicates per dose point). After 12 days, colonies having at least 50 cells were scored as offspring from 1 surviving cell.

The RBE value at 10 % survival, determined by a linear-quadratic model fit was found to be 1.28 ± 0.5. As the photon energy is decreasing, the secondary electron spectrum becomes dominated by low-energy electrons and this leads to higher localisation of damage. The comparison of the energy spectrum of the 25 kV X-ray tube (measured with a Si PIN photodiode) and the 200 kV X-ray tube (modelled) revealed that in the first case the main contribution to the dose is coming by the photons of energy 10 - 20 keV, whereas in the second case, photons of this energy range contribute to the absorbed dose only by 4 %. Although the results obtained are not in contradiction with published data, there is a demand for accurate determination of RBE photon energy dependence.

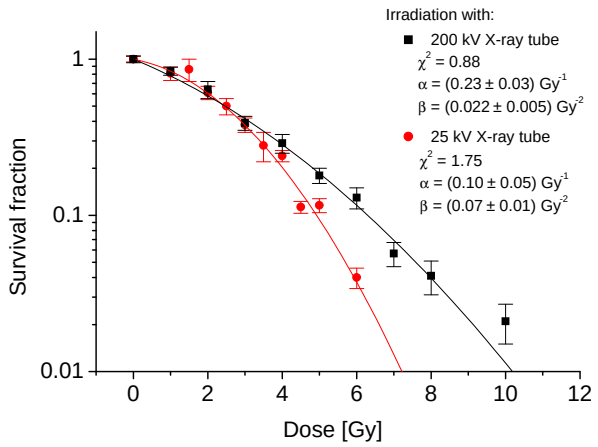

Fig. 1 *Clonogenic survival of NIH/3T3 cells after 25 kV and 200 kV X-ray tube irradiation.*

[1] *Dresden University of Technology, Germany*
[2] *Centre of Oncology, Krakow, Poland*

References

[1] W. Enghardt et. al., Acta Physica Polonica, Vol. 30 (1999), No. 5, pp. 1639-1645
[2] M. Bistrovic et. al., Radiother. Oncol., Vol. 7 (1986), No. 2, pp. 175-180
[3] R.P. Virsik et. al., Radiat. Environ. Biophys., Vol. 14 (1977), No. 2, pp. 109-121

PUBLICATIONS AND TALKS

Publications

From the authors printed in **bold** further information can be obtained

Peculiarities of Isotopic Temperatures Obtained from p+A Collisions at 1 GeV
(Eur. Phys. J. A 8 (2000) 9)

Andronenko, M.N., L.N. Andronenko, **W. Neubert**, D.M. Seliverstov

Abstract: Nuclear temperatures were extracted from fragment yields obtained in inclusive measurements of p+A collisions at 1 GeV. All thermometers based on double-isotopic yield-ratios provide temperatures T$\simeq$ 4 MeV nearly independent of the target mass.

Spin Transfer in Exclusive Λ Production from pp Collisions at 3.67 GeV/c
(Phys. Rev. Lett. 38 (1999) 1534)

Balestra, F., Y. Bedfer, R. Bertini, L.C. Bland, A. Brenschede, F. Brochard, M.P. Bussa, V. Chalyshev, Seonho Choi, **M. Debowski,** M. Dzemidzic, J.-Cl. Faivre, I.V. Falomkin, L. Fava, L. Ferrero, J. Foryciarz, V. Frolov, R. Garfagnini, D. Gill, A. Grasso, S. Heinz, V.V. Ivanov, W.W. Jacobs, W. Kühn A. Maggiora, M. Maggiora, A. Manara, D. Panzieri, H.-W. Pfaff, G. Piragino, G.B. Pontecorvo, A. Popov, J. Ritman, P. Salabura, F. Tosello, S.E. Vigdor, G. Zosi (DISTO Collaboration)

Abstract: We report the first polarization transfer measurements for exclusive hyperon production reactions. The normal spin transfer coefficient D_{NN} for $pp \to pK^+K^-\Lambda$ is large and negative for forward Λ production at a beam momentum of 3.67GeV/c, a result qualitatively consistent with expectations for a mechanism dominated by kaon-exchange and rescattering. The sign of D_{NN} is opposite to that observed in the fragmentation regime for inclusive Λ production at much higher energies.

K^- Meson Production in the Proton–Proton Reactions at 3.67 GeV/c
(Phys. Lett. B 468 (1999) 7)

Balestra, F., Y. Bedfer, R. Bertini, L.C. Bland, A. Brenschede, F. Brochard, M.P. Bussa, V. Tchalyshev, Seonho Choi, **M. Debowski,** M. Dzemidzic, J.-Cl. Faivre, I.V. Falomkin, L. Fava, L. Ferrero, J. Foryciarz, I. Fröhlich, V. Frolov, R. Garfagnini, D. Gill, A. Grasso, **E. Grosse,** S. Heinz, V.V. Ivanov, W.W. Jacobs, W. Kühn, A. Maggiora, M. Maggiora, A. Manara, D. Panzieri, H.-W. Pfaff, G. Piragino, G.B. Pontecorvo, A. Popov, J. Ritman, P. Salabura, F. Tosello, S.E. Vigdor, G. Zosi

Abstract: The total cross section of the reaction $pp \to ppK^+K^-$ has been determined for proton–proton reactions with $p_{beam} = 3.67\ GeV/c$. This represents the first cross section measurement of the $pp \to ppK^-K^+$ channel near threshold, and is equivalent to the inclusive $pp \to ppK^-X$ cross section at this beam momentum. The cross section determined at this beam momentum is about a factor 20 lower than that for inclusive $pp \to ppK^+X$ meson production at the same CM energy above the corresponding threshold. This large difference in the K^+ and K^- meson inclusive production cross sections in proton-proton reactions is in strong contrast to cross sections measured in sub-threshold heavy ion collisions, which are similar in magnitude at the same energy per nucleon below the respective thresholds.

The ANKE Spectrometer at COSY-Jülich and Studies of the Subthreshold K^+ Production
(Nucl. Phys. A 663 (2000) 1107c)

Barsov, S., U. Bechstedt, G. Borchert, W. Borgs, M. Buscher, **M. Debowski**, W. Erven, R. Esser, P. Fedorets, D. Gotta, M. Hartmann, H. Junghans, A. Kacharava, B. Kamys, F. Klehr, H.R. Koch, V.I. Komarov, V. Koptev, P. Kulessa, A. Kulikov, V. Kurbatov, G. Macharashvili, R. Maier, S. Mikirtychyants, S. Merzlyakov, **H. Müller**, A. Mussgiller, M. Nioradze, H. Ohm,

A. Petrus, D. Prasuhn, K. Pysz, F. Rathmann, ¡u¿B. Rimarzig¡/u¿, Z. Rudy, R. Schleichert, **C. Schneider**, H. Schneider, O.W.B. Schult, H. Seyfarth, K. Sistemich, H.J. Stein, H. Ströher (ANKE Collaboration)

Abstract: The new spectrometer ANKE has been put into operation at the accelerator COSY of the Forschungszentrum Jülich. It enables the study of forward going ejectiles from proton-induced reactions at internal targets in COSY. First measurements of the double differential cross sections for the subthreshold K^+-production in pA collisions have been performed at projectile energies as low as 1.0 GeV, i.e. 0.58 GeV below the free nucleon-nucleon threshold.

First Results from Subthreshold K^+ Production Measurements with ANKE
(Nucl. Phys. A 675 (2000) 230c)

Barsov, S., U. Bechstedt, G. Borchert, W. Borgs, M. Buscher, **M. Debowski**, W. Erven, R. Esser, P. Fedorets, D. Gotta, M. Hartmann, H. Junghans, A. Kacharava, B. Kamys, F. Klehr, H.R. Koch, V.I. Komarov, V. Koptev, P. Kulessa, A. Kulikov, V. Kurbatov, G. Macharashvili, R. Maier, S. Mikirtychyants, S. Merzlyakov, **H. Müller**, A. Mussgiller, M. Nioradze, H. Ohm, A. Petrus, D. Prasuhn, K. Pysz, F. Rathmann, **B. Rimarzig**, Z. Rudy, R. Schleichert, **C. Schneider**, H. Schneider, O.W.B. Schult, H. Seyfarth, K. Sistemich, H.J. Stein, H. Ströher (ANKE Collaboration)

Abstract: The new spectrometer ANKE has been put into operation at the accelerator COSY of the Forschungszentrum Jülich. An initial scientific goal is to study K^+-production in pA collisions at subthreshold energies bellow the free NN-threshold of T=1.58 GeV. First measurements of double differtial cross sections in $p^{12}C$ collisions at emission angles around 0^o have been performed at T=1.0, 1.2 and 2.0 GeV. The challenge is to identify the kaons in a huge background of pions and protons, since the signal to background ratio decreases to about 10^{-6} at T=1.0 GeV. For background suppression detectors and a trigger system based on energy-loss and time-of-flight measurements have been developed. In the analysis the decay of kaons (τ=12.4 ns) stopped in the detection system into μ^+ and π^+ is exploited as well as the track information from the wire chambers.

Study of Medium Modifications with the New Spectrometer ANKE at COSY-Jülich
(Acta Phys. Polon B 31 (2000) 357)

Barsov, S., U. Bechstedt, G. Borchert, W. Borgs, M. Buscher, **M. Debowski**, W. Erven, R. Esser, P. Fedorets, D. Gotta, M. Hartmann, H. Junghans, A. Kacharava, B. Kamys, F. Klehr, H.R. Koch, V.I. Komarov, V. Koptev, P. Kulessa, A. Kulikov, V. Kurbatov, G. Macharashvili, R. Maier, S. Mikirtychyants, S. Merzlyakov, **H. Müller**, A. Mussgiller, M. Nioradze, H. Ohm, A. Petrus, D. Prasuhn, K. Pysz, F. Rathmann, **B. Rimarzig**, Z. Rudy, R. Schleichert, **C. Schneider**, H. Schneider, O.W.B. Schult, H. Seyfarth, K. Sistemich, H.J. Stein, H. Ströher (ANKE Collaboration)

Abstract: The accelerator COSY at the Forschungszentrum Juelich provides proton beams with energies up to 2.6 GeV for medium-energy hadron research. ANKE, an internal target magnetic spectrometer at the internal beam of COSY, is used to investigate medium effects in proton–nucleus reactions. It has been installed in the accelerator ring and commissioned in 1998. As a first experiment, subthreshold K^+-production has been studied in $p^{12}C$ collisions.

The COSY-TOF Barrel Detector
(Nucl. Instr. Meth. A 443 (2000) 238)

Böhm, A., K.-Th. Brinkmann, **S. Dshemuchadse**, H. Freiesleben, P. Herrmann, B. Jakob, H. Koch, J. Krug, E. Kuhlmann, J.S. Lange, **P. Michel, K. Möller, A. Schamlott,** P.

Schönmeier, A. Schülke, M. Steinke, G.Y. Sun, M. Würschig-Pörsel, U. Zielinski

Abstract: A barrel-shaped scintillator hodoscope was developed as part of the time-of-flight spectrometer TOF operated at an external beam line of the cooler synchrotron COSY. The COSY-TOF spectrometer is used mainly to perform kinematically complete experiments on light meson production and proton-proton bremsstrahlung in proton-proton collisions for laboratory energies up to 2.5 GeV. The newly developed scintillator hodoscope (BARREL1), one of several detector segments of the COSY-TOF spectrometer, consists of one layer of 96 scintillator bars of 15 mm thickness arranged to form a barrel with 3 m in diameter and 2.85 m in length. For any given interaction process the TOF spectrometer allows to determine the velocity vectors of all charged ejectiles emerging from the target by measuring the time of flight between the start and the stop detector as well as the point of impact on the stop detector. For the BARREL1 detector the position information is obtained by two-sided light read-out of the scintillator bars. For minimum ionizing particles the spatial resolution was measured to be Δ z(FWHM) = 8 cm, corresponding to a polar angle resolution in the range 0.57 to 2.86 degrees, depending on the hit position. The binning in azimuthal angular direction amounts to 360/96 = 3.75 degrees. For the time-of-flight resolution of minimum ionizing particles a value of Δ t(FWHM) = 0.61 ns was obtained.

Shears Mechanism in ^{109}Cd

(Phys. Rev. C 61 (2000) 034318)

Chiara, C.J., S.J. Asztalos, B. Busse, R.M. Clark, M. Cromaz, M.A. Deleplanque, R.M. Diamond, P. Fallon, D.B. Fossan, D.G. Jenkins, S. Juutinen, N.S. Kelsall, R. Krücken, G.J. Lane, I.Y. Lee, A.O. Macchiavelli, R.W. MacLeod, G. Schmid, J.M. Sears, J.F. Smith, F.S. Stephens, K. Vetter, R. Wadsworth, **S. Frauendorf**

Abstract: Lifetimes of high-spin states in two $\Delta I = 1$ bands and one $\Delta I = 2$ band in ^{109}Cd have been measured using the Doppler shift attenuation method in an experiment performed using the ^{96}Zr(^{18}O,5n) reaction with the GAMMASPHERE array. Experimental total angular momenta and reduced transition strengths for both $\Delta I = 1$ bands were compared with tilted axis cranking (shears mechanism) predictions and the $\Delta I = 2$ band with principal axis cranking predictions, based on configurations involving two proton $g_{9/2}$ holes and one or three valence quasineutrons from the $h_{11/2}$ and mixed $g_{7/2}/d_{5/2}$ orbitals. Good overall agreement for angular momentum versus rotational frequency has been observed in each case. The $\Delta I = 2$ band is shown to have a large $\Im^{(2)}/B(E2)$ ratio suggestive of antimagnetic rotation. Additionally, both dipole bands show a decreasing trend in $B(M1)$ strength as a function of spin, a feature of the shears mechanism. The experimental results are also compared with a semiclassical model that employs effective interactions between the proton holes and neutrons as an alternate interpretation for the shears mechanism.

Sideward Flow of K^+ Mesons in Ru+Ru and Ni+Ni Reactions near Threshold

(Phys. Lett. B 486 (2000) 6)

Crochet, P., N. Herrmann, K. Wisniewski, Y. Leifels, A. Andronic, R. Averbeck, A. Devismes, C. Finck, A. Gobbi, O. Hartmann, K.D. Hildenbrand, P. Koczon, T. Kress, R. Kutsche, W. Reisdorf, D. Schüll, J.P. Alard, V. Barret, Z. Basrak, N. Bastid, I. Belyaev, A. Bendarag, G. Berek, R. Caplar, N. Cindro, P. Dupieux, M. Dzelalija, M. Eskef, Z. Fodor, Y. Grishkin, B. Hong, J. Kecskemeti, Y.J. Kim, M. Kirejczyk, M. Korolija, **R. Kotte**, M. Kowalczyk, A. Lebedev, K.S. Lee, V. Manko, H. Merlitz, S. Mohren, D. Moisa, **W. Neubert**, A. Nianine, D. Pelte, M. Petrovici, **C. Plettner**, F. Rami, B. de Schauenburg, Z. Seres, B. Sikora, K.S. Sim, V. Simion, K. Siwek-Wilczynska, V. Smolyankin, A. Somov, M. Stockmeier, G. Stoicea, M.

Vasiliev, P. Wagner, **D. Wohlfarth**, J.T. Yang, I. Yushmanov, A. Zhilin

Abstract: Experimental data on K^+ meson and proton sideward flow measured with the FOPI detector at SIS/GSI in the reactions Ru+Ru at 1.69 AGeV and Ni+Ni at 1.93 AGeV are presented. The K^+ sideward flow is found to be anti-correlated (correlated) with the one of protons at low (high) transverse momenta. When compared to the predictions of a transport model, the data favour the existence of an in-medium repulsive K^+ nucleon potential.

Bestrahlung von Schädelbasistumoren mit Kohlenstoffionen bei der GSI
(Strahlenther. Oncol. 176 5 (2000) 211)

Debus, J., Th. Haberer, D. Schulz-Ertner, O. Jäkel, F. Wenz, **W. Enghardt,** W. Schlegel, G. Kraft, M. Wannenmacher

Abstract: Background: Radiobiological and physical examinations suggest clinical advantages of heavy ion irradiation. We report the results of 23 women and 22 men (median age 48 years) with skull base tumors irradiated with carbon ion beams at the Gesellschaft für Schwerionenforschung (GSI), Darmstadt, from December 1997 until September 1999.
Patients and Methods: The study included patients with chordomas (17), chondrosarcomas (10) and other skull base tumors (Table 1). It is the first time that the intensity-controlled rastercan-technique and the application of positron-emission tomography (PET) for quality assurance was used. All patients had computed tomography for three-dimensionaltreatment planning (Figure 1). Patients with chordomas and chondrosarcomas underwent fractionated carbon ion irradiation in 20 consecutive days (median total dose 60 GyE). Other histologies were treated with a carbon ion boost of 15 to 18 GyE delivered to the macroscopic tumor after fractionated stereotactic radiotherapy (median total dose 63 GyE).
Result: Mean follow-up was 9 months. Irradiation was well tolerated by all patients. Partial tumor remission was seen in 7 patients (15.5%)(Figure 2). One-year local control rate was 94%. One patient (2.2%) deceased. No severe toxicity and no local recurrence within the treated volume were observed.
Conclusion: Clinical effectiveness and technical feasibility of this therapy modality could clearly be demonstrated in our study. To evaluate the clinical relevance of the different beam modalities studies with larger patient numbers are necessary. To continue our projects a new heavy ion accelerator exclusively for clinical use is planned to be constructed in Heidelberg.

A Hybrid Version of the Tilted Axis Cranking Model and its Application to ^{128}Ba
(Phys. Rev. C 62 (2000) 024315)

Dimitrov, V.I., **S. Frauendorf, F. Dönau**

Abstract: A hybrid version the deformed nuclear potential is suggested, which combines a spherical Woods Saxon potential with a deformed Nilsson potential. It removes the problems of the conventional Nilsson potential in the mass 130 region. Based on the hybrid potential, tilted axis cranking calculations are carried out for the magnetic dipole band in ^{128}Ba.

Chirality of Nuclear Rotation
(Phys. Rev. Lett. 84 (2000) 5732)

Dimitrov, V.I., **S. Frauendorf, F. Dönau**

Abstract: It is shown that the rotating mean field of triaxial nuclei can break the chiral symmetry. Two nearly degenerate $\Delta I = 1$ rotational bands originate from the left-handed and right-handed solutions.

Medium Effects in K^+ and K^- Production in Nuclear Collisions at Subthreshold Beam Energies
(Nucl. Phys. A 663/664 (2000) 521c)

Dohrmann, F., for the KaoS Collaboration

Abstract:
We have conducted systematic experimental studies of K^+ and K^- production and propagation in nucleus-nucleus collisions at beam energies close to and below the production threshold for free nucleon-nucleon (NN) collisions. In noncentral Au+Au collision, the K^+ mesons are preferentially emitted perpendicular to the reaction plane and the excitation functions for K^+ and K^- mesons nearly coincide when correcting for the threshold energy. In contrast, for NN collisions the K^+ yield exceeds the K^- yield by two orders of magnitude near the respective NN threshold. Both effects are considered to be experimental signatures of a modification of kaon properties in the nuclear medium.

Note on a Search for the Two-Octupole Phonon 2^+ State in ^{208}Pb with Resonant Photon Scattering
(Nucl. Phys. A 674 (2000) 3)

Enders, J., P. von Brentano , J. Eberth , A. Fitzler , C. Fransen , R.-D. Herzberg, H. Kaiser, **L. Käubler**, P. von Neuman-Cosel, N. Pietralla, V.Yu. Ponomarev, A. Richter, **H. Schnare, R. Schwengner,** S. Skoda, H.G. Thomas, H. Tiesler, D. Weisshaar, I. Wiedenhöver

Abstract: Results of a ^{208}Pb (γ,γ') experiment are presented aiming at an identification of the 2^+ member of the long-sought two-octupole phonon multiplet. Four E2 excitations have been observed below 6.5 MeV excitation energy, two of them for the first time. However, in contrast to new results of calculations within the quasiparticle-phonon nuclear model (QPM), no obvious candidate for the two-octupole phonon vibration could be found in the present study. We discuss the $J = 2^+$ states detected in this as well as previous experiments with respect to their possible two-octupole phonon structure.

Neutrons Produced by 1.22 GeV Antiproton Interactions with Nuclei
(Eur. Phys. J. A 8 (2000) 197)

Egidy von, T., P. Figuera, J. Galin, F. Goldenbaum, Ye.S. Golubeva, M. Hasinoff, D. Hilscher, A.S. Iljinov, U. Jahnke, M. Krause, W. Kurcewicz, X. Ledoux, B. Lott, L. Maier, M. Manrique de Lara, **G. Pausch,** L. Pienkowski, B. Quednau, W. Schott, W.U. Schröder, J. Tőke

Abstract: Inclusive neutron energy spectra were measured by time of flight using 1.22 GeV antiprotons from LEAR,CERN, as projectiles and targets from natural Al, Cu, Ag, Ho, Ta, Au, Pb, Bi, U. The sum of two Maxwellian distributions was fitted to the spectra $d^2\sigma/d\Omega dE$) obtained at several forward and backward angles yielding neutron multiplicities M_i and slope or temperature parameters T_i for the low-energy (evaporative, i=1) and high-energy (pre-equilibrium, i=2) parts, respectively. M_1 increases with A, proportional to the nuclear volume, and M_2 is growing with $A^{1/3}$, proportional to the nuclear radius. The T parameters are nearly independent of A. The results are compared with previous multiplicity measurements with a 4π neutron detector, intranuclear cascade calculations and neutron spectra from stopped antiproton annihilation on nuclei. With the measured proton spectra also the ratio of emitted neutrons to protons was determined for Au.

Positron Emission Tomography for Quality Assurance of Cancer Therapy with Light Ion Beams
(Nucl. Phys. A 654 (1999) 1047)

Enghardt, W., J. Debus, T. Haberer, B.G. Hasch, R. Hinz, O. Jäkel, M. Krämer, **K. Lauckner, J. Pawelke, F. Pönisch**

Abstract:Positron emission tomography (PET) offers the possibility of in-situ monitoring the tumour treatment with light ion beams by means of imaging the spatial distribution of β^+-activity that is produced as a byproduct of the therapeutic irradiation via nuclear fragmentation reactions between the projectiles and the atomic nuclei of the tissue within the target volume. The implementation of this PET technique at the experimental tumour therapy facility at the Gesellschaft für Schwerionenforschung (GSI) in Darmstadt and first results of its clinical application are presented.

Moment of Inertia for Multi-Quasiparticle Configurations
(Phys. Rev. C 61 (2000) 064324)

Frauendorf, S., J.A. Sheikh, P.M. Walker, K. Neergard

Abstract: Tilted-axis cranking calculations have been performed for multi-quasiparticle states in well deformed A≈180 nuclei. In the limit of zero pairing, not only are the calculated moments of inertia substantially smaller than for rigid rotation, but also they are close to the experimental values. The moments of inertia are found to be insensitive to dynamic pair correlations

Description of Multi-Quasiparticle Bands by the Tilted Axis Cranking Model
(Nucl. Phys. A 677 (2000) 115)

Frauendorf, S.

Abstract: The selfconsistent cranking approach is extended to the case of rotation about an axis which is tilted with respect to the principal axes of the deformed potential (Tilted Axis Cranking). Expressions for the energies and the intra bands electromagnetic transition probabilities are given. The mean field solutions are interpreted in terms of quantal rotational states. The construction of the quasiparticle configurations and the elimination of spurious states is discussed. The application of the theory to high spin data is demonstrated by analysing the multi quasiparticle bands in the nuclides with $N = 102, 103$ and $Z = 71, 72, 73$.

Breakup Density in Spectator Fragmentation
(Phys. Lett. B 461 (1999) 315)

Fritz, S., C. Schwarz, R. Bassini, M. Begemann-Blaich, S.J. Gaff-Ejakov, D. Gourio, C. Groß, G. Immè, I. Iori, U. Kleinevoß, G.J. Kunde, W.D. Kunze, U. Lynen, V. Maddalena, M. Mahi, T. Möhlenkamp, A. Moroni, W.F.J. Müller, C. Nociforo, B. Ocker, T. Odeh, F. Petruzzelli, J. Pochodzalla, G. Raciti, G. Riccobene, F.P. Romano, A. Saija, M. Schnittker, A. Schüttauf, **W. Seidel**, V. Serfling, C. Sfienti, W. Trautmann, A. Trzcinski, G. Verde, A. Wörner, Hongfei Xi, B. Zwieglinski

Abstract: Proton-proton correlations and correlations of protons, deuterons and tritons with α particles from spectator decays following ^{197}Au + ^{197}Au collisions at 1000 MeV per nucleon have been measured with two highly efficient detector hodoscopes. The constructed correlation functions, interpreted within the approximation of a simultaneous volume decay, indicate a moderate expansion and low breakup densities, similar to assumptions made in statistical multifragmentation models.

The Rossendorf Radiation Source ELBE and its FEL Projects
(Nucl. Instr. and Meth. B 161-163 (2000) 1143)

Gabriel, F., **P. Gippner, E. Grosse,** D. Janssen, **P. Michel, H. Prade, A. Schamlott, W. Seidel**, A. Wolf, **R. Wünsch** and ELBE-crew

Abstract: The Forschungszentrum Rossendorf (FZR) is constructing a superconducting Electron Linac [F. Gabriel, J. Voigtländer, et al., ELBE Design Report 1998, http://www.fz-rossendorf.de/FWQ/report_d.htm; Annual Report 1996, FZR-179 (1997) 3; Annual Report 1997, FZR-215 (1998) 3] with high Brilliance and low Emittance (ELBE) which can deliver a 1 mA cw beam of 40 MeV. ELBE will be equipped with a free-electron laser (FEL) system for the production of infrared (IR) light in the range 5-300 μm and will thus cover the range from the infrared to the THz regime. The electron beam can also be used to generate X-rays, bremsstrahlung, positrons or fast neutrons.

Is there a Unique Thermal Source of Dileptons in Pb(158 A·GeV + Au, Pb Reactions?
(Phys. Lett. B 473 (2000) 20)

Gallmeister, K., B. Kämpfer, O.P. Pavlenko

Abstract: An analysis of the dilepton measurements in the reactions Pb(158 A·GeV + Au, Pb points to a unique thermal source contributing to the invariant mass and transverse momentum spectra.

Unique Large Thermal Source of Real and Virtual Photons in the Reactions Pb(158A GeV) + Pb, Au
(Phys. Rev. C 62 (2000) 057901)

Gallmeister, K., B. Kämpfer, O.P. Pavlenko

Abstract: The data of direct single-photon measurements of the WA98 Collaboration in the reaction Pb(158A GeV) + Pb are analyzed within a thermal model with a minimum number of parameters adjusted to the dilepton data obtained by the CERES and NA50 Collaborations in the reactions Pb(158A GeV) + Au, Pb. The agreement of our model with the WA98 data points to a unique large thermal source emitting electromagnetic radiation is observable in both the real and virtual photon channels.

A Multidimensional Dynamical-Statistical Model of Fission of Excited Nuclei
(Yadernaja Fizika, 63 (2000) 1778)

Gontchar, I.I., A.E. Gettinger, L.V. Guryan, **W. Wagner**

Abstract: A multidimensional stochastic model of decay of excited nuclei is presented. In the model the dynamics of thermal fluctuations of collective variables as well as dissipation of collective kinetic energy and particle emission are accounted for. Potential energy of deformed nucleus is calculated in the framework of both the liquid drop model with sharp surface and the finite range model. The friction parameters are computed by means of the one-body dissipation model. In order to find the inertia parameters the Werner-Wheeler approximation is used. The drift forces are calculated via the entropy of excited nucleus. The entropy is found in the Fermi-gas approximation with a deformation-dependent level density parameter. In the framework of the stochastic model following quantities are calculated and compared with data: 1) the fission probability, 2) the average multiplicity of the neutrons being emitted before scission (precission neutrons), 3) the variance of fission-fragment mass distribution. Dependence of the values of these quantities upon the parameters of the model is considered in details.

Quantum Mechanical Approach to Planar Position Channeling in a Hypersonic Field (I)
(Radiation Effects & Defects in Solids 152 (2000) 269)

Grigoryan, L.Sh., A.R. Mkrtchyan, B.V. Khachtryan, H.F. Khachtryan, **H. Prade, W. Wagner**

Abstract: The solutions of the Dirac equation for a positron channeled in a single crystal which is excited by a longitudinal hypersonic wave have been obtained for the energy interval of 10 MeV $< E \leq$ 100 MeV, and the resonance condition for the interaction between hypersound and positron was deduced. It is shown that the total intensity of the channeling radiation emitted by the relativistic positron in the hypersonic field is formed by the partial intensities of several dominating radiative transitions for which the appropriate conservation law and the Doppler shift of the photon frequency have been determined. Owing to the hypersound the transverse energy of the positron may increase which leads to a larger bandwidth of the emitted lines.

Quantum Mechanical Approach to Planar Positron Channeling in a Hypersonic Field (II) - Inverse Radiative Transitions
(Radiation Effects & Defects in Solids, 152 (2000) 225)

Grigoryan, L.Sh., A.H. Mkrtchyan, H.F. Khachtryan, R.P. Vardapetian, **H. Prade, W. Wagner**

Abstract: Transition probabilities and the intensity of channeling radiation has been calculated for positrons of energy 10 MeV $< E \leq$ 100 MeV channeled in a longitudinal hypersonic crystal-superlattice. It has been found that the hypersound can excite inverse radiative transitions through which the transverse energy of the channeled positron is increased. These transition have a resonant nature if the wavelengths of the hypersound and of the oscillations of the positron during channeling match. This can lead to a considerable intensification of the positron channeling radiation.

Resonant Influence of Hypersound on the Quantum States of an Axially Channeled Electron
(Radiation Effects & Defects in Solids 153 (2000) 13)

Grigoryan, L.Sh., A.R. Mkrtchyan, H.F. Khachtryan, A.H. Mkrtchyan, **H. Prade, W. Wagner**

Abstract: The wave function of an electron of energy 10 MeV $\leq E \leq$ 100 MeV axially channeled in a longitudinal hypersonic superlattice has been obtained within the framework of a quantum mechanical approach. Conditions for the resonant influence of the hypersonic wave excited in the single crystal on the quantum states of the channeled electron have been deduced.

In-Medium Properties of Kaons and Antikaons as Studied by Threshold Production in Nuclear Collisions
(Nucl. Phys. A 654 (1999) 501c)

Grosse, E.

Abstract: In a systematic experimental study of K^+ and K^- production in nuclear collisions at energies close to and below the free nucleon-nucleon production threshold we have found several features indicating a change of kaon properties within the nuclear medium.

Resolved Dipole Strength below the *E*1 Giant Resonance in ^{138}Ba
(Phys. Rev. C 60 (1999) 051307)

Herzberg, R.-D., C. Fransen, P. von Brentano, J. Eberth, J. Enders, A. Fitzler, **L. Käubler,** H. Kaiser, P. von Neumann-Cosel, N. Pietralla, V.Yu. Ponomarev, H. Prade, A. Richter,

H. Schnare, **R. Schwengner,** S. Skoda, H.G. Thomas, H. Tiesler, D. Weisshaar, I. Wiedenhöver

Abstract: The electromagnetic dipole response of ^{138}Ba was measured up to 6.7 MeV excitation energy in a photon scattering experiment. Two Euroball Cluster detectors were used to detect the scattered photons under 94 and 132 degrees. The Cluster at 94 degrees served as a Compton polarimeter. The total observed dipole cross strength and the electric character of most of the transitions has been determined on a state-by-state basis. The data show a concentration of $E1$ strength around 6 MeV. For one of the strongest excitations $M1$ character is suggested. The results of model calculations using the quasiparticle phonon model (QPM) agree with the observed electric dipole strength distribution.

A Measurement of the Coulomb Dissociation of ^{8}B at 254 MeV/Nucleon and the ^{8}B Solar Neutrino Flux
(Phys. Rev. Lett. 83 (1999) 2910)

Iwasa, N., F. Boué, G. Surówka, K. Sümmerer, T. Baumann, B. Blank, S. Czajkowski, A. Förster, M. Gai, H. Geissel, **E. Grosse,** M. Hellström, P. Koczon, B. Kohlmeyer, R. Kulessa, F. Laue, C. Marchand, T. Motobayashi, H. Oeschler, A. Ozawa, M.S. Pravikoff, E. Schwab, W. Schwab, P. Senger, J. Speer, C. Sturm, A. Surowiec, T. Teranishi, F. Uhlig, **A. Wagner,** W. Walus, C.A. Bertulani

Abstract: We have measured the Coulomb dissociation of ^{8}B into ^{7}Be and proton at 254 MeV/nucleon using a large-acceptance focusing spectrometer. The astrophysical S_{17} factor for the ^{7}Be(p,γ)^{8}B reaction at $E_{c.m.}$ = 0.25-2.78 MeV is deduced yielding $S_{17}(0) = 20.6 \pm 1.2$ (exp.) $\pm$ 1.0 (theor .) eV-b. This result agrees with the presently adopted zero-energy S_{17} factor obtained in direct-reaction and with the results of other Coulomb-dissociation studies performed at 46.5 and 51.2 MeV/nucleon.

Prevalence of Fission and Evaporation in the Decay of Heavy Nuclei Excited up to 1000 MeV with Energetic Antiprotons
(Phys. Rev. Lett. 83 (1999) 4959)

Jahnke, U., W. Bohne, T. von Egidy, P. Figuera, J. Galin, F. Goldenbaum, D. Hilscher, J. Jastrzebski, B. Lott, M. Morjean, **G. Pausch,** A. Péghaire, L. Pienkowski, D. Polster, S. Proschitzki, B. Quednau, H. Rossner, S. Schmid, W. Schmid

Abstract: Annihilation of 1.2 GeV antiprotons has been explored as a means to generate high thermal excitation in heavy nuclei (U, Au, Ho) and to observe their decay with a minimal contribution from dynamical $E^* \approx 1000$ MeV. Both modes are increasingly accompanied by a modest emission of intermediate-mass fragments (up to 1 on average), but true multifragmentation is not observed. These features are in agreement with the predictions of the statistical model with no need for a fission delay $\tau_f > 0.5 \times 10^{-21}$ s.

Magnetic Moment Measurements in the Semi-Magic Nuclei ^{94}Ru and ^{95}Rh after Recoil Implantation Into Iron and Nickel
(Eur. Phys. J. A 6 (1999) 29)

Jungklaus, A., D. Kast, K.P. Lieb, C. Lingk, C. Teich, O. Iordanov, T. Härtlein, D. Schwalm, I.P. Johnstone, **R. Schwengner**

Abstract: The magnetic moments of the 12^+ and 11^- yrast states in ^{94}Ru and of the $25/2^-$, $29/2^+$ and $35/2^+$, levels in ^{95}Rh have been measured via the IMPAD technique. The nuclei were produced in the reaction ^{58}Ni + ^{40}Ca and recoil-implanted into polarized Ni and Fe hosts. The g-factors were deduced from the measured time-integral Larmor precessions. The comparison between the experimental results and large-scale shell model calculations suggests that the

12^+ and 11^- states in ^{94}Ru and the $25/2^-$ level in ^{95}Rh are pure proton states whereas the $29/2^+$ and $35/2^+$ states in ^{95}Rh contain a neutron excitation across the N=50 shell gap. This interpretation supports the conclusion drawn from recent lifetime measurements.

The Ter-Mikaelian and Landau-Pomeranchuk Effects for Induced Soft Gluon Radiation in a QCD Medium
(Phys. Lett. B 477 (2000) 171)

Kämpfer, B., O.P. Pavlenko

Abstract: The polarisation of a surrounding QCD medium modifies the induced gluon radiation spectrum of a high-energy parton at small transverse momenta for a single interaction and for multiple scatterings as well. This effect is an analogue of the Ter-Mikaelian effect in QED, superimposed to the Landau-Pomeranchuk effect. We study the Ter-Mikaelian effect in a phase space region where Abelian radiation does occur. In this region the induced gluon radiation is shown to be suppressed due to polarization properties of the medium

Cosmic Phase Transitions
(Ann. Phys. (Leipzig) 9 (2000) 605)

Kämpfer, B.

Abstract: The sequence of phase transitions during the hot history of the universe is followed within a phenomenological framework. Particular emphasis is put on the QCD confinement transition, which is at reach under earth laboratory conditions. A tepid inflationary scenario on the GUT scale with bubble growth at moderate supercooling is discussed.

Is the 4.742 MeV State in ^{88}Sr the 1^- Two-Phonon State
(Eur. Phys. J. A 7 (2000) 45)

Käubler, L., H. Schnare, R. Schwengner, P. von Brentano, **F. Dönau,** J. Eberth, J. Enders, A. Fitzler, C. Fransen, M. Grinberg, **E. Grosse,** R.-D. Herzberg, H. Kaiser, P. von Neumann-Cosel, N. Pietralla, **H. Prade,** A. Richter, S. Skoda, Ch. Stoyanov, H.-G. Thomas, H. Tiesler, D. Weisshaar, I. Wiedenhöver

Abstract: A nuclear resonance fluorescence experiment on ^{88}Sr has been performed with bremsstrahlung of 6.7 MeV endpoint energy. The γ-ray linear polarisation has been measured with a EUROBALL CLUSTER detector used as a Compton polarimeter. The results indicate positive parity for the J=1 state at 4.742 MeV in ^{88}Sr, in contrast to the previous interpretation as a 1^- two -phonon ($2_1^+ \otimes 3_1^-$) state and in conflict with the predictions of the quasiparticle-phonon model. On the basis of such calculations the 1^+ state at 3.486 MeV may be considered as the 1_1^+ one-phonon state and the very strong $1_1^+ \rightarrow 0_1^+$deexcitation as proton spin-flip $2p_{1/2} \rightarrow 2p_{3/2}$ transition.

Pion-Exchange Effects in Elastic Backward Proton-Deuteron Scattering
(Few-Body Systems 27 (1999) 189)

Kaptari, L.P., **B. Kämpfer,** S.M. Dorkin, S.S. Semikh

Abstract: The elastic backward proton-deuteron scattering is analyzed within a covariant approach based on the deuteron vertex function obtained by the Bethe-Salpeter equation with realistic meson-exchange interaction. Contributions of the one-nucleon and one-pion exchange mechanisms to the cross section and polarization observables are investigated in explicit form. Results of numerical calculations for the cross section, tensor analyzing power and spin transfers are presented. The one-pion exchange contribution is essential for describing the spin-averaged cross section, while in polarization observables it is found to have a small effect.

Solar Proton Burning Process Revisited within a Covariant Model Based on the Bethe-Salpeter Formalism
(J. Phys. G 26 (2000) 1423)

Kaptari, L.P., **B. Kämpfer, E. Grosse**

Abstract: A covariant model based on the Bethe-Salpeter formalism is proposed for investigating the solar proton burning process $pp \to De^+\nu_e$ and the near-threshold deuteron disintegration via electromagnetic and weak interactions. Results of numerical calculations of the energy dependence of relevant cross sections and the astrophysical low-energy cross section factor S_{pp} of the proton burning process are presented. Our results confirm previous canonical values, and the energy dependence of the S_{pp} factor is rather close to phenomenological extrapolations commonly adopted in computations of solar nuclear reaction rates.

A High-Energy Resolution Observed from a YAP:Ce Scintillator
(Nucl. Instr. and Methods in Phys. Research A 421 (1999) 610)

Kapusta, M., M. Balcerzyk, M. Moszyński, **J. Pawelke**

Abstract: A energy resolution of 4.38±0.11% was obtained for 662 keV γ-rays with a 3×3×20 mm^3 YAP: Ce crystal with its long face coupled to an XP2020Q photomultiplier. The measured number of photoelectrons of 5290±80 phe/MeV implies a photoelectron statistical contribution of 4.18±0.04% and hence a YAP intrinsic energy resolution of 1.3±0.5% the lowest value ever observed for scintillators. The relative light output of the YAP crystal measured for energies between 14.4 keV and 1.275 MeV was constant within ±2%. These observations are consistent with the assumption that there is a direct correlation between the energy resolution of scintillators and nonproportionality of their light output versus energy.

Comparison of the Scintillation Properties of LSO:Ce and YSO:Ce as the Detectors for High Resolution Pet
(Acta Phys. Polonica B 31 (2000)101)

Kapusta, M., M. Moszyński, M. Balcerzyk, **J. Pawelke**

Abstract: We investigate the application of LSO and YSO scintillating crystals for Positron Emission Tomography (PET). Properties such as light output, energy resolution, detection efficiency for various energy threshold, and timing resolution are presented. These data allow us to evaluate the usage of finger-like LSO:Ce and YSO:Ce crystals coupled to photomultiplier tube, and to establish optimal operating conditions for high-resolution PET. Both crystals have advantages over BGO currently used in PET and LSO is considered as a possible replacement for BGO based systems.

Evidence for Shears Bands in ^{108}Cd
(Phys. Rev. C 61 (2000) 011301)

Kelsall, N.S., R. Wadsworth, S.J. Asztalos, B. Busse, C.J. Chiara, R.M. Clark, M.A. Deleplanque, R.M. Diamond, P. Fallon, D.B. Fossan, D.G. Jenkins, S. Juutinen, R. Krücken, G.J. Lane, I.Y. Lee, A.O. Macchiavelli, C.M. Parry, G.J. Schmid, J.M. Sears, J.F. Smith, F.S. Stephens, K. Vetter, **S. Frauendorf**

Abstract: High-spin states were populated in ^{108}Cd using the ^{96}Zr(^{16}O,4n) reaction at a beam energy of 72 MeV. Two magnetic dipole bands have been observed, both of which contain weak $E2$ crossover transitions. Lifetimes for the stronger of the two bands were measured via the Doppler shift attenuation method. The configuration assignment for this band has been determined from comparison with tilted axis cranking model calculations to be $\pi[g_{9/2}^{-3}g_{7/2}]$

$\otimes$ $\nu[h_{11/2}(g_{7/2}d_{5/2})^1]$ and $\pi[g_{9/2}g_{7/2}]$ $\otimes$ $\nu[h^3_{11/2}(g_{7/2}d_{5/2})^1]$, before and after the $\nu h^2_{11/2}$ band crossing, respectively. The deduced $B(M1)$ strengths decrease rapidly with increasing spin after the $\nu h^2_{11/2}$ alignment, which is a characteristic behavior of a shears band.

On the Space-Time Difference of Proton and Composite Particle Emission in Central Heavy-Ion Reactions at 400 $A\cdot$ MeV
(Eur. Phys. J. A 6 (1999) 185)

Kotte, R., H.W. Barz, W. Neubert, C. Plettner, D. Wohlfarth, J.P. Alard, A. Andronic, R. Averbeck, Z. Basrak, N. Bastid, N. Bendarag, G. Berek, R. Čaplar, N. Cindro, P. Crochet, A. Devismes, P. Dupieux, M. Dželalija, M. Eskef, Z. Fodor, A. Gobbi, Y. Grishkin, N. Herrmann, K.D. Hildenbrand, B. Hong, J. Kecskemeti, Y.J. Kim, M. Kirejczyk, M. Korolija, M. Kowalczyk, T. Kress, R. Kutsche, A. Lebedev, K.S. Lee, Y. Leifels, V. Manko, H. Merlitz, D. Moisa, A. Nianine, D. Pelte, M. Petrovici, F. Rami, W. Reisdorf, B. de Schauenburg, D. Schüll, Z. Seres, B. Sikora, K.S. Sim, V. Simion, K. Siwek-Wilczyńska, A. Somov, G. Stoicea, M.A. Vasiliev, P. Wagner, K. Wiśniewski, J.T. Yang, Y. Yushmanov, A. Zhilin

Abstract: Small-angle correlations of pairs of nonidentical light charged particles produced in central collisions of heavy ions in the A=100 mass region at a beam energy of 400 $A\cdot$MeV are investigated with the FOPI detector system at GSI Darmstadt. The difference of longitudinal correlation functions with the relative velocity parallel and anti-parallel to the center-of-mass velocity of the pair in the central source frame is studied. This method allows extracting the apparent space-time differences of the emission of the charged particles. Comparing the correlations with results of a final-state interaction model delivers quantitative estimates of these asymmetries. Time delays as short as 1 fm/c or - alternatively - source radius differences of a few tenth fm are resolved. The strong collective expansion of the participant zone introduces not only an apparent reduction of the source radius but also a modification of the emission times. After correcting for both effects a complete sequence of space-time emission points of p, d, t, ^{3}He, α particles is presented for the first time.

Production of Charged Pions, Kaons and Antikaons in Relativistic C+C and C+Au Collisions
(Eur. Phys. J. A 9 (2000) 397)

Laue, F., I. Böttcher, **M. Debowski, E. Grosse**, P. Koczon, B. Kohlmeyer, M. Mang, **L. Naumann,** H. Oeschler, F. Pühlhofer, E. Schwab, P. Senger, Y. Shin, J. Speer, H. Ströbele, C. Sturm, G. Surowka, F. Uhlig, **A. Wagner,** W. Walus

Abstract: Production cross sections of charged pions, kaons and antikaons have been measured in C+C and C+Au collisions at beam energies of 1.0 and 1.8 AGeV for different polar emission angles. The kaon and antikaon energy spectra can be described by Boltzmann distributions whereas the pion spectra exhibit an additional enhancement at low energies. The pion multiplicity per participating nucleon $M(\pi^+)/A_{part}$ is a factor of about 3 smaller in C+Au than in C+C collisions at 1.0 AGeV whereas it differs only little for the C and the Au target at a beam energy of 1.8 AGeV. The K^+ multiplicities per participating nucleon $M(K^+)/A_{part}$ are independent of the target size at 1 AGeV and at 1.8 AGeV. The K^- multiplicity per participating nucleon $M(K^-)/A_{part}$ is reduced by a factor of about 2 in C+Au as compared to C+C collisions at 1.8 AGeV. This effect might be caused by the absorption of antikaons in the heavy target nucleus. Transport model calculations underestimate the K^-/K^+ ratio for C+C collisions at 1.8 AGeV by a factor of about 4 if in-medium modifications of K mesons are neglected.

First Measurement of Antikaon Phase-Space Distributions in Nucleus-Nucleus Collisions at Subthreshold Beam Energies
(Phys. Lett. B 495 (2000) 26)

Menzel, M., I. Böttcher, **M. Debowski, F. Dohrmann,** A. Förster, **E. Grosse,** P. Koczon, B. Kohlmeyer, F. Laue, **L. Naumann**, H. Oeschler, F. Pühlhofer, E. Schwab, P. Senger, Y. Shin, H. Ströbele, C. Sturm, G. Surowka, F. Uhlig, **A. Wagner,** W. Walus (KaoS Collaboration)

Abstract: Differential production cross sections of K^- and K^+ mesons have been measured as function of the polar emission angle in Ni+Ni collisions at a beam energy of 1.93 AGeV. In near-central collisions, the spectral shapes and the widths of the rapidity distributions of K^- and K^+ mesons are in agreement with the assumption of isotropic emission. In non-central collisions, the K^- and K^+ rapidity distributions are broader than expected for a single thermal source. In this case, the polar angle distributions are strongly forward-backward peaked and the nonisotropic contribution to the total yield is about one third both for K^+ and K^- mesons. The K^-/K^+ ratio is found to be about 0.03 independent of the centrality of the reaction. This value is significantly larger than predicted by microscopic transport calculations if in-medium modifications of K mesons are neglected.

Direct Evidence for the Breakdown of the N = 8 Shell Closure in ^{12}Be
(Phys. Rev. Lett. 85 (2000) 266)

Navin, A., D. Anthony, T. Aumann, T. Baumann, D. Bazin, Y. Blumenfeld, B. A. Brown, T. Glasmacher, P. G. Hansen, R.W. Ibbotson, P.A. Lofy, V. Maddalena, K. Miller, T. Nakamura, B.V. Pritychenko, B.M. Sherrill, E. Spears, M. Steiner, J.A. Tostevin, J. Yurkon, **A. Wagner**

Abstract: Partial cross sections and corresponding momentum distributions have been studied in the one-neutron knockout reaction (^{12}Be, $^{11}Be + \gamma$) on a ^{9}Be target at 78 MeV/nucleon. The resulting spectroscopic factors for the only two bound states of ^{11}Be are 0.42±0.06 ($1/2^+$) and 0.37±0.06 ($1/2^-$), where the errors are experimental only. This result shows that N = 8 is not a good closed shell in the neutron-rich 12Be and that the last neutron pair is two-thirds in the ($1s^2 + 0^d2$) intruder configuration.

What is the Physics Behind the ^{3}He-^{4}He Anomaly
(Eur. Phys. J. A 7 (2000) 101)

Neubert, W., A.S. Botvina

Abstract: We show that coalescence of nucleons emitted prior to thermalization in highly excited nuclei can explain the anomaly of kinetic energies of helium fragments. This mechanism accomplishes the statistical approach to nuclear rections formerly used to describe intermediate mass fragment production.

Fragment Kinetic Energies and Modes of Fragment Formation
(Phys. Rev. Lett. 84 (2000) 4557)

Odeh, T., R. Bassini, M. Begemann-Blaich, S. Fritz, S.J. Gaff-Ejakov, D. Gourio, C. Groß, G. Immé, I. Iori, U. Kleinevoß, G.J. Kunde, W.D. Kunze, U. Lynen, V. Maddalena, M. Mahi, T. Möhlenkamp, A. Moroni, W.F.J. Müller, C. Nociforo, B. Ocker, F. Petruzzelli, J. Pochodzalla, G. Raciti, G. Riccobene, F.P. Romano, A. Saija, M. Schnittker, A. Schüttauf, C. Schwarz, **W. Seidel**, V. Serfling, C. Sfienti, W. Trautmann, A. Trzcinski, G. Verde, A. Wörner, Hongfei Xi, B. Zwieglinski

Abstract: Kinetic energies of light fragments (A $\leq$ 10) from the decay of target spectators in ^{197}Au + ^{197}Au collisions at 1000 MeV per nucleon have been measured with high-resolution telescopes at backward angles. Except for protons and apart from the observed evaporation

components, the kinetic-energy spectra exhibit slope temperatures of about 17 MeV, independent of the particle species, but not corresponding to the thermal or chemical degrees of freedom at breakup. It is suggested that these slope temperatures may reflect the intrinsic Fermi motion and thus the bulk density of the spectator system at the instant of becoming unstable.

Potential Application of PET in Quality Assurance of Proton Therapy
(Phys. Med. Biol. 45 (2000) N151-N156)

Parodi, K., W. Enghardt

Abstract: Our investigation supporting the feasibility of *in situ* PET monitoring in proton therapy is presented. We simulated by means of the FLUKA code the number and the spatial distribution of the main β^+ emitters created in PMMA targets by protons at typical therapeutic energies. The quantitative comparison with the activation induced by ^{12}C ions of energies corresponding to the same range shows that the available signal at the same physical dose level should be up to twice as intense for protons than actually successfully used for the control of carbon ion therapy at GSI Darmstadt. The spatal correlation between the activity and the dose profile for protons is poorer than for ^{12}C nuclei. However, an important check of the particle range, dose localization and stability of the treatment during all the fractions seems to be possible.

RoSiB - a 4π Silicon Ball for Charged-Particle Detection in EUROBALL
(Nucl. Instr. and Meth. A 443 (2000) 304)

Pausch, G., **H. Prade, M. Sobiella,** H. Schnare, **R. Schwengner, L. Käubler , C. Borcan,** H.-G. Ortlepp, U. Oehmichen, H. Grawe, R. Schubart, J. Gerl, J. Cederkäll, A. Johnson, A. Kerek, W. Klamra, M. Moszyński, D. Wolski, M. Kapusta, A. Axelsson, M. Weiszflog, T. Härtlein, D. Pansegrau, G. de Angelis, S. Ashrafi, A. Likar, M. Lipoglavšek

Abstract: A 4π silicon ball for detection and identification of light charged particles in large multidetector γ-arrays as EUROBALL is presented. The design is based on a N=42 ball with 12 pentagons and 30 hexagons as used in the GASP array. The absorptive material for γ-rays is minimized to the detector thickness of 300 or 500μm and a 0.63 mm ceramic backing. The geometrical coverage is designed for about 90% of 4π. A pulse shape discrimination method with totally depleted detectors working in the reverse mount allows identifying protons and α-particles above an energy threshold of about 2 MeV. The performances of the ball were tested at the tandem - booster accelerator combination of the MPI Heidelberg in two experiments using the high-recoil reaction of 228 MeV ^{58}Ni+^{46}Ti and the low-recoil reaction of 95 MeV ^{16}O+^{58}Ni. The two-dimensional spectra of zero-crossing (ZC) versus energy confirmed an excellent discrimination of protons and α-particles in all the detectors at different angles. The energy spectra of protons and α-particles measured in the experiments are presented, too. The γ-spectra measured in coincidence with various combinations of emitted particles showed a high selectivity of the ball. The reduced total efficiency for protons of 59% and 55% and α-particles of 44% and 32% measured in a nuclear spectroscopy application is analyzed in a Monte-Carlo simulation (GEANT). It is due to a combined influence of a thick target needed to stop the recoiling residual nuclei and thick absorbers needed to protect the Si-detectors from scattered beam. The results along with the GEANT extrapolation to optimum experimental conditions confirm that RoSiB is a highly efficient and selective device for identification of rare reaction channels with heavy ions.

Quark Dispersion Relation and Dilepton Production in the Quark-Gluon Plasma
(Phys. Rev. Lett. 84 (2000) 841)

Peshier, A., M.H. Thoma

Abstract: Under very general assumptions we show that the quark dispersion relation in the quark-gluon plasma is given by two collective branches, of which one has a minimum at a non-vanishing momentum. This general feature of the quark dispersion relation leads to structures (van Hove singularities, gaps) in the low mass dilepton production rate, which might provide a unique signature for the quark-gluon plasma formation in relativistic heavy ion collisions.

Equation of State of Deconfined Matter at Finite Chemical Potential in a Quasiparticle Description
(Phys. Rev. C 61 (2000) 045203)

Peshier, A., B. Kämpfer, G. Soff

Abstract: A quasiparticle description of the thermodynamics of deconfined matter, reproducing both the perturbative limit and nonperturbative lattice QCD data at finite temperature, is generalized to finite chemical potential. By a flow equation resulting from Maxwell's relation, the equation of state is extended from zero to nonzero quark densities. The impact of the massive strange flavor is considered and implications for cold, charge-neutral deconfined matter in β equilibrium in compact stars are given.

Vaporization and Multifragmentation in the Reaction 1.2 GeV $\bar{p}$ + Cu and Ag
(Phys. Lett. B 472 (2000) 15)

Pienkowski, L., W. Bohne, T. von Egidy, P. Figuera, J. Galin, F. Goldenbaum, D. Hilscher, U. Jahnke, J. Jastrzebski, B. Lott, M. Morjean, **G. Pausch,** A. Péghaire, D. Polster, S. Proschitzki, B. Quednau, H. Rossner, S. Schmid, W. Schmid

Abstract: Reactions of 1.2 GeV antiprotons with Cu and Ag targets have been studied. It was found that in such reactions, excitation energies are generated in excess of the total binding energy of the nuclei involved. Accordingly, one observes in these reactions the onset of vaporization and multifragmentation processes. In the $\bar{p}$ + Cu reaction, the vaporization is observed to set in about 7.5 MeV/nucleon. However, its probability remains relatively small and below 15% up to the highest excitation energies identified in the present studies (approximately 15 MeV/nucleon). The threshold excitation energy for multifragmentation prosesses, defined as the detection of a least 3 intermediate mass fragments, is observed at about 4 MeV/nucleon for both studied reactions. Multifragmentation is seen to account for no more than approximately 5% and 20% of the corresponding inclusive yield for Cu and Ag targets, respectively

Very High Rotational Frequencies and Band Termination in ^{73}Br
(Phys. Rev. C 62 (2000) 014313)

Plettner, C., H. Schnare, **R. Schwengner, L. Käubler, F. Dönau,** I. Ragnarsson, A.V. Afanasjev, A. Algora, G. de Angelis, A. Gadea, D.R. Napoli, J. Eberth, T. Steinhardt, O. Thelen, M. Hausmann, A. Müller, A. Jungclaus, K .P. Lieb, D.G. Jenkins, R. Wadsworth, A. N. Wilson, **S. Frauendorf**

Abstract: Rotational bands in ^{73}Br have been investigated up to spins of $I = 65/2$ using the EUROBALL III spectrometer. One of the negative-parity bands displays the highest rotational frequency $\hbar\omega = 1.85$ MeV reported to date in nuclei with $A \geq 25$. At high frequencies, the experimental $\Im^{(2)}$ dynamic moment of inertia for all bands decreases to very low values, $\Im^{(2)} \leq 10\hbar^2$ MeV^{-1}. The bands are described in the configuration-dependent cranked Nilsson-Strutinsky model. The calculations indicate that one of the negative-parity bands is observed up to its terminating single-particle state at spin 63/2. This result establishes the first band termination in the $A \approx 70$ mass region.

Signature Inversion Caused by Triaxiality and Unpaired Band Crossings in ^{72}Br
(Phys. Rev. Lett. 85 (2000) 2454)

Plettner, C., I. Ragnarsson, H. Schnare, **R. Schwengner, L. Käubler, F. Dönau,** A. Algora, G. de Angelis, D.R. Napoli, A. Gadea, J. Eberth, T. Steinhardt, O. Thelen, M. Hausmann, A. Müller, A. Jungclaus, K.P. Lieb, D.G. Jenkins, R. Wadsworth, A.N. Wilson

Abstract: High-spin states in ^{72}Br were studied with the EUROBALL III spectrometer using the ^{40}Ca(^{40}Ca, $\alpha 3p1n$) reaction. The negative-parity band observed in this experiment displays a signature inversion around spin I=16. The interpretation within the cranked Nilsson-Strutinsky approach shows that this signature pattern is a signal of a substantial triaxial shape change with increasing spin where the nucleus evolves from a triaxial shape with rotation about the intermediate axis at low spin through a collective prolate shape to a triaxial shape but with rotation about the shortest principal axis at high spin

Isospin-Tracing: A Probe of Non-Equilibrium in Central Heavy-Ion Collisions
(Phys. Rev. Lett. 84 (2000) 1120)

Rami, F., Y. Leifels, B. de Schauenburg, A. Gobbi, B. Hong, J.P. Alard, A. Andronic, R. Averbeck, V. Barret, Z. Basrak, N. Bastid, I. Belyaev, N. Bendarag, G. Berek, R. Čaplar, N. Cindro, P. Crochet, A. Devismes, P. Dupieux, M. Dželalija, M. Eskef, C. Finck, Z. Fodor, H. Folger, L. Fraysse, A. Genoux-Lubain, Y. Grigorian, Y. Grishkin, N. Herrmann, K.D. Hildenbrand, J. Kecskemeti, Y.J. Kim, P. Koczon, M. Kirejczyk, M. Korolija, **R. Kotte**, M. Kowalczyk, T. Kress, R. Kutsche, A. Lebedev, K.S. Lee, V. Manko, H. Merlitz, S. Mohren, D. Moisa, **J. Mösner, W. Neubert**, A. Nianine, D. Pelte, M. Petrovici, C. Pinkenburg, C. Plettner, W. Reisdorf, J. Ritman, D. Schüll, Z. Seres, B. Sikora, K.S. Sim, V. Simion, K. Siwek-Wilczyńska, A. Somov, M.R. Stockmeier, G. Stoicea, M.A. Vasiliev, P. Wagner, K. Wiśniewski, **D. Wohlfahrt**, J.T. Yang, Y. Yushmanov, A. Zhilin

Abstract: Four different combinations of $^{96}_{44}$Ru and $^{96}_{40}$Zr nuclei, both as projectile and target, were investigated at the same bombarding energy of 400A MeV using a 4π detector. The degree of isospin mixing between projectile and target nucleons is mapped across a large protion of the phase space using two different isospin-tracer observables, the number of measured protons and the t/^{3}He yield ratio. The experimental results show that the global equilibrium is not reached even in the most central collisions. Quantitative measures of stopping and mixing are extracted from the data. They are found to exhibit a quite strong sensitivity to the in-medium (n,n) cross section used in microscopic transport calculations.

Development of Miniaturized Potentiometric Nitrateand Ammonium Selective Electrodes for Applications in Water Monitoring
(Fresenius J. Anal. Chem. 367 (2000) 396)

Schwarz, J., H. Kaden, **G. Pausch**

Abstract: Mobile analysis with potentiometric sensors is well suited for field measurements. Ion-selective electrodes (ISE) based on polymeric membranes for in-situ determination of nitrate and ammonium contents in ground water, drinking water and surface water have been developed. The ISE are integrated in a multisensor module (MSM) for monitoring these ions over longer time intervals. The receptor is a PVC-membrane with tridodecyl-ammonium nitrate (TDDA) for nitrate- and nonactine for ammonium-electrodes as ionophores. As plasticizer dibutylphthalate (DBT) was used. The main parameters for assessing the efficiency of these ISE are presented.

Kaon and Antikaon Production in Proton Nucleus Collisions
(Acta Phys. Polonica B 31 (2000) 2305)

Scheinast, W.

Abstract: For the first time, a systematic study of differential production cross sections of antikaons in proton nucleus collisions close to threshold has been performed, using the first proton beam a t GSI. Preliminary results on K^+ and K^- production in p+Au collisions at a beam energy of 2.5 GeV are presented

Particle Excitations and Rotational Modes in Nuclei with $A \approx$ 70-90
(BgNS Transactions 5 (2000) 136)

Schwengner, R., H. Schnare, **C. Borcan, F. Dönau, L. Käubler**

Abstract: In nuclei in the mass region of $A \approx$ 70-90 a variety of phenomena is observed which are based on single-particle and collective motion of the nucleons. We discuss the properties of Br and Rb isotopes with neutron numbers of 38-48. In light Br isotopes (N=37,38) rotational bands have been observed up to spins of 65/2 and rotational frequencies of 1.8 MeV. Both features can be described in terms of the cranked Nilsson-Strutinsky formalism. In Rb nuclei with N=45, 47 we found regular magnetic dipole bands evolving at high spin whereas the low-spin structure of those less deformed nuclei is irregular. These magnetic dipole bands represent magnetic rotation, a new rotational mode predicted by the tilted-axis cranking model. In nuclei at N=48 we found small collectivity in low-spin states and multiplets based on multi-particle excitations a high spin. These properties are interpreted in terms of the shell-model.

Magnetic Rotation in the A=80 Region: M1 Bands in Heavy Rb Isotopes
(J. Res. Natl. Stand. Technol. 105 (2000) 133)

Schwengner, R., H. Schnare, **S. Frauendorf, F. Dönau, L. Käubler, H. Prade, E. Grosse**, J. Jungclaus, K.P. Lieb, C. Lingk, S. Skoda, J. Eberth, G de Angelis, A. Gadea, E. Farnea, D.R. Napoli, C.A. Ur, G. Lo Bianco

Abstract: We have studied the isotopes $^{82}Rb_{45}$, $^{83}Rb_{46}$, and $^{84}Rb_{47}$ to search for magnetic rotation which is predicted in the tilted-axis cranking model for a certain mass region around A= 80. Excited states in these nuclei were populated via the reaction ^{11}B + ^{76}Ge with E = 50 MeV at the XTU tandem accelerator of the LNL Legnaro. Based on a γ-coincidence experiment using the spectrometer GASP we have found magnetic dipole bands in each studied nuclide. The regular M1 bands observed in the odd-odd nuclei ^{82}Rb and ^{84}Rb include B(M1)/B(E2) ratios decreasing smoothly with increasing spin in a range of $13^- \leq J^\pi \leq 16^-$. These bands are interpreted in the tilted-axis cranking model on the basis of four-quasiparticle configurations of the type $\pi(fp)\ \pi g_{9/2}^2\ \nu g_{9/2}$. This is the first evidence of magnetic rotation in the $A \approx$ 80 region. In contrast, the M1 sequences in the odd-even nucleus ^{82}Rb are not regular, and the B(M1)/B(E2) ratios show a pronounced staggering.

Influence of Neutron-Core Excitations on High-Spin States in ^{88}Sr
(Phys. Rev. C 62 (2000) 054314)

Stefanova, E.A., **R. Schwengner,** J. Reif, H. Schnare, **F. Dönau,** M. Wilhelm, A. Fitzler, S. Kasemann, P. von Brentano, W. Andrejtscheff

Abstract: High-spin states of the nucleus ^{88}Sr have been studied via the reaction ^{80}Se(^{11}B,$p2n$) at a beam energy of 45 MeV. Gamma rays were detected with the six-detector array OSIRIS CUBE. The level scheme of ^{88}Sr has been extended up to $E\approx$11 MeV and J=17. Mean lifetimes of three levels have been determined using the Doppler-shift-attenuation method.

The level structures in ^{88}Sr have been interpreted in terms of the shell model. The calculations were performed in the configuration space ($0f_{5/2}$,$1p_{3/2}$,$1p_{1/2}$,$0g_{9/2}$) for the protons and ($1p_{1/2}$,$0g_{9/2}$,$1d_{5/2}$ for the neutrons. These calculations describe the high-spin level sequences linked by $M1$ transitions with strengths of $B(M1)\approx$0.3 to 1.4 W.u. as multiplets of seniority v=4 and 6 states including proton configurations and neutron-core excitations.

Production of ϕ Mesons in Near Threshold πN and NN Reactions
(Eur. Phys. J. A7 (2000) 543)

Titov, A.I., **B. Kämpfer,** B.L. Reznik

Abstract: We analyze the production of ϕ mesons in πN and NN reactions in the nearthreshold region, using throughout the conventional "non-strange" dynamics based on such processes which are allowed by the non-ideal ω - ϕ mixing. We show that the occurrence of the direct ϕNN interaction may show up in different unpolarized and polarization observables in $\pi N \to N\phi$ reactions. We find a strong non-trivial difference between observables in the reactions $pp \to pp\phi$ and $pn \to pn\phi$ caused by the different role of the spin singlet and triplet states in the entrance channel. A series of predictions for the experimental study of this effect is presented.

Spectroscopy of ^{44,46}Ti with the Binary Reaction Spectrometer and Euroball
(Physica Scripta. T 88 (2000) 114)

Thummerer, S., B. Gebauer, H.G. Bohlen, W. von Oertzen, D. Bazzacco, S.M. Lenzi, A. Algora, G. de Angelis, A. Gadea, D.R. Napoli, C. Borcan, F. Dönau, **L. Käubler, H. Schnare, R. Schwengner,** I. Peter, C. Beck, C. Bhattacharya, M. Rousseau, R. Nouicer, J. Lisle

Abstract: A first experiment was performed with the Binary Reaction trigger Spectrometer (BRS) for Euroball, as second last experiment of phase III. The reaction ^{24}Mg(^{32}S,^{56}Ni*) at E=163.5 MeV was chosen in order to populate a specific hyperdeformed resonance state in the compound nucleus ^{56}Ni* at E=84 MeV (J^π=46$^+$) and to investigate the spectroscopy of its binary descendents. The experimental setup combined the γ-detector array Euroball III, without the phase I Ge detectors, the two large-area gas detector telescopes of the BRS at forward angles and 31 of the 40 detectors of the 4π silicon ball EUROSiB (now called ROSiB) at backward angles. We report on results of binary reaction triggers collected with one BRS telescope. Binary events are separated from evaporation residues due to (i) the large laboratory scattering angles of the detected reaction fragments, the opening angle of the BRS telescope being θ=12° - 46°, and (ii) by means of particle identification in the telescope. In this paper channels with emission of ^{8}Be plus two protons and of ^{12}C will be discussed.

The Emission Pattern of High-Energy Pions: A New Probe for the Early Phase of Heavy Ion Collisions
(Phys. Rev. Lett. 85 (2000) 18)

Wagner, A., C. Müntz, H. Oeschler, C. Sturm, R. Barth, M. Cieslak, M. Debowski, **E. Grosse,** P. Koczon, F. Laue, M. Mang, D. Miskowiec, E. Schwab, P. Senger, P. Beckerle, D. Brill, Y. Shin, H. Ströbele, W. Walus, B. Kohlmeyer, F. Pühlhofer, J. Speer, I.K. Yoo

Abstract: The emission pattern of charged pions has been measured in Au+Au collisions at 1 GeV/nucleon incident energy. In peripheral collisions and at target rapidities, high-energy pions are emitted preferentially towards the target spectator matter. In contrast, low-energy pions are emitted predominantly in the opposite direction. The corresponding azimuthal anisotropy is explained by the interaction of pions with projectile and target spectator matter. This interaction with the spectator matter causes an effective shadowing which varies with time during the reaction. Our observations show that high-energy pions stem from the early stage of the collision whereas low-energy pions freeze out later.

Energy Resolution and Energy-Light Response of CsI(TI) Scintillators for Charged Particle Detection
(Nucl. Instr. Meth. A 456 (2000) 290)

Wagner, A., W.P. Tan, K. Chalut, R.J. Charity, B. Davin, Y. Larochelle, M.D. Lennek, T.X. Liu, W.G. Lynch, A.M. Ramos, R. Shomin, L.G. Sobotka, R.T. de Souza, M.B. Tsang, G. Verde, H.S. Xu

Abstract: This article describes the crystal selection and quality control utilized to develop and calibrate a high resolution array of CsI(TI) scintillator crystals for the detection of energetic charged particles. Alpha sources are used to test the light output variation due to thallium doping gradients. Selection of crystals with better than 1% non-uniformity in light output is accomplished using this method. Tests with 240 MeV alpha beam reveal that local light output variations within each of the tested CsI(TI) crystals limit the resolution to about 0.5%. Charge and mass dependences in the energy - light output relationship are determined by calibrating with energetic projectile fragmentation beams.

Direct Comparison of Phase-Space Distributions of K^- and K^+ Mesons in Heavy-Ion Collisions at SIS Energies – Evidence for In-Medium Modifications of Kaons?
(Eur. Phys. J. A 9 (2000) 515)

Wisniewski, K., P. Crochet, N. Herrmann, A. Andronic, R. Averbeck, A. Devismes, C. Finck, A. Gobbi, O. Hartmann, K.D. Hildenbrand, P. Koczon, T. Kress, R. Kutsche, Y. Leifels, W. Reisdorf, D. Schüll, J. P. Alard, V. Barret, Z. Basrak, N. Bastid, I. Belyaev, A. Benderag, G. Berek, R. Caplar, N. Cindro, P. Dupieux, M. Dzelalija, M. Eskef, Z. Fodor, Y. Grishkin, B. Hong, J. Kecskemeti, Y.J. Kim, M. Kirejczyk, M. Korolija, **R. Kotte**, M. Kowalczyk, A. Lebedev, K.S. Lee, V. Manko, H. Merlitz, S. Mohren, D. Moisa, **W. Neubert**, A. Nianine, D. Pelte, M. Petrovici, **C. Plettner**, F. Rami, B. de Schauenburg, Z. Seres, B. Sikora, K. Sim, V. Simion, K. Siwek-Wilczynska, V. Smolyankin, A. Somov, M. Stockmeier, G. Stoicea, M. Vasiliev, P. Wagner, **D. Wohlfarth**, J.T. Yang, I. Yushmanov, A. Zhilin

Abstract: The ratio of K^- to K^+ meson yields has been measured in the systems ^{96}Ru+^{96}Ru at 1.69 A GeV, ^{96}Ru+^{96}Zr at 1.69 A GeV, and ^{96}Ni+^{96}Ni at 1.93 A GeV incident beam kinetic energy. The yield ratio is observed to vary across the measured phase space. Relativistic transport-model calculations indicate that the data are best understood if in-medium modifications of the kaons are taken into account.

Isospin Fractionation in Nuclear Multifragmentation
(Phys. Rev. Lett. 85 (2000) 716)

Xu, H.S, M.B. Tsang, T.X. Liu, X.D. Liu, W.G. Lynch, W.P. Tan, A. Vander Molen, G. Verde, **A. Wagner**

Abstract: Isotopic distributions for light particles and intermediate mass fragments have been measured for $^{112}Sn + ^{112}Sn$, $^{112}Sn + ^{124}Sn$, $^{124}Sn + ^{112}Sn$, and $^{124}Sn + ^{124}Sn$ collisions at E/A = 50 MeV. Isotope, isotone, and isobar yield ratios are utilized to estimate the isotopic composition of the gas phase at freeze-out. Analyses within the equilibrium limit imply that the gas phase is enriched in neutrons relative to the liquid phase represented by bound nuclei. These observations suggest that neutron diffusion is commensurate with or more rapid than fragment production.

Subpicosecond Electro-optic Measurement of Relativistic Electron Pulses
(Phys. Rev. Lett. 85 (2000) 3404)

Yan, X., A.M. MacLeod, W.A. Gillespie, G.M.H. Knippels, D. Oepts, A.F.G. van der Meer, **W. Seidel**

Abstract: Time-resolved measurements of the transverse electric field associated with relativistic electron bunches are presented. Using an ultrafast electro-optic sensor close to the electron beam, the longitudinal profile of the electric field was measured with subpicosecond time resolution and without time-reversal ambiguity. Results are shown for two cases: inside the vacuum beam line in the presence of wake fields, and in air behind a beryllium window, effectively probing the near-field transition radiation. Especially in the latter case, reconstruction of the longitudinal electron bunch shape is straightforward.

Conference Contributions
Laboratory Reports and Patents

Almehed, D., S. Frauendorf, F. Dönau:
Pairing Correlations in Rotating Nuclei
Verhandl. DPG (VI) 35, 208 (2000)

Andronenko, M.N., L.N. Andronenko, **W. Neubert**, D.M. Seliverstov:
Nuclear Temperatures obtained from Light Charged Particle Yields in Spontaneous and Neutron Induced Fission
Int. Conf. Bologna 2000- Structure of the Nucleus at the Drawn of the Century, Bologna, May 29 - June 2, 2000

Balcerzyk, M., M. Moszynski, M. Kapusta, D. Wolski, **J. Pawelke**, M. Melcher:
YSO, LSO, GSO and LGSO. A Study of Energy Resolution and Nonproportionality
IEEE Nuclear Science Symposium and Medical Imaging Conference, Seattle, Oct. 24-30 1999
Book of Abstracts(1999)18
Conference Record **N10-4**(2000)1-5

Barz, H.W., B. Kämpfer:
The Role of Three-Body Collisions on ϕ Meson Production Processes near Threshold,
nucl-th/005063

Barz, H.W.:
Compton Backscattering of Laser Light off the ELBE Electron Beam
Workshop on X-rays from Electron Beams, FZ-Rossendorf, Febr. 24-26, 2000
Forschungszentrum Rossendorf, Report FZR-287 (2000)

Borcan, C., H. Schnare, **R. Schwengner, L. Käubler, F. Dönau,** I. Ragnarsson, A.V. Afanasjev, J. Eberth, T. Steinhardt, O. Thelen, M. Hausmann, A. Jungclaus, K.P. Lieb, A. Algora, G. DeAngelis, A. Gadea, D.R. Napoli, D. Jenkins, R. Wadsworth, A. Wilson:
The ^{73}Br Nucleus Investigated at Highest Rotational Frequencies
Verhandl. DPG (VI) 35, 232 (2000)

Borcan, C., H. Schnare, **R. Schwengner, L. Käubler, F. Dönau,** I. Ragnarsson, A.V. Afanasjev, J. Eberth, T. Steinhardt, O. Thelen, M. Hausmann, A. Jungclaus, K.P. Lieb, A. Algora, G. DeAngelis, A. Gadea, D.R. Napoli, D. Jenkins, R. Wadsworth, A. Wilson:
Signature Inversion in the Odd-Odd ^{72}Br Nucleus
Verhandl. DPG (VI) 35, 242 (2000)

Brankovic, K., D. Slonina, **A. Panteleeva,** W. Dörr:
Klonogenes Zellüberleben von Keratinozyten und Fibroblasten nach Bestrahlung mit 25 kV und 200 kV Röntgenstrahlen.
Gemeinsamer Jahreskongress der Deutschen Gesellschaft für Radioonkologie, Strahlenbiologie und Medizinische Physik, der DEGRO und der DGMP, München 06-09 Okt, 2000
Strahlenther. Oncol. **176**(Sondernr.1)(2000)110

Büchner, A., F. Gabriel, **E. Grosse, P. Michel, W. Seidel,** J. Voigtländer and the ELBE-crew, FZR:
The ELBE-Project at Dresden-Rossendorf
Proceedings of the EPC 2000, Wien, July 26-30 2000

Büchner, A., F. Gabriel, **P. Gippner, E. Grosse,** D. Janssen, **P. Michel, A. Schamlott, W. Seidel,** A. Wolf, J. Voigtländer, **R. Wünsch** and the ELBE-crew:

The FEL Projects at the Radiation Source ELBE
Proceedings of the Twenty-first Int. FEL-Conference, DESY, Hamburg, Aug. 23-26, 1999

Chmel, S., H. Hübel, K. Vyey, D.L. Balabanski, D. Boremans, S. Cottenier, N. Coulier, R. Coussement, W. Declercq, G. Gergigiev, N. Nenoff, G. Neyens, S.C. Pancholi, D. Rossbach, **R. Schwengner,** S. Teughels:
Quadrupolmomente isomerer Zustände in ^{194}Pb und ^{196}Pb
Verhandl. DPG (VI) 35, 234 (2000)

Enghardt, W., H. Prade:
Workshop on X-Rays from Electron Beams with Special Emphasis on Possible Developments at ELBE
Transparencies of the Workshop, FZ-Rossendorf, Febr. 24-26, 2000
FZR-287

Gabriel F., **P. Gippner, E. Grosse, D. Janssen, P. Michel, H. Prade, A. Schamlott, W. Seidel,** U. Steegmüller, M. Wenzel, A. Wolf, **R. Wünsch**:
The Rossendorf Radiation Source ELBE and its FEL Projects
Proc. 6^{th} Int. Conf. ECAARD, Dresden 1999

Gabriel F., **P. Gippner, E. Grosse,** D. Janssen, **P. Michel, H. Prade, A. Schamlott, W. Seidel,** U. Steegmüller, M. Wenzel, A. Wolf, **R. Wünsch**:
The FEL Projects at the Rossendorf Radiation Source ELBE
Proc. 21^{st} Int. Conf. on FREE Electron Lasers, Hamburg 1999

Gallerano, G.P., A. Gover, **E. Grosse, W. Seidel,** M. Tecimer, A. Wolf, **R. Wünsch**:
Design Study of a Waveguide Resonator for an Infrared FEL at ELBE
2000 FEL Conference and Workshop, Durham, USA, Aug. 2000

Gallmeister, K., B. Kämpfer, O.P. Pavlenko, C. Chale:
A Unique Parametrization of the Shapes of Secondary Dilepton Spectra Observed in Central Heavy-Ion Collisions at CERN-SPS
nep-ph/ 0010332

Gallmeister, K., B. Kämpfer, O.P. Pavlenko:
Kann man die Pb(158 AGeV)+Au,Pb Dilepton-Daten von CERES und NA50 mit einer einzigen thermischen Quelle beschreiben?
Verhandl. DPG (VI) 35, 243 (2000)

Grigoryan, L.Sh. A.R. Mkrtchyan, H.F. Khachtryan, **W. Wagner**:
Quantum Mechanical Approach to Planar Position Channeling in Longitudinal Hypersonic Field (Poster)
IV International Symposium "RREPS", Lake Baikal,Russia, Sept. 13-16, 1999

Hinz, R., W. Enghardt, B.G. Hasch, **K. Lauckner, J. Pawelke, F. Pönisch, M. Sobiella:**
Simultaneous Monitoring of Heavy-Ion Therapy by Positron Emission Tomography.
Sixth Int. Conf. on Medical Physics, Patras, Hellas, 1-4 Sep, 1999
Physica Medica XV(No.3)(1999)157

Hinz, R., W. Enghardt, B.G. Hasch, **K. Lauckner, J. Pawelke, F. Pönisch, M.**

Sobiella:
PET zur in-situ Dosislokalisation bei der Schwerionen-Tumortherapie
Nuklearmedizin 2000 - Gemeinsame Jahrestagung der Deutschen, Österreichischen und Schweizerischen Gesellschaften für Nuklearmedizin, München, 29-1 Mar/Apr, 2000
Nuklearmedizin 39 (2000)A45

Kämpfer, B., K. Gallmeister, O.P. Pavlenko:
Can Extended Duality Uniquely Explain the Dilepton Data in HICS at SPS?
28th Intern. Workshop on Gross Properties of Nuclei and Nuclear Excitation: Hadrons in Dense Matter, Hirschegg, Austria, Jan. 16-22, 2000, p. 219

Kämpfer, B.:
Kosmische Phasenübergänge
Verhandl. DPG (VI) 35, 187 (2000)

Kämpfer, B.:
Strange Quark Matter: Mapping QCD Lattice Results to Finite Baryon Density by a Quasiparticle Model
5th Intern. Conference on Strangeness in Quark Matter, Berkeley, California, 20-25 July, 2000, nucl-th/0008058

Kämpfer, B., O.P. Pavlenko:
Probing Meson Spectral Functions with Double Differential Dilepton Spectra in Heavy-Ion Collisions,
nucl-th/0011021

Kämpfer, B., K. Gallmeister O.P Pavlenko:
Confinement im Big Bang and Deconfinement in Little Bangs at CERN-SPS
nucl-th/0011088

Käubler, L., K.D. Schilling, D. Belic, P. von Brentano, **F. Dönau,** C. Fransen, **E. Grosse,** U. Kneissl, C. Kohstall, A. Linnemann, P. Matschinsky, A. Nord, N. Petralla, H.H. Pitz, M. Scheck, **R. Schwengner,** F. Stedile, V. Werner:
A Nuclei Resonance Fluorescence Experiment on the N=50 Nucleus ^{87}Rb
Verhandl. DPG (VI) 35, 232 (2000)

Käubler, L.:
A Scissors-Like State on Top of the Quadrupole Vibrational State in ^{88}Sr
Bologna 2000 - Structure of the Nucleus at the Dawn of the Century,
Bologna, Italy, May 5-June 3, 2000

Käubler, L.:
Dynamic Scissors Mode in Spherical Nuclei
Workshop on Nuclear Spectroscopy and Astrophysics
FZ-Rossendorf, April 29, 2000

Kapusta, M., M. Moszynski, M. Balcerzyk, J. Braziewicz, D. Wolski, **J. Pawelke**, W. Klamra:
Comparison of the Scintillation Properties of LSO:Ce Manufactured by Different Laboratories and of LGSO:Ce
IEEE Nuclear Science Symposium and Medical Imaging Conference, Seattle, 24-30 Oct, 1999
Conference Record **N20-27**(2000)1-5

Kotte, R.:
Subthreshold $\phi(1020)$ Meson Production in Central Heavy-Ion Collisions
28th Intern. Workshop on Gross Properties of Nuclei and Nuclear Excitation: Hadrons in Dense Matter, Hirschegg, Austria, Jan. 16-22, 2000, p. 112

Kotte, R., W. Neubert, D. Wohlfarth, FOPI Collaboration:
Produktion und Propagation seltsamer Mesonen bei zentralen Schwerionenstößen
Verhandl. DPG (VI) 35, 205 (2000)

Lauckner, K., W. Enghardt, R. Hinz, J. Pawelke, F. Pönisch:
Schwächungs- und Streukorrektur für die Positronen-Emissions-Tomografie (PET) bei der Schwerionentherapie
Verhandl. DPG (VI) 35, 212 (2000)

Lauckner, K., W. Enghardt, P. Crespo, **J. Pawelke**:
An LSO-Based Scanner for In-Beam PET: A Feasibility Study
IEEE Nuclear Science Symposium and Medical Imaging Conference, Lyon, France, Oct. 15-20, 2000

Lauckner, K., W. Enghardt, F. Pönisch:
Fortschritt bei der Bildkonstruktion
Gemeinsamer Jahreskongress der Deutschen und Österreichischen Gesellschaften für Radioonkologie und der Deutschen Gesellschaft für Medizinische Physik, München, Oct. 6-9, 2000

Michel, P., A. Büchner, **P. Evtushenko, K. Möller, Ch. Schneider,** J. Teichert, F. Gabriel, **E. Grosse**:
Status of the ELBE Accelerator - a Driver for Different Radiation Sources (Poster)
The 22nd Intern. Free Electron Laser Conference and 7th FEL Users Workshop, Durham, North Carolina, USA 13-18 Aug. 2000

Naumann, B., E. Grosse:
Ein gepulster Neutronenstrahl an ELBE
Verhandl. DPG (VI) 35, 222 (2000)

Naumann, L., F. Dohrmann, **R. Dressler, W. Enghardt, E. Grosse, K. Heidel, J. Hutsch, M. Sobiella:**
Großflächige Driftkammern hoher Auflösung für das HADES Spectrometer
Verhandl. DPG (VI) 35, 216 (2000)

Naumann, L., H. Bokemeyer, J.I. Boyard, V. Chepurnov, S. Chernenko, H. Daues, F. Dohrmann, **W.Enghardt,** O. Fateev, C. Garabatos, L. Glonti, **E. Grosse,** J. Hehner, T. Hennino, J. Kempter, W. Koenig, C. Müntz, A. Petrov, J. Pouthas, Ph. Rosier, L. Smykov, H.S. Stelzer, **M.Sobiella,** J. Stroht, J. Wüstenfeld, Yu. Zanevsky, P. Zumbruch:
Development of Low-Mass Drift Chambers for the HADES Spectrometer
5th Int. Conf. on Position-Sensitive, London 13th -17th Sept. 1999

Neubert, W., W. Enghardt, U. Lehnert, B. Naumann, A. Panteleeva, J. Pawelke:
Optimization of a Tunable Quasi- Monochromatic X-Ray Source for Cell Irradiations
Book of Abstracts of Int. Conf. Advanced Monte Carlo an Radiation Physics, Particle Transport Simulation and Applications, Lissabon, Portugal, 23-26 Oct. 2000, p. 27

Neubert, W., W. Enghardt:
1. Bericht zum Forschungsvertrag zwischen der Gamma Service Produktbestrahlung GmbH Leipzig und dem FZ-Rossendorf, Sept. 2000

Neubert, W., W. Enghardt, M.N. Andronenko:
2. Bericht zum Forschungsvertrag der Gamma Service Produktbestrahlung GmbH Leipzig und dem FZ-Rossendorf, Oct. 2000

Neubert, W., B. Naumann, W. Enghardt, M.N. Andronenko:
3. Bericht zum Forschungsvertrag der Gamma Service Produktbestrahlung GmbH Leipzig und dem FZ-Rossendorf, Dec. 2000

Neubert, W.:
Neue Entwicklungen bei Strahlungstransportrechnungen
Workshop Dosimetrie von Teilchenstrahlung und weicher Röntgenstrahlung
Rossendorf, Nov. 10, 2000

Panteleeva, A., W. Enghardt, U. Lehnert, J. Pawelke, H. Prade, W. Wagner, W. Dörr, B. Dörschel:
A Project for Radiobiological Studies with Channeling Radiation
Proc. der 3. Jahrestagung der Gesellschaft für Biologische Strahlenforschung, Dresden, Sep./Oct. 29-1(1999)25

Panteleeva, A., W. Enghardt, U. Lehnert, J. Pawelke, H. Prade, W. Dörr, B. Dörschel:
Cell Survival Studies after X-Ray Irradiation
Workshop on X-rays from Electron Beams, Dresden, 24-26 Feb, 2000
Forschungszentrum Rossendorf, Report FZR-287 (2000)

Panteleeva, A., W. Enghardt, U. Lehnert, J. Pawelke, H. Prade, W. Dörr, B. Dörschel, K. Brankovic, D. Slonina:
Radiobiological Studies with Soft X-Rays
30th Annual Meeting of the European Society for Radiation Biology,
Warszawa, Poland, 27-31 Aug., 2000
Book of Abstracts(2000)55

Panteleeva A., W. Enghardt, U. Lehnert, J. Pawelke, H. Prade, W. Dörr, B. Dörschel, K. Brankovic, D. Slonina:
Radiobiological Studies with Soft X-Rays
Int. Conf. on Modern Problems of Radiobiology, Radioecology and Evolution,
Dubna, Russia, 6-9 Sep., 2000
Book of Abstracts (ISBN 5-85165-572-0)(2000)142

Panteleeva, A., W. Enghardt, U. Lehnert, W. Neubert, J. Pawelke, H. Prade, K. Brankovic, W. Dörr, B. Dörschel, D. Slonina:
Preparation of RBE Measurements of Soft X-Rays at ELBE
Abstracts of the 7th Workshop on Heavy Charged Particles in Biology and Medicine,
Darmstadt, 28-30 Sep., 2000
G. Kraft and K. Langbein (eds.): GSI-Report 2000-04 (2000)Appendix

Panteleeva, A.:
The Estimation of the Absorbed Dose in the Cell
Workshop zur Dosimetrie von Teilchenstrahlung und weicher Röntgenstrahlung,
FZ-Rossendorf, 10 Nov. 2000

Parodi, K., S. Squarcia:
Improvements of the FLUKA Simulation Code for Radiobiological Applications
Verhandl. DPG (VI) 35, 218 (2000)

Parodi, K., P. Crespo, **W. Enghardt,** R. Hinz, **K. Lauckner, J. Pawelke, F. Pönisch:**
The Potential of Positron Emission Tomography for the Monitoring of Proton Therapy
7th Workshop on Heavy Charged Particles in Biology and Medicine,
Darmstadt, Sept. 2000, GSI Report 2000-4

Pawelke, J., W. Enghardt, B.G. Hasch, R. Hinz, **K. Lauckner, F. Pönisch, M. Sobiella:**
In-situ Kontrolle der Strahlentherapie mit Schwerionen durch Positronen-Emissions-Tomographie
Proc. der 3. Jahrestagung der Gesellschaft für Biologische Strahlenforschung,
Dresden, Sep./Oct. 29-1(1999)32

Pawelke, J., W. Enghardt, U. Lehnert, B. Naumann, W. Neubert, A. Panteleeva, H. Prade, W. Wagner:
A Device for Cell Irradiation with Low Energy Quasi-Monochromatic Photons at ELBE
Workshop on X-rays from electron beams, Dresden, 24-26 Feb, 2000
Forschungszentrum Rossendorf, Report FZR-287 (2000)

Pawelke, J., W. Enghardt, U. Lehnert, B. Naumann, W. Neubert, A. Panteleeva, H. Prade, W. Wagner:
Strahlenbiologische Forschung mit Channelingstrahlung an ELBE
Frühjahrstagung des Fachverbandes Strahlenphysik und Strahlenwirkung der Deutschen Physikalischen Gesellschaft, Dresden, 20-24 Mar, 2000
Vortrag ST 4.3, Verhandl. DPG 35 (VI) (2000)

Pawelke, J., K. Brankovic, W. Dörr, B. Dörschel, **W. Enghardt, U. Lehnert, A. Panteleeva, H. Prade,** D. Slonina:
Die relative biologische Wirksamkeit von weicher Röntgenstrahlung
Proc. der 4. Jahrestagung der Gesellschaft für Biologische Strahlenforschung
(ISBN 3-00-006800-7), Bad Kissingen, 4-6 Oct(2000)52

Pflüger, I., **P. Gippner,** A. Swiderski, T. Vieliz, J. Feldhans, H. Weise:
Magnetic Characterisation of the Undulator for the VUV-FEL at the TESLA-Test Facility
Proceedings of the Twenty-first Int. FEL-Conference, DESY, Hamburg, Aug. 23-26, 1999

Pönisch, F., J. Debus, **W. Enghardt,** Th. Haberer, B.G. Hasch, R. Hinz, **K. Lauckner, J. Pawelke:**
PET zur Qualitätskontrolle der Schwerionen-Tumortherapie
5. Deutscher Kongress für Radioonkologie, Strahlenbiologie und Medizinische Physik,
Karlsruhe, Nov. 6-9 1999
Strahlenther. Oncol. 175 (Sondernr.1)(1999)143

Pönisch, F.:
Quality Assurance in Heavy Ion Tumor Therapy by Means of PET
PET 2000-ECAT Users Meeting in Barcelona, Aug. 28, 2000

Rainovski, G., H. Schnare, **R. Schwengner, C. Borcan, L. Käubler, F. Dönau,** V.I. Dimitrov, J. Eberth, T. Steinhardt, O. Thelen, M. Hausmann, A. Müller, A. Jungclaus, K.P. Lieb, D. Jenkins, R. Wadsworth, A. Wilson, G. DeAngelis, A. Gadea, D.R. Napoli, A. Algora:
High Spin Structure of ^{70}Se
Verhandl. DPG (VI) 35, 232 (2000)

Richter, M., H. Freiesleben, K.-Th. Brinkmann, **P. Michel,** F. Gabriel, R. Krause, P. Eckstein, H. Futterschneider:
Realisierung eines Echtzeit-Triggers zur Erkennung elastischer Proton-Proton-Streuereignisse am Flugzeitspektrometer COSY-TOF
Verhandl. DPG (VI) 35, 219 (2000)

Schneider, Ch., H. Müller, ANKE-Kollaboration:
Vergleich erster Ergebnisse zur K^+ Messung an ANKE mit Modellrechnungen
Verhandl. DPG (VI) 35, 22 9 (2000)

Schwengner, R.:
Signature Inversion Caused by Triaxiality in ^{72}Br and Band Termination in ^{73}Br
Bologna 2000 - Structure of the Nucleus at the Dawn of the Century, Bologna, Italy, May 5 - June 3, 2000

Seidel, W., A. Büchner, **W. Enghardt, P. Evtushenko,** F. Gabriel, **P. Gippner, E. Grosse, D. Kalionska, U. Lehnert, P. Michel, A. Schamlott, W. Wagner, D. Wohlfahrt,** A. Wolf, **R. Wünsch:**
Projects for Two-Color Pump-Probe Studies at the Radiation Source
Proceedings of the Twenty-second Int. FEL-Conference, Duke University, Durham, Aug. 13-18, 2000

Seidel, W.:
Infrarotstrahlung vom Rossendorfer Freie Elektronen Laser
BioMet - Innovationsnetzwerk Dresden, April 2000

Stefanova, E., **R. Schwengner,** J. Reif, H. Schnare, **F. Dönau,** M. Wilhelm, A. Fitzler, S. Kaesemann, P. von Brentano:
Influence of Neutron Core Excitations on the High-Spin States of ^{88}Sr
Verhandl. DPG (VI) 35, 242 (2000)

Teichert, J., A. Büchner, **P. Evtushenko, P. Michel, K. Möller, Ch. Schneider**:
Simulation of a Thermionic Electron Gun Including Control Grid Effects Poster at
6th Intern. Computational Accelerator Physics Conference, Darmstadt, Sept. 11-14, 2000

Tomitani, T., **J. Pawelke,** M. Kanazawa, K. Yoshikawa, K. Yoshida, M. Sato, A. Takami, M. Koga, Y. Futami, T. Murakami, A. Kitagawa, E. Urakabe, M. Suda, T. Kanai, H. Matsuura, I. Shinoda, S. Takizawa:
Metabolic Studies of ^{11}C in Rabbit Thigh Muscle Implanted by Secondary Beam of HIMAC.
2nd Japan-Korean Joint Meeting on Medical Physics, Chiba, Japan, 5-6 Nov, 1999

Wagner, A. :
Detector Simulations with GEANT
Workshop on a New High Resolution Array, East Lansing/MI (USA), Nov. 11, 1999

Wagner, W., W. Enghardt, U. Lehnert, B. Naumann, W. Neubert, A. Panteleeva, J. Pawelke, H. Prade:
Quasi-Monochromatic X-rays from ELBE
Workshop on X-rays from electron beams, Dresden, 24-26 Feb, 2000
Forschungszentrum Rossendorf, Report FZR-287 (2000)

Wagner, W., W. Enghardt, U. Lehnert, B. Naumann, W. Neubert, A. Panteleeva, J. Pawelke, H. Prade:
Quasi-Monochromatic X-rays from the ELBE Radiation Source
1^{st} Int. Congress on Radiation Physics,Tomsk, Russia, Sept. 2000

Lectures and Seminars

Barz, H.-W.:
$K^{\pm}$-und Φ-Erzeugung in Transportcodes vom BUU-Typ
FZ Rossendorf, Aug. 1999

Barz, H.-W.:
Mean Field Effects in Two-Particle Correlations
Seminar, KFKI Budapest, Sept. 2000

Barz, H.-W.:
Streutheorie für Elementarteilchen
Vorlesung, TU Dresden WS 2000/2001

Crespo, P.:
A RHICH for the Alpha Magnetic Spectrometer AMS
FZ Rossendorf, Oct. 1999

Debowski, M., B. Kämpfer:
Konferenzbericht Hirschegg, Bormio und EOS 2000
FZ Rossendorf, March 2000

Dohrmann, F.:
Kaon-Electroproduction off Light Nuclei
FZ Rossendorf, Nov. 2000

Dohrmann, F.:
Investigating Kaon Production in pp Collisions with HADES
HADES Collaboration Meeting, Santiago de Compostela, Sept. 1999

Dönau, F.:
Chirale Symmetrie in rotierenden Kernen
FZ Rossendorf, May 2000

Dönau, F.:
Chirale Symmetry in Rotating Nuclei
Physics Division Seminar
Oak Ridge National Lab., June 22, 2000

Dönau, F.:
Symmetry Breaking in Rotating Nuclei
Seminar, Universitiät Tübingen, Nov. 22, 2000

Dönau, F.:
Symmetriebrechung in rotierenden Kernen
Seminar, TU München, Dec. 15, 2000

Dressler, R.:
Zur Auswertung von DISTO-Daten der pp-Reaktion
FZ Rossendorf, March 2000

Enghardt, W., U. Lehnert, W. Wagner:
Berichte über Konferenzbesuche: X-99(Chicago/USA), PSD 5 (London/GB),

RPEPS '99 (Irkutsk/Russland)
FZ Rossendorf, Oct. 1999

Enghardt,W.:
PET Analysis
Vortrag, Meeting of the International Advisory Committee Therapie (ACT),
GSI Darmstadt, Apr. 2000

Enghardt, W.:
Radiotherapie mit Photonen und Elektronen (Teletherapie)
Vorlesung am Institut für biomedizinische Technik an der Fakultät Elektrotechnik der TU Dresden, May 2000

Enghardt, W.:
Moderne Methoden der Strahlentherapie von Tumoren
Beitrag zur Ringvorlesung im Studium generale "Naturwissenschaften aktuell" an der TU Dresden, June 2000

Enghardt, W.:
Dosimetrie von Teilchenstrahlung und weicher Röntgenstrahlung
Workshop FZ-Rossendorf, Nov. 10, 2000

Gallmeister, K.:
A Unique Parametrisation for "Excess" - Dileptons In Heavy Ion Collision at the CERN SPS?
DPG Frühjahrstagung, Dresden March 20-24, 2000

Gallmeister, K.:
A Unique Thermal Parametrisation for Real and Virtual Photons in Heavy Ion Collisions at the CERN SPS?
Rauischholzhausen XII, Rieneck, June 19-21, 2000

Gallmeister, K.:
Dileptonen und Photonen in relativistischen Schwerionenstößen
TU Dresden, Oct. 13, 2000

Gallmeister, K.:
Dileptons and Photons in Relativistic Heavy Ion Collisions
Justus-Liebig-Universität Gießen, Gießen Oct. 31, 2000

Grosse, E.:
The Rossendorf FEL Projects
Workshop on Research with Infrared Radiation,
FZ Rossendorf, Aug. 1999

Grosse, E.:
Bericht über Photonics West (Tagung für Biomedizinische Optik und Laser) in San Jose (USA) und Laborversuche in Berkeley und Stanford
FZ Rossendorf, Febr. 2000

Grosse, E.:
Der supraleitende Elektronen-Linac ELBE in Dresden-Rossendorf als Quelle von Neutronen

und elektromagnetischer Strahlung in ps-Pulsen
Physikalisches Kolloquium Universität Gießen, Dec. 2000

Kämpfer, B.:
Kosmische Phasenübergänge,
Hauptvortrag auf der DPG-Tagung, Dresden, March 2000

Kämpfer, B.:
Can extended duality uniquely explain the dilepton data on HIC'S,
28 th Int. Workshop on Gross Properties of Nuclei and Nuclear Excitation: Hadrons in Dense Matter, Hirschegg, Austria, 16-22 Jan. 2000

Kämpfer, B.:
Kosmische Phasenübergänge,
FZ Rossendorf "Tag der offenen Tür", Sept. 2000

Kämpfer, B.:
Eichfeldtheorie,
Lecture Course, TU Dresden, SS 2000

Kämpfer, B.:
Strange Quark Matter: Mapping QCD Lattice Results to Finite Baryon Density by a Quasiparticle Model,
5th Int. Conference on Strangeness on Quark Matter, Berkely, July 2000

Kämpfer, B.:
Cosmic Phase Transitions
FZ Rossendorf, June 2000

Kämpfer, B.:
Confinement in the Big Bang and Deconfinement in the Little Bangs at CERN-SPS
Kolloquium, Uni Giessen, July 2000

Kämpfer, B.:
Confinement in the Big Bang and Deconfinement in the Little Bangs at CERN-SPS
Seminar, Uni Nantes, Sept. 2000

Kämpfer, B.:
Confinement in the Big Bang and Deconfinement in the Little Bangs at CERN-SPS
Seminar, Uni VI - VII, Paris, Sept. 2000

Kämpfer, B.:
Confinement in the Big Bang and Deconfinement in the Little Bangs at CERN-SPS
Conference "Fundamental and Applied Aspects of Modern Physics", Lüderitz, Nov. 2000

Kämpfer, B.:
Confinement in the Big Bang and Deconfinement in the Little Bangs at CERN-SPS
Kolloquium Uni Cape Town, Nov. 2000

Kotte, R.:
$K^{\pm}$-und Φ-Erzeugung in Schwerionenstößen: FOPI-Resultate

FZ Rossendorf, Sept. 1999

Kotte, R.:
K^+, K^- and ϕ Mesons at Midrapidity and Low Transverse Momentum (Helitron/Plastic Wall data) for the reaction Ru+Ru(Zr) at 1.69 AGeV
FOPI collaboration meeting, Obernai, France, Sept. 29-30, 1999

Kotte, R.:
Zur Reaktion π^- $p^+ \rightarrow \phi$ n am Pionenstrahl der GSI
FZ Rossendorf, April 2000

Martin, J.:
Konfokale Mikroskopie an fluoreszenten und anderen Strukturen im Submikrometerbereich
FZ Rossendorf, June 2000

Michel, P.:
Messungen am 250 keV-Strahl an ELBE
FZ Rossendorf, July 2000

Michel, P.:
Diagnosekonzept an ELBE
FZ Rossendorf, June 2000

Michel, P.:
Sitzung des externen ELBE-MAC
FZ Rossendorf, Oct. 2000

Michel, P.:
Optimierung des thermionischen ELBE-Injektors
FZ Rossendorf, Oct. 2000

Naumann, B.:
Monte-Carlo-Rechnungen zur Vorbereitung von Flugzeitexperimenten mit Neutronen
FZ Rossendorf, May 5, 2000

Naumann, L.:
Status Report of the MDCIII
HADES Collaboration Meeting, Santiago de Compostela, Sept. 1999

Naumann, L.:
Untersuchung derK^+ and K^- Produktion in Au+Au Stößen mit dem Kaonenspektrometer Kaos
FZ Rossendorf, Oct. 1999

Naumann, L.:
Stand der Auswertung K^+ Produktion in Au+Au Stößen bei 1 AGeV
Seminar, GSI, Nov. 1999

Naumann, L.:
Detektierungsmöglichkeiten von K± an HADES
FZ Rossendorf, April 2000

Parodi, K.:
Potential Capabilities of Positron Emission Tomography for Quality Assurance of Proton Therapy
Talk given at Proton Therapy Co-Operative Group PTCOGXXIII, Berlin, Sept. 25-27, 2000

Pawelke, J.:
Positronen-Emissions-Tomographie zur Qualitätssicherung der Schwerionen-Tumortherapie.
Lecture at the Deutsches Krebsforschungszentrum (DKFZ), Heidelberg, Germany, Feb. 14, 2000

Pawelke, J.:
Strahlenwirkung und Strahlenschäden - Biologische Wirkung ionisierender Strahlung.
FZ Rossendorf "Tag der offenen Tür", Sept. 2000

Peshier, A.:
Equation of State of Deconfined Hadronic Matter at Finite Chemical Potential
FZ Rossendorf, Nov. 1999

Plettner, C.:
Band Termination in ^{73}Br
Workshop on Nuclear Structure and Nuclear Astrophysics
FZ Rossendorf, Apr. 2000

Plettner, C.:
Band Termination and Signature Inversion in ^{72,73}Br, Selected Topics on N=Z Nuclei
Lund, Sweden, June 2000

Pönisch, F.:
PET zur Qualitätssicherung der Schwerionentherapie
Seminar in der Strahlenschutzphysik der TU Dresden, May 2000

Pönisch, F.:
Quality Assurance in Heavy Ion Tumour Therapy by Means of PET
PET 2000 - ECAT Users Meeting in Barcelona, Aug. 28, 2000

Pönisch, F.:
PET zur Qualitätskontrolle der Schwerionen-Tumortherapie
5. Deutscher Kongress für Radiologie, Strahlenbiologie und Medizinische Physik,
Karlsruhe, Nov. 1999

Scheinast, W.:
$K^{\pm}$-Erzeugung in pA-Reaktionen: Statusreport zu KaoS-Experimenten
FZ Rossendorf, Oct. 1999

Schwengner, R.:
Der Elektronenbeschleuniger ELBE und seine Möglichkeiten für Experimente mit Infrarot-Laserlicht, Röntgen- und Bremsstrahlung
Seminarvortrag, Fakultät Physik der Universität Stuttgart, June 2000

Schwengner, R.:
Stand der Arbeiten am Gepulsten Injektor - Planungen für den Kernphysikmeßplatz
ELBE Seminar, FZ Rossendorf, July 1999

Schwengner, R.:
Nachweis von Radioaktivität
Lehrerfortbildung 2000 im FZR, FZ Rossendorf, Aug. 2000

Schwengner, R.:
Particle Excitations and Rotational Modes in Nuclei with A=70-90
Invited Lecture at the XIII Int. School on Nuclear Physics, Neutron Physics and Nuclear Energy, Varna, Bulgaria, Sept. 27 - Oct. 3, 1999

Schwengner, R.:
Experimentelle Untersuchung von Teilchenanregungen und Rotationsmoden in mittelschweren Kernen
Seminarvortrag Fachbereich Strahlenschutzphysik der Technischen Universität Dresden, Nov. 1999

Schwengner, R.:
Nuclear Resonance Fluorescence Experiments at the Accelerator ELBE
Invited Talk at the WOG99 Workshop on Spin and Isospin Excitations in Nuclei, Gent, Belgium, Nov. 15-16 1999

Sczepan, M.:
Photophysik und Photochemie von überbrückten Cyanin-Farbstoffen
FZ Rossendorf, April 3, 2000

Seidel, W.:
Bericht über das internationale Arbeitstreffen "Forschung mit Infrarot-Strahlung" zu Anwendungsmöglichkeiten für den zukünftigen "Freie-Elektronen-Laser" in Rossendorf
FZ Rossendorf, Oct. 1999

Seidel, W.:
Beitrag (Poster) zur Präsentation der Projekte
Bio-Med. Netzwerk Hygienemuseum, Dresden, Apr. 2000

Seidel, W.:
Forschung mit Infrarot-Strahlung
FZ Rossendorf "Tag der offenen Tür", Sept. 2000

Wagner, A.:
Experimente zur nuklearen Astrophysik an Elbe
FZ Rossendorf, Sept. 2000

Wagner, A.:
Kerne und Sterne
FZ Rossendorf "Tag der offenen Tür", Sept. 2000

Wagner, W.:
Quasi-Monochromatic X-Rays from the ELBE Radiation Source
IV International Symposium "RREPS '99" Lake Baikal, Russia, Sept. 1999

Wagner, W.:
Resonance Influence of Longitudinal Hypersonic Field on the Radiation from Channeled Electron
IV International Symposium "RREPS '99" Lake Baikal, Russia, Sept. 1999

Wagner, W.:
Quantum Mechanical Approach to Planar Positron Channeling in Longitudinal Hypersonic Field
IV International Symposium "RREPS '99" Lake Baikal, Russia, Sept. 1999

Wagner, W.:
The Superconducting Electron Accelerator ELBE and Application of Secondary Beams for Biomedical Research
Tomsk Polytechnic University, Oct. 2000

Wünsch, R.:
Akzeptanz der aktuellen Injektorparameter und der Erhöhung der Frequenz der Mikrobunche aus der Sicht der FEL's
FZ Rossendorf, ELBE Palaver, Febr. 2000

Wünsch, R.:
Wie funktioniert ein Freie-Elektronen-Laser
FZ Rossendorf "Tag der offenen Tür", Sept. 2000

Talks of Visitors

Aichelin, J., Uni Nantes/SUBATECH:
$K^{\pm}$ Production in AA Collisions: Test of Hadron Properties in Medium and of Reaction Dynamics
May 3, 2000

Andrejtscheff, W., INRNE Sofia:
Nuclear Structure Aspects of ^{176}Lu the Astrophysics Case
April 13, 2000

Brinkmann, K.-Th., TU Dresden:
Neutron Measurements between 1 and 100 MeV
Oct. 16, 2000

Fateev, O., JINR Dubna:
Construction and Investigation of the Multiwire Drift Chambers for the Second Tracking Layer of the HADES Spectrometer
June 5, 2000

Friedland, W., GSF-Institut für Strahlenschutz:
Simulation von Spurstrukturen und DNA-Schäden im biophysikalischen Modell PARTRAC
Nov. 24, 2000

Geltenbort, P., Inst. Laue-Langevin, Grenoble, France:
Detektorenentwicklungen am ILL Grenoble
April 13, 2000

Grigoryan, L.Sh., IAPP NAS, Yerevan, Armenia:
4 Seminare zum Thema: Channeling-Strahlung im Ultraschallfeld
Nov. 3., 17. Dec. 1., 15 2000

Haberer, Th., GSI Darmstadt:
Prinzipien, technische Realisierung und Einsatz der Kohlenstofftherapie an der Gesellschaft für Schwerionenforschung für die Schwerionentherapiekollaboration GSI Darmstadt, Radiologische Klinik und DKFZ Heidelberg
Nov. 23, 1999

Henniger, J., TU Dresden:
AMOS - Ein multivalent nutzbares Programmsystem zur Berechnung von Strahlungstransport-problemen
Nov. 23, 1999

Jordan, K., TJNAF Newport News (Cebaf), VA, USA:
Instrumentation and Controls for Cebaf FEL
Dec. 15, 1999

Jordan, K., TJNAF Newport News (Cebaf), VA, USA:
ELBE Beam Position Monitors a Proposal Based on Beam Line Requirements and General Observations about ELBE Project
Febr. 28, 2000

Kanaki, K., University of Athens:
Study of Passive and Active Shielding of NaI Detection Systems in Gamma Ray Spectroscopy
Sept. 12, 2000

Kaptari, L.P., JINR Dubna:
Estimates of the Solar Burning Reaction pp $\rightarrow$ D $e^+ \bar{\nu}_e$
Dec. 20, 1999

Kaptari, L.P., JINR Dubna:
Polarisation observables in the reaction pn $\rightarrow$ Dϕ
Dec. 20, 2000

Kapusta, M., Soltan Inst. for Nucl. Studies, Otwock/Swierk, Poland:
Applied Scintillation Detection in Medical Diagnostic
March 14, 2000

Kelley, M., William and Mary College and Thomas Jefferson Accelerator Facility
Progress with Jefferson Lab FEL
Nov. 22, 1999

Kulipanov, G., Budker Inst. of Nucl. Phys., Novosibirsk:
The Status of the High Power Infrared FEL Project at Novosibirsk
Aug. 29, 2000

Langanke, K.H., Uni Aarhus:
Kernphysik und Supernovae
May 22, 2000

Moszynski, M., Soltan Inst. for Nucl. Studies, Otwock/Swierk, Poland:
Avalanche Photodiodes in X-Rays and Scintillation Detection
March 14, 2000

Neil, G., T. Jefferson Lab., Newport News, Virginia:
Recent developments and future plans at the TJL-FEL
June 19, 2000

Oepts, D., FOM-Institute for Plasma Physics Rijnhuizen/The Netherlands:
Application of Electro-Optic Sampling in FEL Physics
May 31, 2000

Oepts, D., FOM-Institute for Plasma Physics Rijnhuizen/The Netherlands:
Different Views on the Free-Electron Laser
June 15, 2000

Pavlenko, O.P., ITP Kiev:
Discussion of Photon Rates in High-Energy Nuclear Collisions
Dec. 9, 1999

Pavlenko, O.P., ITP Kiev:
QCD Analog of the Ter-Mikaelian Effect
Dec. 17, 1999

Pavlenko, O.P., ITP Kiev/FZR:
Analysis of WA 98 photon Data
May 5, 2000

Pavlenko, O.P., ITP Kiev/FZR:
Quantum Mechanical Sum Rules
May 16, 2000

Pavlenko, O.P., ITP Kiev/FZR:
A unique thermal source of Real and Virtual Photons in Heavy-Ion Collisions at SPS
May 29, 2000

Pavlenko, O.P., ITP Kiev:
Probing Meson Spectral Functions with Double Differential Dilepton Spectra in Heavy-Ion Collisions
Nov. 27, 2000

Peshier, A., TU Dresden
Equation of state of deconfined matter: The Luttinger-Ward theorem in action
Dec. 21, 2000

Potylitsina, N., Tomsk Polyt. University, Tomsk, Russia:
Diffraction Radiation as a Tool for Electron Beam Diagnostics
June 23, 2000

Rapp, R., Stony Brook:
Chirale Symmetrierestauration und Dileptonen
Jan. 10, 2000

Reshetin, A.I., Inst. for Nucl. Research, Moscow:
Subthreshold K^+, K^--Meson Production in Hadron-Nucleus and Nucleus-Nucleus Interaction
Dec. 2, 1999

Semikh, S.S., JINR/FZR:
Charge - Exchange Reaction pD $\rightarrow$ (pp)n in the Bethe -Salpeter Formalism
May 31, 2000

Sadovski, A., Nucl. Res.Moscow:
The ISTRA - M Experiment at Protvino: - Preliminary Results for $K^- \rightarrow \pi^- \pi^0 \pi^0$ Decay - Calibration and Shower Parameterization of the Electromagnetic Calorimeter
Oct. 24, 2000

Schaffner-Bielich, J., Brookhaven National Lab.:
Kaons and Anti-Kaons in Nuclear Matter
Dec. 14, 2000

Sibirtsev, A., Uni Giessen:
In-Medium Modification of the pi+N $\rightarrow$ K+Y Amplitude and its Relation to KAOS Data
May 8, 2000

Smith, T., HEPL, Stanford University/FZR:
Experiments with the Stanford ps-FEL
March 15, 2000

Stäudner, F., Wissenschaftsgemeinschaft Gottfried Wilhelm Leibnitz:
Gedankenexperimente, Computersimulationen und ihre wissenschaftstheoretischen Probleme
Nov. 1, 1999

Stefanova, E., INRNE Sofia/FZR:
Influence of Neutron-Core Excitations on High Spin States in ^{88}Sr
May 5, 2000

Ströher, H., FZ Jülich:
Hadronenphysik mit Photonen und Protonen
Dec. 13, 1999

Tecimer, M., University Tel-Aviv:
Modeling of Time Dependent Fields in Short-Pulse Waveguide Resonator FELs
Jan. 17, 2000

Titov, A.I., JINR, Dubna:
On Φ Production in Electromagnetic and Hadronic Processes
Nov. 22, 1999

Titov, A.I., JINR, Dubna:
Calculations of Cross Sections πN $\rightarrow$ ϕN, NN within the One-Boson Exchange Model with Final State Interactions
Dec. 17, 1999

Titov, A.I., JINR, Dubna:
Production of ω, ϕ - Mesons in Near-Threshold Reactions: Baryonic Resonances and Validity of OZI-Rule
Dec. 20, 2000

Wolf, Gy., KFKI Budapest:
Vector Mesons in Nuclear Matter
Dec. 12, 1999

Wolf, Gy., KFKI Budapest:
Thermodynamics of Strongly Interacting Matter within Transport Models: a Status Report
Dec. 16, 1999

Zetenyi, M., KFKI Budapest:
Dalitz Decay of Higher Spin Baryon Resonances-Background Estimates for HADES
July 10, 2000

Zschocke, S., TU Dresden:
Second-Order Self-Energy Correction to the Lamp Shift in Strong Electric Fields
May 24, 2000

THE INSTITUTE OF NUCLEAR AND HADRON PHYSICS

Departments of the Institute

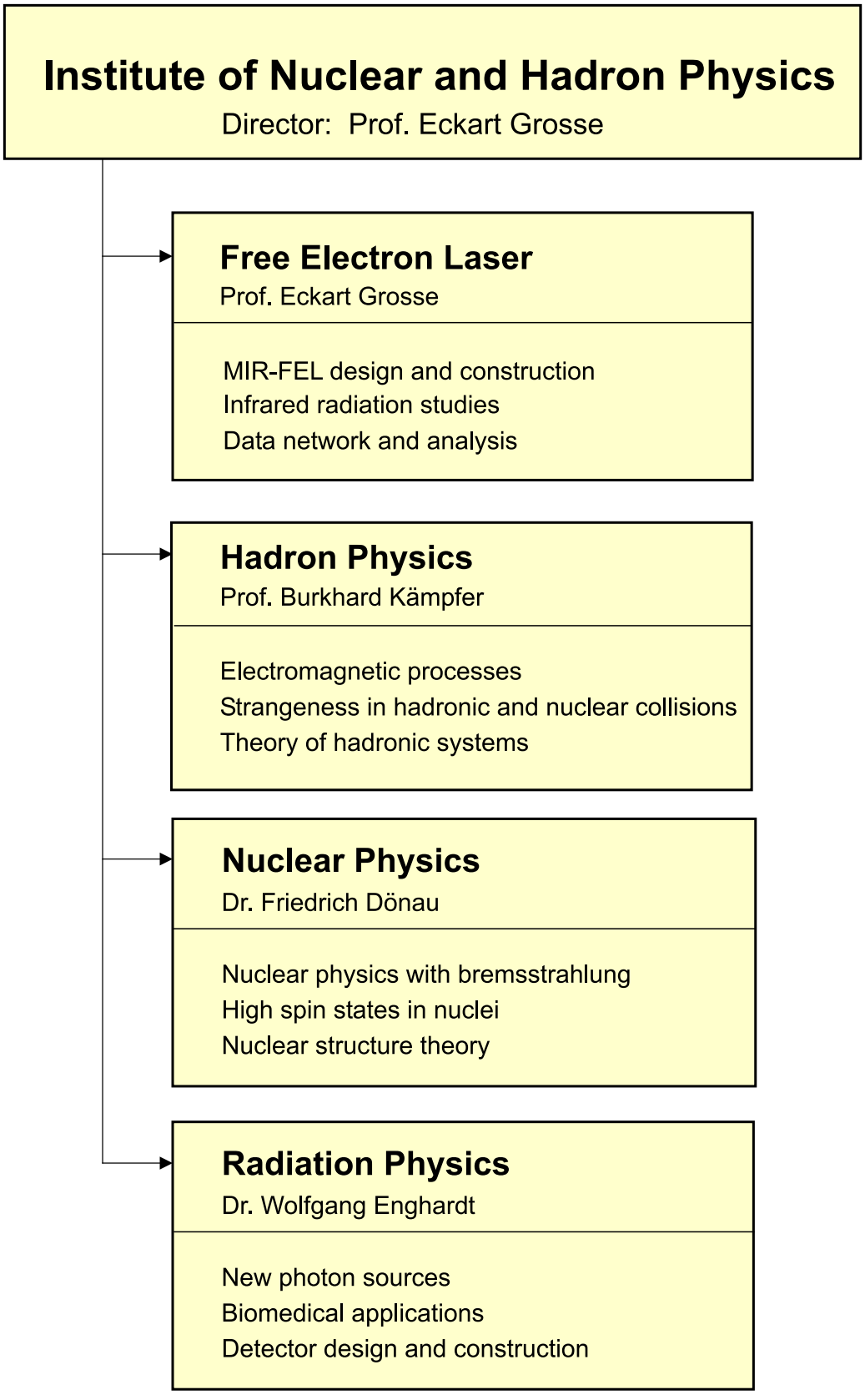

Personnel of the Institute for Nuclear and Hadron Physics

Director: Prof. Dr. E. Grosse[1]

Scientific Personnel

Dr. H.W. Barz
Dr. M. Debowski
Dr. F.Dönau
Dr. F. Dohrmann
Dr. S. Dshemuchadse
Dr. W. Enghardt
Dr. S. Fan
Dr. S. Frauendorf
Dr. P. Gippner
Prof. Dr. B. Kämpfer
Dr. L. Käubler
Dr. R. Kotte
Dr. K. Lauckner
Dr. U. Lehnert
Dr. P. Michel
Dr. K. Möller
Dr. H. Müller
Dr. B. Naumann
Dr. L. Naumann
Dr. W. Neubert
Dr. J. Pawelke
Dr. H. Prade
A. Schamlott
Dr. K.D. Schilling
Dr. M. Schlett
Dr. C. Schneider
Dr. R. Schwengner
Dr. W. Seidel
Dr. A. Wagner
Dr. W. Wagner
D. Wohlfarth
Dr. R. Wünsch

PhD Students

D. Almehed
P. Evtushenko
K. Gallmeister
R. Hinz
D. Kalionska
K. Kanaki
A. Panteleeva
K. Parodi
F. Pönisch
C. Plettner
W. Scheinast

Technical Personnel

M. Altus
H. Angermann
U. Baumann
J.U. Berlin
M. Boeck
M. Böse
R. Förster
M. Freitag
D. Hachenberger
K. Heidel
L. Heinrich
R.R. Hensel
K.H. Hermann
J. Hutsch
J. Kerber
E. Kluge
M. Langer
M. Paul
J. Philipp
I. Probst
B. Rimarzig
H. Römer
C. Schneidereit
W. Schulze
M. Sobiella
U. Wolf

[1]also TU Dresden

Guest Scientists

Andrejtscheff, W.	INRNE Sofia/Bulgaria
Alekseev, V.K.	JINR Dubna, Russia
Andronenko, M.	Inst. of Physics, St. Petersburg/Russia
Byrne, M.	University of Notre Dame, USA
Fateev, O.	JINR Dubna, Russia
Fetea, M.	Nation. Accelerator Centre South Afrika
Friedland, W.	GSF Neuherberg
Dimitrov, V. I.	INRNE Sofia/Bulgaria
Georguieva, E.	Nation. Accelerator Centre South Afrika
Gontchar, I.	Omsk State Railway University/Russia
Grigoryan, L.	Physics Institute, Yerevan/Armenien
Grinberg, M.	INRNE Sofia/Bulgaria
Kalionska, D.	INRNE Sofia/Bulgaria
Kanaki, K.	University Athen/Greece
Kaptari, L. P.	JINR Dubna, Russia
Kapusta, M.	Soltan Institute for Nuclear Studies, Swierk/Poland
Milyov, B. I.	INRNE Sofia/Bulgaria
Moroz, V. D.	JINR Dubna, Russia
Moszynski, I.	Soltan Institute for Nuclear Studies, Swierk/Poland
Nazmitdinov, R.	JINR Dubna, Russia
Oepts, D.	Institute for Plasmaphysics ,Rijnhuizen/Netherlands
Pavlenko, O .P.	Institute for Theor. Physics, Kiev/Ukraine
Potylitsina, N. A.	University Tomsk, Russia
Rapp, R.	State University of New York, USA
Rainovsky, G.	INRNE Sofia/Bulgaria
Rusev, G.	INRNE Sofia/Bulgaria
Semikh, S.	JINR Dubna, Russia
Shteinke,A. R.	BINP Novosibirsk, Russia
Sibirtsev, A.	Institute of Theoretical Physics, Uni Giessen
Stefanova, E.	INRNE Sofia/Bulgaria
Tecimer, M.	Tel Aviv University, Israel
Titov A. I.	JINR Dubna, Russia
Tsakov, I. I.	INRNE Sofia/Bulgaria
Vlaev,K. I.	INRNE Sofia/Bulgaria
Vyvey ,K.	Katholieke Universiteit Leuven/Belgium
Wolf, G.	KFKI Budapest/Hungary
Zetenyi M.	KFKI Budapest/Hungary

Meetings organized by the Institute

Topic	Period	Number of participants
Workshop on X-rays from Electron Beams	February 24-26, 2000	50
Workshop NSA 2000 on Nuclear Spectroscopy and Nuclear Astrophysics	April 27-29, 2000	45
Workshop: Dosimetrie von Teilchenstrahlung und weicher Röntgenstrahlung	November 10, 2000	48